



UiT The Arctic University of Norway

Faculty of Health Sciences
Department of Medical Biology

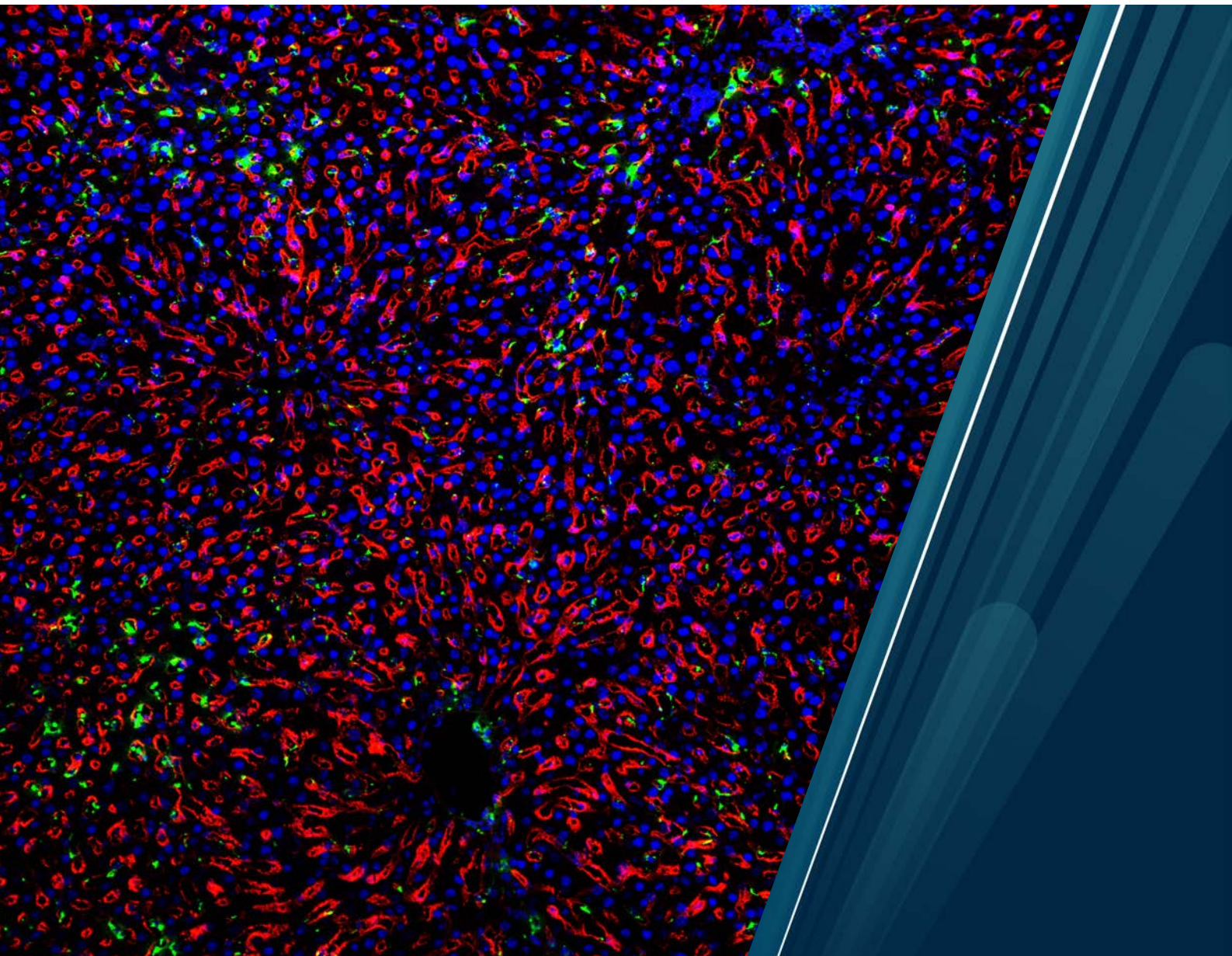
Molecular profiling of the liver sinusoidal endothelial cell – a multi-omics approach

Studies in the rat and mouse model

Sabin Bhandari

A dissertation for the degree of Philosophiae Doctor

May 2021



Molecular profiling of the liver sinusoidal endothelial cell – a multi-omics approach

Studies in the rat and mouse model

Sabin Bhandari

A dissertation for the degree of Philosophiae Doctor



Vascular Biology Research Group

Department of Medical Biology

Faculty of Health Sciences

UiT–The Arctic University of Norway

May 2021

कर्मण्येवाधिकारस्ते मा फलेषु कदाचन ।
मा कर्मफलहेतुर्भूर्मा ते सङ्गोऽस्त्वकर्मणि ॥ 47 ॥

**karmany-evādhikāras te mā phaleṣhu kadāchana
mā karma-phala-hetur bhūr mā te saṅgo 'stvakarmaṇi**

“Do your duty, but do not concern yourself with the results”

Bhagavad Gita: Chapter 2, Verse 47

Acknowledgements

Foremost, I would like to express my utmost veneration and gratitude to my main supervisor Professor Karen Kristine Sørensen, at the Department of Medical Biology, UiT/The Arctic University of Norway. I could not express how grateful I am to find refuge in a learned, compassionate, caring, and wise supervisor like you. You are an accomplished supervisor and a true GURU. You have always showered your grace upon me. I have benefited from the direct guidance and attention you have bestowed upon me and the invaluable career advice you have given me. Thank you immensely for sharing with me your hands-on experiences, nurturing my laboratory and academic skills, and showing me the way forward. With great pride and honour, I could say that you have been my role model. I will feel accomplished if I continue to work towards remaining aspirant in science, sustain optimism even through hard times, compassion and dedications for the study and the students, as you have shown in this project.

The gestation of this dissertation was not easy for both of us due to the unexpectedly long animal house closure. Many times, the helplessness and status quo were maddening and often proved frightening to me, but you always took the personal responsibility to all the troubles and have always been so generous to listen to all my trifles, be it during the weekdays, weekends, holidays, vacations, or sabbaticals or at an office or skype/teams/zoom. Beyond doubts, the boundless optimism, and enthusiasms you maintained and the pragmatic approach you took was the major contributing factor for the success of this Ph.D. projects. I am also grateful for every one-to-one conversation we had throughout this duress. I would also like to beg your pardon if I have in any way failed to absorb, assimilate, practice, or meditated or in any form detriment you or the effort you have put into me to inculcating the core values. My family and I will always remain grateful for the warmest welcome, hospitality, and generosity that you and your family have shown to us from the time we landed on Tromsø lufthavn (airport).

I would also like to pay my sincerest gratitude to Professor Bård Smedsrød, at the Department of Medical Biology, UiT/The Arctic University of Norway, for always sharing your wit and wisdom of your stellar career works on "Liver Sinusoidal Endothelial Cell". Your suggestions and contribution have been proven monumental for the success of these thesis projects beyond any measure. I feel lucky to study the LSECs under your tutelage. I know I could not acknowledge enough the advice and assistance you have bestowed upon me. I would also like to extend my heartfelt appreciation to

the Smedsrød family for all the cordial welcome into your heavenly homes and for titillating our palates with the most satisfying foods.

I am immensely grateful to my co-supervisor, Professor Inigo Zubiavrrre Martinez, at the Department of Clinical Medicine, UiT/The Arctic University of Norway, for being very generous with your time to share your experiences, the expertise concerning "LSEC", career advice, not least for boosting my morale all along these sixth long years. I would also like to express my sincerest appreciation for bringing out much-needed ideas, good strategic advice, not least, the assistance during these periods, and above all, for always being keen on the process and progress in the projects and outside.

I would also like to express my deepest gratitude to my co-supervisor, Professor Peter A.G. McCourt, at the Department of Medical Biology, UiT/The Arctic University of Norway, for your generosity, consideration, and willingness to help no matter whatever, wherever, and whenever despite your busy schedule. I would also like to thank you for making me the beneficiaries of your experience on LSECs and proteins, not least, your English.

I cannot wait to acknowledge the invaluable supervision from my co-supervisor, Dr. Jaione Simon-Santamaria, at the Department of Medical Biology. I could not express how grateful I am to have the opportunity to learn every nook and cranny of the LSEC experimentations and scientific considerations from you. I could not applaud enough your experience, dexterity in the lab, witty and sharp comments, and sophisticated taste for scientific illustrations. You have been instrumental in the success of this thesis project.

I would also like to thank my co-supervisor, Professor Steinar Daae Johansen, at the Faculty of Biosciences and Aquaculture, Nord University, for providing much-needed resources and assistance with RNAseq experiments, the first paper of this thesis.

Anything I would say would fall short to appreciate the expertise and assistance of Dr. Ruomei Li for lifting these thesis projects and converting them into a success. I am glad for the opportunity that I have received to learn and work alongside you. I am an admirer of your lab skills, meticulous planning, fastidiousness in research, and erudition.

I also had the great pleasure of working with Ingelin Kyrrestad, a genuine, kind-hearted person. I want you to know that your assistance has been monumental in the successful completion of my thesis.

I would also take this opportunity to recognize the assistance I had received from Gianina Dumitriu. The excellent liver sections that you prepared amidst various other things have proven indispensable for the success of this thesis. I would also like to pay my heartfelt regard to Dr. Ana Oteiza for sharing with me your immense hands-on expertise in FACS experimentations and analysis. I am also thankful to Dr. Erik Knutsen for introducing me to CLCbio and providing all the technical help I have asked for. I would also like to thank Jack-Ansgar Bruun and Ilona Urbarova for their assistance with proteomics experiments.

I also want to express my sincerest gratitude to Dr. Cristina Ionica Øie for your helpful advice, not least for sharing with us the comfort of your roof in the beginning.

I would also like to express my kind regard to my friend Dr. Hong Mao - for sharing your experience, excitement, and frustrations. I have always admired your frank opinions, not least for never failing to establish that I will always be a year mature than you.

I would also like to extend my thanks to all VBRG members from past and present: Kjell, Kjetil, Montse, Ole Kristian, Jan Ole, Anett, Javier, Christopher, Karolina, Larissa, Bartlomiej, Gahl, Milton, Eirik. I really could not estimate how invaluable you have been along this tortuous Ph.D. journey. Together you have made the VBRG ambiance admirably social, entertaining, helpful, and highly approachable for scientific discussion and small talks. Your company has made us experience a heavenly warmth despite being in the cold arctic Tromsø.

Not least, I want to express my whole-hearted gratitude to my mentor Dr. Kristin Gabestad Nørsett, at the Department of Biomedical Laboratory Science, NTNU, for the training and hands-on laboratory techniques and your invaluable advice that have been fundamental in my Ph.D. success. I would also like to express heartfelt appreciation to all my teachers from the Kathmandu University, Nepal, and my school Nava Ratna English Secondary School, Nepal, for successfully grooming me for this achievement.

I would also like to express my appreciation to all Nepalese families and comrades for making Tromsø home away from home.

Finally, I am eternally grateful to my parents for this graceful life and for providing selfless, unwavering supports, never losing faith in me and my work. To my dearest sister Sarita and brother Rabin, I could not find words to express how grateful I am to have you both in my life. You both

have been my blessings. And to my beloved, beautiful wife Tara for your unrelenting support and profound belief. It is not an exaggeration to say what all I have achieved here will not have been possible without you. I could not imagine life without you. To my dear son Shaswat, you have graced us with your charm. You have never failed to add laughter in and have reinforced purpose in my life. I dedicate this thesis to all of you.

Sabin Bhandari

Tromsø, May 2021

Summary

The endothelium is the innermost cell layer of blood vessels and has a key role in maintaining vascular homeostasis. Beside the general role to prevent blood coagulation and regulate blood flow, endothelial cells of different vascular beds show tissue specific specializations. This thesis focuses on a unique endothelial cell with immune-like properties, namely the liver sinusoidal endothelial cell (LSEC) that make up the perforated wall of the hepatic sinusoids. LSECs, together with liver-resident macrophages (Kupffer cells) constitute an efficient scavenger cell system for removal of microbial products, viruses, and waste macromolecules from blood. However, the spatial co-localization of LSECs and Kupffer cells in the sinusoids, species differences in cell marker expression, and variation in cell culture systems between laboratories have led to confusion around the LSEC phenotype. In addition, LSECs are challenging cells to study as they rapidly lose core functions *in vitro*. In this thesis a multi-omics approach was used to resolve some of the discrepancies in the literature about the LSEC phenotype.

In the first part of the study, mRNA sequencing and label-free proteomics were used to characterize and compare the transcriptomes and proteomes of rat LSECs and KCs at gene, protein, and functional levels. The findings support complementary and partly overlapping scavenging and immune functions of the two cells. Both cells expressed high levels of scavenger receptors and C-type lectins recapitulating their high endocytic activity *in vivo*. Some of these receptors were equally expressed, suggesting functional similitudes of LSECs and Kupffer cells, while several were cell-type specific. Many immune regulatory factors were also differentially expressed in LSECs and KCs, illustrating the complex cytokine milieu of the hepatic sinusoids.

In the second part of the study, tandem mass tag (TMT)-based quantitative proteomics was used to reveal culture-induced changes in rat and mouse LSECs and effects of pro- and anti-inflammatory stimuli on the cells. In both animal models, LSEC showed a rapid shift in metabolism, downregulation of endocytosis receptors, and gain of proinflammatory functions in primary culture. The use of the anti-inflammatory drug dexamethasone repressed LSEC activation, and improved cell survival *in vitro*, and the study presents a detailed overview of biological processes and pathways affected by dexamethasone in the cells.

Abbreviations

AFM	Atomic force microscopy
AGE	Advanced glycation end-product
CAM	Cell adhesion molecule
CPM	Count per million
DE	Differential expression
ECM	Extracellular matrix
ELISA	Enzyme-linked immunosorbent assay
emPAI	Exponentially modified protein abundance index
FACS	Fluorescence activated cell sorting
FDR	False-discovery rate
FITC	Fluorescein isothiocyanate
FPKM	Fragments per kilobase per million mapped reads
FSA	Formaldehyde-treated serum albumin
GSEA	Gene set enrichment analysis
HSC	Hepatic stellate cell
iBAQ	Intensity-based absolute quantification of label free proteomics
KC	Kupffer cell
LCM	Liver capsular macrophage
LDL	Low-density lipoproteins
LSEC	Liver sinusoidal endothelial cell
MACS	Magnetic activated cell sorting
MoMF	Bone marrow monocyte-derived macrophage
mRNAseq	mRNA sequencing
MS	Mass spectrometry
MsigDB	Molecular signature database
NO	Nitric oxide
NPC	Non-parenchymal cell
PRR	Pattern recognition receptor
RNAseq	RNA sequencing
RPKM	Reads per kilobase of transcript, per million mapped reads
scRNAseq	Single cell RNA sequencing
SEM	Scanning electron microscopy
SILAC	Stable isotope labelling with amino acids in cell culture
SIM	Structured illumination microscopy
SR	Scavenger receptor
TF	Transcription factor
TLR	Toll-like receptor
TMT	Tandem mass tag
TPM	Transcripts per million
XIC	Extracted ion chromatogram

List of papers

Paper I:

Sabin Bhandari, Ruomei Li, Jaione Simon-Santamaria, Peter McCourt, Steinar Daae Johansen, Bård Smedsrød, Inigo Martinez-Zubiaurre, and Karen Kristine Sørensen. "**Transcriptome and proteome profiling reveal complementary scavenger and immune features of rat liver sinusoidal endothelial cells and liver macrophages.**" *BMC molecular and cell biology*. 2020 Dec;21(1):1-25. PMID: 33246411; PMCID: PMC7694354; DOI: 10.1186/s12860-020-00331-9

Paper II:

Ruomei Li*, Sabin Bhandari*, Inigo Martinez, Jack-Ansgar Bruun, Ilona Urbarova, Bård Smedsrød, Jaione Simon-Santamaria, Karen Kristine Sørensen. " **Changes in the proteome and secretome of rat liver sinusoidal endothelial cells during early primary culture and effects of dexamethasone.**" *Manuscript*

*Equal contribution

Paper III:

Sabin Bhandari, Ingelin Kyrrestad, Jaione Simon-Santamaria, Ruomei Li, Bård Smedsrød, Karen Kristine Sørensen. "**Mouse liver sinusoidal endothelial cell responses to the glucocorticoid receptor agonist dexamethasone *in vitro*.**" *Manuscript*.

Table of Contents

Acknowledgements	ii
Summary	vi
Abbreviations	vii
List of papers	viii
List of Tables.....	xii
List of Figures.....	xii
1 Introduction.....	1
1.1 Micro-anatomy of the liver – The liver lobule	3
1.2 The hepatic sinusoid	7
1.3 Liver sinusoidal endothelial cells (LSECs)	8
1.3.1 LSEC fenestration and sieve functions.....	9
1.3.2 LSEC endocytosis and scavenger functions	10
1.3.3 LSEC immune functions	12
1.3.4 LSEC activation and dysfunction	13
1.3.5 LSEC-derived angiocrine factors	15
1.3.6 LSEC phenotypic and functional heterogeneity	16
1.3.7 The LSEC phenotype in liver disease.....	17
1.3.8 Concerns regarding <i>in vitro</i> studies of LSECs	19
1.4 Liver macrophages	20
1.4.1 Heterogeneity of liver macrophages.....	20
1.4.2 Scavenger and immune functions of KCs	21
1.4.3 KC molecular signature and markers	22
1.5 General introduction to expression profiling.....	25
1.6 Biological interpretation of expression data.....	26
1.6.1 Differential gene/protein expression (DE) analysis.....	27
1.6.2 Pathway enrichment analysis (gene set analysis)	27
2 Aim of the study	29

3	Methods and methodological considerations.....	31
3.1	Animal models and ethics statement.....	31
3.2	Cell isolation, purification, and cultivation.....	31
3.2.1	Tissue dissociation and differential centrifugation.....	31
3.2.2	Cell purification techniques used for LSECs and KCs.....	32
3.2.3	Cell purification method used in this thesis.....	33
3.3	Methods for LSEC and KC identification.....	36
3.3.1	Scanning electron microscopy (SEM).....	36
3.3.2	Immunofluorescence staining.....	36
3.3.3	Flow cytometry.....	36
3.4	mRNAseq.....	37
3.5	Proteomics.....	38
3.5.1	Label free proteomics.....	39
3.5.2	TMT-based quantitative proteomics.....	40
3.6	Statistical inference of the transcriptomics and proteomics data.....	41
3.7	Design considerations specific to the studies included in this thesis.....	41
3.8	Data validation.....	43
3.9	Genome annotation.....	43
3.10	Enumeration of statistical and bioinformatical tools.....	45
4	Summary of Papers.....	48
	Paper I: Transcriptome and proteome profiling reveal complementary scavenger and immune features of rat liver sinusoidal endothelial cells and liver macrophages.....	48
	Paper II: Changes in the proteome and secretome of rat liver sinusoidal endothelial cells during early primary culture and effects of dexamethasone.....	49
	Paper III: Mouse liver sinusoidal endothelial cell responses to the glucocorticoid receptor agonist dexamethasone <i>in vitro</i>	50
5	General discussion.....	52
5.1	Factors affecting comparative gene and protein expression profiling.....	52
5.2	Gene/protein markers of rat LSECs and KCs.....	54

5.3	Complementary scavenging and immune functions between LSECs and KCs	56
5.4	LSECs <i>in vitro</i> display an activated, pro-inflammatory phenotype.....	57
5.5	Dexamethasone attenuates LSEC activation	57
5.6	LSEC showed a shift in metabolism in culture	58
5.7	Dexamethasone improves LSEC survival in cultures	60
5.8	Effects of dexamethasone on LSEC morphology <i>in vitro</i>	60
5.9	Culture-induced changes in LSEC endocytosis and effects of dexamethasone	61
5.10	Changes in transcription factors and regulators in LSECs during culture.....	62
6	Concluding remarks.....	63
	Works cited.....	64

List of Tables

Table 1. Factors that may stimulate LSEC activation or dysfunction	14
Table 2: Popular markers used for discrimination between liver macrophage populations	24
Table 3. Suits of bioinformatical and statistical software used in the projects included in the thesis	45

List of Figures

Figure 1. The liver micro-anatomy	4
Figure 2. Transmission electron micrographs of rat liver.....	6
Figure 3. Different cell preparation methods used in the present thesis project.....	34

1 Introduction

The liver is the largest internal organ in the body and performs many essential functions connected to metabolism and homeostasis. The functions include production of bile, uptake, storage, and distribution of nutrients and vitamins from the bloodstream, maintenance of blood glucose levels, regulation of iron metabolism, degradation or conjugation of many xenobiotics and toxins, and modification of various hormones. The liver also produces many plasma proteins, including albumin, lipoproteins, coagulation factors, components of the complement system, and proteins involved in iron transport (1, 2). In addition, the liver has vital immune functions (3). Various resident liver cells coordinate to carry out these miscellaneous organ functions. In addition, an intricate liver architectural organization optimizes the cell-cell communication and coordination to match the liver functional demands. Unlike other solid organs, the liver displays a remarkable regenerative capacity, and the liver quickly restores its physiological size and weight following partial hepatectomy and various liver injuries (4).

The resting liver receives approximately 25% of cardiac output from its dual afferent blood supply. About 75-80% of the blood in the sinusoids is from the portal vein and 20-25% from the hepatic artery (5). The portal vein receives blood from the spleen, stomach, and pancreas (via the splenic vein) and the small intestine and colon (apart from the rectum via the mesenteric veins). This blood contains nutrients, toxins, hormones, microbial products, and break-down products of blood cells. The venous blood mixes with the arterial blood in the liver sinusoids (the liver capillary system) (5). The hepatocytes are large polyhedral cells constituting approximately 80% of the liver cell volume (6). The major cell populations of the sinusoids are the liver sinusoidal endothelial cells (LSECs), which make up the sinusoidal wall, the Kupffer cells (KCs), which are liver resident macrophages, and the hepatic stellate cells (HSCs), which are sinusoidal pericytes (7-9). Other liver cells include macrovascular and lymphatic endothelial cells, bile duct epithelial cells (cholangiocytes), connective tissue cells, and several populations of resident and mobile immune cells such as natural killer cells, natural killer T cells, and other lymphocytes (5, 10-13).

Despite an increasing research focus on liver cell biology, particularly in liver disease, our knowledge about the steady-state functions of the various liver cells still lacks sufficient resolution (14-16). The LSECs display some unique functional and morphological features compared to other endothelial cells, such as numerous open fenestrae (7, 8) and a high endocytic capacity towards modified plasma proteins and waste macromolecules from matrix turnover processes (17-19). Increasing evidence also points towards the role of LSECs in liver immunity (17, 18). Despite numerous reports on LSEC

receptor-mediated endocytosis and immune functions since the first publication about LSEC uptake of hyaluronan at the beginning of the 1980s (20), the role of LSECs as scavenger and immune cells is still largely overlooked in textbooks and scientific commentaries. This has caused confusion regarding the identity and functions of LSECs versus KCs. Furthermore, LSEC studies are comparatively sparse and frequently burdened by disparate laboratory practices regarding LSEC isolation, identification, purification, and culture conditions among research groups. Consequently, this makes it challenging to systematically compare results from published LSEC studies.

One major problem has been to find unambiguous LSEC specific molecular and functional markers to discriminate these cells from other sinusoidal cells, especially from the KCs (16, 21-23). Traditionally, endogenous peroxidase activity or latex bead phagocytosis have been used to distinguish KCs from LSECs, and factor VIII immune reactivity to discriminate LSECs from KCs (24). However, depending on the context and species, LSECs display positive endogenous peroxidase activity (25). Cell surface antigens like stabilin-2, Fc γ RIIb2, and LYVE-1, are widely used to distinguish LSECs from other hepatic cells (26). But so far, no markers have achieved consensual approval among different research groups. It is also necessary to pay attention to species differences in expression and avoid generalization about biological information from one species to another. Interspecies generalizations are common in the scientific literature, which also has contributed to creating confusion about the LSEC phenotype (14, 16). Thus, it is necessary to carry out a comprehensive characterization of the cells in different species.

The projects presented in this thesis have focused on molecular characterization of primary LSECs from healthy rats and mice, two commonly used animal species in biomedical research, and looked at changes occurring in the cells in early primary culture. Moreover, we utilized a comparative approach to contrast LSEC molecular signature to that of KCs (in the rat model, **paper I**) to resolve phenotypic and functional issues surrounding them. These two cell types constitute the liver scavenger cell system (17, 18), also known as the liver reticuloendothelial system (18, 27, 28), and show several overlapping functions related to blood waste clearance and immune functions.

Furthermore, the problem to maintain primary LSECs in prolonged (more than 1-2 days) culture, combined with the lack of cell lines that retain the LSEC *in vivo* functions (21), makes the use of animal models and primary cell preparations indispensable. In *in vitro* conditions, LSECs rapidly lose their characteristic morphology and specialized functions. However, the molecular mechanisms driving such changes are yet to be completely characterized. In the second and third papers (**papers II and III**), we have, therefore, characterized culture-induced changes to unravel the molecular basis

for these changes in LSECs (in both rats and mice). We have also looked at the LSEC response towards the widely used anti-inflammatory drug dexamethasone.

Our current knowledge and understanding of the LSECs have also been limited by the methods available to study the cells. Implementation of innovative and novel *modus operandi* is needed to enhance the scope and meaning of scientific interrogations. The rapid evolution in technology has made multi-omics approaches more accessible. Multi-omics implementation may foster a leap towards a more global-integrative understanding of liver cell biology. The projects included in this thesis have applied robust, highly reliable mRNA sequencing (mRNAseq), mass spectrometry (MS) based proteomics methods, and data-driven computational methods to predict and interpret the functions. In **paper I**, we have used ion torrent mRNAseq and label-free shotgun quantitative proteomics for comprehensive global characterization of rat LSECs and KCs. In **papers II and III**, we have used tandem mass tag (TMT)-based quantitative proteomics to characterize rat and mouse LSECs in different *in vitro* conditions.

1.1 Micro-anatomy of the liver – The liver lobule

The liver is an ensemble of repeating morpho-functional modules capable of performing the liver function *per se*, albeit on a small scale. There are three popular models to explain the organization of the liver architecture, namely the classic liver lobule, the portal lobule, and the liver acinus (5, 29, 30).

The classic liver lobule, often named the hepatic lobule, describes a basic structural unit, first defined by Kiernan in 1833 (31). The hepatic lobule contains cords of hepatocytes, mostly one cell thick, radiating around the central venule creating a prismatic polygonal geometry, often referred to as a polyhedron (illustrated in Figure 1A). The portal triads consisting of branches of the portal vein, hepatic artery, and bile duct, occupy the vertices of these polyhedrons (29) The portal canal with the triad also contains connective tissue and lymphatic vessels. In some species, such as pigs, the lobule structure can easily be identified by a thin peripheral border of connective tissue. These connective tissue septa are not so distinct in the rat, mouse, and human liver, and the lobule structure is therefore not as evident.

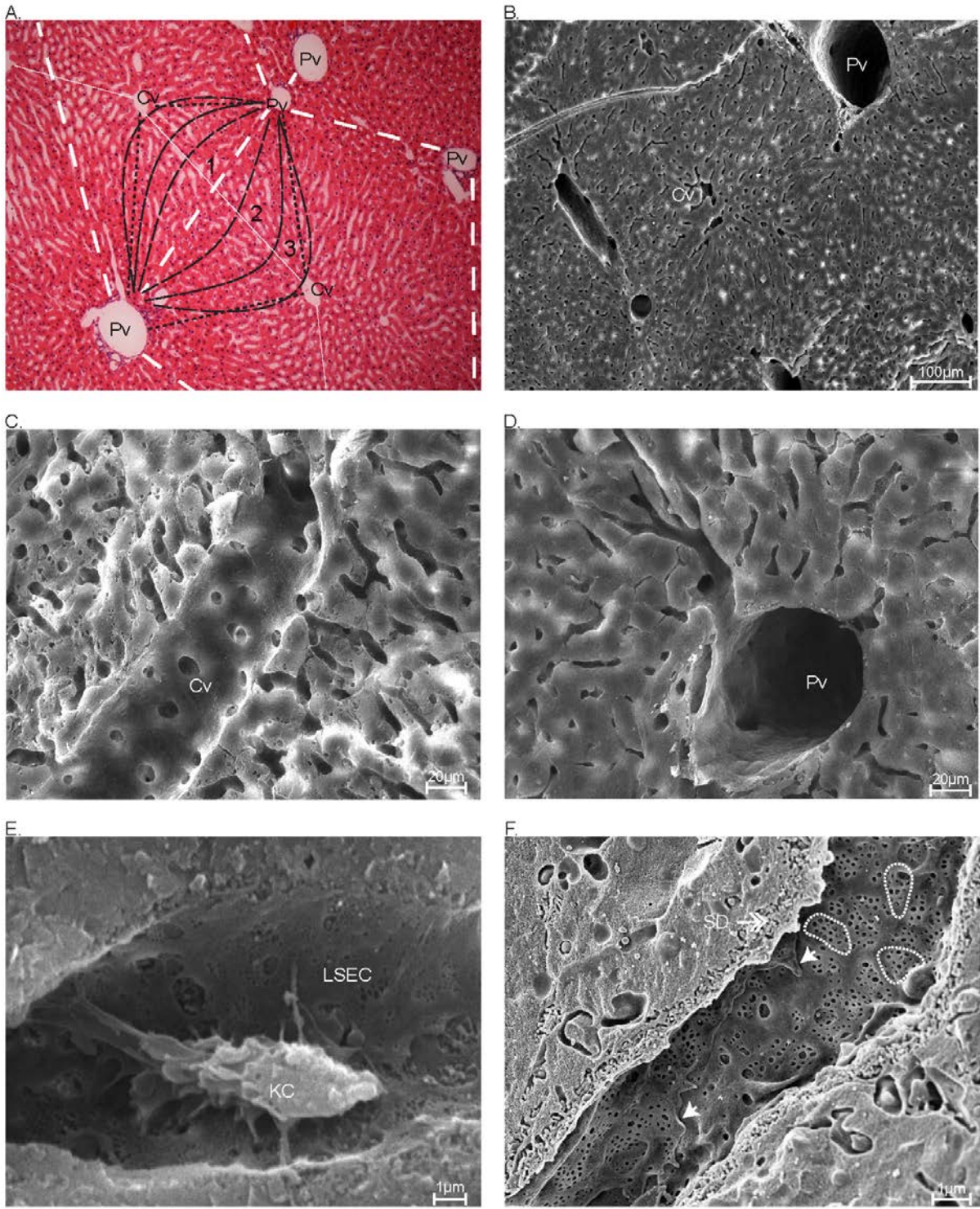


Figure 1. The liver micro-anatomy

A. Hematoxylin and eosin-stained section illustrating the normal histology of the rat liver. The classic hepatic lobule is illustrated with thick, white dashed lines joining several portal triads (Pv, portal veins) at the periphery, and with a central venule (Cv) at the centre of the lobule. Part of a portal unit is depicted with thin solid white lines connecting several central venules (Cv) at the periphery and a portal vein (Pv) in the middle. The liver acinus is depicted with black small, dotted lines joining two portal triads and two central venules (Cv), and the zones 1-3 are shown with black lines. B. Scanning electron micrograph (SEM) of mouse liver – overview image. C-D. SEM of mouse liver showing C) a central vein (Cv) with numerous openings of sinusoids that enter the vein, and D) a portal vein (Pv), and surrounding sinusoids.

E. SEM of a Kupffer cell (KC) with numerous cytoplasmic expansions (protrusions), resting on the luminal surface of a liver sinusoidal endothelial cell (LSEC). F. SEM of a mouse liver sinusoid showing the highly fenestrated endothelium, intercalated cell margins between two LSECs (arrow heads) and sieve plates. Three sieve plates are encircled by white dashed lines. The space of Disse (SD, arrows) with hepatocyte microvilli are visible underneath the sinusoidal wall. The images in A-F are reproduced with permission from Karen Kristine Sørensen, UiT The Arctic University of Norway.

Blood enters the sinusoids from the terminal branches of the portal vein and hepatic artery at the lobule periphery and runs along the cords of hepatocytes towards the central venule. The bile runs in the opposite direction through the bile canaliculi within the chords of hepatocytes and drains into the bile ducts located in the portal triad (32). This arrangement allows the hepatocytes to make multiple contacts with the sinusoids and bile duct networks simultaneously (Figure 2A) and greatly facilitates hepatocyte functions (32, 33).

The portal lobule model, or portal unit, was proposed by Mall in 1906 (34). It represents a structural module with the portal canal with the triad at the centre and the central venules at the peripheral angles of the lobule (Figure 1A) (29, 30). The portal unit provides a better description of the exocrine function of the liver compared to the other organizational modules of the liver (29, 30).

The liver acinus, proposed by Rappaport *et al.* in 1954 (35), describes the smallest functional unit of the liver rather than the strict anatomical organization of the liver parenchyma. The liver acinus has the septal branches of the portal triad (*i.e.*, the distributing blood vessels, indicated by thick dashed lines joining between two portal veins in Figure 1A) at the equator of the lobule and a central venule at each pole (1). The liver acinus, therefore, occupies parts of two adjacent classic lobules (30). The acinus subdivides into three zones representing their proximity to the terminal portal supply axis. Zone 1 is the closest to the distributing vessels and corresponds to the periphery of the classic liver lobule, zone 3 is close to the central venule, whereas zone 2 interposes between the two other zones (30) (Figure 1A). The division, however, is not strict. This model explains best the heterogeneous distribution of oxygen, metabolites, liver enzymes, and various other aspects of liver pathophysiological functions, such as the distribution of pathological changes after toxic insults along the sinusoidal axis (29, 36).

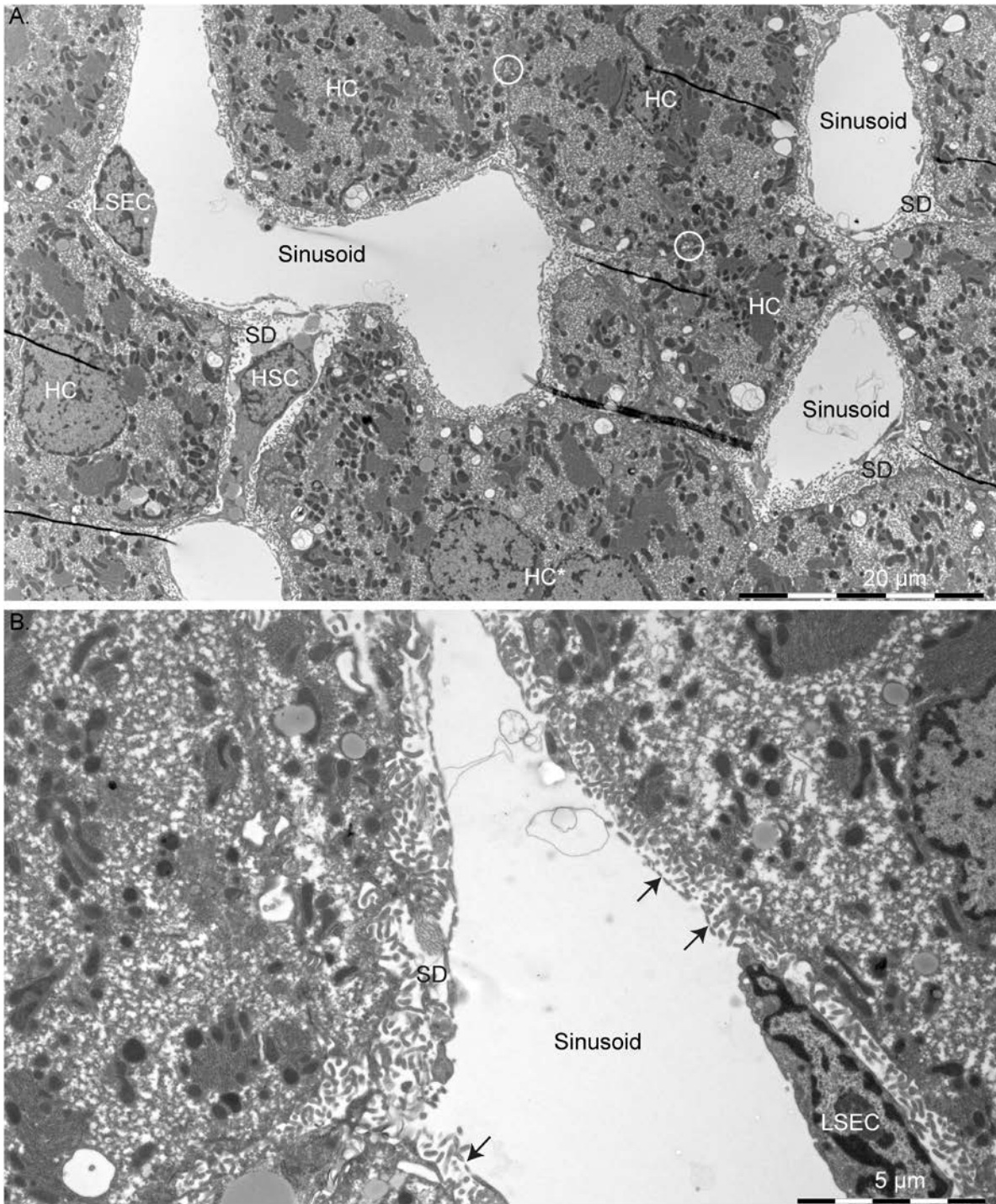


Figure 2. Transmission electron micrographs of rat liver

A. Transmission electron micrograph showing hepatocytes (HC) bordered by thin-walled sinusoids at the basolateral side. One binuclear hepatocyte is marked with HC*. Two biliary canaliculi are encircled with white solid circles, located between two adjacent hepatocytes at the apical side of the cells. One hepatic stellate cell (HSC) can be seen in the space of Disse (SD) stretched between two sinusoids. B. Higher magnification micrograph of a sinusoid, showing LSEC fenestrae (→). Hepatocyte microvilli can be seen in the space of Disse. The images are reproduced with permission from Karen Kristine Sørensen, UiT The Arctic University of Norway.

1.2 The hepatic sinusoid

The hepatic sinusoids represent the liver capillary system and are specialized vascular structures lined by highly fenestrated endothelial cells (Figure 1F). The liver macrophages or KCs are located in the sinusoids, resting on the endothelial cells (Figure 1E), or embedded in the endothelial lining where they also make contact with HSCs and hepatocytes (37, 38). The endothelium is encircled by HSCs (also named Ito cells, or Vitamin A-storing cells), which act as pericytes and are located in the space of Disse (Figure 2A) (5, 7, 8, 32).

At rest, the adult human liver receives around 1500-2000 ml blood per minute that streams into the sinusoidal network (10). The flow within the extensively ramified and highly porous sinusoidal networks results in a substantial drop in the intrahepatic blood pressure, maintaining the sinusoidal pressure gradient essentially lower than 1 mmHg (39-41). For example, within the hepatic lobule, the blood oxygen partial pressure drops from around 54-60 mmHg to 48-50 mmHg along this axis (42, 43). Low pressured blood flowing alongside the highly active and oxygen-demanding hepatocytes creates gradients of oxygen, metabolites, hormones, and other substances along the porto-central axis. This contributes to the generation of a heterogenous microenvironment which supports the functional segregation between hepatocytes in different zones within the liver acinus and affects various aspects of liver pathophysiology and responses (36, 44-50).

Furthermore, the sinusoidal network is highly tortuous and exhibits more anastomoses in the periportal region (zone 1) compared to the pericentral region (zone 3) where the sinusoids run more in parallel (Figure 1A-C) (5, 10, 51). Despite the high degree of tortuosity and anastomosity, the orientation of the sinusoids is not random. In fact, the sinusoids are aligned in the direction of the blood flow, displaying a weak nematic order (32, 52). In addition, the internal diameter of the sinusoids varies among species and studies. Multiple studies have reported a sinusoidal diameter in the range of 5-10 μm (26, 51-54).

At steady-state, the hepatic sinusoid establishes a unique physiological microenvironment conducive to the differentiated functions of the liver cells and consequently the liver. The sinusoidal organization permits intercellular communications between the different liver cells via direct cell-cell contact and/or the release of paracrine factors. Cell-matrix contacts are also important for establishing the sinusoidal niche (55).

1.3 Liver sinusoidal endothelial cells (LSECs)

Endothelial cells are flat cells lining the inner surface of blood and lymphatic vessels. However, endothelial cells from different vascular beds demonstrate a remarkable tissue-specific gene expression, morphology, and functions (56-58). In general, the microvascular bed adopts morphology and function in such a way to optimally support the underlying tissue. For instance, the vascular beds of the central nervous system have a continuous type of endothelium supported by a well-organized continuous basal lamina at the abluminal side and a layer of anionic glycocalyx on the luminal side. Thus, rendering the endothelium refractory to exchange between blood and nerve tissue, contributing to the highly selective blood-brain barrier and shielding the neurons from potentially noxious substances or cells (57). By contrast, the endothelium of the bone marrow sinusoids is discontinuous with minimal adherence junctions and few tight junctions between the adjacent endothelial cells, and an incomplete supporting basal lamina which makes the endothelium highly permeable, which is vital for the proper function of the underlying hematopoietic stem cells and traffic of cells through the endothelial wall (59). The specific needs of the underlying tissue and the variation in the tissue niches may be the main driving force for the tissue-specific specialization of the vascular lining (56). Our knowledge about different endothelial cells from various vascular beds is still insufficient, not least the gene expression, transcriptome, and proteome resources are scant, despite ardent discussion on tissue-specific endothelial specialization and the disparity they exhibit in response to various stimuli. Such multi-omics data are necessary to delineate and better understand the underlying molecular mechanisms governing endothelial cell specialization (60).

The liver sinusoidal endothelium is also unique and displays specialized functions. Despite abundant expression of proteins associated with adherens junctions, rat LSECs were reported to lack specialized tight junction molecules such as claudin-5 and occludins typical of other microvasculatures (61). Furthermore, LSECs display some overlap between the adjacent LSECs (Figure 1F). LSECs are highly fenestrated cells with a poorly organized basal lamina making the sinusoidal wall permeable to many substances (7, 62, 63). The specialized functions performed by the LSECs include: 1) ultrafiltration of plasma (“sieve functions”) through the fenestrae, 2) blood clearance of waste macromolecules and nanoparticles via mostly clathrin-mediated endocytosis (“scavenger functions”), and 3) participation in the induction of liver immune tolerance through modulation of naïve T-cells (“immune functions”) (3, 22, 26, 64).

1.3.1 LSEC fenestration and sieve functions

The most distinctive morphological feature of LSECs is the numerous transcellular pores or fenestrae generally organized in sieve plates, making the cells highly permeable (65). A fenestrated liver endothelium is found in fish, birds, and mammals (17), so fenestration seems to be a general trait of LSECs across vertebrate classes. The presence of open fenestrae is the morphological hallmark or gold standard to differentiate LSECs from other endothelial cells and liver non-parenchymal cells (NPCs) *in vivo*, *in situ*, and *in vitro* (16).

The LSEC fenestrae contains a diaphragm during foetal development, whereas after birth, the diaphragm is lost (7, 8, 66). Fenestrae covers around 2-20% of the LSEC surface area, as measured in perfusion fixed liver samples analysed by scanning electron microscopy (SEM) (9, 67, 68). Fenestration characteristics, such as the number and size of fenestrae, vary along the sinusoids and between species (7, 8, 69-72). Interestingly, Fraser and co-workers reported a link between species-specific differences in LSEC fenestration characteristics and the species vulnerability toward developing atherosclerosis, hyperlipoproteinaemia, and hypercholesterolemia (69, 70, 73, 74). Furthermore, LSEC porosity (percentage of surface area occupied by fenestrae) also depends on the animal age and is reported to be decreased in old age (75-77) and several pathophysiological conditions of the liver (9, 63, 77-82).

Then again, the measurements related to fenestrae characteristics depend on various experimental factors, such as methods used for specimen preparation, instrumentation and image analysis, and statistical methods used in the interpretation of the study (63, 83, 84). Despite discrepancies among studies, the most commonly reported average values for fenestrae diameter usually fall between 100-200 nm (ranging from 50-300 nm) (65, 84). Most fenestrae are therefore smaller than the resolution limit of conventional light microscopes. Therefore, to visualize the structures in detail, electron microscopy (EM) or the recently available super-resolution microscopy technologies including structured illumination microscopy (SIM), atomic force microscopy (AFM), or direct stochastic optical reconstruction microscopy (dSTORM) must be used. Of note, AFM and SIM also allow live-cell imaging. Recent studies employing these later live-cell imaging techniques have revealed LSEC fenestrae as highly dynamic structures, which form, stay open, move around, and coalesce to form a large gap or disappear within minutes to hours (63, 65, 84).

The unimpeded bidirectional exchange of plasma proteins, albumin-bound substances, lipoproteins, and chylomicron remnants over the highly porous sinusoidal endothelium is vital for effective hepatic uptake and metabolism but is in part limited by the size of the fenestrae (76). Additionally, the

biophysical and biochemical nature of the substances crossing the endothelial barrier, exemplified by the molecular weight, charge, and solubility, present constraints to the exchange of molecules between the sinusoidal lumen and the space of Disse (9). Two hypotheses have been put forward to explain how the hepatic sinusoids circumvent the exchange barrier based on sinusoidal hemodynamic characteristics. These are named 1) “Forced sieving” (67), sometimes referred to as “transendothelial massage” and 2) “The counter current hypothesis ” (85). In 1985, Wisse and colleagues proposed the model of forced sieving where white blood cells, while moving quickly or squeezing through the narrow sinusoids, disrupt and restrict the randomness of solutes or particle movements and enhance the chance of escape (*i.e.*, forced sieving) of solutes and particles through the fenestrae towards the space of Disse (67). Popescu and co-workers, in 2000, proposed a second hypothesis, suggesting that differences in hemodynamic forces generated while the blood flows from the narrow periportal sinusoids towards the relatively wide pericentral sinusoids pulls plasma into the space of Disse in the pericentral sinusoids and pushes the plasma out from the periportal sinusoids reinvigorating fluid exchange and renewal (85). The collapse of the space of Disse caused by altered blood flow following stasis of the pulmonary trunk in a rat model is consistent with the counter current hypothesis (86).

1.3.2 LSEC endocytosis and scavenger functions

The second distinctive feature of the LSECs is their very high endocytic capacity (17, 19, 22, 26, 87). The ultrastructural observations from Eddie Wisse published in 1970 and 1972, is an early testament to the very efficient endocytic ability of the LSECs (7, 8). Wisse reported numerous pits in the LSEC plasma membrane and vesicles in the cytoplasm of the cells. The vesicles comprised both “bristle-coated macropinocytic vesicles”, with a diameter of $\sim 0.18 \mu\text{m}$ (corresponding to clathrin-coated vesicles, first described in 1976 (88)), and “smooth macropinocytic vesicles” with a diameter of $\sim 0.7 \mu\text{m}$ (7).

The first reports on the selective and rapid uptake of extracellular matrix (ECM) macromolecules in LSECs came at the beginning of the 1980s when it was found that the connective tissue polysaccharide hyaluronan injected intravenously into rat was taken up and metabolized almost exclusively in the LSECs (20). In the subsequent years, many ECM waste macromolecules, lysosomal enzymes, and toxins were found to be actively endocytosed by LSECs (19). It is noteworthy that over the last four decades, the role and importance of the LSEC as an indefatigable scavenger cell and indispensable member of the body scavenger cell system (17, 18), also termed “the reticuloendothelial system” (18, 27), has been firmly established (17, 27, 89-110). Historically, liver scavenger or clearance functions were attributed solely to the liver resident macrophages, the KCs

(19). Not least, we now know that LSECs are actively involved in the clearance and disposal of a wide range of tissue turnover waste products, modified plasma proteins, and lipoproteins, biopharmaceuticals, nanoparticles, and several blood-borne viruses (17, 27, 89-110).

LSECs are essentially non-phagocytic cells, specialized in clathrin-mediated endocytosis (reviewed in (17, 19, 111, 112)). The cells express a diverse repertoire of endocytosis receptors (16, 17, 26, 87, 113). The LSEC scavenger function has been attributed mainly to four highly expressed receptors: the two members of scavenger receptor (SR) class H, stabilin-1 (SR-H1; STAB1) and stabilin-2 (SR-H2; STAB2), the mannose receptor (MRC1; CD206), and the isoform IIB2 of the low-affinity immunoglobulin gamma Fc region receptor II (FcγRIIb2; CD32b) (17).

Stabilin-1 and stabilin-2 are expressed in sinusoidal endothelial cells from various organs, including liver, spleen, adrenal cortex, bone marrow, and pancreas, with stabilin-1 also expressed by alternatively activated macrophages (114-119). The two stabilin proteins are homologous receptors and display highly similar ligand binding properties (114). Both receptors bind to oxidized low-density lipoproteins (LDL) (100), acetylated LDL (120), formaldehyde-treated serum albumin (FSA) (100), advanced glycation end-product albumin (AGE-albumin) (120-122), and phosphorothioate-modified antisense oligonucleotides (123). Stabilin-1 and stabilin-2 also show some non-overlapping functions; the ECM protein SPARC is exclusively bound by stabilin-1 (124), whereas hyaluronan is recognized by stabilin-2 but not stabilin-1 (125-127).

The mannose receptor (CD206) in LSECs mediates removal of blood-borne ECM waste, including C-terminal procollagen propeptides and collagen alpha-chains (94, 98), lysosomal enzymes (99), tissue plasminogen activator (93), amylase (110), and yeast invertase (93). Ovalbumin, a ligand frequently used in studies of immunological functions of LSECs, is also endocytosed via the mannose receptor (128). The mannose receptor is also a pattern recognition receptor (PRR) that binds and removes microbial glycans, playing a crucial role in innate immunity (129).

The FcγRIIb2 is a low-affinity FcγR (130), expressed primarily on dendritic cells and LSECs (131). The receptor inhibits other activating FcγRs via its conserved cytoplasmic domain (ITIM motif) or crosslinking along with those receptors (130). The receptor also binds to and mediates endocytosis of small, soluble IgG immune complexes (132, 133). LSECs are the predominant cell type expressing the FcγRIIb2 in the liver (132, 133) and are actively involved in the blood clearance of intravenously injected small, soluble IgG complexes (134, 135).

The LSECs exhibit an unparalleled rate of endocytosis, unequivocally complemented by their efficient endolysosomal catabolic capacity. In addition, the specific activity of several lysosomal enzymes in LSECs is relatively high compared with other liver cells, facilitating the degradation of endocytosed ligands (99, 136-138). In addition to constitutive expression of lysosomal enzymes such as cysteine proteinases, aspartic proteinases, lipases, acid phosphatases, DNases, and aminoglycosylases (137, 139, 140), LSECs may also supplement their inventory by mannose receptor-mediated uptake of extracellular lysosomal enzymes (99, 136-138). Accordingly, evidence from a study in mannose receptor knockout mice indicated that the high catabolic capacity of the LSECs might in part be dependent on the mannose receptor-mediated recruitment of lysosomal enzymes from the cell exterior (99).

1.3.3 LSEC immune functions

LSECs are exposed continuously to portal blood laden with immunogens, endotoxins, viruses, microbial components, and other exogenous molecules originating from the gut. If not removed rapidly from the blood circulation, such substances may accumulate and cause inadvertent immune activation in various tissues, ultimately disrupting normal organ/tissue functioning. The cells have a diverse repertoire of PRRs, including several SRs and toll-like receptors (TLRs) (141-143). SRs and TLRs not just bind and silently remove immunogens from circulation but can initiate intracellular signalling cascades to promote an inflammatory response. For instance, in mouse LSECs, LPS binds to TLR4 via CD14 and stimulates the translocation of nuclear factor kappa-B (NF- κ B) into the nucleus inducing expression of the pro-inflammatory cytokine interleukin-6 (IL-6) and tumour necrosis factor α (TNF α) (141). In response to immunogenic stimulation, LSECs respond by upregulating the expression of cytokines, chemokines, SRs, and cell adhesion molecules (CAMs), enhancing leukocyte recruitment, and modulating the immune milieu of the liver (64, 141, 144-153).

Moreover, multiple studies in mice *in vivo* and *in vitro* suggest the role of LSECs in eliciting immune responses and sustaining the immune homeostasis in the liver (reviewed in (3, 64, 154).

Under normal physiological conditions, LSECs have been shown to prime T cells (CD8⁺ and CD4⁺) to induce a tolerogenic differentiation via MHC-I mediated antigen presentation, leading to enhanced immune tolerance in the liver (155-162). However, under inflammatory or pathological conditions, or in the presence of higher antigen density, LSECs can upregulate MHC-II and co-stimulatory molecules and activate immunogenic T cell effector responses (131, 163-166). Of note, the LSEC fenestrae may passively modulate the hepatic immune surveillance, as the fenestrae provide a window

for other immune cells to contact the hepatocytes and continuously survey the perisinusoidal space of Disse (66, 69, 167).

Furthermore, LSECs serve as a cell system for the clearance of virus particles from the circulation (17, 168). In mice, LSECs rapidly cleared adenoviruses (168), BK- and JC polyomavirus-like particles (101), and HIV-like particles (169) after intravenous injection. LSECs also respond to hepatitis C virus infection by eliciting antiviral responses (170).

1.3.4 LSEC activation and dysfunction

Upon inflammatory stimuli or during various liver pathologies, LSECs respond by upregulating the expression of CAMs like CD31, VCAM-1, and ICAM-1 and increasing the production of pro-inflammatory cytokines, including IL-6, TNF α , and TGF β (64, 171-173). These changes correlates to core changes described in endothelial activation (174-176). The upregulation of CAMs, chemokines, and cytokines in LSECs facilitates adhesion and extravasation of leukocytes (152, 177). At the same time, LSECs during inflammation fail to keep up the supply of nitric oxide (NO) through endothelial NO synthase (eNOS), needed for normal vasodilation, and instead increase the expression of thromboxane A2 and endothelin 1, which favors vessel constriction (15, 178). Such alterations represent LSEC dysfunction (178). Dysfunctional LSECs fails to maintain the sinusoidal vascular tone, HSC quiescence, control of blood coagulation, and vascular integrity (177, 178). The increase in intrahepatic resistance induces local and systemic changes in the hemodynamic, which impairs the mechano-sensing and responses that further exacerbate the LSEC dysfunction (178). Table 1 lists some of the factors that may lead to LSEC dysfunction.

Table 1. Factors that may stimulate LSEC activation or dysfunction

Factor	Proposed mechanism	References
Oxidative stress	An elevated level of reactive oxygen species (ROS) hampers NO production by eNOS which limits NO availability by transforming NO into peroxynitrite (ONOO [•]) in a reaction with superoxide (O ₂ [•]). ROS can induce eNOS uncoupling, switching eNOS to produce O ₂ [•] instead of NO. Furthermore, ROS can enhance interactions between caveolin-1 and eNOS which significantly ablates the eNOS dependent NO production.	(178, 179)
Pathological angiogenesis	Angiopoietin-2/Tie2, VEGF, and adipokines induce angiogenesis during chronic liver disease which may result in LSEC capillarization and dysfunction.	(180, 181)
Mechanical stimulus	LSECs acutely respond to mechanical cues via modulating the expression of Krüppel-like factor 2 (KLF2). KLF2 expression enhances NO production, preventing eNOS uncoupling and stimulates the expression of several vasoactive proteins such as thrombomodulin.	(182, 183)
Endothelial to mesenchymal transition (EndMT)	This process refers to trans-differentiation of endothelial cells into myofibroblast-like cells through downregulation of endothelial-specific genes including eNOS vis-a-vis the enhancement of expression of fibrillar collagens, α -smooth muscle actin, N-cadherin, and vimentin. An expression program indicative of EndMT has been described in LSECs derived from cirrhotic livers, and genetic lineage tracing illustrated a very small subpopulation of Tie2-lineage cells undergoing EndMT.	(184-186)
Autophagy	Autophagy is a process used by cells to eliminate or rejuvenate cell organelles and might be critical for the ability to adapt to stressful situations during acute/chronic injury. Elevated autophagy is reported in rats with liver injury induced by CCL ₄ . Diminished autophagy augments endothelial inflammation, EndMT, and endothelial cell apoptosis in the murine cell line, TSECs. Diminished autophagy was also reported in mice with non-alcoholic fatty liver disease (NAFLD). Deregulation of autophagic mechanisms may accentuate inflammation and ultimately lead to endothelial dysfunction.	(187-189)

1.3.5 LSEC-derived angiocrine factors

LSECs express diverse angiocrine factors (190). Angiocrine factors comprise divergent endothelium-derived instructive macromolecules, including secreted and membrane-bound trophic factors, morphogens, cytokines, chemokines, and components associated with ECM and exosomes, typically eliciting trophogenic and pro-regenerative responses mediating self-renewal, differentiation, repair, and regeneration in adult tissue (191). These factors are not only means for physiological communication among neighbouring cells but are also vital in maintaining hepatic metabolism and sustaining liver homeostasis (191). For example, LSEC-derived BMP2 and BMP6 communicate with and induce hepatocytes to release hepcidin, a critical regulator of systemic iron homeostasis (192-194). Thus, the physiological expression of angiocrine factors determines the vascular niche and maintains niche functions.

During liver development, angiocrine factors such as NOTCH and WNT determine the gut endoderm specification and stimulate differentiation of the biliary tree (195-197) and affect the LSEC phenotype (195, 198). For instance, a study using tamoxifen-induced endothelial-specific activation of NOTCH1 in C57BL/6J mice suggested the activation not just affects other angiocrine factors such as WNT2A, WNT9B, and hepatocyte growth factor (HGF) but also promote capillarization in LSEC (195). Similarly, under homeostatic conditions in the adult liver, WNT2 induces hepatocyte proliferation and maintains the self-renewing pericentral population of AXIN⁺ TBX3⁺ hepatocytes (199). Even though endothelial cells in the central vein are the predominant source of WNT2 in the liver, LSEC specific ablation of *Wnt2* or the mediator of WNT secretion *Wls* impair hepatic zonation (46, 200) and disrupt hepatic tissue organization (32), suggesting that LSECs derived WNTs are unequivocally essential for the healthy liver organization and functions.

Moreover, following acute or chronic hepatic injuries and in response to partial hepatectomy, LSECs upregulate angiocrine factors such as WNT2, RSP03, and HGF that initiate hepatocyte proliferation and induce regeneration of liver tissue (46, 190, 200). Of note, in addition to WNT2 and HGF, other angiocrine factors such as TGF- β and Angiopoietin-2 (ANG2) are also essential to coordinate liver regeneration after partial hepatectomy (201). It has been shown that the expression of ANG2 during the regeneration determines the hepatocytes or LSECs proliferation. In mice, downregulation of ANG2 subsequently decreases TGF- β production, favouring the hepatocyte proliferation, while the upregulation of ANG2 during angiogenic phase induces angiogenic endothelial proliferation (201). Elevated hepatocyte proliferation in ANG2 deficient mice in response to CCL4-induced chronic liver injury supports the ANG2 mediated negative regulation of hepatocyte proliferation (201). Another

study using inducible VE-cadherin-dependent *Cxcr7* and *Cxcr4* gene knock-out mice models demonstrated differential expression and function of angiocrine factors in response to liver regeneration triggered by acute liver injury (202). Acute liver injury due to a single injection of CCL₄ augmented the LSEC expression of stromal-derived factor 1 (SDF-1; CXCL12) and the chemokine receptors CXCR7 and CXCR4 (202). CXCR7 is an inducible LSEC specific receptor for SDF-1. SDF-1 activated CXCR7 interacted with CXCR4 to enhance DNA-binding protein inhibitor ID-1 expression, a major transcriptional regulator of angiocrine factors. SDF-1 stimulation induced a pro-regenerative angiocrine response in LSECs from wild-type mice, whereas mice that lacked the expression of CXCR7 or CXCR4 failed to upregulate ID-1 in response to liver injury (measured in LSECs *in vitro*). Furthermore, the authors also reported that SDF-1-mediated CXCR7 activation in human LSEC cultures enhanced the expression of anti-fibrotic genes such as follistatin-like 1 (FSTL1) and apelin (APLN) (202).

1.3.6 LSEC phenotypic and functional heterogeneity

The metabolic segregation of hepatocytes, traditionally called liver zonation has been extensively examined (46, 47). The term zonation is no longer limited to metabolism but has extended to spatial differences in gene and protein expression along the sinusoidal axis. Recently, studies from Shalev Itzkovitz' lab have implemented state-of-the-art techniques, including single-molecule fluorescence *in situ* hybridization, single cell RNA sequencing (scRNAseq), and bulk proteomics and mRNA sequencing of spatially sorted hepatocytes based on the pericentral expression of CD73 and periportal expression of E-cadherin in hepatocytes to confirm and extend the hepatocyte phenotypic heterogeneity (45, 203).

Like hepatocytes, it is increasingly evident that LSECs also constitute a heterogeneous cell population. Differential responses of LSECs from different spatiotemporal localizations along the sinusoids against various stimuli were reported already in the 1990s (204-206). Even earlier, in 1983, Wisse and colleagues reported differences regarding morphometric features (fenestrae size and number) of LSECs along the porto-central axis. They observed that the porosity of the sinusoidal endothelium, *i.e.*, percentage of surface area occupied by fenestrae, was noted to increase from the portal towards the central vein (9).

Interestingly, a study in rats also reported the differential expression of the pan-leukocyte marker CD45 in rat LSECs. LSECs from zone 1 displayed higher expression of CD45 compared with LSECs from zone 2, whereas CD45 expression was absent in zone 3 (207). Nevertheless, the expression of

CD45 in LSECs is debated in the literature and is reported to be absent in mouse and human LSECs (16, 21).

In 2017, Strauss and co-workers added to evidence supporting the heterogeneity of LSECs by demonstrating a differential immunoreactivity pattern for purported LSECs markers including LYVE-1, CD36, CD14, CD54, and CD32 along the porto-central sinusoidal axis on tissue sections from normal human liver (208). Moreover, evidence suggests that LSECs in the adult liver might have a mixed ontogeny. Using lineage tracing in a mouse model, Plein and co-workers estimated that approximately 60% of LSECs in the adult liver originate from yolk-sac erythromyeloid progenitor cells and the rest from mesoderm-derived hemangioblasts (209).

In 2018, Halpern and co-workers used a paired scRNAseq workflow and smFISH to identify and reconstruct mouse LSEC heterogeneity with reference to the mouse hepatocyte gene expression pattern as a reference for spatiotemporal zonation (210). Recent scRNAseq studies have also supported a remarkable heterogeneity and complexity within the LSEC population (11-13). However, unlike hepatocytes, information on the heterogeneity of LSECs still has a limited spatial resolution. The reported phenotypic differences are usually limited to periportal (zone1), transitional/midzonal (zone2), and perivenous zones (zone3) (11-13, 210-212). Although scRNAseq studies agree on LSEC heterogeneity, the discrepant numbers (varying from 2 to 8) of LSEC subpopulations (clusters) reported have raised concerns over the method of cluster identification and markers chosen to annotate the cluster (213). Above all, none of these scRNAseq studies looked closely into the morphological (*e.g.*, the appearance of cell fenestration) or functional details of the cells annotated as LSECs. Nor have they provided the complete overview of LSEC heterogeneity under normal physiological conditions and in liver disease.

1.3.7 The LSEC phenotype in liver disease

LSEC may lose their specialized functions and phenotype during sustained hepatic injuries, chronic liver disease, and liver regeneration (21, 22, 63). LSECs that have lost their specialized features may no longer exert hepatoprotective functions exacerbating inflammation and ultimately leading to fibrosis (121, 214, 215). The sinusoidal endothelium in the liver of patients with alcoholic liver disease, non-alcoholic steatohepatitis (NASH), liver fibrosis, and cirrhosis is reported to look more like continuous capillaries of other vascular beds (181, 216, 217). This “capillarization” of LSECs refers to the phenomenon where LSECs display significantly diminished cell porosity while increasing tight junctions and concomitant accumulation of ECM to create a continuous basal lamina underneath the cells (218, 219). Diminished porosity and a thickened sinusoidal wall may lead to a

detrimental reduction in the bi-directional exchange of substances across the sinusoidal interface (76, 220). A mild form of LSEC capillarization, named pseudocapillarization, is reported in old livers of rodents, humans, and other primates (80-82). Sinusoidal capillarization consequently orchestrates more severe changes like an increase in intrahepatic vascular resistance, enhanced hepatocyte atrophy, and stimulation of fibrogenesis, which may ultimately lead to liver failure (221).

LSEC-derived angiocrine signals, especially Notch ligand Delta-like 4 (DLL4) and BMP9 are reported to regulate LSEC fenestrae and progression of fibrosis (222, 223). LSEC-specific upregulation of DLL4 was reported in fibrotic livers of both humans and mice (222). A recent scRNAseq study showed upregulation of DLL4, JAG1, and JAG2 in a subpopulation of endothelial cells isolated from fibrotic livers, compared to non-fibrotic livers, supporting the involvement of DLL4 during capillarization (12). However, this endothelial cell subpopulation was different from CD34⁻CLEC4M⁺ cells, defined as LSECs in that study (12). The authors suggested that interaction between the DLL4 ligand expressed on liver endothelial cells and NOTCH3 expressed in scar-associated HSCs can activate the HSCs and stimulate fibrillar collagen production by these cells.

A hallmark function of LSECs is their high endocytic activity. However, the expression level of LSEC endocytosis receptors in liver disease is only reported in a few studies. Immune labeling of tissue microarrays of human hepatocellular carcinoma (HCC) biopsies and tissue sections from an HCC mouse model (C57BL/6 AST mice) showed that most of the tumor-associated and peritumorous microvasculature displayed loss of expression of the LSEC markers stabilin-1, stabilin-2, LYVE-1, and FcγRIIb2, and increased expression of the pan endothelial marker CD31 (224). Ishikawa and co-workers found significant downregulation in immunoreactivity to FcγRIIb in human biopsies from patients with non-alcoholic steatohepatitis (NASH) (225). Moreover, only a few studies have looked into the alteration in LSEC endocytic function implementing quantitative ligand uptake experiments *in vivo* or *in vitro*. Intriguingly, Connolly and co-workers showed enhanced *in vitro* uptake of several mannose receptor ligands (dextran, albumin, and mannose-albumin) in LSECs isolated from fibrotic livers, compared to normal LSECs (171). Tamaki and co-workers reported an increase in serum hyaluronan concentration in a thioacetamide-induced liver cirrhosis model in rats. LSECs derived from these cirrhotic rats displayed a significant decrease in binding and uptake of hyaluronan *in vitro*, supporting the notion that diminished LSEC-mediated clearance of hyaluronan was the chief cause for the elevated serum level of this ECM glucosaminoglycan (226).

1.3.8 Concerns regarding *in vitro* studies of LSECs

The sinusoidal microenvironment is critical for maintaining phenotype and function of liver cells, including LSECs (227, 228). LSECs in primary culture display rapid loss of cell fenestration and decline in endocytosis (43). LSECs maintained *in vitro* also display diminished expression of LSEC markers, including stabilin-2, LYVE-1, Fc γ RIIb2, and mannose receptor (CD206), and rather upregulates the expression of continuous endothelial markers such as CD31 and CD14 (43, 228, 229). Then again, the comprehensive overview regarding gene and protein expression changes induced *in vitro* is still elusive. Moreover, recent *in vitro* studies attempting to induce deterministic differentiation of embryonic stem cells (230), induced pluripotent stem cells (231, 232), or other endothelial cells (233) towards an LSEC phenotype further underline the significance of the complex yet imperative physiological niche for the housekeeping of LSEC differentiated features. Cultured LSECs, however, is devoid of the stimuli provided by the physiological liver tissue architecture, heterotypic cell-cell contacts, local paracrine signals typical to the sinusoids, and not least, the shear stress from the laminar sinusoidal blood flow, which may be the reason for the phenotypic alterations. For example, a simple addition of vascular endothelial growth factor (VEGF) in culture supplements is reported to maintain well-fenestrated features of rat LSECs *in vitro* for up to 2 days (234, 235). In addition, the LSECs cultured in a 5% oxygen atmosphere, which is closer to the physiological oxygen tension in the sinusoids, could substantially improve survival and better preserve endocytosis compared with LSECs incubated in the commonly used 21% oxygen atmosphere (43). Species differences may also be an issue. The record for keeping primary LSEC in culture is probably in the pig model, where primary LSECs showed well-preserved endocytosis functions for up to 21 days, with special serum-free supplements (236). Unfortunately, these supplements are no longer available. Similarly, physicochemical characteristics of the ECM substrate used influence on LSEC features *in vitro* (229, 237, 238). Not least, the cultivation of LSECs with other cell types or under flow in microfluidic bioreactors also had a positive effect on the maintenance of LSEC features compared to conventional static culture condition (235, 239-241).

LSEC cell lines are increasingly used in place of primary LSECs for ease and convenience during fabrications of a bioreactor and liver-on a chip (21, 55, 242). Although such cell lines might be an alternative in some types of experiments, the applicability is limited. Most available cell lines of LSEC origin could not recapitulate the well-fenestrated morphology and high scavenger activity reflective of LSECs (21). It is, therefore, necessary to compare the molecular phenotype and functions of the cell line with freshly isolated primary LSECs, if cell lines are to be used.

In conclusion, although various approaches have been used to improve LSEC survival, functions, and features in prolonged cultures, the success is still limited, which sets limitations to the type of experiments feasible in these cells *in vitro*. At present, even with highly sophisticated and advanced biofabrication techniques, we are still falling short to maintain LSECs with *in vivo* like phenotype for a prolonged period *in vitro* (243). The recommendation is still to use short-term primary cultures for studying LSEC features. It is further necessary to be vigilant of phenotypic and functional changes in LSECs *in vitro* to avoid misinterpretation of the experimental outcomes.

1.4 Liver macrophages

1.4.1 Heterogeneity of liver macrophages

Macrophages are tissue-resident immune sentinels mainly derived from the terminal differentiation of monocytes (244, 245). Like endothelial cells, macrophages constitute a highly heterogeneous cell population demonstrating remarkable tissue specificity. The observed heterogeneity of macrophages can partly be attributed to the distinct origin or ontogeny of the cells (245, 246). The complex population of macrophages in many tissues stem from successive waves of hematopoiesis: primitive hematopoiesis (extraembryonic, yolk sac derived), pro-definitive hematopoiesis (embryonic derived), and definitive hematopoiesis (from circulating monocytes) (246). At the same time, macrophages exhibit diverse cellular states in response to various environmental and molecular cues usually referred to as cellular plasticity (247). The phenotypic heterogeneity and cellular plasticity of macrophages and their high phagocytic activity privilege these cells to exhibit a wide range of physiological functions. Functions include cleansing of harmful immunogens and dead/dying cells, local and systemic immune surveillance, and orchestration of immune reactions (248).

Liver-associated macrophages can be categorized into three major populations namely resident liver macrophages (KCs), liver capsular macrophages (LCMs), and bone marrow monocyte-derived macrophages (MoMFs) (249).

KCs represent the largest population of tissue-resident macrophages in healthy livers and constitute around 30% of non-parenchymal liver cells, as measured in young adult rats (250). Fate mapping studies in mice using colony-stimulating factor 1 receptor (*Csf1r*) and the KIT proto-oncogene, receptor tyrosine kinase (*Kit*) revealed that KCs first appear around E 10.5 day in the embryonic liver originating from the differentiation of erythromyeloid progenitors (251, 252). KCs are located chiefly at the luminal side of the sinusoidal wall and possess large cytoplasmic extrusions that make contact with HSCs and hepatocytes (249). A recently published study in mice reported that the cell bodies of

KCs (*i.e.*, CLEC4F positive cells) distributed equally between the luminal location and the abluminal side of the sinusoidal wall (37). Moreover, LSEC fenestrae also permits the cytoplasmic extensions of KCs in the sinusoidal lumen to protrude their cytoplasmic extensions and constantly survey the perisinusoidal space of Disse and be in touch with hepatocytes and HSCs (253).

Moreover, strategic positioning of KCs along the sinusoids allows efficient blood and tissue surveillance (37). The density of KCs is highest in the periportal areas along the porto-central axis, but KCs can be found all along the sinusoids (250, 254). KCs further represent a complex cell population with diverse phenotypic and functional characteristics (37, 255). KCs in the periportal area display 2-3 times more efficient phagocytosis than pericentrally located KCs, measured as a function of uptake of FITC-labelled zymosan after intravenous injection (254).

KCs represent a long-lived and self-maintaining macrophage population (256, 257). But in cases of massive KC ablation following liver injury, intoxication, or other pathologies, the KC pool is quickly replenished by MoMFs (255, 258, 259).

Liver MoMFs are macrophages differentiated from circulating monocytes that infiltrate the organ following liver injury or after substantial depletion of KCs. MoMFs can rapidly accumulate, and multiply, and acquire a wide range of phenotypes which allow them to respond vigorously during acute liver inflammation and injuries (249). Compared with the sessile, long-lived KCs, MoMFs are mobile, short-lived, and more rounded macrophages. MoMFs possess few cytoplasmic expansion and are continuously patrolling the liver tissue (249). Of note, the understanding of the sequence of events leading to MoMF differentiation and the detailed characterization of consequent phenotypes is still limited (37, 255, 258).

LCMs are the least studied liver macrophages, defined as macrophages “present at the level of the liver capsule” (260). In mice, they express the macrophage markers CD64 and F4/80 and typical dendritic cell markers such as MHCII and CD11c (261, 262). However, they lack the expression of the KC-specific markers TIM-4 and CLEC4F.

In specific circumstances following infection, trauma, and cancer, peritoneal macrophages will also migrate into the liver, preferentially to the subcapsular region (263).

1.4.2 Scavenger and immune functions of KCs

KCs are in the vanguard of the hepatic defence system and are renowned for their high phagocytic activity empowered by the abundant expression of a diverse repertoire of SRs (264). SRs expressed

in KCs include CD36, CD163, CD68, MARCO, and SR-A1 (MSR1), which are involved in the clearance of insoluble particles, endotoxins, altered-self molecules, and recognition of bacterial membrane components by phagocytosis and receptor-mediated endocytosis (265). KCs express the complement receptor of the immunoglobulin family (CRIg (266)) at high density enabling it to catch C3b opsonized bacteria from the circulation under shear stress. As a result, KCs can efficiently remove and kill pathogenic bacteria such as *Escherichia coli*, *Pseudomonas aeruginosa*, *Bacillus cereus*, and *Borrelia burgdorferi* (267). Moreover, KC-associated CD1d dependent activation of invariant natural killer T cells was shown to give direct immune protection by preventing bacterial dissemination to the hepatic parenchyma and other extrahepatic tissues (268).

In most cases of systemic infection, KCs bind to pathogens and consequently elevate cell expression of CAMs and cytokines release necessary to augment the recruitment of neutrophils needed for efficient bacterial killing, as shown with *Listeria monocytogenes* infection in the liver (269). KCs are apt for efferocytosis (*i.e.*, removal of aged and damaged cells) (270) by virtue of the expression of the phosphatidylserine receptors MerTK and TIM-4, and SR-F1 (SCARF1). Moreover, increased expression of phosphatidylserine on dead/damaged cells or high expression of bridging molecules such as MFG-E8, GAS6, protein S, and C1q by KCs and LSECs enhance efferocytosis (270, 271). Of note, SRs highly expressed on LSECs, including stabilin-1 and stabilin-2, bind to phosphatidylserine with high affinity (272, 273). Given that, LSECs might help to segregate apoptotic bodies from circulation for further phagocytosis by KCs (270). Moreover, Dectin-2 (Clec6a) expression also enables KCs to remove cancer cells via phagocytosis (274).

Interestingly, KC-mediated clearance of exogenous and endogenous antigens may induce anti-inflammatory and tolerogenic immune responses compared with macrophages in other tissues (275). Studies in mouse models have shown that KC-mediated antigen presentation can directly induce local or systemic immune tolerance by activating naïve CD4⁺ T cells to differentiate into regulatory T cells (275). Regulatory T cells produce a high amount of the immunosuppressive cytokine IL-10 (275). It has also been shown that KCs can directly suppress effector T cell responses *in vitro* by expressing immunosuppressive mediators such as prostaglandin E₂ (276), 15d-PGJ₂, indoleamine 2,3-dioxygenase (277), and apoptotic inducer Fas ligand (278). KCs also express the programmed death ligand 1 (PD-L1), an immunosuppressive costimulatory molecule that inhibits T cell activation (275).

1.4.3 KC molecular signature and markers

KCs may be distinguished from other hepatic cells and MoMFs by their signature gene expression mostly studied in mice. Signature genes may vary between species, however, KCs in humans, mice,

and rats are primarily positive for CD45, F4/80, CR1g (VSIG4), and CD11b (249, 260, 279). In mice, CLEC4F has been used as a KC marker alone or in addition to the above markers (280). In humans, CD68 and MARCO expression are reported to differentiate KCs from other macrophages, and liver NPCs (11, 281). Similarly, in rats, CD163, CD68, and CR1g have been used to identify KCs (100, 266, 282). The expression of popular markers used for discriminating KCs and other liver macrophage populations are listed in Table 2.

Table 2: Popular markers used for discrimination between liver macrophage populations

Markers			Expression level at steady-state			References
Common name	Symbol	Species	KCs	MoMFs	LCMs	
F4/80	<i>Emr1</i>	Mouse	High	Intermediate	+	(283)
Clec4f	<i>Clec4f</i>	Mouse	+	-	-	(261, 280)
TIM-4	<i>Timd4</i>	Mouse	+	-	-	(261)
Langerin	<i>Cd207</i>	Mouse			+	(261)
CD11b	<i>Itgam</i>	Mouse	Low	High	Low	(284-286)
Ly6c	<i>Ly6c1</i>	Mouse	-	High	Low	(284, 287)
Csf1r	<i>Csf1r</i>	Mouse	+	+	+	(288)
Cx3cr1	<i>Cx3cr1</i>	Mouse	low	High	+	(261, 284)
CD163	<i>CD163</i>	Human	+	Intermediate		(11)
MARCO	<i>MARCO</i>	Human	+	-		(11)
CD68	<i>CD68</i>	Human	+	+		(11)
CR1g	<i>VSIG4</i>	Human	+	-		(11)
CD163	<i>Cd163</i>	Rat	+	-		(289-292)
CD68	<i>Cd68</i>	Rat	+	+		(289, 290, 292)
CD11b/c	<i>Itgam</i> and <i>Itgax</i>	Rat	+	+		(293-295)

Expression level: “+” present, “-” absence, and the empty cells represents no discrete information available.

1.5 General introduction to expression profiling

The genome is mostly invariant across the cells and tissues of an individual. Each diploid cell will bear the same DNA compared to any other cell from the same individual in its entirety, with a few exceptions. The genome stores the information inherited across progenies. Despite the same inherited genome, most cells display their characteristic cell type and cell state-specific traits/phenotype because of differential genome activity, in other words, differential gene expression patterns across various cell types.

Genome activity can be quantitatively measured both at the level of transcription and translation. The complete set of RNA transcribed from the genome constitutes the transcriptome. The term transcriptome has been synonymously used for RNA subsets, most predominantly to set of mRNAs. The mRNA transcripts translate into proteins. Proteins produced in each organism, system, or biological context in their entirety represent the proteome. Both the transcriptome and the proteome are functional units of the genome. They are highly dynamic entities, sensitive to various internal and external stimuli. The existence of many proteoforms (*i.e.*, the different forms of a protein produced from the genome, including sequence variations, splice isoforms, and posttranslational modifications) and the high dispersion in expression level between proteins makes the proteome more complex and dynamic compared to the transcriptome (296).

The expression patterns or the profiles of the genes and proteins in a cell determine the cellular identity and dictate specialization. Therefore, it is of great biological value to generate accurate and precise information regarding the transcriptome and proteome. Gene and protein expression profiling represents the methods that identify and catalogue the expressed mRNA transcripts (the transcriptome) and proteins (the proteome) in a specific cell and context to create a holistic overview of the cellular function.

Methods such as RNAseq allow precise quantitative measurement of a transcriptomic outcome at a genome-wide scale. RNAseq is an unbiased yet highly effective and powerful exploratory tool in both experimental and clinical settings. In the clinics, RNAseq methods offer a high resolution, wide dynamic range, and higher genomic coverage strengthening clinical prediction (297). RNAseq is also used to find novel genes, other active transcript isoforms, small RNAs, microRNAs, and long noncoding RNAs (298, 299). Convincingly, today the RNAseq methods are have become more reliable and affordable to use in the laboratory and the clinic (299).

Other contemporary transcriptomic techniques such as microarrays are also widely in use. Unlike RNAseq, microarrays employ hybridization of fluorescently labelled RNAs to a known set of complementary short oligomeric probes arrayed to a surface to measure the relative abundances of the transcripts. However, the probe design requires prior information about the gene assemblies of interest. Microarray data might also suffer from high background noise because of cross-hybridization and constrained dynamic range (300).

Although RNAseq can sensitively enumerate the expressed genes and provide their relatively accurate and precise expression level, the information merely captures an event (out of a sequence of regulating events) conferring to the cell phenotype and function. The cell-specific proteomic landscape embodies another fundamentally deterministic regulatory event. Several methods are available to explore protein abundance, including Western blotting, enzyme-linked immunosorbent assay (ELISA), flow cytometry, fluorescence-activated cell sorting (FACS), and 2-D gel electrophoresis. However, today the most preferred approach for large-scale protein exploration is based on mass spectrometry (MS). MS-based methods not merely support the speed and scale necessary for the characterization of the proteome but also enable reliable identification and quantification of peptides/proteins in complex biological samples (301).

Briefly, MS-based proteomics relies on enzymatic fragmentation of the proteins, ionization of the resulting peptides, separation with regard to the peptide mass-to-charge (m/z) ratio, and the generation of a mass spectrum according to the ion intensity and the mass-to-charge ratio. The relative ion intensity accurately measures the protein abundance, and the mass spectrum allows precise identification.

Several proteomics techniques can separate between different proteoforms and posttranslational modifications with very high resolution permitting more precise functional prediction. The list of various applications of proteomics techniques and their biological utility is enormous (301). Therefore, only proteomics methods applied in the studies included in this thesis will be further described (section 3.5).

1.6 **Biological interpretation of expression data**

The quantitative expression data from both transcriptomic and proteomic experiments are rich in biological information and can presumably predict and model the cell function and the behaviour at a particular moment of interest. The manual search of the literature for biologically relevant telltale clues across the enormous gene/protein list generated is laborious and impractical. One of the easiest

ways to make an enormous list more tractable is to subdivide the list into meaningful subsets. The standard approach to generate informative subsets is to use statistics-driven differential gene/protein expression analysis and pathway enrichment analysis.

1.6.1 Differential gene/protein expression (DE) analysis

The differentially expressed genes/proteins ought to signify the prominent phenotypic variation or the functional differences implicit between the states of interest in the experiment. The expression of genes/proteins within a condition can be directly compared using normalized expression values (RPKM, FPKM, or TPM) for mRNA and ion intensities for proteins. However, these values are not appropriate to compare relative abundance between different conditions.

Various statistical strategies can be implemented to identify the differentially expressed genes/proteins. Differentially expressed genes/proteins between cellular states are ones with an expression difference significantly higher than would be expected by chance. Both “limma+voom” (302) and “edgeR” (303) are widely used tools for testing differential expression (DE) and were used in this thesis following the published recommendations (304-306). The limma+voom tool is more conservative compared to edgeR and provides better control regarding false positives. However, edgeR performs better regarding sensitivity and specificity when the biological replicates are few (307). We have used the normalized counts at the level of genes and the normalized ion intensities or the reporter intensities at the level of protein groups for the DE analysis. The list of differentially expressed genes/proteins will be substantially shorter than the original gene/protein list (given that this method assumes that most of the genes/proteins remain unaffected between states). The DE analysis may lose subtle biological information and may not represent a unifying biological theme. Above all, the interpretation can still be *ad hoc*, depending on the expertise of an analyst (308). Nevertheless, DE analyses can be useful in identifying biomarkers and genetic mechanisms contributing to the phenotypic variations between the cells and the state of interest (309).

1.6.2 Pathway enrichment analysis (gene set analysis)

Biological interpretation requires the association of the gene list to its respective functions. One way to do this is to look for gene-function association one by one from the list of selected genes/proteins. However, this approach is not practical, as a single gene/protein might be associated with multiple functions, the interpretation of which can easily overwhelm researchers and make the study intimidating to discern and discuss. To address such pitfalls, a researcher can implement statistics-driven enrichment analysis to subset the genes into unified, standardized, and easy to interpret biological themes.

Enrichment analysis refers to the statistical test devised to identify the over-representation of any biological theme (gene sets) on the experimental gene list compared to what can be expected by chance. Compared to single gene analysis, gene enrichment analysis can identify more subtle yet concordant changes in genes belonging to a gene set. In physiological systems, a group of genes rather than a single gene works in concert to carry out a specific task, so the gene set analysis is biologically more insightful than the single gene analysis (310). However, enrichment analysis depends on *a priori* knowledge about gene sets. Gene sets comprise genes that are co-expressed or are involved together in a biological pathway. The information regarding the gene sets is stored and organized in well-structured databases such as the Molecular signature database (MsigDB (311)). In this thesis project, we have used gene set collections from MSigDB with gene set enrichment analysis (GSEA) for functional enrichment in all three subprojects (**papers I, II, and III**) included in the thesis.

2 Aim of the study

LSECs, together with KCs, constitute the liver reticuloendothelial system, or scavenger cell system (17). Both cells are involved in immune surveillance and blood clearance of tissue turnover waste macromolecules, oxidized proteins/lipoproteins, toxins, viruses, microbial products, and other potentially dangerous substances that gain access to the general circulation. The spatial co-localization of the two cells in the liver sinusoid and partly overlapping functions, as well as species differences in cell marker expression, heterogeneity within LSEC and KC populations, and variation in cell isolation and culture systems, have led to confusion around the LSEC phenotype and functions (14). Furthermore, LSECs are challenging cells to study as they rapidly change their *in vivo* phenotype in culture (43, 228, 229). Thorough descriptions of LSEC *in vitro* changes as well as the underlying mechanisms for these changes are scarce, which makes it difficult to make biologically relevant interpretations of experiments done in LSECs cultured for several days. This also contributes to the confusion around the LSEC phenotype.

In this thesis, we used a multi-omics approach to try to resolve some of the discrepancies about the LSEC phenotype in the literature. The overall aim of the study was to provide a comprehensive molecular characterization of LSECs and KCs using high-throughput mRNA sequencing and proteomics methods. First, the transcriptome and proteome of freshly isolated rat LSECs and KCs were analysed and compared with a focus on features related to their roles as a scavenger and immune cells, as well as on cell-specific markers. The project further aimed to characterize changes in LSEC protein expression *in vitro*, as well as to examine how LSECs are affected by pro- and anti-inflammatory factors. As two previous reports (312, 313) showed an effect of the pro-inflammatory cytokine IL-1 β and the anti-inflammatory drug dexamethasone on LSEC endocytosis, we focused our study on these two factors. Dexamethasone is a frequently used additive in primary culture systems, for instance, in hepatocytes, and is also an essential drug for treating several liver diseases. However, the detailed effect of this drug on the LSEC is unknown.

Based on the above research questions, the thesis project was divided into the following subprojects:

1. To conduct a transcriptome and proteome profiling of rat LSECs and KCs and compare the expression profiles between the two cell types to determine cell-specific and overlapping scavenger and immune features of the cells (**paper I**).

2. To characterize the proteome and secretome of rat LSECs in early *in vitro* culture and the effect of IL-1 β , IL-1 β plus dexamethasone, and dexamethasone alone on protein expression, using multiplexed TMT-based quantitative proteomics (**paper II**).

3. Based on the results of the study in **paper II** showing a culture-induced early activation of rat LSECs and dexamethasone-mediated abrogation of the activated phenotype, a more detailed time-course quantitative proteomics study was carried out in the mouse model to describe and nuance the effects of dexamethasone on LSECs during prolonged primary culture, including comparative aspects between rat and mice (**paper III**).

3 Methods and methodological considerations

3.1 Animal models and ethics statement

Rats and mice are widely used animal models in biomedical research. They are preferred not merely because of their small size, ease of maintenance, high fertility, short life span, and abundant available genetic resources, but they also share a resemblance to humans in various aspects of their anatomy, physiology, and genome traits (314). The complete genome information is available for both rats and mice. Approximately 95% of the genes are shared between these rodents and humans (314). Furthermore, the liver of rats and mice share the microarchitectural organization with that of the human liver (315). There is, however, a lack of literature that systematically compares LSECs between rat, mouse, and human. In the present study, we used the outbred Sprague Dawley rat and the inbred C57BL/6 mouse. These are two commonly used rodent models and much of their proteogenomic and physiological data are readily available. There is also some transcriptomics and proteomics data (58, 228, 316, 317), as well as functional data available for LSECs, obtained from these rodent models, which made the cross-validation of the present data and subsequent interpretation of the studies easier.

The experimental protocols using rats and mice were approved by the institutional authority at UiT The Arctic University of Norway, and the National Animal Research Authority at the Norwegian Food Safety Authority (Mattilsynet), as described in **paper I** (318), **II**, and **III**. Housing, and handling of the animals, and the experimental procedures were performed in compliance with Directive 2010/63/EU and the European Convention for the protection of Vertebrate Animals used for Experimental and Other Scientific Purposes (ETS 123, European Council).

3.2 Cell isolation, purification, and cultivation

3.2.1 Tissue dissociation and differential centrifugation

Rat and mouse liver cells were isolated as described in (319) with some modifications as described in **papers I** (318), **II**, and **III**. In short, a catheter linked to a peristaltic pump-driven perfusion system was inserted into the portal vein of the anaesthetized rat (**papers I** (318) and **II**), or the newly dead mouse (**paper III**). The liver was perfused free of blood with a calcium-free buffer, followed by perfusion with collagenase in perfusion buffer with calcium (calcium is needed for the enzyme to function optimally). After digestion of the liver, the liver cells in suspension were subjected to differential centrifugation to remove hepatocytes before purification of LSECs or KCs from the resulting NPC fraction.

In differential centrifugation, different speeds (g forces) are used to separate different cell types based on their density or size, which determine their sedimentation rate. Larger and denser cells pellet earlier than smaller and less dense cells. Differential centrifugation is the simplest way to separate NPCs from hepatocytes but lacks the specificity to separate KCs or LSECs from other NPCs (25).

3.2.2 Cell purification techniques used for LSECs and KCs

Various methods are available for isolation and purification of LSECs and KCs from the NPC single cell suspension. All methods have their strengths, weaknesses, and technical requirements resulting in different yields and purity. Either of the following four strategies is used to purify LSECs and KCs: 1) centrifugal elutriation (320); 2) selective adherence to a substrate (321); 3) magnetic-activated cell sorting (MACS) (322, 323), and 4) fluorescent activated cell sorting (FACS) (324). Each of these methods is often preceded by isopycnic sedimentation, using a density gradient to enrich LSECs and KCs before the final purification step.

Centrifugal elutriation, like differential centrifugation, separates different cell types based on their sedimentation velocity determined by the cellular shape and size. The major merit of this method is the ability to separate a large number of similar cells in a relatively short time. However, the method has been used for LSEC isolation with a variable degree of success. According to the literature, elutriation centrifugation may give high cell yields but is inconsistent when it comes to cell purity and requires high technical skills (23).

Selective adherence is commonly used for the separation of LSECs from NPC suspension in both rats and mice (18, 321, 325) and was used in **paper II** of this thesis. The method takes advantage of the differential ability of cells to attach to different cell culture substrates. Macrophages quickly and readily adhere to uncoated plastic culture plates compared to LSECs. Hence, a short incubation of the NPC suspension in a plastic culture dish without an ECM coating effectively removes KCs from the cell suspension. The remaining LSEC-enriched cell suspension can be removed and seeded onto collagen- or fibronectin-coated culture dish to produce pure LSECs cultures. This method is simple, fast, and does not require additional chemical treatment or labelling. At the same time, the selective adherence method can handle large quantities of cells and can give a high yield of pure LSECs (321). However, factors including time allowed for the attachment of cells, type of tissue culture plates, and technical skills of the researcher, determine the end purity of the cultures.

MACS and FACS are commonly used methods for cell separation. Both methods separate cells based on their molecular phenotypes. In typical MACS and FACS workflows, the cells are labelled with an

antibody (conjugated with magnetic beads or a fluorophore) to a cell surface antigen. The antibody binds to the antigen target with high affinity and specificity and allows the cells to be discriminately separated based on the magnetic or photonic properties. The advantages of MACS over FACS are basically that MACS is gentler to the cells and can handle a large number of cells in parallel batches, significantly reducing the running time and offers relatively low cell loss (7-9%) (326). On the other hand, FACS allows simultaneous measurements of multiple parameters increasing the discriminatory power to separate cell types from the heterogeneous mix. FACS measures all the parameters in every single cell sequentially, hence this method is limited by the speed of operation especially in the case of low proportion samples. In addition, due to the limited speed and harsh procedures, FACS results in high cell loss (approximately 70%) (326). Overall, MACS often results in high yield of cells with high viability (327).

In the present project, we have used MACS to purify rat LSECs and KCs in **paper I** and mouse LSECs in **paper III**.

3.2.3 Cell purification method used in this thesis

The choice of method for cell isolation and purification determines the cell purity, viability, and cell yield. Consequently, the methods used will significantly affect the outcome and biological interpretation of the experiment as discussed in (14, 16, 23).

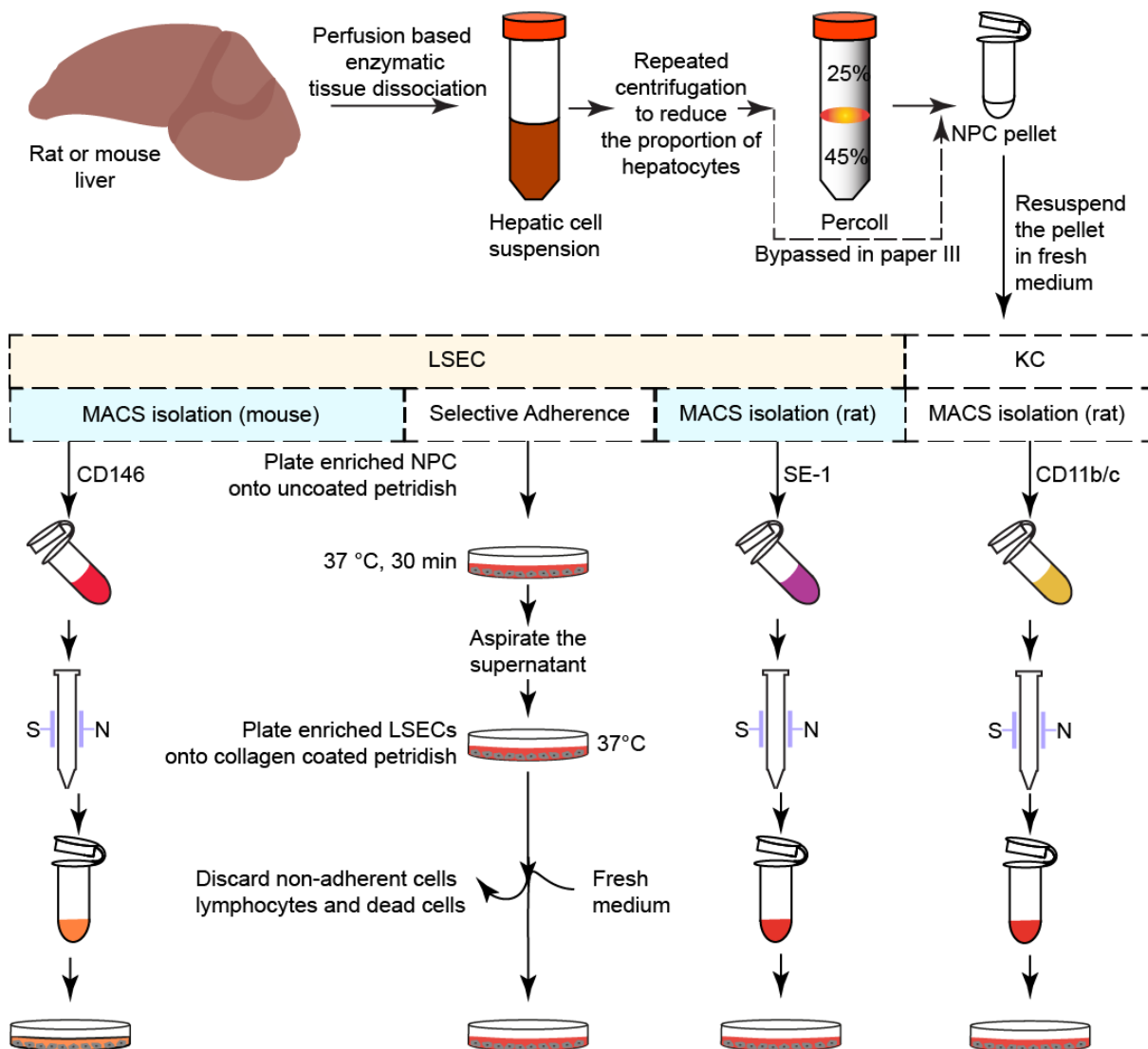


Figure 3. Different cell preparation methods used in the present thesis project.

The studies in this thesis implemented a combination of differential centrifugation (to remove hepatocytes) and density centrifugation and selective adherence (**paper II**), or MACS (**paper I**), or MACS without density centrifugation (**paper III**, as illustrated in Figure 3). In **paper II**, we used differential centrifugation followed by density centrifugation using a two-layered Percoll-gradient, and then selective adherence of KCs to enrich the LSECs (321). This method was used to maximize the LSEC yield, as the experimental design used in paper II required many cells to be able to include all treatments in the proteomics experiments at the same time.

In **paper I**, we chose MACS to maximize cell purity and viable cell yield, this was essential for the type of experiments where two different cell types were compared to describe both differential and overlapping features. Proteomics experiments from the small and mRNA poor LSEC, we used the

separation regime giving the highest cell yield. FACS could also have been used to generate pure cells, however, the cell yield and probably also viability (326) would have been compromised. In addition, MACS is faster and gentler compared with FACS and reduces stress-induced changes in expression profiling (328).

MACS-based purification of LSECs and KCs faces similar challenges in terms of specificity of antigen and available antibodies. The recently reported heterogeneity of the two cell types from single cell transcriptome studies (reported after the production of the transcriptomes in the present thesis) has further added complexity to the selection and use of particular markers for purification (16). The following markers were chosen in our study based on literature searches and commercially available antibodies: The HSEC antibody (SE-1) (323, 329), and biotinylated CD11b/c (OX-42) (321) were used for MACS-based purification of rat LSECs and KCs, respectively (**paper I**), whereas CD146 (131, 330) was used for MACS purification of mouse LSECs from liver NPCs (**paper III**).

The HSEC/SE-1 antibody is a validated monoclonal antibody for MACS-based purification of rat LSECs (323, 331). It targets Fc γ RIIb2 which is selectively expressed in LSECs in the rat liver (229). In **paper I**, we also validated the LSEC specific expression of Fc γ RIIb2 (CD32b) in frozen sections from rat liver (318). In contrast to the reported zone-dependent disparate expression of Fc γ RIIb2 in LSECs in human liver (208), we found that the expression of this receptor in the young healthy rat was homogeneous along the porto-central axis as also reported by (331). The method produced highly pure LSECs (appr. 97% fenestrated cells) (318).

For the isolation of mice LSECs, we used CD146, a popular marker used for the purification of mouse LSECs (23, 131, 330). To reduce the workflow time and prevent cell loss, the Percoll-gradient density centrifugation step was excluded. Of note, CD146 is expressed by many endothelial cells and may not differentiate LSECs from other vascular endothelial cell types in the liver. Nonetheless, since CD146⁺LYVE-1⁺ cells (interpreted as LSECs) constitute greater than 95% of endothelial cells in the liver (332), almost all cells obtained using CD146 as a marker would represent LSECs. In accordance with this, we obtained cultures with greater than 95% (up to 99%) LSECs (*i.e.*, fenestrated endothelial cells) when using this antibody in MACS-based LSEC isolation from enriched NPC suspensions (**paper III**).

Regarding KCs, several markers are available and accepted for use in mice, including F4/80, CLEC4F, and CD11b/c (249, 260, 279, 280). Nevertheless, little is known about the rat KC phenotype in contrast to the extensive literature in mice. In the absence of other validated and functional

antibodies for MACS-based rat KC isolation, we have used CD11b/c (293). The CD11b/c antibody showed a more limited immunoreactivity in comparison to CD68 in liver tissue sections, being more restricted to KCs in the periportal area, suggesting that we may have excluded some KC subpopulations in the analyses in **paper I** (318).

3.3 Methods for LSEC and KC identification

3.3.1 Scanning electron microscopy (SEM)

SEM is an imaging technique where a focused beam of electrons is used to scan the surface of the specimen and secondary electrons emitted from the specimen surface are used to generate a 3D-like image of the cell topography. In all three studies, we used SEM for LSEC identification and purity assessment of LSEC cultures. SEM enables detection of the most important ultrastructural hallmark of LSEC, *i.e.*, the numerous open fenestrae. The presence of fenestrae is the gold standard for the identification of LSECs (16, 21, 26, 65).

3.3.2 Immunofluorescence staining

Immunostaining is a powerful technique to localize specific antigens within a tissue or cell based on antigen-antibody interactions. Samples are incubated with an antibody specific to the target protein to identify its expression pattern. In direct immune fluorescence, the primary antibody is covalently bound to a fluorophore, whereas in indirect immune fluorescence, a fluorophore-conjugated secondary antibody binding to the primary antibody is used to visualize antigen expression. Indirect fluorescence can significantly amplify the signal but at the same time increase the risk of false-positive results due to the increased probability of unspecific binding. Therefore, for unambiguous interpretations and to avoid false outcomes, a set of controls including a negative control, positive control, the match-isotype control, and fluorescence minus one control constitute good laboratory practice (333). In this thesis, we have utilized indirect immunofluorescence on liver tissue sections and cultured cells for three major purposes; 1) to examine the cellular distribution and expression pattern of proteins in liver sections; 2) to identify different liver cell types in culture, and 3) to validate gene/protein expression in cells.

3.3.3 Flow cytometry

Flow cytometry is a widely used single cell technique that measures various optical properties of cells with high sensitivity and precision enabling exploration of a wide range of scientific questions. Flow cytometry has been routinely used for the identification and quantification of target protein

expression. Above all, flow cytometry is a powerful tool to evaluate and characterize rare cell populations within complex and highly heterogeneous samples (334-336).

Within the flow cytometer, single cell suspensions with fluorescence (genetically labelled or labelled with fluorescence-antibody conjugates) are focused on the flow chamber (hydro-dynamically, or by microcapillary methods, or acoustophoresis) before passing through the laser beam (337). When cells pass through the laser beam, they emit optical signals. Photomultiplier tubes or photodiodes are used to detect the optical signals (*e.g.*, scattering features or fluorescence emission). The scattering features of the cells are dependent on the size and the cellular complexity associated with the cells, while the fluorescence emission corresponds to the level of expression of the protein of interest (335).

Although flow cytometry and other FACS methods allow simultaneous measurements of multiple parameters, the throughput is limited by the range of suitable fluorescent dyes and the optical configuration. The emission spectrum of some fluorophores is broad and spills over to other channels. Therefore, compensation to reduce fluorophore interference between channels is necessary when multiple fluorophores are used in the analysis (336).

In **paper I**, flow cytometry was used to evaluate the expression of CD45 (PTPRC) on rat LSECs along with the two discriminatory LSEC markers SE-1 (*i.e.*, FcγRIIb2) and the pan-endothelial marker CD31.

3.4 mRNAseq

RNAseq has matured immensely over the last decade. At present, it allows transcriptome-wide analysis of various aspects of RNA biology and used to generate reliable and reproducible identification and quantification of gene expression which can be used to make an unequivocal distinction of cell and tissue phenotypes and to predict phenotype-specific function (299).

A general mRNAseq workflow contains RNA extraction, mRNA enrichment, cDNA synthesis, adaptor ligation, and library preparation in the laboratory in succession. This is followed by computational methods post data acquisition, including adapter trimming and other quality checks, read alignment to reference transcriptome, expression quantification, filtering and normalization of the read counts, and finally differential expression analysis (299).

A comparative transcriptomics approach generally relies on statistical evaluation of gene expression differences between samples, or cell types, especially at the level of single genes. Although the depth of sequencing affects the sensitivity of differential gene expression analysis primarily for low

abundant genes, mapping short reads (on average of 100-150 bp), such as the reads in the **paper I**, with the well-annotated *Rattus norvegicus* reference genome (338) allowed sufficient quantitative assessment of composition and complexity of the transcriptome landscape. Different mapping methods are reported to have little influence on the outcome if a well-annotated reference genome is used for aligning reads, as used in **paper I** (339). Additionally, various known and unknown elements of the experimental design (section 3.6) and settings, including quality and purity of the sample, number of biological replicates, read alignments parameters, sequencing depth, sequencing coverages, and choice of computational analyses might have an impact on the outcome of RNAseq (304).

In this thesis, we used Ion PGMTM sequencing of polyA-enriched RNA from LSECs and KCs. Ion PGMTM is based on Ion Torrent next-generation semiconductor high-throughput sequencing technology relying on measurements of pH changes during nucleotide elongation. Ion Torrent technology is distinct from Illumina, which is the most popular platform that uses fluorescence to read nucleotide bases in a sequence (340). Despite the differences, both platforms perform substantially similar in terms of gene quantification and detection of differential gene expression and putative functions (340-342). Ion PGMTM sequencing using Ion chip 316 generates single-end short reads with decent throughput or sequencing depth (approximately 1-3 million reads per chip).

3.5 Proteomics

Proteomics is a powerful analytic technique that refers to a set of approaches implemented to explore the proteome of a cell or tissue. We have implemented two very different bottom-up shotgun proteomics approaches for protein identification and quantification at a larger scale: 1) Label-free proteomics (**paper I**), and 2) TMT-labelled proteomics (**papers II and III**). These approaches were applied either to contrast the proteome differences between the two sinusoidal cells, LSECs and KCs (**paper I**), or to measure changes in the proteome that were induced in culture in the presence/absence of the synthetic glucocorticoid agonist dexamethasone (**papers II and III**), and the pro-inflammatory cytokine IL-1 β (**paper II**).

The mass spectrometer instruments used in this study were Q ExactiveTM HF-X Hybrid Quadrupole-OrbitrapTM (**paper I and paper II**), and Orbitrap FusionTM LumosTM TribridTM (Lumos) (**paper III**). The mass analyser used by Q-Exactive HF-X is a hybrid of quadrupoles with Orbitrap Fourier transform-based mass analyser. This provides high mass accuracy and is ideal for analysing highly complex (high dynamic range) protein extract from LSECs and KCs at very high resolution. The second instrument, Orbitrap Fusion Lumos, a state-of-the-art high-performance mass spectrometer,

is a tribrid that consists of three different mass analysers including Q1 quadrupole, ultra-high field Orbitrap, and Dual-pressure linear ion trap. Compared to the Q-Exactive HF-X, the Lumos provides better fragmentation, enabling the use of SPS MS³-based methods to minimize ratio compression resulting in enhanced detection sensitivity and improved quantitative precision (343).

Generally, in bottom-up shot-gun proteomics approaches, the mass spectrometric analysis is performed on the peptides subsequently generated after enzymatic digestion (by trypsin or lysyl endopeptidase) of the protein extract. The third study (**paper III**) additionally included pre-fractionation of the peptides. The digested peptide mixes are generally sorted *a priori* during liquid chromatography (LC) in concert with high-resolution tandem mass spectrometry (MS/MS). The sorted peptides are protonated into ions at the electrospray ion source inlets and are guided into a series of mass spectrometers. For example, in the Q-Exactive HF-X mass spectrometer, the ions are guided using series of ion guides into a quadrupole for selection. The quadrupoles generate a full MS spectrum, and the intensities of ions recorded in the MS1 scan correspond to the peptide abundance in the sample. The “top-N” precursor ions are selected in a data-dependent acquisition in quadrupoles and transferred into a C-trap/octopole collision cell for fragmentation using higher-energy collisional dissociation (HCD). The resulting fragmented peptides were analysed in an Orbitrap mass analyser.

3.5.1 Label free proteomics

Label-free proteomics offers the simplest biochemical workflow at a low cost for whole proteome analysis. The approach is superior to handle large numbers of samples. At the same time, it suffers from limited throughput and precision in the identification and quantification of low expressed proteins in samples (344). Label-free proteomics generally employs two different methods based on ion spectral counting or spectral intensities in conjugation with the retention times from chromatogram data (XIC; extracted ion chromatogram) to measure absolute or relative quantitation of the protein.

In the first study (**paper I**), we implemented intensity-based absolute quantification of label-free proteomics (iBAQ) to compare the LSEC and KC proteomes. iBAQ is an XIC-based method of quantification. The XIC-based methods provide more sensitivity and accuracy compared to spectral count methods such as protein abundance index (PAI) or exponentially modified protein abundance index (emPAI) (345). Label-free quantification is based on the proportional relationship between the spectral counts, intensity, and the protein abundance. In other words, the more abundant the proteins are the greater number of times it gets sequenced in the MS/MS events. The peak height or area under the curve information from the LC is equally proportional to the abundance of the peptide. The

retention time can be used to integrate the protein identification from the MS² event to the quantification from LC, generating XIC. The XIC is normalized against the protein length to obtain the iBAQ value, or by the possible number of tryptic peptides as in emPAI (346). The iBAQ value (*i.e.*, the total intensities divided by the identified peptides for one protein) represents the most accurate label-free quantitation and is less biased towards the quantitation of smaller proteins. With the need for higher accuracy in protein quantification, label-based approaches are recommended (344).

3.5.2 TMT-based quantitative proteomics

Peptides can be labelled metabolically using stable isotopes as in SILAC (stable isotope labelling with amino acids in cell culture), or chemically with isobaric tags such as TMT (tandem-mass tag), and iTRAQ (isobaric tag for relative and absolute quantitation). Implementation of SILAC in *in vitro* LSEC systems is challenging due to the short survival of cells in culture, and pilot experiments prior to this thesis work resulted in poor isotope incorporation of rat LSECs. TMT-labelling, on the other hand, was suitable as the peptides are covalently modified with isobaric tags later in the workflow subsequently after protein digestion.

TMT-labelling allows multiplexing of the sample and provides high precision quantification with minimal missing values (344, 347). The TMT labelling approach is advantageous when performing a time series, dose-response experiment, or other experimental designs where multiple samples are compared. Multiplexing greatly minimizes technical bias, allowing improved and accurate comparative proteomics. Primarily, TMT contains an amine reactive dye that chemically labels the peptide, which is linked to a mass balancer moiety, and a mass reporter (344). The mass reporter is separated from the balancer by a weak linker susceptible to dissociation. Fragmentation of labelled peptides during MS² releases the reporter ions, and the ratio of these reporter ion intensities are used for relative quantification.

The ability to select a single peptide precursor for MS² fragmentation is fundamental for the accurate quantification in TMT-based proteomics. The existence of near isobaric peptide precursor ions causes a co-isolation and co-fragmentation of precursor peptides resulting in underestimation of the actual differences in abundance, sometimes termed ratio compression. Ratio compression may lead to inaccurate reporting of true fold differences between two reporter ion intensities (344). Ratio compression is intrinsic to TMT-based proteomics irrespective of instrumentation. Nevertheless, ratio compression issues can be mitigated using prefractionation of peptide mixture and additional MS³ isolation and fragmentation as allowed by Lumos (348) as done in **paper III**.

The Q-Exactive HF-X (**paper II**) only favours MS¹ and MS² isolation and fragmentation and the data may suffer from the ratio compression, whereas Lumos (used in **paper III**) allows additional MS³ isolation and fragmentation. The Lumos not only mitigates the ratio compression problem but also allows deeper proteome analysis. The prefractionation of the peptide mixture and the use of the Lumos may be the reason why we have approximately 6000 proteins identified in the mouse LSEC proteomics experiments (**paper III**), compared to approximately 3000 proteins in the rat LSEC proteomics experiments (**paper II**).

3.6 Statistical inference of the transcriptomics and proteomics data

Transcriptomics and proteomics experiments measure tens of thousands of genes or gene products in a single run. Although mRNAseq or MS-based proteomics technologies generate highly reliable and highly reproducible (*i.e.*, little technical variation) measurements; the measurements may have limited accuracy and precision due to interfering, inadvertent, and nuisance variations. For example, in an mRNAseq experiment, systematic variation (noises and biases) may arise from intrinsic gene expression variation, library construction (cDNA conversion, PCR amplification, adaptor ligation), sequencing cycling, and base-calling (349). Such variation easily masks the true biological signal and poses challenges for statistical inferences and may lead to an erroneous biological inference.

Including biological replicates in an experiment, as we have done in all studies in this thesis, allows the researcher to estimate and address technology-specific effects. However, the sample size in an omics experiment is often kept small for various logistic and economic reasons. Enormous numbers of data attributes (genes/gene products) and limited biological replicates make the omics data inherently highly dimensional. The high dimensionality of the omics data adds further difficulty for statistical inference. Generally, an incidence of random association of variables to the desired phenotype or an outcome is more common in high dimensional data due to combinatorial effects of the multiple genes/gene products, often referred to as multiple testing problems (350).

3.7 Design considerations specific to the studies included in this thesis

A priori decisions regarding design elements such as sample size, mRNAseq/LC-MS platforms, enrichments methods, library constructions, single/paired-end sequencing, sequencing depth, multiplexing, and normalization aspects are essential to appropriately detect and address nuisance variation for judicious inference of the transcriptomic and proteomic data (304, 349). Elements of the experimental design mostly depend on the nature of the biological question being studied. Apart from

the biological interest, several other factors influence the design including cost, technical skills, type and availability of samples, and the accessibility of platforms.

Regarding the platform (sections 3.4 and 3.5) we were restricted by accessibility and the availability of the choices. Nonetheless, to ensure the validity and reliability of the data, the studies in this thesis considered the following:

1. Utmost considerations have been paid to optimize purity and viability of the LSEC and KC preparations as cross-contamination between samples limit the discriminative power of the omics experiments and may lead to misinterpretation.
2. Rigorous quality control measures
 - a. In the mRNAseq experiment, this included testing the quality of mRNA used for library construction, quality of the libraries, quality of sequencing reads, filtering out the ambiguous or low-quality base-calls prior to alignment with the annotated rat reference genome, and increasing the penalty while mapping for mismatch, insertion, and deletion.
 - b. In the proteomics experiments, the quality control included data-dependent acquisition of the peptide spectra and filtering out the low confidence peptide identification.
3. Checking the quality and distribution of all the data values to determine intra and inter experimental quality and setting out of filtering thresholds.
4. All studies included in this thesis have at least 3 biological replicates in each experimental group.
5. Well-established statistical methods were used to account for biases and noises. This included scaling normalization to control sequencing depth bias or total intensity differences in RNAseq and proteomics, respectively, internal reference scaling to account for sampling variations between TMT runs, and trimmed mean of the log expression ratios (TMM) normalization to account for compositional bias.
6. The experimental design was always accounted for while testing for the differential expression of genes/proteins. The log-CPM (count per million) and iBAQ per million, respectively for mRNAseq data and label-free proteomics data were used in linear modelling via the limma's `voomWithQualityWeights` function with empirical Bayes moderation for determining differentially expressed genes/proteins (305). This way of testing DE provides better control to false-positive results. The normalized TMT reporter intensities were used in edgeR based negative binomial distributions including empirical Bayes moderation for DE identification with exact tests. The edgeR provides more sensitivity and specificity (351).

7. False-discovery rate (FDR) approach was implemented for corrections of multiple testing problems.

3.8 Data validation

Data validation is another important aspect of the experimental design to ensure the reliability of the experimental data. Batch effect, sparsity of data, challenges in data integrations, and high intrinsic noise are some of the factors that influence biological interpretation. Moreover, algorithms for identification and quantification along with the statistical pipelines used for analytical purpose are prone to generate false positive outcomes (304). Therefore, it is necessary to validate results using alternative and/or orthologous technologies to the extent possible. Again, the validation may suffer from the limitations of available samples, technologies, and the cost of experiments. For example, in the study of molecular phenotyping of rat LSECs and KCs (**paper I**), we primarily chose an orthologous approach to validate the result of the RNAseq experiment, in terms of protein abundance. Label-free proteomics was preferred for the validation due to limited availability of specific, sensitive, and functional antibodies. Nevertheless, we performed immune-staining and flow cytometry experiments to validate the expression of some of the surface markers identified in the omics dataset. Furthermore, the study also applied published data and information to cross-validate the datasets (58, 228). In **paper II**, alternative protein measurement methods such as ELISA and Luminex were used for validating the abundance of target proteins. In the mouse LSEC study in **paper III**, we primarily focused on validating the differential protein abundance at a functional level, (*e.g.*, apoptosis, endocytosis, glutathione assays), investigating the alteration in functions associated with the proteins of interest.

3.9 Genome annotation

Genome annotation primarily refers to the process of associating sequences of biological elements such as genes and long noncoding RNAs, to their putative functions. A well annotated genome is an invaluable resource for analysis and interpretation of any omics study. An accurate reference genome adds quality and accuracy to genes/proteins identification, read/spectral mapping, and quantitation in shotgun sequencing approaches such as Ion torrent mRNAseq or bottom-up label-free/labelled proteomics. None of the annotation databases are 100% complete warranting a need for being scrupulous while performing the data interpretation.

In the first study we have used the rat genome assembly (Rnor_6.0) from Ensemble database for alignment and assembly of RNAseq reads (338) because this was the most updated database, with

coding and non-coding genes including the Y chromosome, as we used male rats in our study. The RNAseq data sets used in annotation of the assembly also included samples from liver along with 11 other organs (338). Similarly, we used the UniProtKB/Swiss-Prot database (352) to annotate the MS data in all studies. UniProtKB/Swiss-Prot follow gene-centric proteome curation (353).

3.10 Enumeration of statistical and bioinformatical tools

Statistical and bioinformatical tools used in the thesis projects are summarized in Table 3.

Table 3. Suits of bioinformatical and statistical software used in the projects included in the thesis

Tools	Version	Details	Applications	Descriptions	Purpose
CLC Genomics Grid Worker	7.0.1	Qiagen® Bioinformatics	Adaptor trimming and quality control of raw reads Read alignment and quantification	Sequence trimming to remove poor quality bases (ambiguous) and the Ion adaptor. Quality control including analysis of the GC content, overrepresentation of k-mers and duplicated reads. Only the sequences homogeneous regarding k-mers were used in the alignment with the reference genome.	Enhance mappability Alignment with the reference sequence Generate reads count matrix
The R Project for Statistical Computing	From 3.4.1 to 4.0.4	https://www.r- project.org/abo ut.html	Used as the environment for statistical analysis of the data	Simple and effective programming language that provides a coherent system for data wrangling, integrations, and visualization. It also includes a library of very useful packages for sequence analysis, and implementation of modern statistics	Differential expression analyses

Bioconductor	From 3.5 to 3.11	https://bioconductor.org/about/related-projects/	For the analysis of RNAseq and proteomics data in combinations with other software tools	Several packages used in the analyses, functional annotation and the visualization of the datasets requires the Bioconductor environment for loading and execution.	Used to access statistical methods used in RNAseq and proteomics data analysis. Also, contains meta data packages and annotation packages.
MaxQuant	From 1.5.6.0 to 1.6.10	https://www.maxquant.org/	Identification and quantification of peptides	The MaxQuant software package allows analysis of high-resolution large MS datasets. It allows inspection of the raw data and offers reliable identification and quantification. It also includes the probabilistic scoring-based peptide search engine Andromeda	Identification and quantification of peptides from raw MS data
Perseus	From 1.5.6.0 to 1.6.14.0	https://maxquant.net/perseus/	Proteomic data processing	Perseus supports analysis and interpretation of proteomic data. A user-friendly workflow and data wrangling tools make the software platform easy to work with.	Data processing including scaling and normalization

GSEA	From 3.0.0 to 4.1.0	http://software.broadinstitute.org/cancer/software/gsea/wiki/index.php/Main_Page	Gene set enrichment analysis (GSEA)	GSEA provides a computational method for identification of enriched gene sets from <i>a priori</i> defined sets of genes/proteins for transcriptomics and proteomics. GSEA use reference annotated gene sets defined and collected in the MSigDB	Functional analysis of the transcriptomic and proteomic data
Cytoscape	From 3.4.0 to 3.8.2	https://cytoscape.org/what_is_cytoscape.html	Functional analysis and network analysis with various plugins (ClueGo, EnrichmentMap, STRING, etc.)	Cytoscape is a free software platform for annotation, network analysis and biological pathway analysis	For visualization of enriched processes and pathways
FlowJo software	V10.7.1	https://www.flowjo.com/solutions/flowjo	Analysis and visualization of flow cytometric data	Proprietary software for analysis and visualization of flow cytometric data	Flow cytometric data analysis

4 Summary of Papers

Paper I: Transcriptome and proteome profiling reveal complementary scavenger and immune features of rat liver sinusoidal endothelial cells and liver macrophages

LSECs lack comprehensive characterization and have often been confused or misidentified with KCs. In this study, we conducted comparative and integrative transcriptome and proteome analyses for resolving some of the impending issues of LSECs' identity and functions compared to the KCs.

We have implemented two omics strategies, mRNAseq and label-free proteomics, and successfully catalogued 10,306 mRNAs and 2996 proteins in samples from freshly plated and highly pure LSECs and KCs isolated from Sprague Dawley rat liver. The inclusion of both mRNA and protein data to compare LSECs and KCs added rigor, power, and validity to the study. We found a robust correlation ($r = 0.74$, $p < 2.2 * 10^{-16}$) considering \log_2 fold changes between the respective transcriptomes and proteomes of the cells. We have used data-driven, statistical differential expression and functional enrichment analyses to determine and distinguish the phenotype and functions between LSECs and KCs. The integrative analysis of the global molecular profile of the two cell types showed the constitutive expression of several immune genes and corresponding proteins in LSECs that bore resemblance with the expression observed in KCs. Both cells contained high levels of SRs and C-type lectins. Equivalent expression of SR-A1 (*Msr1*), mannose receptor (*Mrc1*), SR-B1 (*Scarb1*), and SR-B3 (*Scarb2*) suggested functional similarity between these two cell types, while the functional distinction between the cells was evidenced by LSEC-specific expression of the SRs stabilin-1 (*Stab1*) and stabilin-2 (*Stab2*), and the C-type lectins LSECTin (*Clec4g*) and DC-SIGNR (*Clec4m*) and KC-specific expression of CRIG (*Vsig4*), at both mRNA and protein level, and CD163, and CD68 at the protein level. On the other hand, many immune regulatory factors were differentially expressed in LSECs and KCs, with one cell predominantly expressing a specific cytokine/chemokine and the other cell the cognate receptor, illustrating the complex cytokine milieu of the sinusoids. Both cells expressed genes and proteins involved in antigen processing and presentation and lymphocyte co-stimulation.

Our findings support complementary and partly overlapping scavenging and immune functions between LSECs and KCs, highlighting the importance of including LSECs in studies of liver immunity, liver clearance, and toxicity of pharmaceuticals and nano-formulations.

Paper II: Changes in the proteome and secretome of rat liver sinusoidal endothelial cells during early primary culture and effects of dexamethasone

In this paper, we examined the cell-associated proteome and secretome of Sprague Dawley rat LSECs and checked for responses to the pro-inflammatory cytokine IL-1 β and the anti-inflammatory drug dexamethasone during the first 24 h in culture, to understand biological processes and pathways affected during early-stage primary culture, and with treatment. The cells were incubated in a DMEM-based medium with serum-free supplements in a 5% O₂ and 5% CO₂ atmosphere.

We here utilized a TMT-based proteomic strategy and LC-MS/MS to generate quantitative proteomes of cell lysates and supernatants of non-treated and IL-1 β or dexamethasone-treated LSECs at 2 and/or 24 h post-seeding for comparison of relative differences in protein expression. This study quantitatively catalogued 2537 protein IDs in the cell lysates (*i.e.*, cell-associated proteins) and 1432 proteins in the filtered supernatants of the LSEC cultures. The differential expression analysis and functional enrichment analysis of the data revealed that rat LSECs cultured for 24 h showed a pro-inflammatory phenotype both in the presence and absence of IL-1 β . The proteome revealed upregulation of proteins associated with cellular responses to cytokines and interferon- γ , cell-cell adhesion, and glycolysis, and downregulation of proteins involved in pyruvate metabolism, citric acid cycle, fatty acid elongation, amino acid metabolism, and oxidation-reduction processes, as well as downregulation of several membrane receptors and endocytosis receptors including CD146 (MCAM), stabilin-1 (STAB1), stabilin-2 (STAB2), LYVE-1, and LSECtin (CLEC4G). Dexamethasone improved LSEC survival in culture, reduced the culture-induced stimulation of glycolysis, and repressed the culture-induced stimulation of inflammatory and immune regulatory pathways and production of pro-inflammatory cytokines while increasing interleukin-10 release from the cells.

LSEC morphology was assessed by SEM and endocytic function by measuring uptake and degradation of the SR ligand formaldehyde-treated serum albumin (FSA). Dexamethasone did not prevent loss of sieve plates in LSECs *in vitro* but the dexamethasone-treated cells otherwise showed a healthier morphology compared with non-treated cells, with smooth cell borders, few gaps, and close contact between cells. At 24 h, uptake of FSA was higher in cultures with dexamethasone, but this difference could also be explained by increased cell survival with dexamethasone treatment.

In conclusion, rat LSECs become activated during the early phase of primary cultures. Dexamethasone represses LSEC activation and improves cell viability in culture.

Paper III: Mouse liver sinusoidal endothelial cell responses to the glucocorticoid receptor agonist dexamethasone *in vitro*

Based on the results in **paper II**, we performed a detailed time-course quantitative proteomics study in primary mouse LSECs (C57BL/6) to describe and nuance the culture-induced changes and cell responses to dexamethasone observed in the rat study. We further investigated dose- and time-dependent effects (up to 5 days) of dexamethasone on LSEC ultrastructure, viability, and scavenger functions. The cells were cultured in AIM-V medium in 5% O₂ and 5% CO₂ atmosphere. The cultures were confluent for at least 5 days with or without dexamethasone treatment. However, dexamethasone improved mouse LSEC survival *in vitro*, and doses up to at least 100 μM were well tolerated by the cells. LSECs gradually lost their fenestrae in culture both in the presence and absence of dexamethasone, but the dexamethasone-treated cells exhibited a more quiescent morphology and showed more fenestrated cells at later time points.

Cell lysates from LSECs treated with 1 μM dexamethasone or untreated control cultures at 1, 10, or 48h post-seeding were collected and subsequently prepared for TMT-based proteomics. We applied the SPS MS³ method on an Lumos mass spectrometer to gain deeper proteome coverage. With this method, more than 6000 protein IDs were quantified (FDR value 1%). The differential expression analysis showed significant alteration in the LSEC proteomes *in vitro* and responses to dexamethasone. The enrichment of hallmark gene sets from the Molecular Signatures Database showed early activation of mouse LSECs towards a pro-inflammatory phenotype and a rapid shift in LSEC metabolism *in vitro*, with upregulation of glycolysis and concomitant downregulation of the tricarboxylic acid cycle and oxidative phosphorylation. Dexamethasone suppressed the culture-induced LSEC activation, downregulating immune-inflammatory genes such as NOS2, IL-6, ICAM-1, and VCAM-1. In addition, we evaluated the concentration of ICAM-1 and VCAM-1 in LSECs supernatants with or without treatment at various periods during the culture to approximate the extent of endothelial activation and validate the dexamethasone mediated expression repression of ICAM-1 and VCAM-1. Dexamethasone also improved the survival of LSECs through anti-apoptotic mechanisms, which was validated with a caspase 3/7 bioassay.

Mouse LSECs in AIM-V kept their ability to rapidly endocytose trace amounts of the scavenger receptor ligand FSA for 3-5 days in culture (best with dexamethasone at day 5). The maximum endocytic capacity, nevertheless, was significantly reduced at 48h, also with dexamethasone. This reduction corroborates the time-dependent downregulation of scavenger receptors and altered expression of the endocytic machinery *in vitro*.

Conclusion: This study presents a detailed overview of biological processes and pathways affected by dexamethasone in mouse LSEC *in vitro*. Like in rats, dexamethasone significantly inhibits mouse LSEC activation and improves cell survival in culture.

5 General discussion

5.1 Factors affecting comparative gene and protein expression profiling

In this thesis, we have used next-generation RNAseq and proteomics methods for comparative gene and protein expression profiling of LSECs and KCs. These methods allow simultaneous measurement of thousands of genes and gene products and provide the power and scale needed to differentiate previously unrecognized biological differences between cell populations with accuracy and precision. Methods such as gene/protein microarray, qPCR, flow cytometry, immune histochemistry, and western blot techniques are widely used to elucidate cell-specific features and function of cells and tissues and are indispensable for many purposes. However, as these techniques depend on *a priori* knowledge and, except for microarrays, are highly limited in scale, so are not suitable for global characterization of gene and protein expression in cells. In many cases, single gene/gene products do not have sufficient power to discriminate between cell types, especially if the cells are poorly characterized. Expression of a single gene is also more likely to vary between the conditions or samples due to stochastic noise compared with the expression of a set of signature genes. Next-generation omics studies have surpassed several of these challenges and enable hypothesis-free investigations and comprehensive cellular characterization on a global scale (299).

In our studies, we employed a bulk shotgun approach for sequencing and quantification of mRNA and proteins. Bulk sequencing measures the average level of mRNA or protein expression of a population. However, bulk omics are unsuitable for investigation of the cellular heterogeneity or tissue composition and therefore must be combined with cell and tissue labelling methods, and/or flow cytometry to distinguish subpopulations. To address cellular heterogeneity of gene/protein expression on a global scale, one should consider single cell omics analysis like scRNAseq. Nonetheless, the cellular constitution can be computationally modelled, even from bulk expression data, if the cell types present in the data are known (354, 355).

The development of techniques for gene and protein expression profiling is very fast, and an increasing number of publications present single-cell analyses, including a growing number of scRNAseq studies of liver cells (11-13, 45, 210, 281, 356-358). At the time of submitting this thesis, no single cell liver proteome studies have been published. scRNAseq has the strength to define developmental trajectories and distinguishing nuances of the cell state and/or cell subpopulations within a complex sample. However, the method still relies on landmark genes (a gene with large variation in scRNAseq data) to define the cellular identity of the cluster or subpopulations or their spatial stratification. As many potential sources could contribute to expression variation in

scRNAseq, not all variations are biologically informative. The data generated in this thesis will be helpful to define and validate such landmark genes to identify LSECs clusters accurately.

Even though mRNAseq and labelled/label-free LC-MS-based methods are highly reliable and reproducible, the outcome is sensitive to the integrity of the library/sample preparations, sequencing depth, coverage, and to some extent to the choice of the computational methods (discussed earlier in section 3.6). In bulk cell analyses the purity of cell preparations is also important. Compromised purity may add unintended factors to the experiments intended to resolve the spectrum of cell type-dependent and/or cell state-specific phenotype. Therefore, all studies in this thesis have put high importance on controlling the purity of the cells. As mentioned in Methods and methodological considerations (section 3.2.3), we further plated the cells and used the fenestrated feature of LSECs to determine the purity of the LSECs by SEM (**papers I, II, and III**). Additionally, cultures were also assessed with immune histochemistry with published cell markers for LSECs, KCs, and HSCs in **papers I and II**.

The use of freshly plated cells instead of cells in suspension has the advantage that plated cultures include only viable cells (*i.e.*, cells that can adhere and spread on the substrate), whereas non-viable cells will be eliminated during washing. Cell plating also allows inspection of cells to assess the quality of the culture in the microscope before RNA/protein harvesting. In **paper I**, we harvested RNA or protein immediately following culture establishment to reduce the extent of culture-induced changes to allow a reliable and comprehensive characterization of LSECs and KCs at a steady state. Cells are also normally attached to other cells and a matrix. However, since plating the cells requires cell suspensions to be brought to normothermic temperature on a non-physiological substrate, the stress of the culture establishment (approximately 30 min-1h) may favour the activation/stress-induced reactions more than in cold cell suspensions (4, 5), and tissue culture plates are not physiological substrates.

Other factors, such as cell dissociation protocols also affect the outcome of the downstream procedures and analyses (7). Studies have shown that the dissociation of cells from tissue induces substantial transcriptomic changes in the cells (4-6). Warm collagenase (37°C) perfusion as used in **papers I, II, and III** has been shown to elicit cell stress responses, especially in scRNAseq protocols (4, 5). At the same time, the warm perfusion protocol used by us generates high-quality, viable single cell suspensions. Fortunately, the due effect of the dissociation protocol is reported to be equivalent across cell types (5), making the comparative study between LSECs and KCs (**paper I**) relevant. However, our finding of a low and variable expression of immune genes among the biological

replicates in both cell types short after plating warrants extra caution regarding activation (see also the discussion in section 5.5). For example, genes such as MHC class I contain heat shock-inducible elements and can be readily induced in response to tissue dissociation by collagenase (5).

Undoubtedly, low abundant genes/proteins present a challenge to the DE analysis. The availability of well-characterized reference genomes of rats (8, 9) and mice (8) provides an advantage for mapping and quantification of short sequencing reads, peptide identification, and DE analysis. Especially for RNAseq data, the reference genome-guided mapping makes the DE outcomes less dependent on the choice of the computational mapping methods (10). Still, one should be vigilant when considering low expressed genes and proteins as their quantifications tend to suffer from low accuracy (10, 11).

5.2 Gene/protein markers of rat LSECs and KCs

In **paper I**, we used the gene/protein expression patterns to accurately discriminate SE-1-MACS purified LSECs from CD11b/c-MACS purified KCs (318). As discussed in the Methods section (3.2.3), SE-1 is a monoclonal antibody reacting specifically against Fc γ RIIb2, constitutively expressed in LSECs (229, 323). Of note, in the human liver, Fc γ RIIb2 present a zone-II-III specific pattern of expression in LSECs (208), different from what we observed in rat LSECs where all sinusoids were positive, whereas other liver endothelia were negative (**paper I** (318)).

The identity of the LSEC and KC samples for the RNAseq experiments was cross-validated against genes/protein signatures corresponding to other sinusoidal cells. For example, the LSEC samples displayed significantly and much higher expression of stabilin-1 and stabilin-2 (STAB1, STAB2), LYVE-1, and VEGFR3 (FLT4), as previously reported for these cells (105, 115, 117, 125, 190, 359, 360) while the KC samples displayed much higher expression of CRIG (VSIG4) and CD11b (ITGAM) (266, 293, 295). Nonetheless, we cannot exclude that the KC population that we analysed was enriched in KCs from the periportal area, as discussed in section 3.2.3 and in **paper I** (318). HSCs markers such as GFAP (Glial fibrillary acidic protein) and DES (Desmin) were consistently very low in the transcriptomes and proteomes of both cell types. Furthermore, the LSEC-specific expression of GATA4 (361) and GPR128 (362) supported the distinct identity of the samples included in the comparative analyses. Additionally, the gene sets enrichment analysis showed overrepresentations of the processes typical for the respective physiological roles of LSECs and KCs (318).

We also included a reanalysis of a previously published microarray study of primary microvascular endothelial cells isolated from different mouse organs, including the liver (58) to validate the results in **paper I** (318). The set of liver endothelial-specific genes from this study (Additional file 9 in **paper I** (318)) supported LSEC-specific expression of CLEC4G, STAB2, and MRC1 (CD206) compared with endothelial cells from other vascular beds, as well as expression of many immune genes. Of note, FcγRIIb2, although expressed abundantly in our LSEC RNAseq and proteomic datasets (**papers I, II, and III**), was not listed among the liver-specific genes in the reanalysed study (58) because FcγRIIb2 expression in spleen endothelium was comparable to that of the liver. Additionally, newly published microarray data from mouse liver also established CLEC4G, STAB2, CD206, and FcγRIIb2 as signature markers of LSECs (233). CLEC4G, STAB2, and FcγRIIb2 were recently also used to differentiate LSECs from other liver endothelial cells in complex scRNAseq datasets from mice and humans (11, 13, 356). In human liver, the expression level of these LSEC signature markers varies along the sinusoids, which have been used to define zone-specific populations of LSECs (11, 13, 208). In addition, some LSEC markers also highlight species differences. For instance, CD36 is expressed at very low density in rat LSECs compared to KCs, in contrast to human LSECs where CD36 is regarded as a good marker (208).

The expression of the pan-leukocyte marker CD45 in LSECs across species is controversial. LSECs derived from mouse and human healthy livers presumably do not express CD45 (16, 207). Hence, the depletion of CD45⁺ cells from NPC suspensions results in LSEC enrichment. Intriguingly, CD45 is reported in rat LSECs, with the highest expression in LSECs of hepatic zone I and low/intermediate in zone II (207). We also observed mRNA and protein evidence for CD45 expression in the bulk omics data from rat and mouse LSECs, albeit the abundance was low (**papers I** (318) and **III**). We, therefore, could not conclude if the observed expression was because of weak expression across all LSECs, a small LSEC subpopulation expressing CD45 at a high level, or KC contamination. Immune staining of frozen rat liver sections was not sensitive enough to unambiguously demonstrate LSEC staining. We therefore did flow cytometry, which allows immunophenotyping of non-parenchymal liver cells at the single cell level. The flow cytometric analyses suggested CD45 expression in a minor subpopulation of LSECs (approximately 5% of the LSECs analysed). The expression was, however, far lower than reported previously in the same rat model (207). To eliminate circulating leukocytes (CD45⁺), we used two endothelial markers, the LSEC-specific SE-1, and CD31 (general endothelial cell marker), along with the CD45 marker. scRNAseq studies, as well, do not exclude CD45 expression on mouse and human LSECs, as a low level of its transcripts can be detected in most clusters purported to be LSECs (13). Moreover, the suggested mixed ontogeny of the LSEC

populations indicates that a larger fraction of the LSEC population share common erythromyeloid progenitors with myeloid cells making the CD45 expression may not be surprising (209, 251, 252).

5.3 Complementary scavenging and immune functions between LSECs and KCs

In **paper I**, we presented that both LSECs and KCs from healthy rats express numerous genes/proteins associated with immune functions, albeit at a low level.

As discussed in 5.1 genes/proteins expressed at very low density pose challenges for accurate quantification. It also warrants caution about the sources and the interpretation of results. A minor contribution of other liver cell types cannot be totally excluded when using MACS isolation. However, the contribution due to cross-contamination is likely to be infinitesimally small when the proportional difference in expression of the genes/proteins of interest is itself low between compared samples (363). In such instances, the amplitude of the proportional difference in expression of low expressed genes and the variation in expression within the cell types provides more relevant information about biological differences than the quantified expression level alone. Our findings in LSECs corroborate and also validate results from functional studies in mice that suggest that LSEC have important roles in liver immunity by cross-presenting endocytosed exogenous antigen to CD8⁺ T cells via major histocompatibility complex (MHC) class I (64, 131, 154-157, 159, 364).

In **paper I**, we additionally catalogued the expression of a wide array of SRs, C-type lectins, and TLRs in rat LSECs and KCs. Some of those SRs and C-type lectins show differential expression between LSECs and KCs. These receptors are involved in the clearance of immunogens (foreign or endogenously modified) that protect against undue immune activations or damages. Moreover, given the promiscuous nature of SRs towards their ligands, preferential cell type-specific expression of some SRs may also be a complementary mechanism to ensure the highly efficacious scavenging activity that goes on in the liver sinusoids. Redundancy in SR functions has been demonstrated for stabilin-1 and stabilin-2 in LSECs, where both had to be deleted to produce phenotypic changes in organs (122, 365).

High expression of SRs and C-type lectins in LSECs was also evident in **paper II** in rats and **paper III** in mice. Furthermore, the transcriptomic and proteomics data from **papers I, II, and III** illustrated the expression of genes/proteins associated with exogenous antigen uptake, processing, and presentation machinery, which gives support to the previous literature on the ability of LSECs to induce naïve T cells (CD4⁺ and CD8⁺) activation (155-162)..

5.4 LSECs *in vitro* display an activated, pro-inflammatory phenotype

Data from **papers II** and **III** highlighted the elevated expression of pro-inflammatory cytokines including IL-6, IL-1 β , MCP1 (CCL2), and MCP3 (CCL7) and various CAMs, including selectins (SELE, SELP), ICAM-1, and VCAM-1 in cultured LSECs, reflecting early activation of LSECs in primary culture even in the absence of added stimulants (IL-1 β , **paper II**). In addition, the observed upregulation of MHC class I histocompatibility antigens in the LSEC proteomes from both rat and mouse, despite differences in purification protocols and cell culture medium in the two studies, further supports the notion that LSECs are activated in primary culture. Given that LSECs are exposed to various non-physiological factors and stimuli during tissue dissociation, cell isolation, and culture establishment as discussed in section 5.1, and lack quiescence promoting signals from other liver cells, the activation of LSECs during culture may not be surprising after all.

The sign of culture-induced activation was evident also in the rat LSEC transcriptome dataset derived from very fresh LSEC cultures in **paper I**, although not emphasized in the paper (318), where we found enrichment of the hallmark gene set “TNF α mediated NF- κ B signalling activation [GeneID=7124]” in LSECs compared with KCs, consistent with the activation reported in **papers II** and **III**.

5.5 Dexamethasone attenuates LSEC activation

Glucocorticoids, like dexamethasone, abrogate TNF α - or sepsis-induced endothelial cell activation (366, 367). However, the dexamethasone effect, be it via a single gene or via pathways and processes, depends on cell type and may evoke disparate magnitude or direction of response on different cell types (368). The details about the effect of dexamethasone on LSECs are limited (312, 369-371) despite its popularity in the treatment of immune-inflammatory hepatic and extrahepatic diseases (372, 373).

Both **papers II** and **III** showed an immunosuppressive role of dexamethasone on LSECs *in vitro*, indicated by diminished expression of CAMs, downregulation of pro-inflammatory cytokines, and immune regulatory and inflammatory pathways in the cells. This has also been reported in other endothelial cells where dexamethasone attenuates the expression of CAMs to reduce recruitment and extravasation of leukocytes to the site of inflammation (374). The suppression of pro-inflammatory cytokines and the attenuation of cytokine-cytokine receptor signalling (374) contributes to the immune-suppressive action of dexamethasone. Cytokines are small proteins that cells deploy to propagate signals and modulate cell responses to activation of PRRs by pathogen-associated or

danger-associated molecular patterns (374). Congruently, the supernatants from rat LSECs cultured with dexamethasone for 24 h (**paper II**) displayed significantly lower pro-inflammatory cytokines levels in contrast to the supernatant from non-treated LSECs. Generally, the immunosuppressive effect of dexamethasone is chiefly due to trans-repression of NF- κ B and AP1-mediated transcription and upregulation of anti-inflammatory genes (374). In addition to diminished expression of CAMs and pro-inflammatory cytokines, the data in **papers II** and **III** also suggest diminished NF- κ B induction during culture in the presence of dexamethasone corroborated by the downregulation of the transcription factors NFKB1 (NF- κ B1, p105) and NFKB2 (NF- κ B2, p100).

Interestingly, the proteomics data in **paper III** showed time-dependent downregulation of the glucocorticoid receptor (NR3C1) in LSECs *in vitro*, regardless of treatment. The presence of dexamethasone in culture further decreased the NR3C1 abundance. Several factors affect the protein turnover apart from the transcription and translation processes, including protein degradation. Notably, in various cell lines, including PC12 (dexamethasone dose: 20 μ M), and COS-1 (dexamethasone dose: 100nM), dexamethasone-induced proteasome-mediated degradation of NR3C1 was observed (375-377), which may lead to dexamethasone resistance over time in culture. From this, it may be that it is better to use dexamethasone early in culture establishment to avoid the initial culture-induced activation, rather than to use it continuously during culture.

5.6 LSEC showed a shift in metabolism in culture

Recent publications are increasingly showing a correlation between changes in metabolism with changes in cell phenotype (378-381). The metabolic shift that we observed in cultured rat and mouse LSECs may be due to the activated cell phenotype *in vitro* but the altered metabolism may also have triggered cell activation, similar to what is reported in macrophages (380, 381). Accordingly, activated proliferating endothelial cells in response to angiogenic stimuli substantially augmented the glycolytic activity compared with quiescent endothelial cells (382, 383). Furthermore, the *in vitro* induced metabolic alteration is not limited to LSECs but also reported in hepatocytes *in vitro* (227). However, the available data, including the data presented in this thesis, could not discriminate or confirm the association between activation and metabolism, and is therefore, merely presented as a consequence of culturing in **papers II** and **III**.

Paper II underscored the downregulation of proteins involved in fatty acid and branched-chain amino acid degradation and indicated diminished oxidative phosphorylation in rat LSECs at 24 h compared to 2 h post-seeding. The data from mouse LSECs (**paper III**), which included data from 1, 10 and 48 h post-seeding supported the *in vitro* induced decrease in fatty acid and branched-chain amino acid

degradation at 48 h. The observed elevated glycolysis may be a compensatory response to the loss in TCA and oxidative phosphorylation.

Intriguingly, the results from **papers II and III** suggest a slightly differential metabolic response in rat and mouse LSECs as a result of dexamethasone treatment. In rats, dexamethasone repressed the culture-induced increase in the expression of some glycolytic enzymes in the cell-associated LSEC proteome at 24 h. In mice, comparisons between the time-matched proteomes of non-treated and dexamethasone-treated LSECs showed an elevated expression of major rate-limiting glycolytic enzymes at 48 h in cultures with dexamethasone, whereas at 10 h pathways associated with glucose metabolism was repressed with dexamethasone (not evident at protein level at this time point). These differences may chiefly reflect differences in time-dependent responses or could in part be the species differences. Despite differences between the two studies regarding cell purification protocols, substrate coating (type-1 collagen used for rat LSECs and fibronectin for mouse), culture medium (DMEM-based medium used for rat and AIM-V for mouse LSECs), and dose of dexamethasone used (1 $\mu\text{g}/\text{ml}$ (=2.5 μM) used in rat and 1 μM in mouse cultures) the dexamethasone effect on LSECs seems to be conserved between rats and mice.

Notably, the knowledge about the metabolism of LSECs *in vivo* is limited. A report suggested that LSECs predominately generate ATPs from glycolysis, glutamine, and palmitate oxidation (384). Moreover, it has been suggested that LSECs metabolism is chiefly anaerobic and generates the required ATPs and other biosynthetic precursors from catabolic conversion of monosaccharides or amino acids into lactate or acetate (385). Interestingly, LSECs may also generate their glycolytic substrate from endolysosomal degradation of various endocytosed macromolecules as they are highly active scavenger cells (89, 90, 385). The endolysosomal products contain monosaccharides and many gluconeogenic amino acids (385). However, glycolysis generates comparatively lower amounts of ATPs but protects endothelial cells from oxidative damage by reducing the production of reactive oxygen species compared with mitochondrial oxidative phosphorylation (383). In general, the more oxygen-independent metabolism of endothelial also enables them to vascularize regions deprived of oxygen (383).

Although not emphasized in **paper I** (318), the comparative analyses of the transcriptomics and proteomics data generated a significant enrichment of hallmark genes/proteins of oxidative phosphorylation and fatty acid oxidation in the KC data compared with LSECs'. Interestingly, a previously published study reported high expression of proteins associated with oxidative phosphorylation and fatty acid oxidation in KCs compared to monocytes (386). Not least, studies

have shown that a high level of oxidative phosphorylation is characteristic of M2 polarized macrophages and regulatory T cells (380, 381).

5.7 Dexamethasone improves LSEC survival in cultures

One major challenge associated with the studies of LSECs in *in vitro* systems is the rapid loss of cells in culture. Both studies showed a time-dependent increase in LSEC death in culture. In **paper II**, we used live/dead cell imaging and cell counts to estimate cell death, and we also checked for the differential level of ribosomes and histones released into the supernatant (387). In **paper III**, we used a caspase activity assay and the average expressions of the proteins associated with various cell death modalities defined in the Cancer Proteomics Database to determine the cause of cell loss. This showed activation of apoptosis, pyroptosis, and autophagy. The latter may also be a protective response (187, 188).

Dexamethasone significantly improved LSEC survival *in vitro*. Elevated expression of anti-apoptotic proteins and diminished expression of pro-apoptotic proteins in the presence of dexamethasone may, in part, be the reason for the observed pro-survival effect of LSECs, as also reported in rat and human hepatocytes (388). Dexamethasone significantly abrogated FasL-induced apoptosis in LSECs (**paper III**) as reported in various cancerous cells (389, 390), and significantly reduced the expression of TNFRSF10B, reflecting the enhanced survival and better confluency of the cultures.

Pro-survival effect of dexamethasone *in vitro* is reported to be dose-dependent and cell type-specific (391-393). For instance, dexamethasone reduces the viability of thymocytes and T cells *in vitro* while showing a biphasic effect on osteoblast viability *in vitro*, with low doses (1-10 nM) promoting survival and doses $\geq 1 \mu\text{M}$ inducing cell death (391-393). In our study dexamethasone was well tolerated by LSECs even in high doses (up to 100 μM , **paper III**) for at least 48 h.

5.8 Effects of dexamethasone on LSEC morphology *in vitro*

LSEC cultures, in the presence of dexamethasone, exhibited better confluency and had cells with less membrane ruffling and smoother cell borders compared to non-treated cultures (**papers II and III**). Long-term (5 days) dexamethasone-treated mouse LSEC cultures still displayed some cells with preserved sieve plates, whereas the cells without dexamethasone were nearly totally defenestrated at this time point. Nonetheless, LSEC sieve plates disappeared over time *in vitro* also in the presence of dexamethasone. Loss of LSEC fenestrae *in vitro* and during the progression of diverse hepatic diseases is a well-known phenotypic alteration in the cells (15, 16, 21, 26, 63).

To understand the fenestration loss, one should consider the non-physiological monocellular culture system. *In vitro*, LSECs lose their native physiological microenvironment comprising the heterotypic cell-cell interactions, paracrine and endocrine factors and loss of fenestrae has often been correlated with diminished VEGF (234) and activated Hedgehog signalling (394). Interestingly, our results did not reveal any culture/treatment-induced pathway-level changes in VEGF or Hedgehog signalling but we found a consistent downregulation of VEGF receptors (KDR and FLT4, **paper III**), which may pose a challenge when trying to use VEGF to improve LSEC fenestration in culture.

In addition, the mouse study (**paper III**) showed significant downregulation of GATA4 *in vitro*, a suggested master regulator of the LSEC phenotype (361, 395). The data also showed the downregulation of endothelial nitric oxide synthase (eNOS), reflecting compromised NO-sGC-cGMP signalling (nitric oxide (NO), soluble guanylate cyclase (sGC), and cyclic guanosine monophosphate (cGMP), crucial for maintaining LSEC fenestrae *in vivo* and *in vitro* (396). In addition, we did not observe BMP-9 expression (also linked to normal LSEC fenestration (223)), either in the supernatant of cultured rat LSECs (**paper II**) or in the cell-associated proteomes of rat and mouse LSECs.

5.9 Culture-induced changes in LSEC endocytosis and effects of dexamethasone

In accordance with (43, 397), we found that LSECs rapidly decreased their endocytic capacity for the SR ligand FSA in culture, with a marked decrease in the maximum capacity of ligand uptake per cell at 48h (**paper III**). This was further reflected in the observed downregulation in LSECs of several endocytosis receptors and various components of the endocytic machinery (**papers II and III**). Dexamethasone slightly abrogated the time-dependent downregulation of some SRs and C-type lectins but this effect on protein expression was not sufficient to preserve the LSEC endocytic capacity for FSA.

However, the presence of dexamethasone LSECs showed efficient uptake of trace amount of ¹²⁵I-FSA for a longer time in culture compared to non-treated cells (**papers II and III**). A direct cause-effect relationship between dexamethasone treatment and endocytosis could not be established in these experiments given that the higher uptake of ¹²⁵I-FSA with dexamethasone could merely be explained by improved LSEC survival in culture.

LSECs cultured with dexamethasone were less activated compared to the non-treated time-matched controls, which may also have influenced the outcome of the endocytosis experiments. Interestingly, previous studies in rat LSECs showed that a short treatment (6 h) with LPS and the pro-inflammatory

cytokines IL-1 β and TNF α markedly increased mannose receptor-mediated and SR-mediated endocytosis of radioiodinated ligands, while treatment for 24 h was counterproductive for endocytosis (313). The authors also reported that dexamethasone diminished the negative effect of IL-1 β on rat LSECs at 24 h and enhanced the rate of ligand uptake at this time point (312). Of note, IL-10 treatment significantly decreased mannose receptor-mediated endocytosis in LSECs *in vitro* (161). In the present proteomics study, dexamethasone increased IL-10 expression in LSECs, and this may have counteracted any positive effects of dexamethasone on LSEC endocytosis via other mechanisms. In conclusion, more studies are needed to fully understand the effects of dexamethasone on the LSEC scavenger function.

5.10 Changes in transcription factors and regulators in LSECs during culture

LSEC specific knockout of GATA4 established the critical importance of GATA4 for LSEC development and phenotype (361). Furthermore, ectopic addition of GATA4 in other endothelial cells elevates LSEC-associated gene expression (233, 361). Apart from GATA4, several other transcription factors (TFs) such as LMO3, MEIS2, and c-MAF have been added to the list of essential TFs for maintaining the LSECs differentiated phenotype and functions (233, 361). The proteomic analyses in **paper III** showed a time-dependent downregulation of GATA4 irrespective of dexamethasone treatment, corresponding with the time-dependent dedifferentiation of LSECs *in vitro*, confirming the previous studies (228, 233).

Paper III tabulated additional TFs such as NOTCH1, NR3C1, IRF9, FOXO1 that likely also mediate LSEC dedifferentiation or phenotypic changes *in vitro* or cause reduced viability *in vitro*. For instance, deregulation of NOTCH signalling was reported to induce loss of LSEC-specific gene expression, decrease fenestration, and elevated the deposition of basal lamina in space of Disse (195). The study also revealed an association between the number of LSECs positive for NIC (intracellular NOTCH signalling domain) and liver cirrhosis in humans (195).

The TFs predicted as vital for LSEC phenotype and functions in this thesis are, however, based purely on the transcriptome and proteome data of cultured LSECs obtained from rat and mouse liver perfusions. Therefore, the role of these TFs needs to be validated primarily utilizing both gain-of-function and loss-of-function experiments in animal models and culture systems. Our finding that mouse LSECs can be maintained for prolonged periods in AIM-V in a 5% O₂ atmosphere may allow in transfection studies to validate these TFs.

6 Concluding remarks

In conclusion, we implemented a comparative approach for comprehensive molecular characterization of rat LSECs and KCs with good resolution between these two cell types in the **paper I**. The evidence from the **paper I** did not just illustrate overlapping phenotypic attributes between LSECs and KCs but also complementary scavenging and immune functions. High and, to some extent, disparate expression of SRs and c-type lectins in LSECs and KCs affirm the complementary immune functions of LSECs and KCs. Our study highlights the importance of considering both cells in studies of liver immunity. Of note, comparative studies in different animal models at steady-state and pathophysiological conditions are still essential to identify inter-species differences, phenotypic changes in LSECs (and KCs) in pathophysiological conditions, and the role of LSECs in the pathogenesis of liver diseases.

In **papers II** and **III**, we report that rat and mouse LSECs in culture acquire an inflammatory-like phenotype. The cultured LSECs displayed enhanced expression of pro-inflammatory cytokines and cell adhesion molecules. Dexamethasone treatment significantly abrogated the inflammatory-like phenotype of LSECs, endowing the cultures with a more quiescent phenotype. **Paper III** provides a detailed overview of the dexamethasone effects on LSECs. In addition, both studies support pro-survival effects of dexamethasone on rat and mouse LSECs in cultures in the doses tested, but dexamethasone alone was insufficient to maintain the LSECs differentiated phenotype *in vitro*.

In addition, these studies also catalogued the differentially expressed proteins and TFs involved in culture-induced changes in LSECs *in vitro* and the response to dexamethasone. These studies also predicted and supported the imperative role of GATA4, NR3C1, and other TFs in sustaining the expression of LSEC signature genes/proteins (228, 233), indicating a concomitant time-dependent decrease in these TFs and LSEC signature genes/proteins. Maintaining NR3C1 and GATA4 expression *in vitro* may improve the culture fitness and prevent the time-dependent deterioration of the LSEC phenotype *in vitro*.

Of note, care should be taken when using long-term cultures of LSECs since gene expression is significantly altered over time in LSEC cultures, both in rats and mice ((228, 233), **papers II** and **III**).

Works cited

1. Ross MH. *Histology : a text and atlas : with correlated cell and molecular biology*. 6th ed. ed. Pawlina W, editor. Philadelphia: Wolters Kluwer/Lippincott Williams & Wilkins Health; 2011.
2. Casotti V, D'Antiga L. Basic Principles of Liver Physiology. In: D'Antiga L, editor. *Pediatric Hepatology and Liver Transplantation*. Cham: Springer International Publishing; 2019. p. 21-39.
3. Kubes P, Jenne C. Immune Responses in the Liver. *Annu Rev Immunol*. 2018;36(1):247-77.
4. Michalopoulos GK, Bhushan B. Liver regeneration: biological and pathological mechanisms and implications. *Nat Rev Gastroenterol Hepatol*. 2021;18(1):40-55.
5. McCuskey RS. The hepatic microvascular system in health and its response to toxicants. *Anat Rec* 2008;291(6):661-71.
6. Shami GJ, Cheng D, Huynh M, Vreuls C, Wisse E, Braet F. 3-D EM exploration of the hepatic microarchitecture - lessons learned from large-volume in situ serial sectioning. *Sci Rep*. 2016;6:36744.
7. Wisse E. An electron microscopic study of the fenestrated endothelial lining of rat liver sinusoids. *J Ultrastruct Res*. 1970;31(1):125-50.
8. Wisse E. An ultrastructural characterization of the endothelial cell in the rat liver sinusoid under normal and various experimental conditions, as a contribution to the distinction between endothelial and Kupffer cells. *J Ultrastruct Res*. 1972;38(5-6):528-62.
9. Wisse E, De Zanger RB, Jacobs R, McCuskey RS. Scanning electron microscope observations on the structure of portal veins, sinusoids and central veins in rat liver. *Scan Electron Microsc*. 1983(Pt 3):1441-52.
10. Nagy P, Thorgeirsson SS, Grisham JW. *Organizational Principles of the Liver*. The Liver2020. p. 1-13.
11. MacParland SA, Liu JC, Ma XZ, Innes BT, Bartczak AM, Gage BK, et al. Single cell RNA sequencing of human liver reveals distinct intrahepatic macrophage populations. *Nat Commun*. 2018;9(1):4383.
12. Ramachandran P, Dobie R, Wilson-Kanamori JR, Dora EF, Henderson BEP, Luu NT, et al. Resolving the fibrotic niche of human liver cirrhosis at single-cell level. *Nature*. 2019;575(7783):512-8.
13. Aizarani N, Saviano A, Sagar, Maily L, Durand S, Herman JS, et al. A human liver cell atlas reveals heterogeneity and epithelial progenitors. *Nature*. 2019;572(7768):199-204.
14. Elvevold K, Smedsrød B, Martinez I. The liver sinusoidal endothelial cell: a cell type of controversial and confusing identity. *Am J Physiol Gastrointest Liver Physiol*. 2008;294(2):G391-400.
15. Gracia-Sancho J, Caparros E, Fernandez-Iglesias A, Frances R. Role of liver sinusoidal endothelial cells in liver diseases. *Nat Rev Gastroenterol Hepatol*. 2021.
16. DeLeve LD, Maretta-Mira AC. Liver Sinusoidal Endothelial Cell: An Update. *Semin Liver Dis*. 2017;37(4):377-87.
17. Sørensen KK, McCourt P, Berg T, Crossley C, Le Couteur D, Wake K, et al. The scavenger endothelial cell: a new player in homeostasis and immunity. *Am J Physiol Regul Integr Comp Physiol*. 2012;303(12):R1217-30.
18. Seternes T, Sørensen K, Smedsrød B. Scavenger endothelial cells of vertebrates: a nonperipheral leukocyte system for high-capacity elimination of waste macromolecules. *Proc Natl Acad Sci U S A*. 2002;99(11):7594-7.
19. Smedsrød B, Pertoft H, Gustafson S, Laurent TC. Scavenger functions of the liver endothelial cell. *Biochem J*. 1990;266(2):313-27.
20. Smedsrød B, Eriksson S, Fraser JRE, Laurent TC, Pertoft H. Properties of liver endothelial cells in primary monolayer cultures. *Sinusoidal Liver Cells*. Amsterdam, The Netherlands: Elsevier; 1982. p. 263-70.
21. Poisson J, Lemoinne S, Boulanger C, Durand F, Moreau R, Valla D, et al. Liver sinusoidal endothelial cells: Physiology and role in liver diseases. *J Hepatol*. 2017;66(1):212-27.
22. Sørensen KK, Smedsrød B. The Liver Sinusoidal Endothelial Cell. *The Liver2020*. p. 422-34.
23. Meyer J, Gonelle-Gispert C, Morel P, Buhler L. Methods for Isolation and Purification of Murine Liver Sinusoidal Endothelial Cells: A Systematic Review. *PLoS One*. 2016;11(3):e0151945.
24. Morin O, Normand C. Long-term maintenance of hepatocyte functional activity in co-culture: requirements for sinusoidal endothelial cells and dexamethasone. *J Cell Physiol*. 1986;129(1):103-10.
25. Pertoft H, Smedsrød B. Separation and Characterization of Liver Cells. In: Pretlow TG, Pretlow TP, editors. *Cell Separation*: Academic Press; 1987. p. 1-24.

26. Sørensen KK, Simon-Santamaria J, McCuskey RS, Smedsrød B. Liver Sinusoidal Endothelial Cells. *Compr Physiol*. 2015;5(4):1751-74.
27. Kawai Y, Smedsrød B, Elvevold K, Wake K. Uptake of lithium carmine by sinusoidal endothelial and Kupffer cells of the rat liver: new insights into the classical vital staining and the reticulo-endothelial system. *Cell Tissue Res*. 1998;292(2):395-410.
28. Wake K, Kawai Y, Smedsrød B. Re-evaluation of the reticulo-endothelial system. *Ital J Anat Embryol*. 2001;106(2 Suppl 1):261-9.
29. Maynard RL, Downes N. Liver. In: Maynard RL, Downes N, editors. *Anatomy and Histology of the Laboratory Rat in Toxicology and Biomedical Research*: Academic Press; 2019. p. 159-68.
30. Carotti S, Morini S, Carpino G, Gaudio E. Liver Histology. In: Radu-Ionita F, Pyrsopoulos NT, Jinga M, Tintoiu IC, Sun Z, Bontas E, editors. *Liver Diseases*. Cham: Springer International Publishing; 2020. p. 17-28.
31. Kiernan F. The Anatomy and Physiology of the Liver. *Philos Trans R Soc*. 1833;123:711-70.
32. Morales-Navarrete H, Nonaka H, Scholich A, Segovia-Miranda F, de Back W, Meyer K, et al. Liquid-crystal organization of liver tissue. *Elife*. 2019;8:e44860.
33. Teutsch HF. The modular microarchitecture of human liver. *Hepatology*. 2005;42(2):317-25.
34. Mall FP. A study of the structural unit of the liver. *Am J Anat*. 1906;5(3):227-308.
35. Rappaport AM, Borowy ZJ, Loughheed WM, Lotto WN. Subdivision of hexagonal liver lobules into a structural and functional unit; role in hepatic physiology and pathology. *Anat Rec*. 1954;119(1):11-33.
36. Lamers WH, Hilberts A, Furt E, Smith J, Jonges GN, van Noorden CJ, et al. Hepatic enzymic zonation: a reevaluation of the concept of the liver acinus. *Hepatology*. 1989;10(1):72-6.
37. Bonnardel J, T'Jonck W, Gaublomme D, Browaeys R, Scott CL, Martens L, et al. Stellate Cells, Hepatocytes, and Endothelial Cells Imprint the Kupffer Cell Identity on Monocytes Colonizing the Liver Macrophage Niche. *Immunity*. 2019;51(4):638-54 e9.
38. Wisse E. Ultrastructure and function of Kupffer cells and other sinusoidal cells in the liver. *Med Chir Dig*. 1977;6(7):409-18.
39. Nakata K, Leong GF, Brauer RW. Direct measurement of blood pressures in minute vessels of the liver. *Am J Physiol*. 1960;199:1181-8.
40. Goresky CA. A linear method for determining liver sinusoidal and extravascular volumes. *Am J Physiol*. 1963;204:626-40.
41. Maass-Moreno R, Rothe CF. Distribution of pressure gradients along hepatic vasculature. *Am J Physiol*. 1997;272(6 Pt 2):H2826-32.
42. Tsukada K, Suematsu M. Visualization and analysis of blood flow and oxygen consumption in hepatic microcirculation: application to an acute hepatitis model. *J Vis Exp*. 2012(66):e3996.
43. Martinez I, Nedredal GI, Oie CI, Warren A, Johansen O, Le Couteur DG, et al. The influence of oxygen tension on the structure and function of isolated liver sinusoidal endothelial cells. *Comp Hepatol*. 2008;7:4.
44. Kietzmann T. Metabolic zonation of the liver: The oxygen gradient revisited. *Redox Biol*. 2017;11:622-30.
45. Halpern KB, Shenhav R, Matcovitch-Natan O, Tóth B, Lemze D, Golan M, et al. Single-cell spatial reconstruction reveals global division of labour in the mammalian liver. *Nature*. 2017;542:352.
46. Ma R, Martinez-Ramirez AS, Borders TL, Gao F, Sosa-Pineda B. Metabolic and non-metabolic liver zonation is established non-synchronously and requires sinusoidal Wnts. *Elife*. 2020;9:e46206.
47. Ben-Moshe S, Itzkovitz S. Spatial heterogeneity in the mammalian liver. *Nat Rev Gastroenterol Hepatol*. 2019;16(7):395-410.
48. Kietzmann T. Liver Zonation in Health and Disease: Hypoxia and Hypoxia-Inducible Transcription Factors as Concert Masters. *Int J Mol Sci*. 2019;20(9):2347.
49. Cheng X, Kim SY, Okamoto H, Xin Y, Yancopoulos GD, Murphy AJ, et al. Glucagon contributes to liver zonation. *Proc Natl Acad Sci U S A*. 2018;115(17):E4111-E9.
50. Jungermann K, Katz N. Functional specialization of different hepatocyte populations. *Physiol Rev*. 1989;69(3):708-64.
51. Vollmar B, Menger MD. The hepatic microcirculation: mechanistic contributions and therapeutic targets in liver injury and repair. *Physiol Rev*. 2009;89(4):1269-339.
52. Karschau J, Scholich A, Wise J, Morales-Navarrete H, Kalaidzidis Y, Zerial M, et al. Resilience of three-dimensional sinusoidal networks in liver tissue. *PLoS Comput Biol*. 2020;16(6):e1007965.

53. Liebig M, Hassanzada A, Kammerling M, Genz B, Vollmar B, Abshagen K. Microcirculatory disturbances and cellular changes during progression of hepatic steatosis to liver tumors. *Exp Biol Med.* 2018;243(1):1-12.
54. Fan J, Chen CJ, Wang YC, Quan W, Wang JW, Zhang WG. Hemodynamic changes in hepatic sinusoids of hepatic steatosis mice. *World J Gastroenterol.* 2019;25(11):1355-65.
55. Ehrlich A, Duche D, Ouedraogo G, Nahmias Y. Challenges and Opportunities in the Design of Liver-on-Chip Microdevices. *Annu Rev Biomed Eng.* 2019;21:219-39.
56. Aird WC. Endothelial cell heterogeneity. *Cold Spring Harb Perspect Med.* 2012;2(1):a006429.
57. Potente M, Makinen T. Vascular heterogeneity and specialization in development and disease. *Nat Rev Mol Cell Biol.* 2017;18(8):477-94.
58. Nolan DJ, Ginsberg M, Israely E, Palikuqi B, Poulos MG, James D, et al. Molecular signatures of tissue-specific microvascular endothelial cell heterogeneity in organ maintenance and regeneration. *Dev Cell.* 2013;26(2):204-19.
59. Itkin T, Gur-Cohen S, Spencer JA, Schajnovitz A, Ramasamy SK, Kusumbe AP, et al. Distinct bone marrow blood vessels differentially regulate haematopoiesis. *Nature.* 2016;532(7599):323-8.
60. Jambusaria A, Hong Z, Zhang L, Srivastava S, Jana A, Toth PT, et al. Endothelial heterogeneity across distinct vascular beds during homeostasis and inflammation. *Elife.* 2020;9:e51413.
61. Geraud C, Evdokimov K, Straub BK, Peitsch WK, Demory A, Dorflinger Y, et al. Unique cell type-specific junctional complexes in vascular endothelium of human and rat liver sinusoids. *PLoS One.* 2012;7(4):e34206.
62. Naito M, Wisse E. Filtration effect of endothelial fenestrations on chylomicron transport in neonatal rat liver sinusoids. *Cell Tissue Res.* 1978;190(3):371-82.
63. Cogger VC, Hunt NJ, Le Couteur DG. Fenestrations in the Liver Sinusoidal Endothelial Cell. *The Liver2020.* p. 435-43.
64. Shetty S, Lalor PF, Adams DH. Liver sinusoidal endothelial cells - gatekeepers of hepatic immunity. *Nat Rev Gastroenterol Hepatol.* 2018;15(9):555-67.
65. Braet F, Wisse E. Structural and functional aspects of liver sinusoidal endothelial cell fenestrae: a review. *Comp Hepatol.* 2002;1(1):1.
66. Auvinen K, Lokka E, Mokkalä E, Jappinen N, Tyystjarvi S, Saine H, et al. Fenestral diaphragms and PLVAP associations in liver sinusoidal endothelial cells are developmentally regulated. *Sci Rep.* 2019;9(1):15698.
67. Wisse E, De Zanger RB, Charels K, Van Der Smissen P, McCuskey RS. The liver sieve: considerations concerning the structure and function of endothelial fenestrae, the sinusoidal wall and the space of Disse. *Hepatology.* 1985;5(4):683-92.
68. Horn T, Henriksen JH, Christoffersen P. The sinusoidal lining cells in "normal" human liver. A scanning electron microscopic investigation. *Liver.* 1986;6(2):98-110.
69. Fraser R, Bosanquet AG, Day WA. Filtration of chylomicrons by the liver may influence cholesterol metabolism and atherosclerosis. *Atherosclerosis.* 1978;29(2):113-23.
70. Wright PL, Smith KF, Day WA, Fraser R. Small liver fenestrae may explain the susceptibility of rabbits to atherosclerosis. *Arteriosclerosis.* 1983;3(4):344-8.
71. Wright PL, Clemett JA, Smith KF, Day WA, Fraser R. Hepatic sinusoidal endothelium in goats. *Aust J Exp Biol Med Sci.* 1983;61 (Pt 6):739-41.
72. Wright PL, Smith KF, Day WA, Fraser R. Hepatic sinusoidal endothelium in sheep: an ultrastructural reinvestigation. *Anat Rec.* 1983;206(4):385-90.
73. Fraser R, Day WA, Fernando NS. The liver sinusoidal cells. Their role in disorders of the liver, lipoprotein metabolism and atherogenesis. *Pathology.* 1986;18(1):5-11.
74. Fraser R, Heslop VR, Murray FE, Day WA. Ultrastructural studies of the portal transport of fat in chickens. *Br J Exp Pathol.* 1986;67(6):783-91.
75. Fraser R, Dobbs BR, Rogers GW. Lipoproteins and the liver sieve: the role of the fenestrated sinusoidal endothelium in lipoprotein metabolism, atherosclerosis, and cirrhosis. *Hepatology.* 1995;21(3):863-74.
76. Fraser R, Cogger VC, Dobbs B, Jamieson H, Warren A, Hilmer SN, et al. The liver sieve and atherosclerosis. *Pathology.* 2012;44(3):181-6.

77. Simon-Santamaria J, Malovic I, Warren A, Oteiza A, Le Couteur D, Smedsrød B, et al. Age-related changes in scavenger receptor-mediated endocytosis in rat liver sinusoidal endothelial cells. *J Gerontol A Biol Sci Med Sci*. 2010;65(9):951-60.
78. Cogger VC, Warren A, Fraser R, Ngu M, McLean AJ, Le Couteur DG. Hepatic sinusoidal pseudocapillarization with aging in the non-human primate. *Exp Gerontol*. 2003;38(10):1101-7.
79. McLean AJ, Cogger VC, Chong GC, Warren A, Markus AM, Dahlstrom JE, et al. Age-related pseudocapillarization of the human liver. *J Pathol*. 2003;200(1):112-7.
80. Le Couteur DG, Fraser R, Cogger VC, McLean AJ. Hepatic pseudocapillarisation and atherosclerosis in ageing. *Lancet*. 2002;359(9317):1612-5.
81. Le Couteur DG, Cogger VC, Markus AM, Harvey PJ, Yin ZL, Ansellin AD, et al. Pseudocapillarization and associated energy limitation in the aged rat liver. *Hepatology*. 2001;33(3):537-43.
82. Le Couteur DG, Warren A, Cogger VC, Smedsrød B, Sørensen KK, De Cabo R, et al. Old age and the hepatic sinusoid. *Anat Rec*. 2008;291(6):672-83.
83. Cogger VC, O'Reilly JN, Warren A, Le Couteur DG. A standardized method for the analysis of liver sinusoidal endothelial cells and their fenestrations by scanning electron microscopy. *J Vis Exp*. 2015;2015(98):e52698.
84. Zapotoczny B, Szafranska K, Kus E, Braet F, Wisse E, Chlopicki S, et al. Tracking Fenestrae Dynamics in Live Murine Liver Sinusoidal Endothelial Cells. *Hepatology*. 2019;69(2):876-88.
85. Popescu D, Movileanu L, Ion S, Flonta ML. Hydrodynamic effects on the solute transport across endothelial pores and hepatocyte membranes. *Phys Med Biol*. 2000;45(11):N157-65.
86. Gieling RG, Ruijter JM, Maas AA, Van Den Bergh Weerman MA, Dingemans KP, ten Kate FJ, et al. Hepatic response to right ventricular pressure overload. *Gastroenterology*. 2004;127(4):1210-21.
87. Smedsrød B. Clearance function of scavenger endothelial cells. *Comp Hepatol*. 2004;3 Suppl 1(SUPPL. 1):S22.
88. Pearse BM. Clathrin: a unique protein associated with intracellular transfer of membrane by coated vesicles. *Proc Natl Acad Sci U S A*. 1976;73(4):1255-9.
89. Eriksson S, Fraser JR, Laurent TC, Pertoft H, Smedsrød B. Endothelial cells are a site of uptake and degradation of hyaluronic acid in the liver. *Exp Cell Res*. 1983;144(1):223-8.
90. Smedsrød B, Kjellen L, Pertoft H. Endocytosis and degradation of chondroitin sulphate by liver endothelial cells. *Biochem J*. 1985;229(1):63-71.
91. Smedsrød B, Johansson S, Pertoft H. Studies in vivo and in vitro on the uptake and degradation of soluble collagen alpha 1(I) chains in rat liver endothelial and Kupffer cells. *Biochem J*. 1985;228(2):415-24.
92. Laakso T, Smedsrød B. Cellular-Distribution in Rat-Liver of Intravenously Administered Polyacryl Starch and Chondroitin Sulfate Microparticles. *Int J Pharm*. 1987;36(2-3):253-62.
93. Smedsrød B, Einarsson M. Clearance of tissue plasminogen activator by mannose and galactose receptors in the liver. *Thromb Haemost*. 1990;63(1):60-6.
94. Smedsrød B, Melkko J, Risteli L, Risteli J. Circulating C-terminal propeptide of type I procollagen is cleared mainly via the mannose receptor in liver endothelial cells. *Biochem J*. 1990;271(2):345-50.
95. Melkko J, Hellevik T, Risteli L, Risteli J, Smedsrød B. Clearance of NH₂-terminal propeptides of types I and III procollagen is a physiological function of the scavenger receptor in liver endothelial cells. *J Exp Med*. 1994;179(2):405-12.
96. Smedsrød B, Melkko J, Araki N, Sano H, Horiuchi S. Advanced glycation end products are eliminated by scavenger-receptor-mediated endocytosis in hepatic sinusoidal Kupffer and endothelial cells. *Biochem J*. 1997;322 (Pt 2):567-73.
97. Falkowska-Hansen B, Oynebråten I, Uhlin-Hansen L, Smedsrød B. Endocytosis and degradation of serglycin in liver sinusoidal endothelial cells. *Mol Cell Biochem*. 2006;287(1-2):43-52.
98. Malovic I, Sørensen KK, Elvevold KH, Nedredal GI, Paulsen S, Erofeev AV, et al. The mannose receptor on murine liver sinusoidal endothelial cells is the main denatured collagen clearance receptor. *Hepatology*. 2007;45(6):1454-61.
99. Elvevold K, Simon-Santamaria J, Hasvold H, McCourt P, Smedsrød B, Sørensen KK. Liver sinusoidal endothelial cells depend on mannose receptor-mediated recruitment of lysosomal enzymes for normal degradation capacity. *Hepatology*. 2008;48(6):2007-15.
100. Li R, Oteiza A, Sørensen KK, McCourt P, Olsen R, Smedsrød B, et al. Role of liver sinusoidal endothelial cells and stabilins in elimination of oxidized low-density lipoproteins. *Am J Physiol Gastrointest Liver Physiol*. 2011;300(1):G71-81.

101. Simon-Santamaria J, Rinaldo CH, Kardas P, Li R, Malovic I, Elvevold K, et al. Efficient uptake of blood-borne BK and JC polyomavirus-like particles in endothelial cells of liver sinusoids and renal vasa recta. *PLoS One*. 2014;9(11):e111762.
102. Oie CI, Wolfson DL, Yasunori T, Dumitriu G, Sørensen KK, McCourt PA, et al. Liver sinusoidal endothelial cells contribute to the uptake and degradation of entero bacterial viruses. *Sci Rep*. 2020;10(1):898.
103. Eskild W, Smedsrød B, Berg T. Receptor mediated endocytosis of formaldehyde treated albumin, yeast invertase and chondroitin sulfate in suspensions of rat liver endothelial cells. *Int J Biochem*. 1986;18(7):647-51.
104. Magnusson S, Kjekken R, Berg T. Characterization of two distinct pathways of endocytosis of ricin by rat liver endothelial cells. *Exp Cell Res*. 1993;205(1):118-25.
105. Magnusson S, Berg T. Endocytosis of ricin by rat liver cells in vivo and in vitro is mainly mediated by mannose receptors on sinusoidal endothelial cells. *Biochem J*. 1993;291 (Pt 3)(Pt 3):749-55.
106. Nagelkerke JF, Barto KP, van Berkel TJ. In vivo and in vitro uptake and degradation of acetylated low density lipoprotein by rat liver endothelial, Kupffer, and parenchymal cells. *J Biol Chem*. 1983;258(20):12221-7.
107. Vanberkel TJC, Derijke YB, Kruijt JK. Different Fate In vivo of Oxidatively Modified Low-Density-Lipoprotein and Acetylated Low-Density-Lipoprotein in Rats - Recognition by Various Scavenger Receptors on Kupffer and Endothelial Liver-Cells. *J Biol Chem*. 1991;266(4):2282-9.
108. Blomhoff R, Eskild W, Berg T. Endocytosis of formaldehyde-treated serum albumin via scavenger pathway in liver endothelial cells. *Biochem J*. 1984;218(1):81-6.
109. Oynebraten I, Hansen B, Smedsrød B, Uhlin-Hansen L. Serglycin secreted by leukocytes is efficiently eliminated from the circulation by sinusoidal scavenger endothelial cells in the liver. *J Leukoc Biol*. 2000;67(2):183-8.
110. Niesen TE, Alpers DH, Stahl PD, Rosenblum JL. Metabolism of glycosylated human salivary amylase: in vivo plasma clearance by rat hepatic endothelial cells and in vitro receptor mediated pinocytosis by rat macrophages. *J Leukoc Biol*. 1984;36(3):307-20.
111. Kjekken R, Mousavi SA, Brech A, Gjoen T, Berg T. Fluid phase endocytosis of [125I]iodixanol in rat liver parenchymal, endothelial and Kupffer cells. *Cell Tissue Res*. 2001;304(2):221-30.
112. Falkowska-Hansen B, Falkowski M, Metharom P, Kronic D, Goerd S. Clathrin-coated vesicles form a unique net-like structure in liver sinusoidal endothelial cells by assembling along undisrupted microtubules. *Exp Cell Res*. 2007;313(9):1745-57.
113. Pandey E, Nour AS, Harris EN. Prominent Receptors of Liver Sinusoidal Endothelial Cells in Liver Homeostasis and Disease. *Front Physiol*. 2020;11:873.
114. Politz O, Gratchev A, McCourt PA, Schledzewski K, Guillot P, Johansson S, et al. Stabilin-1 and -2 constitute a novel family of fasciclin-like hyaluronan receptor homologues. *Biochem J*. 2002;362(Pt 1):155-64.
115. Falkowski M, Schledzewski K, Hansen B, Goerd S. Expression of stabilin-2, a novel fasciclin-like hyaluronan receptor protein, in murine sinusoidal endothelia, avascular tissues, and at solid/liquid interfaces. *Histochem Cell Biol*. 2003;120(5):361-9.
116. Qian H, Johansson S, McCourt P, Smedsrød B, Ekblom M, Johansson S. Stabilins are expressed in bone marrow sinusoidal endothelial cells and mediate scavenging and cell adhesive functions. *Biochem Biophys Res Commun*. 2009;390(3):883-6.
117. Martens JH, Kzhyshkowska J, Falkowski-Hansen M, Schledzewski K, Gratchev A, Mansmann U, et al. Differential expression of a gene signature for scavenger/lectin receptors by endothelial cells and macrophages in human lymph node sinuses, the primary sites of regional metastasis. *J Pathol*. 2006;208(4):574-89.
118. Li R, McCourt P, Schledzewski K, Goerd S, Moldenhauer G, Liu X, et al. Endocytosis of advanced glycation end-products in bovine choriocapillaris endothelial cells. *Microcirculation*. 2009;16(7):640-55.
119. Sandberg M, Johansson S, Sagulin L, Jansson L, Johansson S. Scavenging Endothelium of Pancreatic Islets: Differential Expression of Stabilin-1 and Stabilin-2 in Mice and Humans. *Pancreas*. 2017;46(1):e4-e5.
120. Hansen B, Longati P, Elvevold K, Nedredal GI, Schledzewski K, Olsen R, et al. Stabilin-1 and stabilin-2 are both directed into the early endocytic pathway in hepatic sinusoidal endothelium via interactions with clathrin/AP-2, independent of ligand binding. *Exp Cell Res*. 2005;303(1):160-73.
121. Terkelsen MK, Bendixen SM, Hansen D, Scott EAH, Moeller AF, Nielsen R, et al. Transcriptional Dynamics of Hepatic Sinusoid-Associated Cells After Liver Injury. *Hepatology*. 2020;72(6):2119-33.

122. Hansen B, Arteta B, Smedsrød B. The physiological scavenger receptor function of hepatic sinusoidal endothelial and Kupffer cells is independent of scavenger receptor class A type I and II. *Mol Cell Biochem.* 2002;240(1-2):1-8.
123. Miller CM, Donner AJ, Blank EE, Egger AW, Kellar BM, Ostergaard ME, et al. Stabilin-1 and Stabilin-2 are specific receptors for the cellular internalization of phosphorothioate-modified antisense oligonucleotides (ASOs) in the liver. *Nucleic Acids Res.* 2016;44(6):2782-94.
124. Kzhyshkowska J, Workman G, Cardo-Vila M, Arap W, Pasqualini R, Gratchev A, et al. Novel function of alternatively activated macrophages: stabilin-1-mediated clearance of SPARC. *J Immunol.* 2006;176(10):5825-32.
125. McCourt PA, Smedsrød BH, Melkko J, Johansson S. Characterization of a hyaluronan receptor on rat sinusoidal liver endothelial cells and its functional relationship to scavenger receptors. *Hepatology.* 1999;30(5):1276-86.
126. Pandey MS, Baggenstoss BA, Washburn J, Harris EN, Weigel PH. The hyaluronan receptor for endocytosis (HARE) activates NF-kappaB-mediated gene expression in response to 40-400-kDa, but not smaller or larger, hyaluronans. *J Biol Chem.* 2013;288(20):14068-79.
127. Zhou B, McGary CT, Weigel JA, Saxena A, Weigel PH. Purification and molecular identification of the human hyaluronan receptor for endocytosis. *Glycobiology.* 2003;13(5):339-49.
128. Magnusson S, Berg T. Extremely rapid endocytosis mediated by the mannose receptor of sinusoidal endothelial rat liver cells. *Biochem J.* 1989;257(3):651-6.
129. Stahl PD, Ezekowitz RA. The mannose receptor is a pattern recognition receptor involved in host defense. *Curr Opin Immunol.* 1998;10(1):50-5.
130. Rogharian A, Stopforth RJ, Dahal LN, Cragg MS. New revelations from an old receptor: Immunoregulatory functions of the inhibitory Fc gamma receptor, FcgammaRIIB (CD32B). *J Leukoc Biol.* 2018.
131. Schurich A, Berg M, Stabenow D, Bottcher J, Kern M, Schild HJ, et al. Dynamic regulation of CD8 T cell tolerance induction by liver sinusoidal endothelial cells. *J Immunol.* 2010;184(8):4107-14.
132. Mousavi SA, Sporstol M, Fladeby C, Kjekken R, Barois N, Berg T. Receptor-mediated endocytosis of immune complexes in rat liver sinusoidal endothelial cells is mediated by FcgammaRIIb2. *Hepatology.* 2007;46(3):871-84.
133. Ganesan LP, Kim J, Wu Y, Mohanty S, Phillips GS, Birmingham DJ, et al. FcgammaRIIb on liver sinusoidal endothelium clears small immune complexes. *J Immunol.* 2012;189(10):4981-8.
134. Johansson AG, Lovdal T, Magnusson KE, Berg T, Skogh T. Liver cell uptake and degradation of soluble immunoglobulin G immune complexes in vivo and in vitro in rats. *Hepatology.* 1996;24(1):169-75.
135. Skogh T, Blomhoff R, Eskild W, Berg T. Hepatic uptake of circulating IgG immune complexes. *Immunology.* 1985;55(4):585-94.
136. Hubbard AL, Wilson G, Ashwell G, Stukenbrok H. An electron microscope autoradiographic study of the carbohydrate recognition systems in rat liver. I. Distribution of 125I-ligands among the liver cell types. *J Cell Biol.* 1979;83(1):47-64.
137. Praaning-van Dalen DP, de Leeuw AM, Brouwer A, Knook DL. Rat liver endothelial cells have a greater capacity than Kupffer cells to endocytose N-acetylglucosamine- and mannose-terminated glycoproteins. *Hepatology.* 1987;7(4):672-9.
138. Bijsterbosch MK, Donker W, van de Bilt H, van Weely S, van Berkel TJ, Aerts JM. Quantitative analysis of the targeting of mannose-terminal glucocerebrosidase. Predominant uptake by liver endothelial cells. *Eur J Biochem.* 1996;237(2):344-9.
139. Markmann S, Krambeck S, Hughes CJ, Mirzaian M, Aerts JM, Saftig P, et al. Quantitative Proteome Analysis of Mouse Liver Lysosomes Provides Evidence for Mannose 6-phosphate-independent Targeting Mechanisms of Acid Hydrolases in Mucopolipidosis II. *Mol Cell Proteomics.* 2017;16(3):438-50.
140. Knook DL, Sleyster EC. Isolated parenchymal, Kupffer and endothelial rat liver cells characterized by their lysosomal enzyme content. *Biochem Biophys Res Commun.* 1980;96(1):250-7.
141. Uhrig A, Banafsche R, Kremer M, Hegenbarth S, Hamann A, Neurath M, et al. Development and functional consequences of LPS tolerance in sinusoidal endothelial cells of the liver. *J Leukoc Biol.* 2005;77(5):626-33.
142. Martin-Armas M, Simon-Santamaria J, Pettersen I, Moens U, Smedsrød B, Sveinbjornsson B. Toll-like receptor 9 (TLR9) is present in murine liver sinusoidal endothelial cells (LSECs) and mediates the effect of CpG-oligonucleotides. *J Hepatol.* 2006;44(5):939-46.

143. Wu J, Meng Z, Jiang M, Zhang E, Trippler M, Broering R, et al. Toll-like receptor-induced innate immune responses in non-parenchymal liver cells are cell type-specific. *Immunology*. 2010;129(3):363-74.
144. Lalor PF, Edwards S, McNab G, Salmi M, Jalkanen S, Adams DH. Vascular adhesion protein-1 mediates adhesion and transmigration of lymphocytes on human hepatic endothelial cells. *J Immunol*. 2002;169(2):983-92.
145. Lalor PF, Shields P, Grant A, Adams DH. Recruitment of lymphocytes to the human liver. *Immunol Cell Biol*. 2002;80(1):52-64.
146. Edwards S, Lalor PF, Nash GB, Rainger GE, Adams DH. Lymphocyte traffic through sinusoidal endothelial cells is regulated by hepatocytes. *Hepatology*. 2005;41(3):451-9.
147. Patten DA, Wilson GK, Bailey D, Shaw RK, Jalkanen S, Salmi M, et al. Human liver sinusoidal endothelial cells promote intracellular crawling of lymphocytes during recruitment: A new step in migration. *Hepatology*. 2017;65(1):294-309.
148. Shetty S, Weston CJ, Adams DH, Lalor PF. A flow adhesion assay to study leucocyte recruitment to human hepatic sinusoidal endothelium under conditions of shear stress. *J Vis Exp*. 2014(85).
149. Shetty S, Weston CJ, Oo YH, Westerlund N, Stamataki Z, Youster J, et al. Common lymphatic endothelial and vascular endothelial receptor-1 mediates the transmigration of regulatory T cells across human hepatic sinusoidal endothelium. *J Immunol*. 2011;186(7):4147-55.
150. Oo YH, Weston CJ, Lalor PF, Curbishley SM, Withers DR, Reynolds GM, et al. Distinct roles for CCR4 and CXCR3 in the recruitment and positioning of regulatory T cells in the inflamed human liver. *J Immunol*. 2010;184(6):2886-98.
151. Aspinall AI, Curbishley SM, Lalor PF, Weston CJ, Blahova M, Liaskou E, et al. CX(3)CR1 and vascular adhesion protein-1-dependent recruitment of CD16(+) monocytes across human liver sinusoidal endothelium. *Hepatology*. 2010;51(6):2030-9.
152. Patten DA, Shetty S. More Than Just a Removal Service: Scavenger Receptors in Leukocyte Trafficking. *Front Immunol*. 2018;9(2904):2904.
153. Wadkin JCR, Patten DA, Kamarajah SK, Shepherd EL, Novitskaya V, Berditchevski F, et al. CD151 supports VCAM-1-mediated lymphocyte adhesion to liver endothelium and is upregulated in chronic liver disease and hepatocellular carcinoma. *Am J Physiol Gastrointest Liver Physiol*. 2017;313(2):G138-G49.
154. Knolle PA, Wohlleber D. Immunological functions of liver sinusoidal endothelial cells. *Cell Mol Immunol*. 2016;13(3):347-53.
155. Limmer A, Ohl J, Wingender G, Berg M, Jungerkes F, Schumak B, et al. Cross-presentation of oral antigens by liver sinusoidal endothelial cells leads to CD8 T cell tolerance. *Eur J Immunol*. 2005;35(10):2970-81.
156. Limmer A, Ohl J, Kurts C, Ljunggren HG, Reiss Y, Groettrup M, et al. Efficient presentation of exogenous antigen by liver endothelial cells to CD8+ T cells results in antigen-specific T-cell tolerance. *Nat Med*. 2000;6(12):1348-54.
157. Berg M, Wingender G, Djandji D, Hegenbarth S, Momburg F, Hammerling G, et al. Cross-presentation of antigens from apoptotic tumor cells by liver sinusoidal endothelial cells leads to tumor-specific CD8+ T cell tolerance. *Eur J Immunol*. 2006;36(11):2960-70.
158. Burgdorf S, Kautz A, Bohnert V, Knolle PA, Kurts C. Distinct pathways of antigen uptake and intracellular routing in CD4 and CD8 T cell activation. *Science*. 2007;316(5824):612-6.
159. Diehl L, Schurich A, Grochtmann R, Hegenbarth S, Chen L, Knolle PA. Tolerogenic maturation of liver sinusoidal endothelial cells promotes B7-homolog 1-dependent CD8+ T cell tolerance. *Hepatology*. 2008;47(1):296-305.
160. Hochst B, Schildberg FA, Bottcher J, Metzger C, Huss S, Turler A, et al. Liver sinusoidal endothelial cells contribute to CD8 T cell tolerance toward circulating carcinoembryonic antigen in mice. *Hepatology*. 2012;56(5):1924-33.
161. Knolle PA, Uhrig A, Hegenbarth S, Loser E, Schmitt E, Gerken G, et al. IL-10 down-regulates T cell activation by antigen-presenting liver sinusoidal endothelial cells through decreased antigen uptake via the mannose receptor and lowered surface expression of accessory molecules. *Clin Exp Immunol*. 1998;114(3):427-33.
162. Lohse AW, Knolle PA, Bilo K, Uhrig A, Waldmann C, Ibe M, et al. Antigen-presenting function and B7 expression of murine sinusoidal endothelial cells and Kupffer cells. *Gastroenterology*. 1996;110(4):1175-81.

163. Liu Y, Gardner CR, Laskin JD, Laskin DL. Classical and alternative activation of rat hepatic sinusoidal endothelial cells by inflammatory stimuli. *Exp Mol Pathol*. 2013;94(1):160-7.
164. Bottcher JP, Schanz O, Garbers C, Zaremba A, Hegenbarth S, Kurts C, et al. IL-6 trans-signaling-dependent rapid development of cytotoxic CD8+ T cell function. *Cell Rep*. 2014;8(5):1318-27.
165. Wittlich M, Dudek M, Bottcher JP, Schanz O, Hegenbarth S, Bopp T, et al. Liver sinusoidal endothelial cell cross-priming is supported by CD4 T cell-derived IL-2. *J Hepatol*. 2017;66(5):978-86.
166. Huang S, Wu J, Gao X, Zou S, Chen L, Yang X, et al. LSECs express functional NOD1 receptors: A role for NOD1 in LSEC maturation-induced T cell immunity in vitro. *Mol Immunol*. 2018;101:167-75.
167. Warren A, Le Couteur DG, Fraser R, Bowen DG, McCaughan GW, Bertolino P. T lymphocytes interact with hepatocytes through fenestrations in murine liver sinusoidal endothelial cells. *Hepatology*. 2006;44(5):1182-90.
168. Ganesan LP, Mohanty S, Kim J, Clark KR, Robinson JM, Anderson CL. Rapid and efficient clearance of blood-borne virus by liver sinusoidal endothelium. *PLoS Pathog*. 2011;7(9):e1002281.
169. Mates JM, Yao Z, Cheplowitz AM, Suer O, Phillips GS, Kwiek JJ, et al. Mouse Liver Sinusoidal Endothelium Eliminates HIV-Like Particles from Blood at a Rate of 100 Million per Minute by a Second-Order Kinetic Process. *Front Immunol*. 2017;8(35):35.
170. Giugliano S, Kriss M, Golden-Mason L, Dobrinskikh E, Stone AE, Soto-Gutierrez A, et al. Hepatitis C virus infection induces autocrine interferon signaling by human liver endothelial cells and release of exosomes, which inhibits viral replication. *Gastroenterology*. 2015;148(2):392-402 e13.
171. Connolly MK, Bedrosian AS, Malhotra A, Henning JR, Ibrahim J, Vera V, et al. In hepatic fibrosis, liver sinusoidal endothelial cells acquire enhanced immunogenicity. *J Immunol*. 2010;185(4):2200-8.
172. Lee WY, Kubes P. Leukocyte adhesion in the liver: distinct adhesion paradigm from other organs. *J Hepatol*. 2008;48(3):504-12.
173. Oteiza A, Li R, McCuskey RS, Smedsrød B, Sørensen KK. Effects of oxidized low-density lipoproteins on the hepatic microvasculature. *Am J Physiol Gastrointest Liver Physiol*. 2011;301(4):G684-93.
174. Sardu C, Gambardella J, Morelli MB, Wang X, Marfella R, Santulli G. Hypertension, Thrombosis, Kidney Failure, and Diabetes: Is COVID-19 an Endothelial Disease? A Comprehensive Evaluation of Clinical and Basic Evidence. *J Clin Med*. 2020;9(5):1417.
175. Avogaro A, Albiero M, Menegazzo L, de Kreutzenberg S, Fadini GP. Endothelial dysfunction in diabetes: the role of reparatory mechanisms. *Diabetes Care*. 2011;34 Suppl 2(Suppl 2):S285-90.
176. Hunt BJ, Jurd KM. Endothelial cell activation. A central pathophysiological process. *BMJ*. 1998;316(7141):1328-9.
177. Pober JS, Sessa WC. Evolving functions of endothelial cells in inflammation. *Nat Rev Immunol*. 2007;7(10):803-15.
178. Iwakiri Y. Endothelial dysfunction in the regulation of cirrhosis and portal hypertension. *Liver Int*. 2012;32(2):199-213.
179. Incalza MA, D'Oria R, Natalicchio A, Perrini S, Laviola L, Giorgino F. Oxidative stress and reactive oxygen species in endothelial dysfunction associated with cardiovascular and metabolic diseases. *Vascul Pharmacol*. 2018;100:1-19.
180. Taura K, De Minicis S, Seki E, Hatano E, Iwaisako K, Osterreicher CH, et al. Hepatic stellate cells secrete angiopoietin 1 that induces angiogenesis in liver fibrosis. *Gastroenterology*. 2008;135(5):1729-38.
181. Furuta K, Guo Q, Hirsova P, Ibrahim SH. Emerging Roles of Liver Sinusoidal Endothelial Cells in Nonalcoholic Steatohepatitis. *Biology*. 2020;9(11):12.
182. Parmar KM, Larman HB, Dai G, Zhang Y, Wang ET, Moorthy SN, et al. Integration of flow-dependent endothelial phenotypes by Kruppel-like factor 2. *J Clin Invest*. 2006;116(1):49-58.
183. Gracia-Sancho J, Russo L, Garcia-Caldero H, Garcia-Pagan JC, Garcia-Cardena G, Bosch J. Endothelial expression of transcription factor Kruppel-like factor 2 and its vasoprotective target genes in the normal and cirrhotic rat liver. *Gut*. 2011;60(4):517-24.
184. Kovacic JC, Dimmeler S, Harvey RP, Finkel T, Aikawa E, Krenning G, et al. Endothelial to Mesenchymal Transition in Cardiovascular Disease: JACC State-of-the-Art Review. *J Am Coll Cardiol*. 2019;73(2):190-209.
185. Ribera J, Pauta M, Melgar-Lesmes P, Cordoba B, Bosch A, Calvo M, et al. A small population of liver endothelial cells undergoes endothelial-to-mesenchymal transition in response to chronic liver injury. *Am J Physiol Gastrointest Liver Physiol*. 2017;313(5):G492-G504.

186. Li Z, Chen B, Dong W, Kong M, Fan Z, Yu L, et al. MKL1 promotes endothelial-to-mesenchymal transition and liver fibrosis by activating TWIST1 transcription. *Cell Death Dis.* 2019;10(12):899.
187. Ruart M, Chavarria L, Camprecios G, Suarez-Herrera N, Montironi C, Guixe-Muntet S, et al. Impaired endothelial autophagy promotes liver fibrosis by aggravating the oxidative stress response during acute liver injury. *J Hepatol.* 2019;70(3):458-69.
188. Hammoutene A, Biquard L, Lasselin J, Kheloufi M, Tanguy M, Vion AC, et al. A defect in endothelial autophagy occurs in patients with non-alcoholic steatohepatitis and promotes inflammation and fibrosis. *J Hepatol.* 2020;72(3):528-38.
189. Guixe-Muntet S, de Mesquita FC, Vila S, Hernandez-Gea V, Peralta C, Garcia-Pagan JC, et al. Cross-talk between autophagy and KLF2 determines endothelial cell phenotype and microvascular function in acute liver injury. *J Hepatol.* 2017;66(1):86-94.
190. Ding BS, Nolan DJ, Butler JM, James D, Babazadeh AO, Rosenwaks Z, et al. Inductive angiocrine signals from sinusoidal endothelium are required for liver regeneration. *Nature.* 2010;468(7321):310-5.
191. Rafii S, Butler JM, Ding BS. Angiocrine functions of organ-specific endothelial cells. *Nature.* 2016;529(7586):316-25.
192. Koch PS, Olsavszky V, Ulbrich F, Sticht C, Demory A, Leibing T, et al. Angiocrine Bmp2 signaling in murine liver controls normal iron homeostasis. *Blood.* 2017;129(4):415-9.
193. Petrillo S, Manco M, Altruda F, Fagoonee S, Tolosano E. Liver Sinusoidal Endothelial Cells at the Crossroad of Iron Overload and Liver Fibrosis. *Antioxid Redox Signal.* 2020.
194. Canali S, Wang CY, Zumbrennen-Bullough KB, Bayer A, Babitt JL. Bone morphogenetic protein 2 controls iron homeostasis in mice independent of Bmp6. *Am J Hematol.* 2017;92(11):1204-13.
195. Duan JL, Ruan B, Yan XC, Liang L, Song P, Yang ZY, et al. Endothelial Notch activation reshapes the angiocrine of sinusoidal endothelia to aggravate liver fibrosis and blunt regeneration in mice. *Hepatology.* 2018;68(2):677-90.
196. Shido K, Chavez D, Cao Z, Ko J, Rafii S, Ding BS. Platelets prime hematopoietic and vascular niche to drive angiocrine-mediated liver regeneration. *Signal Transduct Target Ther.* 2017;2(1):16044.
197. Klein D, Demory A, Peyre F, Kroll J, Augustin HG, Helfrich W, et al. Wnt2 acts as a cell type-specific, autocrine growth factor in rat hepatic sinusoidal endothelial cells cross-stimulating the VEGF pathway. *Hepatology.* 2008;47(3):1018-31.
198. Zhang P, Yue K, Liu X, Yan X, Yang Z, Duan J, et al. Endothelial Notch activation promotes neutrophil transmigration via downregulating endomucin to aggravate hepatic ischemia/reperfusion injury. *Sci China Life Sci.* 2020;63(3):375-87.
199. Wang B, Zhao L, Fish M, Logan CY, Nusse R. Self-renewing diploid Axin2(+) cells fuel homeostatic renewal of the liver. *Nature.* 2015;524(7564):180-5.
200. Leibing T, Geraud C, Augustin I, Boutros M, Augustin HG, Okun JG, et al. Angiocrine Wnt signaling controls liver growth and metabolic maturation in mice. *Hepatology.* 2018;68(2):707-22.
201. Hu J, Srivastava K, Wieland M, Runge A, Mogler C, Besemfelder E, et al. Endothelial cell-derived angiopoietin-2 controls liver regeneration as a spatiotemporal rheostat. *Science.* 2014;343(6169):416-9.
202. Ding BS, Cao Z, Lis R, Nolan DJ, Guo P, Simons M, et al. Divergent angiocrine signals from vascular niche balance liver regeneration and fibrosis. *Nature.* 2014;505(7481):97-102.
203. Ben-Moshe S, Shapira Y, Moor AE, Manco R, Veg T, Bahar Halpern K, et al. Spatial sorting enables comprehensive characterization of liver zonation. *Nat Metab.* 2019;1(9):899-911.
204. Scoazec JY, Racine L, Couvelard A, Flejou JF, Feldmann G. Endothelial cell heterogeneity in the normal human liver acinus: in situ immunohistochemical demonstration. *Liver.* 1994;14(3):113-23.
205. Asumendi A, Alvarez A, Martinez I, Smedsrød B, Vidal-Vanaclocha F. Hepatic sinusoidal endothelium heterogeneity with respect to mannose receptor activity is interleukin-1 dependent. *Hepatology.* 1996;23(6):1521-9.
206. Dini L, Carla EC. Hepatic sinusoidal endothelium heterogeneity with respect to the recognition of apoptotic cells. *Exp Cell Res.* 1998;240(2):388-93.
207. Xie G, Wang L, Wang X, Wang L, DeLeve LD. Isolation of periportal, midlobular, and centrilobular rat liver sinusoidal endothelial cells enables study of zoned drug toxicity. *Am J Physiol Gastrointest Liver Physiol.* 2010;299(5):G1204-10.
208. Strauss O, Phillips A, Ruggiero K, Bartlett A, Dunbar PR. Immunofluorescence identifies distinct subsets of endothelial cells in the human liver. *Sci Rep.* 2017;7:44356.

209. Plein A, Fantin A, Denti L, Pollard JW, Ruhrberg C. Erythro-myeloid progenitors contribute endothelial cells to blood vessels. *Nature*. 2018;562(7726):223-8.
210. Halpern KB, Shenhav R, Massalha H, Toth B, Egozi A, Massasa EE, et al. Paired-cell sequencing enables spatial gene expression mapping of liver endothelial cells. *Nat Biotechnol*. 2018;36(10):962-70.
211. Ramachandran P, Matchett KP, Dobie R, Wilson-Kanamori JR, Henderson NC. Single-cell technologies in hepatology: new insights into liver biology and disease pathogenesis. *Nat Rev Gastroenterol Hepatol*. 2020;17(8):457-72.
212. Zhao Q, Molina-Portela MDP, Parveen A, Adler A, Adler C, E H, et al. Heterogeneity and chimerism of endothelial cells revealed by single-cell transcriptome in orthotopic liver tumors. *Angiogenesis*. 2020;23(4):581-97.
213. Diaz-Mejia JJ, Meng EC, Pico AR, MacParland SA, Ketela T, Pugh TJ, et al. Evaluation of methods to assign cell type labels to cell clusters from single-cell RNA-sequencing data. *F1000Res*. 2019;8(296).
214. Lafoz E, Ruart M, Anton A, Oncins A, Hernandez-Gea V. The Endothelium as a Driver of Liver Fibrosis and Regeneration. *Cells*. 2020;9(4).
215. Sun X, Harris EN. New aspects of hepatic endothelial cells in physiology and nonalcoholic fatty liver disease. *Am J Physiol Cell Physiol*. 2020;318(6):C1200-C13.
216. Zapotoczny B, Braet F, Wisse E, Lekka M, Szymonski M. Biophysical nanocharacterization of liver sinusoidal endothelial cells through atomic force microscopy. *Biophys Rev*. 2020;12(3):625-36.
217. Wilkinson AL, Qurashi M, Shetty S. The Role of Sinusoidal Endothelial Cells in the Axis of Inflammation and Cancer Within the Liver. *Front Physiol*. 2020;11(990):990.
218. Xu B, Broome U, Uzunel M, Nava S, Ge X, Kumagai-Braesch M, et al. Capillarization of hepatic sinusoid by liver endothelial cell-reactive autoantibodies in patients with cirrhosis and chronic hepatitis. *Am J Pathol*. 2003;163(4):1275-89.
219. Schaffner F, Poper H. Capillarization of hepatic sinusoids in man. *Gastroenterology*. 1963;44(3):239-42.
220. DeLeve LD. Liver sinusoidal endothelial cells in hepatic fibrosis. *Hepatology*. 2015;61(5):1740-6.
221. Babbs C, Haboubi NY, Mellor JM, Smith A, Rowan BP, Warnes TW. Endothelial cell transformation in primary biliary cirrhosis: a morphological and biochemical study. *Hepatology*. 1990;11(5):723-9.
222. Chen L, Gu T, Li B, Li F, Ma Z, Zhang Q, et al. Delta-like ligand 4/DLL4 regulates the capillarization of liver sinusoidal endothelial cell and liver fibrogenesis. *Biochim Biophys Acta Mol Cell Res*. 2019;1866(10):1663-75.
223. Desroches-Castan A, Tillet E, Ricard N, Ouarne M, Mallet C, Belmudes L, et al. Bone Morphogenetic Protein 9 Is a Paracrine Factor Controlling Liver Sinusoidal Endothelial Cell Fenestration and Protecting Against Hepatic Fibrosis. *Hepatology*. 2019;70(4):1392-408.
224. Geraud C, Mogler C, Runge A, Evdokimov K, Lu S, Schledzewski K, et al. Endothelial transdifferentiation in hepatocellular carcinoma: loss of Stabilin-2 expression in peri-tumourous liver correlates with increased survival. *Liver Int*. 2013;33(9):1428-40.
225. Ishikawa T, Yokoyama H, Matsuura T, Fujiwara Y. Fc gamma RIIb expression levels in human liver sinusoidal endothelial cells during progression of non-alcoholic fatty liver disease. *PLoS One*. 2019;14(1):e0211543.
226. Tamaki S, Ueno T, Torimura T, Sata M, Tanikawa K. Evaluation of hyaluronic acid binding ability of hepatic sinusoidal endothelial cells in rats with liver cirrhosis. *Gastroenterology*. 1996;111(4):1049-57.
227. Cassim S, Raymond VA, Lapierre P, Bilodeau M. From in vivo to in vitro: Major metabolic alterations take place in hepatocytes during and following isolation. *PLoS One*. 2017;12(12):e0190366.
228. Geraud C, Schledzewski K, Demory A, Klein D, Kaus M, Peyre F, et al. Liver sinusoidal endothelium: a microenvironment-dependent differentiation program in rat including the novel junctional protein liver endothelial differentiation-associated protein-1. *Hepatology*. 2010;52(1):313-26.
229. March S, Hui EE, Underhill GH, Khetani S, Bhatia SN. Microenvironmental regulation of the sinusoidal endothelial cell phenotype in vitro. *Hepatology*. 2009;50(3):920-8.
230. Arai T, Sakurai T, Kamiyoshi A, Ichikawa-Shindo Y, Inuma N, Iesato Y, et al. Induction of LYVE-1/stabilin-2-positive liver sinusoidal endothelial-like cells from embryoid bodies by modulation of adrenomedullin-RAMP2 signaling. *Peptides*. 2011;32(9):1855-65.
231. Gage BK, Liu JC, Innes BT, MacParland SA, McGilvray ID, Bader GD, et al. Generation of Functional Liver Sinusoidal Endothelial Cells from Human Pluripotent Stem-Cell-Derived Venous Angioblasts. *Cell Stem Cell*. 2020;27(2):254-69 e9.

232. Kouji Y, Kido T, Ito T, Oyama H, Chen SW, Katou Y, et al. An In Vitro Human Liver Model by iPSC-Derived Parenchymal and Non-parenchymal Cells. *Stem Cell Reports*. 2017;9(2):490-8.
233. de Haan W, Øie C, Benkheil M, Dheedene W, Vinckier S, Coppiello G, et al. Unraveling the transcriptional determinants of liver sinusoidal endothelial cell specialization. *Am J Physiol Gastrointest Liver Physiol*. 2020;318(4):G803-G15.
234. Xie G, Wang X, Wang L, Wang L, Atkinson RD, Kanel GC, et al. Role of differentiation of liver sinusoidal endothelial cells in progression and regression of hepatic fibrosis in rats. *Gastroenterology*. 2012;142(4):918-27 e6.
235. DeLeve LD, Wang X, Hu L, McCuskey MK, McCuskey RS. Rat liver sinusoidal endothelial cell phenotype is maintained by paracrine and autocrine regulation. *Am J Physiol Gastrointest Liver Physiol*. 2004;287(4):G757-63.
236. Elvevold KH, Nedredal GI, Revhaug A, Smedsrød B. Scavenger properties of cultivated pig liver endothelial cells. *Comp Hepatol*. 2004;3(1):4.
237. Juin A, Planus E, Guillemot F, Horakova P, Albiges-Rizo C, Genot E, et al. Extracellular matrix rigidity controls podosome induction in microvascular endothelial cells. *Biol Cell*. 2013;105(1):46-57.
238. Kidambi S, Natarajan V, Casey C, Harris E. Matrix Stiffness Regulate Liver Sinusoidal Endothelial Cells (LSECs) Function: Importance for Liver Fibrosis Progression. *Faseb J*. 2019;33(S1):496.39-.39.
239. Yang H, Li N, Du Y, Tong C, Lu S, Hu J, et al. Neutrophil adhesion and crawling dynamics on liver sinusoidal endothelial cells under shear flow. *Exp Cell Res*. 2017;351(1):91-9.
240. Tegge AN, Rodrigues RR, Larkin AL, Vu L, Murali TM, Rajagopalan P. Transcriptomic Analysis of Hepatic Cells in Multicellular Organotypic Liver Models. *Sci Rep*. 2018;8(1):11306.
241. Ware BR, Durham MJ, Monckton CP, Khetani SR. A Cell Culture Platform to Maintain Long-term Phenotype of Primary Human Hepatocytes and Endothelial Cells. *Cell Mol Gastroenterol Hepatol*. 2018;5(3):187-207.
242. Ozkan A, Stolley D, Cressman ENK, McMillin M, DeMorrow S, Yankeelov TE, et al. The Influence of Chronic Liver Diseases on Hepatic Vasculature: A Liver-on-a-chip Review. *Micromachines*. 2020;11(5).
243. Deng J, Wei W, Chen Z, Lin B, Zhao W, Luo Y, et al. Engineered Liver-on-a-Chip Platform to Mimic Liver Functions and Its Biomedical Applications: A Review. *Micromachines*. 2019;10(10):676.
244. van Furth R, Cohn ZA, Hirsch JG, Humphrey JH, Spector WG, Langevoort HL. The mononuclear phagocyte system: a new classification of macrophages, monocytes, and their precursor cells. *Bulletin of the World Health Organization*. 1972;46(6):845-52.
245. Davies LC, Taylor PR. Tissue-resident macrophages: then and now. *Immunology*. 2015;144(4):541-8.
246. Sreejit G, Fleetwood AJ, Murphy AJ, Nagareddy PR. Origins and diversity of macrophages in health and disease. *Clin Transl Immunology*. 2020;9(12):e1222.
247. Locati M, Curtale G, Mantovani A. Diversity, Mechanisms, and Significance of Macrophage Plasticity. *Annu Rev Pathol*. 2020;15(1):123-47.
248. Wynn TA, Vannella KM. Macrophages in Tissue Repair, Regeneration, and Fibrosis. *Immunity*. 2016;44(3):450-62.
249. Guillot A, Tacke F. Liver Macrophages: Old Dogmas and New Insights. *Hepatol Commun*. 2019;3(6):730-43.
250. Bouwens L, Baekeland M, De Zanger R, Wisse E. Quantitation, tissue distribution and proliferation kinetics of Kupffer cells in normal rat liver. *Hepatology*. 1986;6(4):718-22.
251. Gomez Perdiguero E, Klapproth K, Schulz C, Busch K, Azzoni E, Crozet L, et al. Tissue-resident macrophages originate from yolk-sac-derived erythro-myeloid progenitors. *Nature*. 2015;518(7540):547-51.
252. Hoeffel G, Chen J, Lavin Y, Low D, Almeida FF, See P, et al. C-Myb(+) erythro-myeloid progenitor-derived fetal monocytes give rise to adult tissue-resident macrophages. *Immunity*. 2015;42(4):665-78.
253. Wisse E. On the endothelial cells of rat liver sinusoids. *Bibl Anat*. 1977(16 Pt 2):373-6.
254. Bykov I, Ylipaasto P, Eerola L, Lindros KO. Phagocytosis and LPS-stimulated production of cytokines and prostaglandin E2 is different in Kupffer cells isolated from the periportal or perivenous liver region. *Scand J Gastroenterol*. 2003;38(12):1256-61.
255. Sakai M, Troutman TD, Seidman JS, Ouyang Z, Spann NJ, Abe Y, et al. Liver-Derived Signals Sequentially Reprogram Myeloid Enhancers to Initiate and Maintain Kupffer Cell Identity. *Immunity*. 2019;51(4):655-70 e8.

256. Soucie EL, Weng Z, Geirsdottir L, Molawi K, Maurizio J, Fenouil R, et al. Lineage-specific enhancers activate self-renewal genes in macrophages and embryonic stem cells. *Science*. 2016;351(6274):aad5510.
257. Hagemeyer N, Kierdorf K, Frenzel K, Xue J, Ringelhan M, Abdullah Z, et al. Transcriptome-based profiling of yolk sac-derived macrophages reveals a role for Irf8 in macrophage maturation. *EMBO J*. 2016;35(16):1730-44.
258. Lefere S, Degroote H, Van Vlierberghe H, Devisscher L. Unveiling the depletion of Kupffer cells in experimental hepatocarcinogenesis through liver macrophage subtype-specific markers. *J Hepatol*. 2019;71(3):631-3.
259. Borst K, Graalman T, Kalinke U. Reply to: "Unveiling the depletion of Kupffer cells in experimental hepatocarcinogenesis through liver macrophage subtype-specific markers". *J Hepatol*. 2019;71(3):633-5.
260. Bleriot C, Ginhoux F. Understanding the Heterogeneity of Resident Liver Macrophages. *Front Immunol*. 2019;10(2694):2694.
261. Sierro F, Evrard M, Rizzetto S, Melino M, Mitchell AJ, Florido M, et al. A Liver Capsular Network of Monocyte-Derived Macrophages Restricts Hepatic Dissemination of Intraperitoneal Bacteria by Neutrophil Recruitment. *Immunity*. 2017;47(2):374-88 e6.
262. David BA, Rezende RM, Antunes MM, Santos MM, Freitas Lopes MA, Diniz AB, et al. Combination of Mass Cytometry and Imaging Analysis Reveals Origin, Location, and Functional Repopulation of Liver Myeloid Cells in Mice. *Gastroenterology*. 2016;151(6):1176-91.
263. Wang J, Kubes P. A Reservoir of Mature Cavity Macrophages that Can Rapidly Invade Visceral Organs to Affect Tissue Repair. *Cell*. 2016;165(3):668-78.
264. Hughes DA, Fraser IP, Gordon S. Murine macrophage scavenger receptor: in vivo expression and function as receptor for macrophage adhesion in lymphoid and non-lymphoid organs. *Eur J Immunol*. 1995;25(2):466-73.
265. PrabhuDas MR, Baldwin CL, Bollyky PL, Bowdish DME, Drickamer K, Febbraio M, et al. A Consensus Definitive Classification of Scavenger Receptors and Their Roles in Health and Disease. *J Immunol*. 2017;198(10):3775-89.
266. Helmy KY, Katschke KJ, Jr., Gorgani NN, Kljavin NM, Elliott JM, Diehl L, et al. CR1g: a macrophage complement receptor required for phagocytosis of circulating pathogens. *Cell*. 2006;124(5):915-27.
267. He JQ, Katschke KJ, Jr., Gribling P, Suto E, Lee WP, Diehl L, et al. CR1g mediates early Kupffer cell responses to adenovirus. *J Leukoc Biol*. 2013;93(2):301-6.
268. Lee WY, Moriarty TJ, Wong CH, Zhou H, Strieter RM, van Rooijen N, et al. An intravascular immune response to *Borrelia burgdorferi* involves Kupffer cells and iNKT cells. *Nat Immunol*. 2010;11(4):295-302.
269. Gregory SH, Sagnimeni AJ, Wing EJ. Bacteria in the bloodstream are trapped in the liver and killed by immigrating neutrophils. *J Immunol*. 1996;157(6):2514-20.
270. Horst AK, Tiesg G, Diehl L. Contribution of Macrophage Efferocytosis to Liver Homeostasis and Disease. *Front Immunol*. 2019;10(2670):2670.
271. Lee SJ, Park SY, Jung MY, Bae SM, Kim IS. Mechanism for phosphatidylserine-dependent erythrophagocytosis in mouse liver. *Blood*. 2011;117(19):5215-23.
272. Park SY, Jung MY, Lee SJ, Kang KB, Gratchev A, Riabov V, et al. Stabilin-1 mediates phosphatidylserine-dependent clearance of cell corpses in alternatively activated macrophages. *J Cell Sci*. 2009;122(Pt 18):3365-73.
273. Park SY, Jung MY, Kim HJ, Lee SJ, Kim SY, Lee BH, et al. Rapid cell corpse clearance by stabilin-2, a membrane phosphatidylserine receptor. *Cell Death Differ*. 2008;15(1):192-201.
274. Kimura Y, Inoue A, Hangai S, Saijo S, Negishi H, Nishio J, et al. The innate immune receptor Dectin-2 mediates the phagocytosis of cancer cells by Kupffer cells for the suppression of liver metastasis. *Proc Natl Acad Sci U S A*. 2016;113(49):14097-102.
275. Heymann F, Peusquens J, Ludwig-Portugall I, Kohlhepp M, Ergen C, Niemietz P, et al. Liver inflammation abrogates immunological tolerance induced by Kupffer cells. *Hepatology*. 2015;62(1):279-91.
276. You Q, Cheng L, Kedl RM, Ju C. Mechanism of T cell tolerance induction by murine hepatic Kupffer cells. *Hepatology*. 2008;48(3):978-90.
277. Frumento G, Rotondo R, Tonetti M, Damonte G, Benatti U, Ferrara GB. Tryptophan-derived catabolites are responsible for inhibition of T and natural killer cell proliferation induced by indoleamine 2,3-dioxygenase. *J Exp Med*. 2002;196(4):459-68.
278. Sun Z, Wada T, Maemura K, Uchikura K, Hoshino S, Diehl AM, et al. Hepatic allograft-derived Kupffer cells regulate T cell response in rats. *Liver Transpl*. 2003;9(5):489-97.

279. Wen Y, Lambrecht J, Ju C, Tacke F. Hepatic macrophages in liver homeostasis and diseases-diversity, plasticity and therapeutic opportunities. *Cell Mol Immunol*. 2021;18(1):45-56.
280. Scott CL, Zheng F, De Baetselier P, Martens L, Saeys Y, De Prijck S, et al. Bone marrow-derived monocytes give rise to self-renewing and fully differentiated Kupffer cells. *Nat Commun*. 2016;7:10321.
281. Zhao J, Zhang S, Liu Y, He X, Qu M, Xu G, et al. Single-cell RNA sequencing reveals the heterogeneity of liver-resident immune cells in human. *Cell Discov*. 2020;6(1):22.
282. Zeng Z, Surewaard BG, Wong CH, Geoghegan JA, Jenne CN, Kubes P. CR1g Functions as a Macrophage Pattern Recognition Receptor to Directly Bind and Capture Blood-Borne Gram-Positive Bacteria. *Cell Host Microbe*. 2016;20(1):99-106.
283. Hume DA, Perry VH, Gordon S. The mononuclear phagocyte system of the mouse defined by immunohistochemical localisation of antigen F4/80: macrophages associated with epithelia. *Anat Rec*. 1984;210(3):503-12.
284. Zigmond E, Samia-Grinberg S, Pasmanik-Chor M, Brazowski E, Shibolet O, Halpern Z, et al. Infiltrating monocyte-derived macrophages and resident kupffer cells display different ontogeny and functions in acute liver injury. *J Immunol*. 2014;193(1):344-53.
285. Nishiyama K, Nakashima H, Ikarashi M, Kinoshita M, Nakashima M, Aosasa S, et al. Mouse CD11b+Kupffer Cells Recruited from Bone Marrow Accelerate Liver Regeneration after Partial Hepatectomy. *PLoS One*. 2015;10(9):e0136774.
286. Ikarashi M, Nakashima H, Kinoshita M, Sato A, Nakashima M, Miyazaki H, et al. Distinct development and functions of resident and recruited liver Kupffer cells/macrophages. *J Leukoc Biol*. 2013;94(6):1325-36.
287. Nascimento M, Huang SC, Smith A, Everts B, Lam W, Bassity E, et al. Ly6Chi monocyte recruitment is responsible for Th2 associated host-protective macrophage accumulation in liver inflammation due to schistosomiasis. *PLoS Pathog*. 2014;10(8):e1004282.
288. Stutchfield BM, Antoine DJ, Mackinnon AC, Gow DJ, Bain CC, Hawley CA, et al. CSF1 Restores Innate Immunity After Liver Injury in Mice and Serum Levels Indicate Outcomes of Patients With Acute Liver Failure. *Gastroenterology*. 2015;149(7):1896-909 e14.
289. Xiang S, Dong HH, Liang HF, He SQ, Zhang W, Li CH, et al. Oval cell response is attenuated by depletion of liver resident macrophages in the 2-AAF/partial hepatectomy rat. *PLoS One*. 2012;7(4):e35180.
290. Dijkstra CD, Dopp EA, Joling P, Kraal G. The heterogeneity of mononuclear phagocytes in lymphoid organs: distinct macrophage subpopulations in the rat recognized by monoclonal antibodies ED1, ED2 and ED3. *Immunology*. 1985;54(3):589-99.
291. Santos M, Marcos R, Santos N, Malhao F, Monteiro RA, Rocha E. An unbiased stereological study on subpopulations of rat liver macrophages and on their numerical relation with the hepatocytes and stellate cells. *J Anat*. 2009;214(5):744-51.
292. Damoiseaux JG, Dopp EA, Beelen RH, Dijkstra CD. Rat bone marrow and monocyte cultures: influence of culture time and lymphokines on the expression of macrophage differentiation antigens. *J Leukoc Biol*. 1989;46(3):246-53.
293. Robinson AP, White TM, Mason DW. Macrophage heterogeneity in the rat as delineated by two monoclonal antibodies MRC OX-41 and MRC OX-42, the latter recognizing complement receptor type 3. *Immunology*. 1986;57(2):239-47.
294. Damoiseaux JG, Dopp EA, Neefjes JJ, Beelen RH, Dijkstra CD. Heterogeneity of macrophages in the rat evidenced by variability in determinants: two new anti-rat macrophage antibodies against a heterodimer of 160 and 95 kd (CD11/CD18). *J Leukoc Biol*. 1989;46(6):556-64.
295. Van den Berg TK, Dopp EA, Breve JJ, Kraal G, Dijkstra CD. The heterogeneity of the reticulum of rat peripheral lymphoid organs identified by monoclonal antibodies. *Eur J Immunol*. 1989;19(9):1747-56.
296. Harper JW, Bennett EJ. Proteome complexity and the forces that drive proteome imbalance. *Nature*. 2016;537(7620):328-38.
297. Zhang W, Yu Y, Hertwig F, Thierry-Mieg J, Zhang W, Thierry-Mieg D, et al. Comparison of RNA-seq and microarray-based models for clinical endpoint prediction. *Genome Biol*. 2015;16(1):133.
298. Van den Berge K, Hembach KM, Soneson C, Tiberi S, Clement L, Love MI, et al. RNA Sequencing Data: Hitchhiker's Guide to Expression Analysis. *Annu Rev Biomed Data Sci*. 2019;2(1):139-73.
299. Stark R, Grzelak M, Hadfield J. RNA sequencing: the teenage years. *Nat Rev Genet*. 2019;20(11):631-56.

300. Wang Z, Gerstein M, Snyder M. RNA-Seq: a revolutionary tool for transcriptomics. *Nat Rev Genet.* 2009;10(1):57-63.
301. Aslam B, Basit M, Nisar MA, Khurshid M, Rasool MH. Proteomics: Technologies and Their Applications. *J Chromatogr Sci.* 2017;55(2):182-96.
302. Ritchie ME, Phipson B, Wu D, Hu Y, Law CW, Shi W, et al. limma powers differential expression analyses for RNA-sequencing and microarray studies. *Nucleic Acids Res.* 2015;43(7):e47.
303. Robinson MD, McCarthy DJ, Smyth GK. edgeR: a Bioconductor package for differential expression analysis of digital gene expression data. *Bioinformatics.* 2010;26(1):139-40.
304. Conesa A, Madrigal P, Tarazona S, Gomez-Cabrero D, Cervera A, McPherson A, et al. A survey of best practices for RNA-seq data analysis. *Genome Biol.* 2016;17(1):13.
305. Law CW, Alhamdoosh M, Su S, Dong X, Tian L, Smyth GK, et al. RNA-seq analysis is easy as 1-2-3 with limma, Glimma and edgeR. *F1000Res.* 2016;5:1408.
306. Plubell DL, Wilmarth PA, Zhao Y, Fenton AM, Minnier J, Reddy AP, et al. Extended Multiplexing of Tandem Mass Tags (TMT) Labeling Reveals Age and High Fat Diet Specific Proteome Changes in Mouse Epididymal Adipose Tissue. *Mol Cell Proteom.* 2017;16(5):873-90.
307. Schurch NJ, Schofield P, Gierlinski M, Cole C, Sherstnev A, Singh V, et al. How many biological replicates are needed in an RNA-seq experiment and which differential expression tool should you use? *RNA.* 2016;22(6):839-51.
308. Subramanian A, Tamayo P, Mootha VK, Mukherjee S, Ebert BL, Gillette MA, et al. Gene set enrichment analysis: a knowledge-based approach for interpreting genome-wide expression profiles. *Proc Natl Acad Sci U S A.* 2005;102(43):15545-50.
309. McDermaid A, Monier B, Zhao J, Liu B, Ma Q. Interpretation of differential gene expression results of RNA-seq data: review and integration. *Brief Bioinform.* 2019;20(6):2044-54.
310. Garcia-Campos MA, Espinal-Enriquez J, Hernandez-Lemus E. Pathway Analysis: State of the Art. *Front Physiol.* 2015;6:383.
311. Liberzon A, Birger C, Thorvaldsdottir H, Ghandi M, Mesirov JP, Tamayo P. The Molecular Signatures Database (MSigDB) hallmark gene set collection. *Cell Syst.* 2015;1(6):417-25.
312. Martinez I, Sveinbjörnsson B, Smedsrød B. Nitric oxide down-regulates endocytosis in rat liver endothelial cells. *Biochem Biophys Res Commun.* 1996;222(3):688-93.
313. Martinez I, Sveinbjörnsson B, Vidal-Vanaclocha F, Asumendi A, Smedsrød B. Differential cytokine-mediated modulation of endocytosis in rat liver endothelial cells. *Biochem Biophys Res Commun.* 1995;212(1):235-41.
314. Bryda EC. The Mighty Mouse: the impact of rodents on advances in biomedical research. *Mo Med.* 2013;110(3):207-11.
315. Kruepunga N, Hakvoort TBM, Hikspoors J, Kohler SE, Lamers WH. Anatomy of rodent and human livers: What are the differences? *Biochim Biophys Acta Mol Basis Dis.* 2019;1865(5):869-78.
316. Ding C, Li Y, Guo F, Jiang Y, Ying W, Li D, et al. A Cell-type-resolved Liver Proteome. *Mol Cell Proteomics.* 2016;15(10):3190-202.
317. Azimifar SB, Nagaraj N, Cox J, Mann M. Cell-type-resolved quantitative proteomics of murine liver. *Cell Metab.* 2014;20(6):1076-87.
318. Bhandari S, Li R, Simon-Santamaria J, McCourt P, Johansen SD, Smedsrød B, et al. Transcriptome and proteome profiling reveal complementary scavenger and immune features of rat liver sinusoidal endothelial cells and liver macrophages. *BMC Mol Cell Biol.* 2020;21(1):85.
319. Smedsrød B, Pertoft H. Preparation of pure hepatocytes and reticuloendothelial cells in high yield from a single rat liver by means of Percoll centrifugation and selective adherence. *J Leukoc Biol.* 1985;38(2):213-30.
320. Knook DL, Sleyster EC. Separation of Kupffer and endothelial cells of the rat liver by centrifugal elutriation. *Exp Cell Res.* 1976;99(2):444-9.
321. Smedsrød B, Pertoft H, Eggertsen G, Sundstrom C. Functional and morphological characterization of cultures of Kupffer cells and liver endothelial cells prepared by means of density separation in Percoll, and selective substrate adherence. *Cell Tissue Res.* 1985;241(3):639-49.
322. Gomez DE, Hartzler JL, Corbitt RH, Nason AM, Thorgeirsson UP. Immunomagnetic separation as a final purification step of liver endothelial cells. *In Vitro Cell Dev Biol Anim.* 1993;29A(6):451-5.

323. Tokairin T, Nishikawa Y, Doi Y, Watanabe H, Yoshioka T, Su M, et al. A highly specific isolation of rat sinusoidal endothelial cells by the immunomagnetic bead method using SE-1 monoclonal antibody. *J Hepatol.* 2002;36(6):725-33.
324. Bartneck M, Topuz F, Tag CG, Sauer-Lehnen S, Warzecha KT, Trautwein C, et al. Molecular response of liver sinusoidal endothelial cells on hydrogels. *Mater Sci Eng C Mater Biol Appl.* 2015;51:64-72.
325. Smedsrød B. Protocol for preparation of mouse liver Kupffer cells and liver sinusoidal endothelial cells. 2012.
326. Sutermaister BA, Darling EM. Considerations for high-yield, high-throughput cell enrichment: fluorescence versus magnetic sorting. *Sci Rep.* 2019;9(1):227.
327. Pan J, Wan J. Methodological comparison of FACS and MACS isolation of enriched microglia and astrocytes from mouse brain. *J Immunol Methods.* 2020;486:112834.
328. Durack G, Robinson JP. Emerging tools for single-cell analysis : advances in optical measurement technologies. New York: Wiley-Liss; 2000.
329. Ohmura T, Enomoto K, Satoh H, Sawada N, Mori M. Establishment of a novel monoclonal antibody, SE-1, which specifically reacts with rat hepatic sinusoidal endothelial cells. *J Histochem Cytochem.* 1993;41(8):1253-7.
330. Schrage A, Loddenkemper C, Erben U, Lauer U, Hausdorf G, Jungblut PR, et al. Murine CD146 is widely expressed on endothelial cells and is recognized by the monoclonal antibody ME-9F1. *Histochem Cell Biol.* 2008;129(4):441-51.
331. Yoshida M, Nishikawa Y, Omori Y, Yoshioka T, Tokairin T, McCourt P, et al. Involvement of signaling of VEGF and TGF-beta in differentiation of sinusoidal endothelial cells during culture of fetal rat liver cells. *Cell Tissue Res.* 2007;329(2):273-82.
332. Thomann S, Weiler SME, Marquard S, Rose F, Ball CR, Toth M, et al. YAP Orchestrates Heterotypic Endothelial Cell Communication via HGF/c-MET Signaling in Liver Tumorigenesis. *Cancer Res.* 2020;80(24):5502-14.
333. Cossarizza A, Chang HD, Radbruch A, Akdis M, Andra I, Annunziato F, et al. Guidelines for the use of flow cytometry and cell sorting in immunological studies. *Eur J Immunol.* 2017;47(10):1584-797.
334. O'Donnell EA, Ernst DN, Hingorani R. Multiparameter flow cytometry: advances in high resolution analysis. *Immune Netw.* 2013;13(2):43-54.
335. Adan A, Alizada G, Kiraz Y, Baran Y, Nalbant A. Flow cytometry: basic principles and applications. *Crit Rev Biotechnol.* 2017;37(2):163-76.
336. Bajgelman MC. Principles and applications of flow cytometry. In: Misra G, editor. *Data Processing Handbook for Complex Biological Data Sources*: Academic Press; 2019. p. 119-24.
337. Vembadi A, Menachery A, Qasaimeh MA. Cell Cytometry: Review and Perspective on Biotechnological Advances. *Front Bioeng Biotechnol.* 2019;7(147):147.
338. Zerbino DR, Achuthan P, Akanni W, Amode MR, Barrell D, Bhai J, et al. Ensembl 2018. *Nucleic Acids Res.* 2018;46(D1):D754-D61.
339. Costa-Silva J, Domingues D, Lopes FM. RNA-Seq differential expression analysis: An extended review and a software tool. *PLoS One.* 2017;12(12):e0190152.
340. Lahens NF, Ricciotti E, Smirnova O, Toorens E, Kim EJ, Baruzzo G, et al. A comparison of Illumina and Ion Torrent sequencing platforms in the context of differential gene expression. *BMC Genom.* 2017;18(1):602.
341. Chen S, Li S, Xie W, Li X, Zhang C, Jiang H, et al. Performance comparison between rapid sequencing platforms for ultra-low coverage sequencing strategy. *PLoS One.* 2014;9(3):e92192.
342. Loman NJ, Misra RV, Dallman TJ, Constantinidou C, Gharbia SE, Wain J, et al. Performance comparison of benchtop high-throughput sequencing platforms. *Nat Biotechnol.* 2012;30(5):434-9.
343. Levy MJ, Washburn MP, Florens L. Probing the Sensitivity of the Orbitrap Lumos Mass Spectrometer Using a Standard Reference Protein in a Complex Background. *J Proteome Res.* 2018;17(10):3586-92.
344. Pappireddi N, Martin L, Wuhr M. A Review on Quantitative Multiplexed Proteomics. *Chembiochem.* 2019;20(10):1210-24.
345. Ankney JA, Muneer A, Chen X. Relative and Absolute Quantitation in Mass Spectrometry-Based Proteomics. *Annu Rev Anal Chem.* 2018;11(1):49-77.
346. Drabovich AP, Pavlou MP, Batruch I, Diamandis EP. Proteomic and Mass Spectrometry Technologies for Biomarker Discovery. In: Issaq HJ, Veenstra TD, editors. *Proteomic and Metabolomic Approaches to Biomarker Discovery*. Boston: Academic Press; 2013. p. 17-37.

347. Arul AB, Robinson RAS. Sample Multiplexing Strategies in Quantitative Proteomics. *Anal Chem.* 2019;91(1):178-89.
348. Myers SA, Klaeger S, Satpathy S, Viner R, Choi J, Rogers J, et al. Evaluation of Advanced Precursor Determination for Tandem Mass Tag (TMT)-Based Quantitative Proteomics across Instrument Platforms. *J Proteome Res.* 2019;18(1):542-7.
349. Fang Z, Cui X. Design and validation issues in RNA-seq experiments. *Brief Bioinform.* 2011;12(3):280-7.
350. Yamada R, Okada D, Wang J, Basak T, Koyama S. Interpretation of omics data analyses. *J Hum Genet.* 2021;66(1):93-102.
351. Rajkumar AP, Qvist P, Lazarus R, Lescai F, Ju J, Nyegaard M, et al. Experimental validation of methods for differential gene expression analysis and sample pooling in RNA-seq. *BMC Genom.* 2015;16(1):548.
352. UniProt C. UniProt: the universal protein knowledgebase in 2021. *Nucleic Acids Res.* 2021;49(D1):D480-D9.
353. Breuza L, Poux S, Estreicher A, Famiglietti ML, Magrane M, Tognolli M, et al. The UniProtKB guide to the human proteome. *Database* 2016;2016:bav120.
354. Wang X, Park J, Susztak K, Zhang NR, Li M. Bulk tissue cell type deconvolution with multi-subject single-cell expression reference. *Nat Commun.* 2019;10(1):380.
355. Menden K, Marouf M, Oller S, Dalmia A, Magruder DS, Kloiber K, et al. Deep learning-based cell composition analysis from tissue expression profiles. *Sci Adv.* 2020;6(30):eaba2619.
356. Tabula Muris C, Overall c, Logistical c, Organ c, processing, Library p, et al. Single-cell transcriptomics of 20 mouse organs creates a Tabula Muris. *Nature.* 2018;562(7727):367-72.
357. Payen VL, Lavergne A, Alevra Sarika N, Colonval M, Karim L, Deckers M, et al. Single-cell RNA sequencing of human liver reveals hepatic stellate cell heterogeneity. *JHEP Reports.* 2021;3(3):100278.
358. Chen T, Oh S, Gregory S, Shen X, Diehl AM. Single-cell omics analysis reveals functional diversification of hepatocytes during liver regeneration. *JCI Insight.* 2020;5(22).
359. Lalor PF, Lai WK, Curbishley SM, Shetty S, Adams DH. Human hepatic sinusoidal endothelial cells can be distinguished by expression of phenotypic markers related to their specialised functions in vivo. *World J Gastroenterol.* 2006;12(34):5429-39.
360. Mouta Carreira C, Nasser SM, di Tomaso E, Padera TP, Boucher Y, Tomarev SI, et al. LYVE-1 is not restricted to the lymph vessels: expression in normal liver blood sinusoids and down-regulation in human liver cancer and cirrhosis. *Cancer Res.* 2001;61(22):8079-84.
361. Geraud C, Koch PS, Zierow J, Klapproth K, Busch K, Olsavszky V, et al. GATA4-dependent organ-specific endothelial differentiation controls liver development and embryonic hematopoiesis. *J Clin Invest.* 2017;127(3):1099-114.
362. Schmid CD, Schledzewski K, Mogler C, Waldburger N, Kalna V, Marx A, et al. GPR182 is a novel marker for sinusoidal endothelial differentiation with distinct GPCR signaling activity in vitro. *Biochem Biophys Res Commun.* 2018;497(1):32-8.
363. Labaj PP, Leparo GG, Linggi BE, Markillie LM, Wiley HS, Kreil DP. Characterization and improvement of RNA-Seq precision in quantitative transcript expression profiling. *Bioinformatics.* 2011;27(13):i383-91.
364. Schildberg FA, Hegenbarth SI, Schumak B, Scholz K, Limmer A, Knolle PA. Liver sinusoidal endothelial cells veto CD8 T cell activation by antigen-presenting dendritic cells. *Eur J Immunol.* 2008;38(4):957-67.
365. Schledzewski K, Geraud C, Arnold B, Wang S, Grone HJ, Kempf T, et al. Deficiency of liver sinusoidal scavenger receptors stabilin-1 and -2 in mice causes glomerulofibrotic nephropathy via impaired hepatic clearance of noxious blood factors. *J Clin Invest.* 2011;121(2):703-14.
366. Zielinska KA, Van Moortel L, Opdenakker G, De Bosscher K, Van den Steen PE. Endothelial Response to Glucocorticoids in Inflammatory Diseases. *Front Immunol.* 2016;7:592.
367. Li R, Kowalski PS, Morselt HWM, Schepel I, Jongman RM, Aslan A, et al. Endothelium-targeted delivery of dexamethasone by anti-VCAM-1 SAINT-O-Somes in mouse endotoxemia. *PLoS One.* 2018;13(5):e0196976.
368. Franco LM, Gadkari M, Howe KN, Sun J, Kardava L, Kumar P, et al. Immune regulation by glucocorticoids can be linked to cell type-dependent transcriptional responses. *J Exp Med.* 2019;216(2):384-406.

369. Melgert BN, Weert B, Schellekens H, Meijer DK, Poelstra K. The pharmacokinetic and biological activity profile of dexamethasone targeted to sinusoidal endothelial and Kupffer cells. *J Drug Target.* 2003;11(1):1-10.
370. Melgert BN, Olinga P, Jack VK, Molema G, Meijer DKE, Poelstra K. Dexamethasone coupled to albumin is selectively taken up by rat nonparenchymal liver cells and attenuates LPS-induced activation of hepatic cells. *J Hepatol.* 2000;32(4):603-11.
371. Broering R, Montag M, Jiang M, Lu M, Sowa JP, Kleinehr K, et al. Corticosteroids shift the Toll-like receptor response pattern of primary-isolated murine liver cells from an inflammatory to an anti-inflammatory state. *Int Immunol.* 2011;23(9):537-44.
372. Yeoman AD, Westbrook RH, Zen Y, Bernal W, Al-Chalabi T, Wendon JA, et al. Prognosis of acute severe autoimmune hepatitis (AS-AIH): the role of corticosteroids in modifying outcome. *J Hepatol.* 2014;61(4):876-82.
373. Xue R, Meng Q. The Management of Glucocorticoid Therapy in Liver Failure. *Front Immunol.* 2019;10(2490):2490.
374. Cain DW, Cidlowski JA. Immune regulation by glucocorticoids. *Nat Rev Immunol.* 2017;17(4):233-47.
375. Sengupta S, Wasyluk B. Ligand-dependent interaction of the glucocorticoid receptor with p53 enhances their degradation by Hdm2. *Genes Dev.* 2001;15(18):2367-80.
376. Webster JC, Jewell CM, Bodwell JE, Munck A, Sar M, Cidlowski JA. Mouse glucocorticoid receptor phosphorylation status influences multiple functions of the receptor protein. *J Biol Chem.* 1997;272(14):9287-93.
377. Wallace AD, Cidlowski JA. Proteasome-mediated glucocorticoid receptor degradation restricts transcriptional signaling by glucocorticoids. *J Biol Chem.* 2001;276(46):42714-21.
378. Rinaldi G, Rossi M, Fendt SM. Metabolic interactions in cancer: cellular metabolism at the interface between the microenvironment, the cancer cell phenotype and the epigenetic landscape. *Wiley Interdiscip Rev Syst Biol Med.* 2018;10(1):e1397.
379. McMahan RH, Porsche CE, Edwards MG, Rosen HR. Free Fatty Acids Differentially Downregulate Chemokines in Liver Sinusoidal Endothelial Cells: Insights into Non-Alcoholic Fatty Liver Disease. *PLoS One.* 2016;11(7):e0159217.
380. Jha AK, Huang SC, Sergushichev A, Lampropoulou V, Ivanova Y, Loginicheva E, et al. Network integration of parallel metabolic and transcriptional data reveals metabolic modules that regulate macrophage polarization. *Immunity.* 2015;42(3):419-30.
381. Sadiku P, Walmsley SR. Hypoxia and the regulation of myeloid cell metabolic imprinting: consequences for the inflammatory response. *EMBO Rep.* 2019;20(5).
382. Kalucka J, Bierhansl L, Conchinha NV, Missiaen R, Elia I, Bruning U, et al. Quiescent Endothelial Cells Upregulate Fatty Acid beta-Oxidation for Vasculoprotection via Redox Homeostasis. *Cell Metab.* 2018;28(6):881-94 e13.
383. Falkenberg KD, Rohlenova K, Luo Y, Carmeliet P. The metabolic engine of endothelial cells. *Nat Metab.* 2019;1(10):937-46.
384. Spolarics Z, Lang CH, Bagby GJ, Spitzer JJ. Glutamine and fatty acid oxidation are the main sources of energy for Kupffer and endothelial cells. *Am J Physiol.* 1991;261(2 Pt 1):G185-90.
385. Smedsrød B. Cellular events in the uptake and degradation of hyaluronan. *Adv Drug Deliv Rev.* 1991;7(2):265-78.
386. Elchaninov A, Lokhonina A, Nikitina M, Vishnyakova P, Makarov A, Arutyunyan I, et al. Comparative Analysis of the Transcriptome, Proteome, and miRNA Profile of Kupffer Cells and Monocytes. *Biomedicines.* 2020;8(12).
387. Tanzer MC, Frauenstein A, Stafford CA, Phulphagar K, Mann M, Meissner F. Quantitative and Dynamic Catalogs of Proteins Released during Apoptotic and Necroptotic Cell Death. *Cell Rep.* 2020;30(4):1260-70 e5.
388. Bailly-Maitre B, de Sousa G, Boulukos K, Gugenheim J, Rahmani R. Dexamethasone inhibits spontaneous apoptosis in primary cultures of human and rat hepatocytes via Bcl-2 and Bcl-xL induction. *Cell Death Differ.* 2001;8(3):279-88.
389. van Roosmalen IA, Quax WJ, Kruyt FA. Two death-inducing human TRAIL receptors to target in cancer: similar or distinct regulation and function? *Biochem Pharmacol.* 2014;91(4):447-56.

390. Jeon MY, Woo SM, Seo SU, Kim SH, Nam JO, Kim S, et al. Dexamethasone Inhibits TRAIL-Induced Apoptosis through c-FLIP(L) Upregulation and DR5 Downregulation by GSK3beta Activation in Cancer Cells. *Cancers* 2020;12(10).
391. Zhang S, Liu Y, Liang Q. Low-dose dexamethasone affects osteoblast viability by inducing autophagy via intracellular ROS. *Mol Med Rep.* 2018;17(3):4307-16.
392. Guess A, Agrawal S, Wei CC, Ransom RF, Benndorf R, Smoyer WE. Dose- and time-dependent glucocorticoid receptor signaling in podocytes. *Am J Physiol Renal Physiol.* 2010;299(4):F845-53.
393. Berki T, Palinkas L, Boldizsar F, Nemeth P. Glucocorticoid (GC) sensitivity and GC receptor expression differ in thymocyte subpopulations. *Int Immunol.* 2002;14(5):463-9.
394. Xie G, Choi SS, Syn WK, Michelotti GA, Swiderska M, Karaca G, et al. Hedgehog signalling regulates liver sinusoidal endothelial cell capillarisation. *Gut.* 2013;62(2):299-309.
395. Winkler M, Staniczek T, Kurschner SW, Schmid CD, Schonhaber H, Cordero J, et al. Endothelial GATA4 controls liver fibrosis and regeneration by preventing a pathogenic switch in angiocrine signaling. *J Hepatol.* 2021;74(2):380-93.
396. Lu J, Zhao YL, Zhang XQ, Li LJ. The vascular endothelial growth factor signaling pathway regulates liver sinusoidal endothelial cells during liver regeneration after partial hepatectomy. *Expert Rev Gastroenterol Hepatol.* 2021;15(2):139-47.
397. Elvevold K, Nedredal GI, Revhaug A, Bertheussen K, Smedsrød B. Long-term preservation of high endocytic activity in primary cultures of pig liver sinusoidal endothelial cells. *Eur J Cell Biol.* 2005;84(9):749-64.

Paper I

Bhandari, S., Li, R., Simon-Santamaria, J., McCourt, P., Johansen, S.D., Smedsrød, B., Martinez, I.Z. & Sørensen, K.K. (2020).

Transcriptome and proteome profiling reveal complementary scavenger and immune features of rat liver sinusoidal endothelial cells and liver macrophages.

BMC molecular and cell biology, 21(1), 85.

<https://doi.org/10.1186/s12860-020-00331-9>

RESEARCH ARTICLE

Open Access



Transcriptome and proteome profiling reveal complementary scavenger and immune features of rat liver sinusoidal endothelial cells and liver macrophages

Sabin Bhandari¹, Ruomei Li¹, Jaione Simón-Santamaría¹, Peter McCourt¹, Steinar Daae Johansen^{1,2}, Bård Smedsrød^{1*} , Inigo Martinez-Zubiaurre³ and Karen Kristine Sørensen¹

Abstract

Background: Liver sinusoidal endothelial cells (LSECs) and Kupffer cells (KCs; liver resident macrophages) form the body's most effective scavenger cell system for the removal of harmful blood-borne substances, ranging from modified self-proteins to pathogens and xenobiotics. Controversies in the literature regarding the LSEC phenotype pose a challenge when determining distinct functionalities of KCs and LSECs. This may be due to overlapping functions of the two cells, insufficient purification and/or identification of the cells, rapid dedifferentiation of LSECs in vitro, or species differences. We therefore characterized and quantitatively compared expressed gene products of freshly isolated, highly pure LSECs (fenestrated SE-1/FcγRIIb2⁺) and KCs (CD11b/c⁺) from Sprague Dawley, Crl:CD (SD), male rats using high throughput mRNA-sequencing and label-free proteomics.

Results: We observed a robust correlation between the proteomes and transcriptomes of the two cell types. Integrative analysis of the global molecular profile demonstrated the immunological aspects of LSECs. The constitutive expression of several immune genes and corresponding proteins of LSECs bore some resemblance with the expression in macrophages. LSECs and KCs both expressed high levels of scavenger receptors (SR) and C-type lectins. Equivalent expression of SR-A1 (Msr1), mannose receptor (Mrc1), SR-B1 (Scarb1), and SR-B3 (Scarb2) suggested functional similarity between the two cell types, while functional distinction between the cells was evidenced by LSEC-specific expression of the SRs stabilin-1 (Stab1) and stabilin-2 (Stab2), and the C-type lectins LSECtin (Clec4g) and DC-SIGNR (Clec4m). Many immune regulatory factors were differentially expressed in LSECs and KCs, with one cell predominantly expressing a specific cytokine/chemokine and the other cell the cognate receptor, illustrating the complex cytokine milieu of the sinusoids. Both cells expressed genes and proteins involved in antigen processing and presentation, and lymphocyte co-stimulation.

(Continued on next page)

* Correspondence: bard.smedsrod@uit.no

¹Department of Medical Biology, Vascular Biology Research Group, University of Tromsø (UiT) -The Arctic University of Norway, Hansine Hansens veg 18, N-9037 Tromsø, Norway

Full list of author information is available at the end of the article



© The Author(s). 2020 **Open Access** This article is licensed under a Creative Commons Attribution 4.0 International License, which permits use, sharing, adaptation, distribution and reproduction in any medium or format, as long as you give appropriate credit to the original author(s) and the source, provide a link to the Creative Commons licence, and indicate if changes were made. The images or other third party material in this article are included in the article's Creative Commons licence, unless indicated otherwise in a credit line to the material. If material is not included in the article's Creative Commons licence and your intended use is not permitted by statutory regulation or exceeds the permitted use, you will need to obtain permission directly from the copyright holder. To view a copy of this licence, visit <http://creativecommons.org/licenses/by/4.0/>. The Creative Commons Public Domain Dedication waiver (<http://creativecommons.org/publicdomain/zero/1.0/>) applies to the data made available in this article, unless otherwise stated in a credit line to the data.

(Continued from previous page)

Conclusions: Our findings support complementary and partly overlapping scavenging and immune functions of LSECs and KCs. This highlights the importance of including LSECs in studies of liver immunity, and liver clearance and toxicity of large molecule drugs and nano-formulations.

Keywords: Sprague Dawley rat, Sinusoidal endothelial cells, Kupffer cells, Macrophages, Transcriptomics, Proteomics, Immune functions, cell markers, Scavenger receptors

Background

The liver has a central role in host defense [1, 2]. Its extensive capillary network, the sinusoids, houses the body's most effective scavenger cell system comprising the Kupffer cells (KCs; the body's largest reservoir of resident macrophages [3]), and liver sinusoidal endothelial cells (LSECs). For decades KCs, facing the sinusoidal lumen, were believed to be the only liver cell responsible for the clearance of blood-borne material [4, 5]. This view was challenged by a series of studies throughout the 1980s and 1990s showing that a number of physiological macromolecules and colloids were cleared chiefly by LSECs, but only to a minor extent by KCs [6–15]. Today it is accepted that LSECs and KCs together make up the hepatic “dual cell principle of waste clearance”, with LSECs being geared to effective clathrin-mediated endocytosis of nanoparticles (< 200 nm), colloids, and macromolecules, and KCs taking up larger material [5]. The discovery that these cells share the task of blood clearance in this way suggested that LSECs are a highly specialized endothelium with characteristics in common with KCs, not only functionally, but at the molecular level as well. The present study was undertaken to study the similarities and differences of the two cells, by comparing their transcriptomes and proteomes.

The liver receives approximately 25% of cardiac output, exposing the sinusoidal cells to large volumes of blood, thus placing these cells in a unique position to monitor blood content. Approximately 80% of the organ blood supply drains the gut and contains (in addition to nutrients) toxins, bacterial components, viruses, and various waste products that are efficiently removed from blood by uptake in LSECs and KCs [5, 15], thus preventing deposition and deleterious effects of such components elsewhere. LSECs show an extraordinarily high capacity for uptake of soluble macromolecules and nanoparticles, including virus [10, 11, 15–23]. For this purpose, LSECs express several high affinity endocytosis receptors, some of which are pattern recognition receptors. These include the scavenger receptors (SRs) stabilin-1 and stabilin-2 [24, 25], the macrophage mannose receptor (CD206) [17], and the endocytic Fc-gamma receptor IIb2 (FcγRIIb2, CD32b) [26]. In addition, LSECs express several Toll-like receptors (TLRs) [27–29], and in mice, the cells are reported to

possess adaptive immune functions, including cross-presentation of endocytosed antigens to naïve CD8⁺ T-cells contributing to the generation of memory T-cells important for liver immune tolerance [1, 27, 30–32]. In contrast to KCs, LSECs are normally not phagocytic but can take up 1 μm particles if KCs are depleted [33].

Due to the overlapping functions of LSECs and KCs as scavenger cells [1, 2, 5], the large endothelial cell diversity between different vascular beds [34, 35], and the lack of standardized methods for LSEC isolation and identification between different research groups [36, 37], LSECs have been described as a cell of controversial and confusing identity [37]. For instance, the pan-leukocyte marker CD45 is often used as a negative selection criterion for isolation of mouse and human LSECs by immune based methods but is reported to be expressed in rat LSECs [36, 38]. Furthermore, LSECs rapidly dedifferentiate in culture [39, 40], which poses a problem for long-term co-cultures with e.g. lymphocytes in immune assays. This highlights the importance of using early primary cells when exploring cell functions and molecular expression patterns, and mapping LSEC and KC gene and protein expression in different species used in biomedical research.

In order to resolve some of the discrepancies in the literature regarding LSEC and KC markers and molecular phenotypes, we directly compared the transcriptome and proteome of freshly isolated rat LSECs and KCs. Studies comparing the gene/protein expression of LSECs and KCs are rare. To the best of our knowledge only two studies, both done in C57Bl/6 mice, have compared the proteome of liver resident cell populations [41, 42], but without discussing LSEC scavenger or immune functions. Our study represents the first comprehensive multiomics profiling and comparison of rat KCs and LSECs. Based on our findings we conclude that LSECs differ from other types of endothelial cells due to their distinct immunological features.

Results

Isolation of LSECs and KCs using SE-1 and CD11b/c yields highly pure cell preparations

An overview of the transcriptomics and proteomics experiments and purity tests of cells used in the experiments is given in Fig. 1. LSECs and KCs were purified

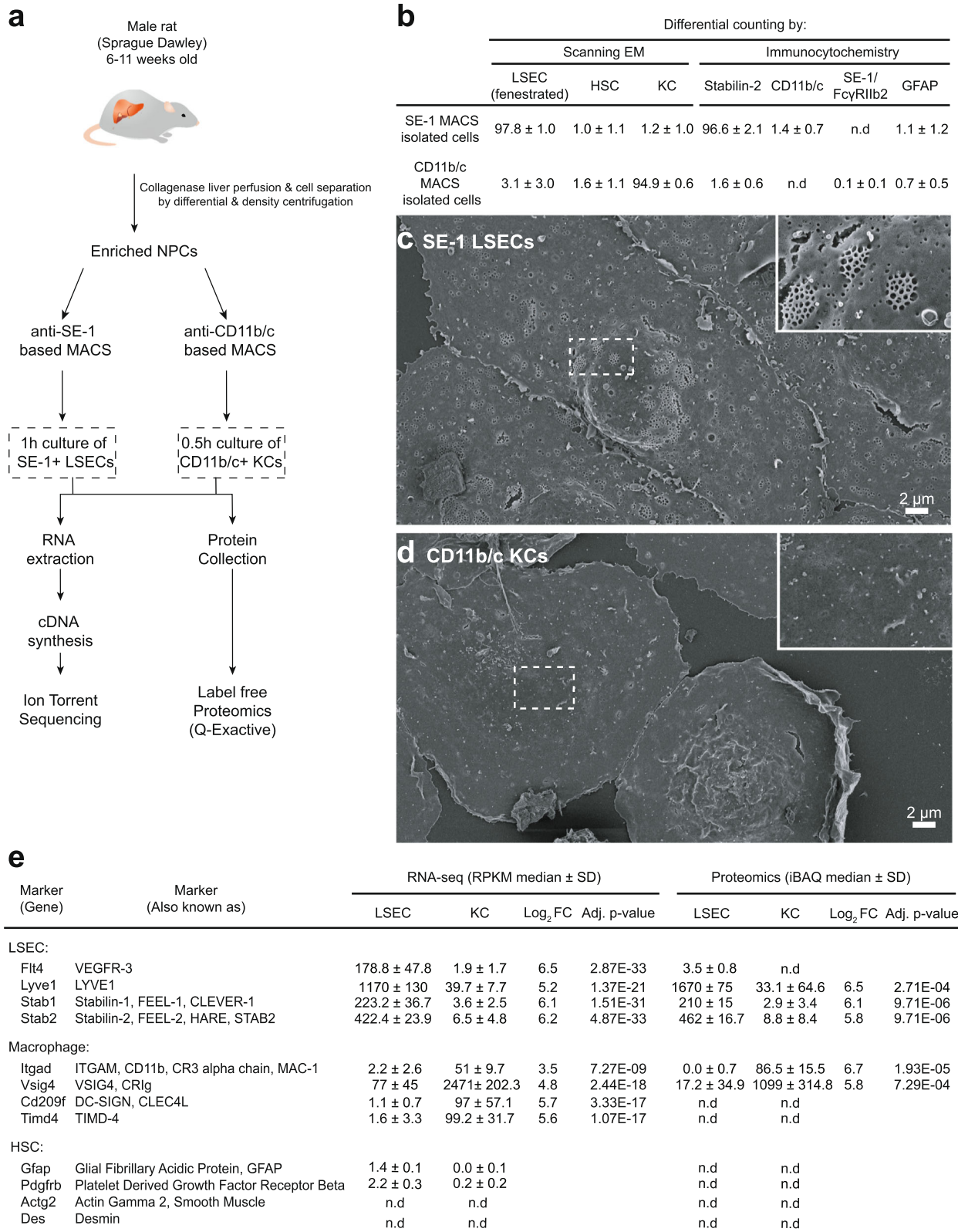


Fig. 1 (See legend on next page.)

(See figure on previous page.)

Fig. 1 Overview of experimental workflows and cell purity tests. **a.** Schematic overview of the high-throughput transcriptomics and label-free proteomics workflows. **b.** Purity of SE-1-MACS-isolated liver sinusoidal endothelial cells (LSECs) and CD11b/c-MACS-isolated Kupffer cells (KCs). Cell isolates were analyzed by scanning electron microscopy (EM) (LSECs: $n = 6$, including all cell isolates for proteomics and RNA sequencing; KCs: $n = 4$, including all isolates for proteomics), and immune cytochemistry (KC: $n = 4$, LSEC: $n = 3$, including all cell isolates for proteomics). Results are presented as % of total cell count (mean \pm standard deviation). Antibodies (Table 1) targeted either stabilin-2 (LSEC marker), SE-1/Fc γ RIIb2 (LSEC marker), CD11b/c (KC marker), or glial fibrillar acidic protein (GFAP, stellate cell marker). N.d., not determined. **c-d.** Scanning electron micrographs showing the typical morphology of MACS-isolated cells. Insert in c shows LSEC fenestrations (hallmark of LSECs), which were absent in KCs (d). **e.** Expression level of marker genes for LSECs, KCs, and hepatic stellate cells (HSC) in the KC and LSEC transcriptomes and proteomes. Expression values are given as RPKM (RNA-seq), and iBAQ (label-free proteomics), as described in Methods

by magnetic-activated cell separation (MACS) of non-parenchymal liver cell (NPC) suspensions generated from collagenase perfused rat liver, then plated for 0.5 h (KCs) or 1 h (LSECs) and washed with medium before RNA and protein extraction (Fig. 1a). For LSEC, we used the SE-1 monoclonal antibody [43, 44] (Table 1), which targets Fc γ RIIb2 [45] and has been previously tested for

MACS-based purification of rat LSECs [43]. The isolated cells were > 97% LSECs (i.e. fenestrated endothelial cells), as examined by scanning electron microscopy (SEM), and 96.6% were stabilin-2 positive by immune staining (Fig. 1b-d). The few contaminating cells were KCs and stellate cells. A monoclonal antibody to CD11b/c (Table 1), targeting complement receptor 3 (CR3) was used to

Table 1 Antibodies used in the study

Antibody (clone)	Target	Company/Reference	Catalog #	Working concentration
Flow cytometry antibodies and isotype controls				
CD45-PE (OX-1)	CD45, PTPRC	Novus Biologicals	NB100-64895PE	0.85 μ g/ million cells
PE Mouse IgG1	IgG1 κ isotype control	BD Pharmingen	555749	0.2 μ g/ million cells
HSEC ^a antibody (SE-1) -AF488	CD32b, Fc γ RIIb2	Novus Biologicals	NB110-68095AF488	1 μ g/ million cells
Mouse IgG2a AF488 (MG2a-53)	IgG2a κ isotype control	Novus Biologicals	NB600-986AF488	0.65 μ g/ million cells
CD31-eFluor 660 (TLD-3A12)	CD31, PECAM-1	eBioscience	50-0310-82	0.2 μ g/ million cells
Mouse IgG1k- eFluor 660 (P3.6.2.8.1)	IgG1 κ isotype control	eBioscience	50-4714	0.2 μ g/ million cells
Immune staining of cells and tissues				
HSEC ^a antibody (SE-1)	CD32b, Fc γ RIIb2	Novus Biologicals	NB110-68095	10 μ g/ml
CD11b/c Biotin (OX-42)	CD11b/c, CR3	Cedarlane	CL042B	2 μ g/ml
CD163 (ED2)	CD163	AbD Serotec	MCA342GA	10 μ g/ml
CD68 (ED-1)	CD68 antigen, macrophage	Abcam	ab31630	20 μ g/ml
GFAP	Glial fibrillary acidic protein	Dako	Z0334	15 μ g/ml
Human MMR/CD206	CD206, macrophage mannose receptor	R&D Systems	AF2534	2 μ g/ml
SR-A1/MSR	Macrophage scavenger receptor A1	Novus Biologicals	NBP1-00092	12 μ g/ml
SR-B1	Scavenger receptor B1	Novus Biologicals	NB400-104	10 μ g/ml
Rabbit anti-rat HA/SR serum ^b	Stabilin-2, STAB2	(24)		1:200
CD45 (OX-1)	CD45, PTPRC	Novus Biologicals	NB100-64895	10 μ g/ml
CD31 (TLD-3A12)	CD31, PECAM-1	Invitrogen	MA1-81051	10 μ g/ml
Magnetic-activated cell sorting				
HSEC ^a antibody (SE-1)	CD32b, Fc γ RIIb2	Novus Biologicals	NB110-68095	0.2 μ g/million NPCs
CD11b/c Biotin (OX-42)	CD11b/c, CR3	Cedarlane	CL042B	0.1 μ g/million NPCs
Anti-Mouse IgG2a + b MicroBeads	IgG2a + b	Miltenyi	130-047-201	2 μ l/million NPCs

^aHSEC, hepatic sinusoidal endothelial cell

^bStabilin-2 was named the hyaluronan-scavenger receptor (HA/SR) in reference [24]

Secondary antibodies used for immune labeling of cells and tissues were all species-matched AlexaFluor antibodies from Invitrogen (ThermoFischer)

purify KCs. This yielded 94.9% KCs - contaminating cells were 3.1% LSECs and 1.6% stellate cells (Fig. 1b).

Quantitative expression of marker genes used for cross validation of the transcriptomics and proteomics data are listed in Fig. 1e. Consistent with SEM and immunocytochemistry analysis of MACS-isolated cells, expression of macrophage and stellate cell markers were low in the LSEC transcriptomes and proteomes, whereas expression of LSEC and stellate cell markers were low in the KC transcriptomes and proteomes.

To check the hepatic intralobular distribution of cells expressing SE-1 (i.e. FcγRIIb2), and CD11b/c, frozen rat liver sections were stained with the same antibodies used for MACS-isolation of cells (Fig. 2). The SE-1 antibody showed a strict sinusoidal staining pattern, colocalizing with the LSEC marker stabilin-2 [24, 46, 47] in all sinusoids (Fig. 2a, b). Most CD11b/c positive cells were

located in the periportal region and showed a different staining pattern than stabilin-2 (Fig. 2c).

Global information generated from omics data profiling

In the RNA-seq experiment 10,306 genome features were deemed expressed and included in the subsequent analyses, while in the label-free proteomics experiment 2996 non-redundant protein IDs were deemed expressed and included in the further analyses. Principal component analysis (Fig. 3a) segregated the LSEC and KC samples into disparate clusters coherent with the distinct biology of the cells.

Figure 3b illustrates the total number of gene products identified with the respective techniques, and their overlap, in the LSEC and KC groups. The proteome covered 26–27% of the transcriptome. Notably, most proteins (90.8–91.5%) identified in the proteome had valid

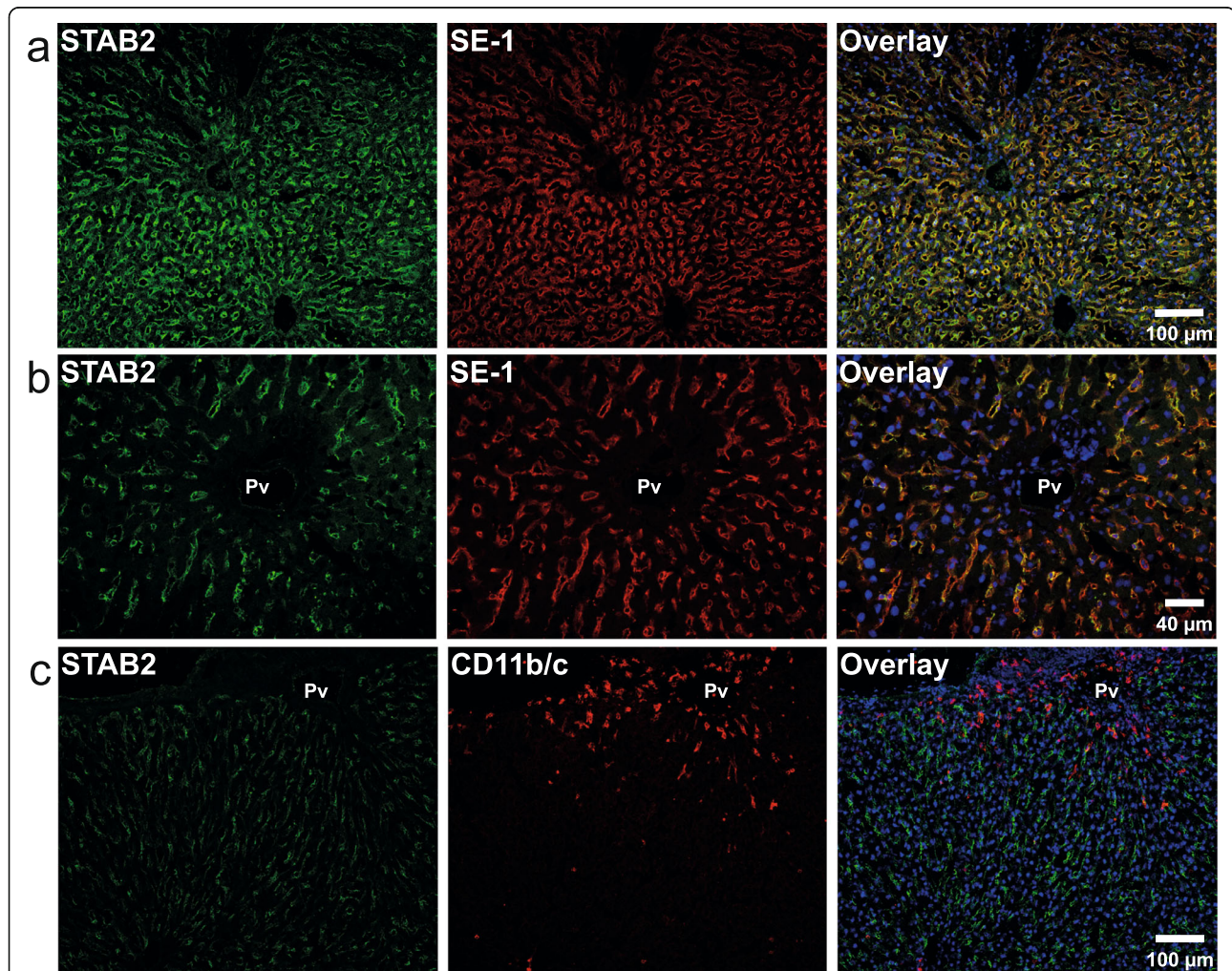
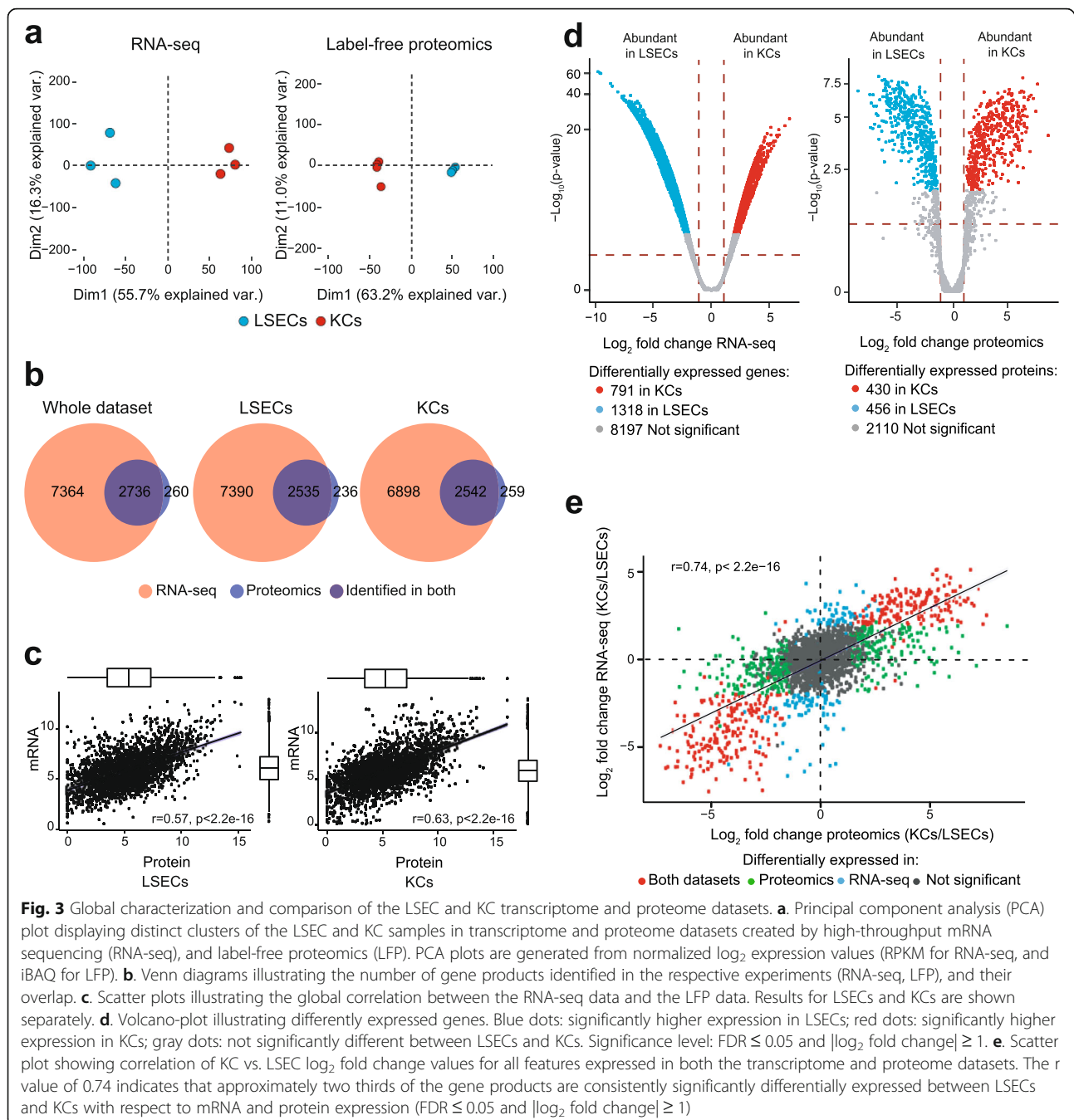


Fig. 2 Immune histochemistry of acetone-fixed frozen rat liver sections. The sections were double immune-labeled with primary antibodies against **a-b**) stabilin-2 (STAB2; green fluorescence), and FcγRIIb2 (SE-1; red fluorescence), or against **c**) stabilin-2 (STAB2; green fluorescence), and CD11b/c (red fluorescence). Antibodies are listed in Table 1. Pv, portal vein. Nuclei were stained with DAPI (blue fluorescence in overlay images)



corresponding mRNA in the transcriptome. To evaluate the coherence between the transcriptome and proteome, we calculated the global Pearson correlation coefficient r using the expression data between the omics datasets for each cell type. The global correlation r value was 0.57 for LSECs, and 0.63 for KCs (Fig. 3c) which are in the upper end of the previously reported range of 0.4–0.6 [41, 48] supporting the reliability of the data.

Differentially expressed gene products are key to understanding phenotypic and functional variation between

cell types. The results of the differential expression analyses of the RNA-seq data, and the proteomics data are summarized in Fig. 3d. We identified 2109 gene products in the transcriptome (20.5%) as significantly differentially expressed (with cutoff of FDR (false discovery rate) ≤ 0.05 and |log₂ fold change| ≥ 1) in LSECs and KCs. Similarly, in the proteome, 886 proteins (~ 30%) were significantly differentially expressed in the two cells (with cutoff of FDR ≤ 0.05 and |log₂ fold change| ≥ 1). Despite differences in percentage of differentially

expressed gene products in the RNA-seq and proteomics experiments, the \log_2 fold changes for the unique gene products identified in both datasets showed high correlation ($r = 0.74$ [95% CI: 0.72–0.75]) (Fig. 3e), suggesting good congruence between the two techniques.

LSECs and KCs show enrichment of terms reflecting their ontogeny

We used ranked gene lists based on expression level from the RNA-seq experiment as input for gene set enrichment analysis (GSEA) [49, 50] to identify the intrinsic functional characteristics of LSECs and KCs. GSEA showed enrichment of 268 biological processes in LSECs and 121 biological processes in KCs with FDR q -value ≤ 0.05 corresponding to Gene Ontology (GO) terms [51, 52] in the Molecular Signatures Database [49, 53] that concur with the generic role of these cells (Additional file 1; Fig. 4). Like other endothelial cells, LSECs are involved in development, morphogenesis, patterning and maintenance of blood vessels, and displayed enrichment of gene sets associated with response to vascular endothelial growth factor and regulation of WNT, BMP, and TGF β signalling pathways. KCs, being macrophages, displayed enrichment of terms related to adaptive and innate immune responses.

Expression of genes associated with endocytic function, cytoskeleton organization, and positive regulators of endocytosis, such as 1-phosphatidylinositol-4-phosphate 5-kinase (Pip5k1c), phospholipase D1/2 (Pld2), integrin subunit beta1 (Itgb1), GTPase Hras, clathrin adaptor protein (Dab2), caveolin1 (Cav1), and E3 ligase NEDD4 (Nedd4) were higher in LSECs than in KCs (Additional file 2). Moreover, LSECs showed higher expression of transport-related proteins such as EH domain-containing protein 3 (Ehd3), which is suggested to be involved in transport of stabilin-1-positive vesicles [39], adaptor-related protein complex 1 beta 1 subunit (Ap1b1), and sorting nexin (Snx) 8 and 33, which are associated with vesicular transport (Additional file 2). Interestingly, RNA-seq of LSECs revealed high expression of genes coding for connective tissue components such as Sparc, Col4a1, Col4a2, Egfl7, and Mfge8, indicating a significant role of these cells in extracellular matrix maintenance and remodeling of liver (Additional file 2). Transcription factor Gata4, which is essential for LSEC differentiation [39, 47] was specifically expressed in the LSEC transcriptome (Additional file 2).

Most gene products involved in KC immune functions are also expressed in LSECs

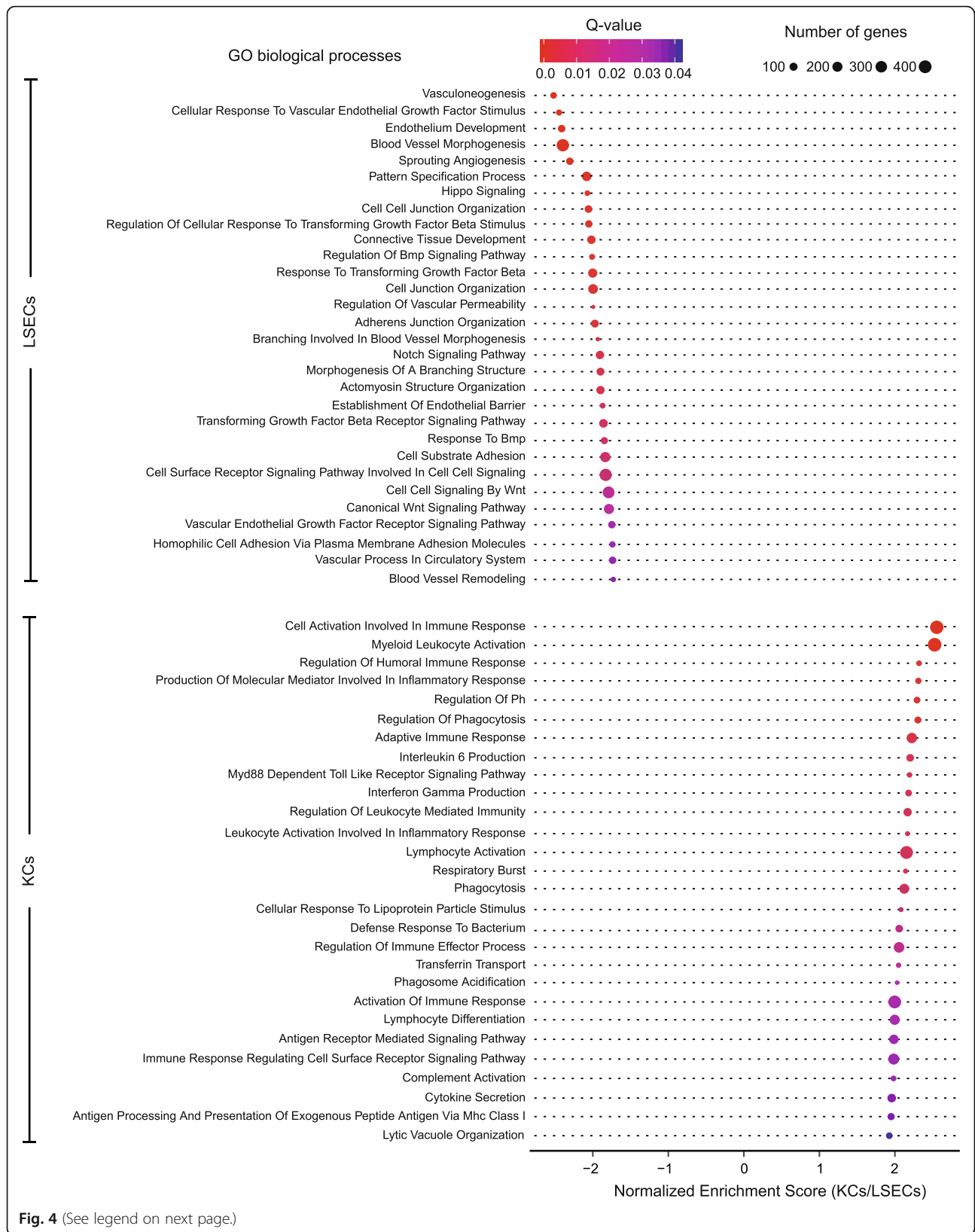
Genes associated with the term immune system processes (GO:0002376) include 2645 annotated objects in the rat genome database (December 13, 2019). Of these, we found 1466 expressed genes in the RNA-seq data,

and 554 expressed genes in the label-free proteomics experiments that were associated with the term (Fig. 5a; Additional file 3). Both cells expressed numerous immune genes - the majority of which were expressed at low density but more abundant in KCs compared to LSECs. To ascertain the immunological role of expressed genes we performed functional enrichment analysis (DAVID 6.8 [54, 55]) of genes with expression values ≥ 10 RPKM (reads per kilobase of exon model per million mapped reads [56]) separately in the LSEC and KC RNA-seq datasets. The threshold 10 RPKM was set to increase the confidence of the results. The immune terms that were significantly enriched (FDR ≤ 0.05) in KC and LSEC transcriptomes were similar, and each term contained almost similar number of expressed genes in the two cells (Fig. 5b).

Both cell types show high expression of scavenger receptors and immune lectins

LSECs and KCs express a variety of SRs, C-type lectins, and TLRs [16, 17, 27–29]. We found that both cells expressed many SRs and immune lectin gene products at high densities, of which some were cell type specific (Fig. 6a; Additional file 4), providing the capacity of rapid sensing and clearance of various danger molecules. Among these were the macrophage mannose receptor (Mrc1) and macrophage SR-A1 (Msr1) which were abundantly expressed both in the LSEC and KC transcriptomes and proteomes (Fig. 6a) and confirmed by immune cytochemistry (Fig. 6c). The high-density lipoprotein receptor SR-B1 (Scarb1) was also equally expressed in the rat LSEC and KC transcriptomes, but at low density, and were not identified in the cell proteomes. However, immune labelling experiments validated SR-B1 protein expression in both LSECs and KCs (Fig. 6c), in accordance with [57]. Of note, CD36, a reliable LSEC marker in human liver [58] was evidently expressed in rat KCs but was very low in rat LSECs (Fig. 6a). Same receptor was previously reported to be absent from Sprague Dawley rat LSECs in western blot and immune fluorescence experiments [59].

Stabilin-1 (Stab1) and stabilin-2 (Stab2) were expressed at much higher densities in the LSECs than in KCs (Fig. 6a-b). Immune labeling of NPCs (Fig. 6c) and frozen rat liver sections (Fig. 2) for stabilin-2 confirmed LSEC specific expression and a typical LSEC distribution pattern in all hepatic zones of this protein, in accordance with [60] supporting the use of stabilin-2 as a specific pan-LSEC marker. Furthermore, rat LSECs showed high mRNA and protein expression of Clec4g (LSEctin) and Clec4m (DC-SIGNR) (Fig. 6a, b), as was also reported in a study of human LSECs [61], where Clec4g was used as a specific LSEC marker in liver single cell transcriptome studies [62].



(See figure on previous page.)

Fig. 4 Dot plot showing selected enriched terms in KC and LSEC transcriptomes, belonging to GO biological processes in the Molecular Signatures Database (MSigDB) [53]. The Normalized Enrichment Score reflects the degree of overrepresentation of the genes in a gene set across the entire ranked list of genes after adjusting for differences in gene set size, and correlation between the gene sets and the RNA-seq expression data. Dot size represents the number of genes assigned to the specific process, and dot colour represents the associated FDR q-value generated from the GSEA analysis

Some of the receptors reported in the literature to discriminate KCs from other liver cells, were also expressed in the LSEC transcriptome. These included Marco, Cd5l, Clec4f, Cd163, Igals3, and Cd68 (Fig. 6a, b). However, their transcript level in KCs were significantly higher compared to LSECs, and their abundance in the LSEC proteome was low. Immune labeling of NPCs for CD163 (not shown) and CD68 showed staining of KCs only (Fig. 6c) and labeling of rat liver sections for CD68 together with the LSEC marker stabilin-2 showed a staining pattern of CD68 that is typical for KCs (Additional file 5), supporting the proteomic results.

Several TLRs were detected in LSECs and KCs transcriptomes (Additional file 3). The abundance of Tlr4, 5, 6, 7, 8, 10, 11, and 12 mRNA was significantly higher ($FDR \leq 0.05$) in KCs, whereas Tlr2, 3, and 13 were not significantly different. The only TLR identified by proteomics at steady state was TLR3 which was identified in both cells.

Immune regulatory factors expressed by LSECs and KCs

When reviewing genes annotated with cytokine receptor binding (GO:0005126), cytokine receptor activity (GO:0004896), complement activation (GO:0006956), and complement receptor activity (GO:0004875), we identified 209 genes in the transcriptome (out of 551 objects associated under the terms), and 54 proteins in the proteome (Additional file 6). Low protein identification may be due to the fact that these genes are normally expressed at low levels in non-stimulated cells from healthy animals (as analyzed in this study), and many gene products associated with the terms represent secreted proteins, mostly found extracellularly. Thus, the bulk of gene products affiliated with the terms were only detected in the transcriptome, and at low level. Many were also differently expressed in the LSEC and KC transcriptomes (Fig. 7a).

Figure 7b-c reflects the complex cytokine milieu of the sinusoids. LSECs showed significantly higher expression of the cytokine receptors Tgfb3, Il6st, Osmr, Il1r1 and Lifr (Fig. 7b) enabling them to sense and respond to the cytokines Tgfb3, Osm, Il1b and Lif in paracrine and autocrine manners. Tgfb3, Osm, and Il18 were more abundantly expressed by KCs (Fig. 7c). LSECs also expressed high levels of Ackr3 (Fig. 7b) which is involved in scavenging and degradation of chemokines,

thus regulating their levels in the hepatic sinusoids. KCs showed significantly higher expression of the cytokine receptors Il6r and Csf3r, and chemokine receptor Cxcr4 (Fig. 7b), which allow KCs to respond to Ccl24, Cxcl12, Ccl2, Ccl6, and Ccl7 in an autocrine or paracrine manner (Fig. 7c).

The expression of colony stimulating factor receptors Csf1r, Csf2ra and Csf3r were also higher in KCs (Fig. 7b). Of these, Csf1r and Csf2ra were detected by proteomics, being significantly higher in KCs (Additional file 6). Interaction of colony stimulating factor receptors with their ligands, e.g. Csf1 and Csf2 which were abundantly expressed in LSECs (Fig. 7c), affects KC maturation [63], underlining the importance of LSECs for proper KC function.

The complement system is an important part of the innate immune system. Hepatocytes are major producers of complement proteins, whereas NPCs regulate complement activation [42]. Gene products representing complement receptors (Fig. 7d), and triggers of complement activation (C1qa, C1qb, C1qc; Fig. 7e) were significantly more abundant in the KC transcriptome and proteome datasets, whereas the expression of the C1 inhibitors C1qbp and Serping1 was similar in the two cells (detected only in the transcriptome; Fig. 7e).

LSECs express the machinery needed for antigen presentation and lymphocyte activation

A series of studies in mouse models suggest that LSEC cross-presentation of exogenous soluble antigens to naïve T cells is central to maintaining liver immune tolerance (reviewed in [1]). However, there are some controversies [37]. As LSECs rapidly dedifferentiate in culture [39, 40] and cells are cultured for several days in lymphocyte stimulation experiments, the in vivo contribution of LSECs in adaptive immunity may be difficult to extrapolate from in vitro experiments. There may also be species differences. We therefore investigated the basal expression of gene products associated with antigen processing and presentation (GO:0019882), and lymphocyte co-stimulation (GO:0031294) in rat LSECs and KCs (Additional file 7). The expression of tap-transporters, immunoproteases, and lysosomal enzymes involved in processing and intracellular traffic of antigens, were similar in the transcriptomes and proteomes of both cells except for Ctse (cathepsin E) and Ctss



Fig. 5 (See legend on next page.)

(See figure on previous page.)

Fig. 5 Expression of immune genes in rat LSECs and KCs. **a.** Unscaled heatmaps of normalized \log_2 expression values (\log_2 (RPKM+ 1), and \log_2 (iBAQ+ 1)) for all gene products associated with the term immune system processes (GO:0002376) in the KC and LSEC transcriptome and proteome. **b.** The figure shows significantly enriched GO terms ($FDR \leq 0.05$) associated with immune functions, and the density of corresponding genes with expression ≥ 10 RPKM in the LSEC and KC transcriptomes

(cathepsin S) which were significantly more abundant in the KCs (Fig. 8a-b). Expression of MHC class II genes was detected in both cells, but significantly higher in KCs (Fig. 8c). Concerning co-stimulatory molecules, LSECs expressed significantly higher levels of some gene products involved in activation of T-cells (Cav-1, Dpp4, Cd40, Cd320, and Efnb1), while KCs showed an abundance of gene products from the B7/CD28 superfamily (Cd80, Cd86, Btla, Icoslg) (Fig. 8d). Btla, Icoslg, and Cd4 were expressed in both cells, but significantly higher in KCs. BTLA [64], and CD4 [65] are also reported in human LSECs.

A minor subset of rat LSECs expresses the pan leukocyte marker CD45

CD45 is reported to be widely expressed in rat LSECs, with high expression in periportal located LSECs, and low expression in mid-zonal LSECs [38, 66]. We here report low expression of CD45 in the LSEC transcriptome, and an even lower expression in the LSEC proteome compared to KCs (Fig. 9a). In order to explore this further, we did flow cytometry of NPCs, and CD45 and stabilin-2 double immune labelling of rat liver sections (Additional file 8). We did not observe a clear colocalization of CD45 with the LSEC marker stabilin-2 in the sinusoids, suggesting either absence or low expression of CD45 in rat LSECs in general or expression in a small subpopulation of these cells. We then performed multicolor flow cytometry (Fig. 9b-f) of rat liver NPCs labeled with antibodies to CD45, SE-1/Fc γ RIIb2 (specific LSEC marker), and CD31 (pan endothelial cell marker; Additional file 8). NPCs from the 25–45% Percoll gradient interface were used instead of SE-1-MACS-isolated LSECs to eliminate any selection bias. Using strict gating (Additional file 8), we found that 4.0% (± 1.06 , $n = 4$) of small, low complex, live-gated SE-1 $^+$ cells were CD31 $^+$ CD45 $^+$ (Fig. 9g), suggesting expression of CD45 in a small subpopulation of LSECs.

LSECs from normal liver have been reported to not express CD31 on the cell surface [67] but in our flow cytometry experiments (Fig. 9g) this marker was shown to be expressed in 97.4% (± 1.80 , $n = 4$) of SE-1 positive cells. Immune staining of liver sections showed positive staining in all vasculature, albeit weaker in LSECs than in other endothelia (Additional file 8).

Discussion

The liver cells facing the blood are represented almost entirely by KCs and LSECs. These two cells make up the most important clearance system for removal of blood borne macromolecules and particles that are incompatible with blood homeostasis [5]. This avid scavenger activity thus fulfills a central role in liver immunity [1, 2] but at the same time poses a serious challenge, namely unwanted uptake of large molecule drug compounds [23]. Curiously, few studies have been undertaken to determine similarities and differences between LSECs and KCs on gene expression and/or proteome levels. Only two comprehensive studies, both done in the inbred C57Bl/6 mouse, have compared liver resident cell populations at the proteome level [41, 42]. The study by Azimifar et al. [41] focused on the distinct functional roles of various hepatic cell types in cholesterol flux, cellular trafficking, and growth receptor signaling, whereas Ding et al. [42] presented an integrated omics analysis focusing on communication and co-ordination between hepatocytes and NPCs, in particular KCs. Against this background we found it timely to carry out a high-throughput mRNA transcriptome and proteome expression study of the two types of specialised hepatic scavenger cells in rat, and focus on the analysis of immune function genes. We chose the outbred Sprague Dawley rat to cover a wide number of genotypes. This rat strain has been widely used in LSEC blood clearance and hepatotoxicity studies [16].

Our omics analysis revealed expression of a great number of genes related to immune functions in both cells. As expected in non-stimulated cells, most of these genes were expressed at low density; however, the great number of expressed immune genes supports the central role for both cells in liver immunity. LSECs seem to be unique among endothelial cells in this respect. Nolan et al. [35] used microarray profiling to compare primary microvascular endothelial cells isolated from liver and several other organs in C57BL/6 mice, and found significant heterogeneity between transcriptomes of the different endothelial cell populations. We did DAVID enrichment analysis [54, 55] on the liver specific gene list (Additional file 9) obtained by pairwise comparison of their LSEC gene expression data (GEO public database-Series GSE47067 [35]) with expression data for other organ-specific endothelial cells included in their study, and found enrichment of terms associated with

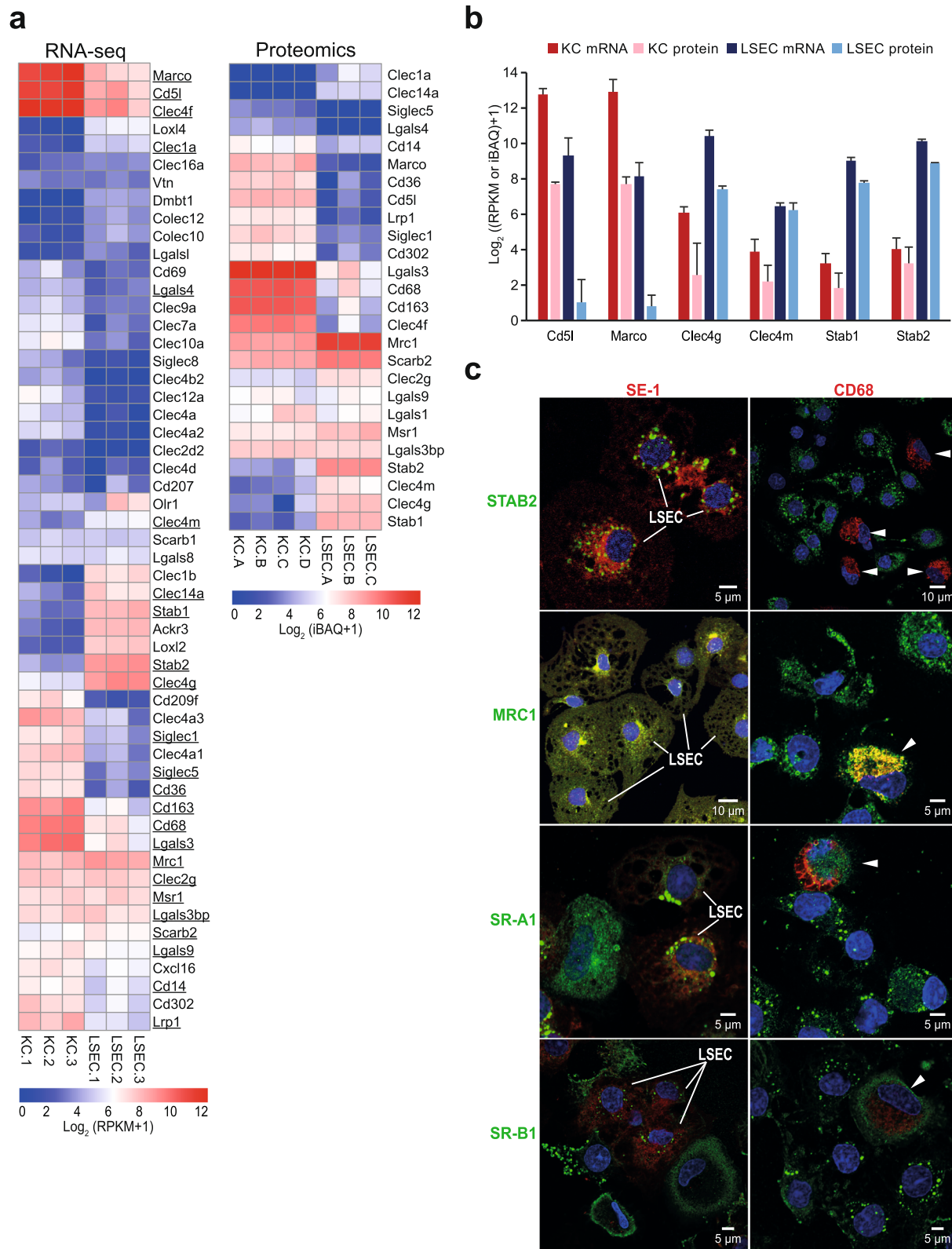


Fig. 6 (See legend on next page.)

(See figure on previous page.)

Fig. 6 Expression of scavenger receptors and immune lectins in rat LSECs and KCs. **a.** Unscaled heatmaps of normalized \log_2 expression values (\log_2 (RPKM+ 1), and \log_2 (iBAQ+ 1)) for scavenger receptors (SR) and C-type lectins in the KC and LSEC transcriptomes and proteomes. Underlined: Genes expressed in the transcriptome that were also present in the proteome. **b.** Absolute abundance of selected SR gene products in the KC and LSEC transcriptomes and proteomes. The bar height reflects good correlation between the transcriptome and proteome data for gene products of Clec4g, Clec4m, Stab1, and Stab2 in both cell types. The abundance of gene products of Marco and Cd51 were well correlated between the KC transcriptome and proteome, while LSECs showed high abundance of these gene products only at mRNA level. **c.** Immune labeling of non-parenchymal liver cell (NPC) cultures for selected SRs and C-type lectins. NPCs from the 25–45% interface on the Percoll gradient were incubated for 1 h, then fixed 15 min in 4% paraformaldehyde, and double immune-labeled with antibodies to FcγRIIb2 (SE-1; red fluorescence; left column), or CD68 (red fluorescence; right column), and to either stabilin-2 (STAB2; green), mannose receptor (MRC1; green), SR-A1 (green), or SR-B1 (green). Overlap of green and red fluorescence is seen as yellow staining in the overlay images. Antibodies are listed in Table 1. Cell nuclei were stained with DAPI (blue). Arrow heads point to CD68 positive KCs. Antibodies to stabilin-2 and FcγRIIb2 (SE-1) specifically labeled LSECs and the CD68-antibody specifically labeled KCs, whereas positive labeling for the mannose receptor, SR-A1, and SR-B1 was observed in both LSECs and KCs

immune functions in the LSECs (Additional file 9). Neither this mouse study [35], nor our present study in rat address the possibility of the existence of functionally different LSEC subpopulations. A recent single-cell transcriptomics analysis of human liver cells grouped the LSECs into two populations, of which the group enriched in LSECs from the acinar midzone and central venous zone displayed highly enriched immune pathways [68]. This supports the existence of functionally distinct LSEC subpopulations.

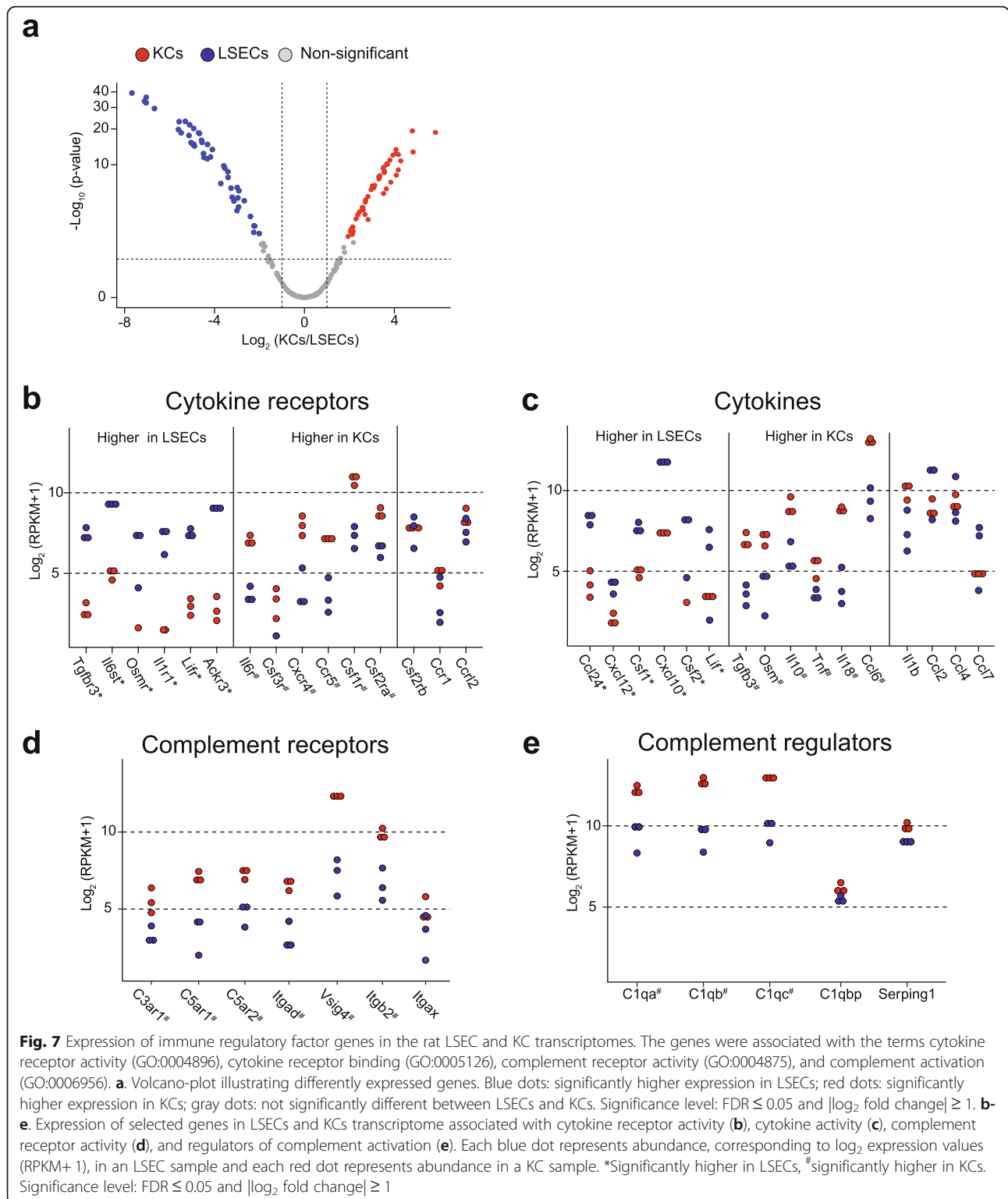
Reliable omics studies of isolated cell populations require access to highly pure cell preparations. Several popular markers used to identify LSECs have been associated with controversies regarding their sensitivity, specificity, selection bias, or lack proper validation [36, 37]. Here, we used SE-1-based MACS [43] to purify rat LSECs. This method utilizes the specific targeting of FcγRIIb2 [45], and has been previously reported to yield highly pure LSEC preparations [43]. The SE-1-MACS isolated cells in our experiments consisted of > 97% cells displaying the highly characteristic fenestration which is the structural hallmark of LSECs [16]. Moreover, the cell yield was relatively high (30–40 million LSECs per liver), and immune staining of liver sections using this antibody showed continuous staining along all sinusoids, similar to the LSEC specific endocytosis receptor stabilin-2, further validating SE-1/FcγRIIb2 as a reliable LSEC marker in rat. The same co-distribution of SE-1 and stabilin-2 in rat liver was reported by [46]. Moreover, flow cytometry of rat NPCs showed that 97.4% of SE-1/FcγRIIb2 positive cells were also CD31 positive, supporting their endothelial identity. Rat LSEC expression of CD31 was confirmed by positive staining in rat liver sections, albeit more weakly than in endothelial cells in other vessels, consistent with [69]. Of note, CD31 is upregulated in LSECs in liver inflammation [36, 69, 70]. CD31 has been reported in KCs. However, a recent study employing macrophage and endothelial reporter mice concluded that what seemed to be a

population of CD31 positive KCs after FACS were instead contaminating endothelial cells [71]. CD31 is regularly used as endothelial marker in studies of KC functions in mice [72]. In the present study CD31 staining was only observed along vessel structures in the liver tissue, and co-localized with stabilin-2 in the sinusoids.

The expression level and intralobular distribution of FcγRIIb2, and other LSEC markers may vary between species. Recently, the lack of periportal expression of FcγRIIb2, and LYVE-1, another commonly used LSEC marker, was reported on immune stained human liver sections [58], suggesting that isolating LSECs from human liver using these receptors as targets may introduce selection bias [36]. Notably, we found that CD36, a recommended LSEC marker in human liver [58], showed low gene and protein expression in rat LSECs, and high expression in KCs, consistent with a previous report in Sprague Dawley rat showing positive immune labeling for CD36 in KCs, but not in LSECs [59]. This shows a clear difference in the cellular distribution of CD36 in rat and human liver.

Interestingly, liver inflammation and fibrosis further affect the LSEC molecular phenotype, leading to down-regulation of LYVE-1 in liver cancer and cirrhosis [73], and of FcγRIIb2 in non-alcoholic steatohepatitis [74]. These studies show that the optimal choice of markers of LSECs and KCs depends on animal species and the health condition of the liver.

Lack of consensus markers and heterogeneity in KCs pose challenges for rat KC isolation. As rat KCs universally express complement receptors for inactivated complement component 3b [75], we used anti-rat-CD11b/c to isolate KCs by MACS with good cell yields. Staining of liver sections showed a scattered distribution with the majority of positive cells located in the periportal region where most KCs reside [76]. However, selection bias towards subpopulations of KCs cannot be excluded, as we found that CD68 positive cells showed a wider distribution within the hepatic lobule than CD11b/c positive



cells. Nonetheless, both markers showed the highest density of positive cells in the periportal region. Compared to the extensive literature in mice on the origin of KCs and differences in cell marker expression in

subpopulations of liver macrophages [77], little is known about rat liver macrophage subpopulations and markers. In mouse, liver resident macrophages are reported to have the CD11b low, or CD11b negative phenotype, and

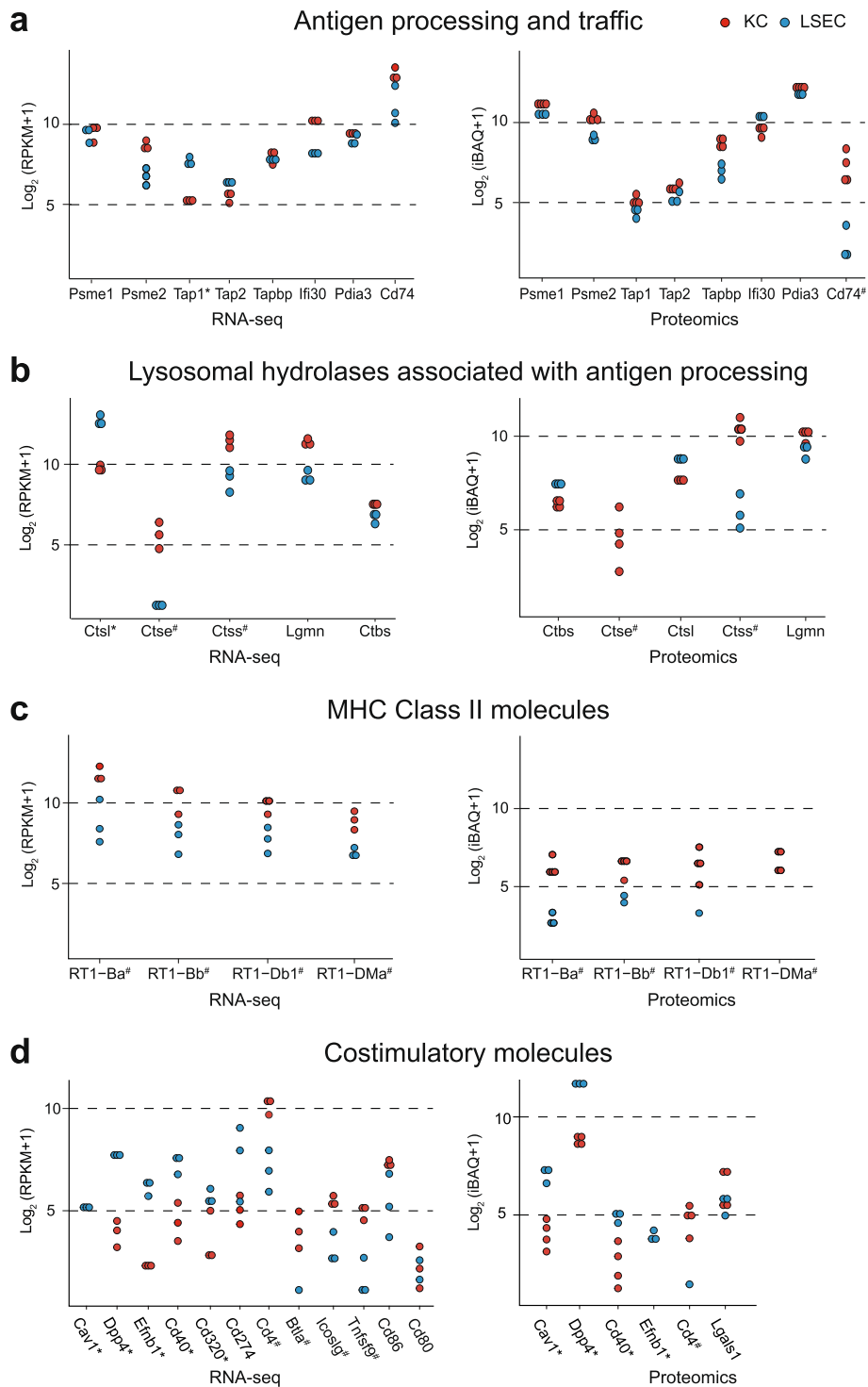


Fig. 8 (See legend on next page.)

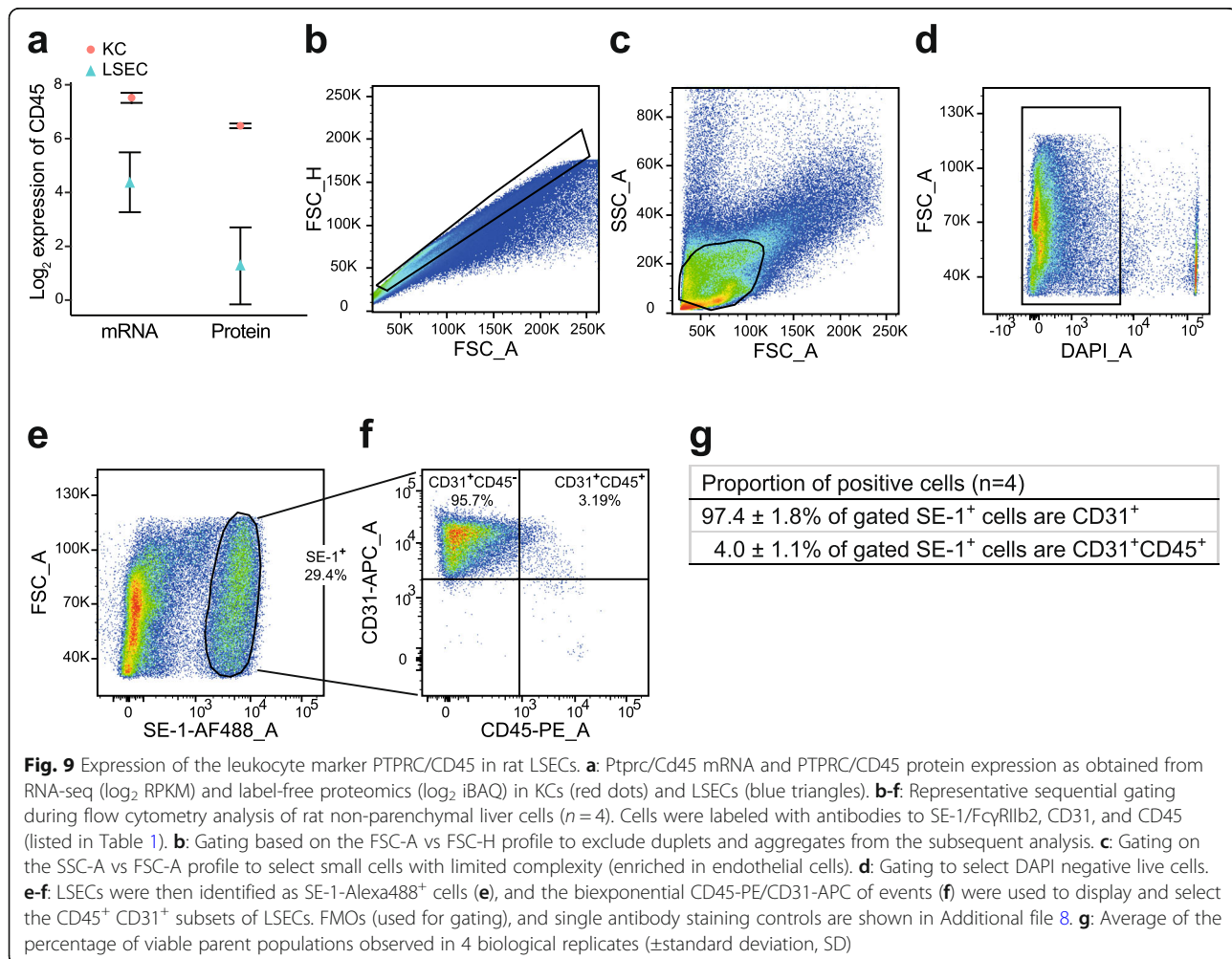
(See figure on previous page.)

Fig. 8 Expression of selected gene products associated with antigen processing and presentation (GO:0019882), and lymphocyte co-stimulation (GO:0031294) in the rat LSECs and KCs transcriptome and proteome. Each blue dot represents abundance of gene products in an LSEC sample and each red dot represents abundance in a KC sample. The dot plots on the left illustrate the abundance of mRNA (\log_2 (RPKM+ 1)) in the transcriptome, and the right plots illustrate the corresponding gene expression value in the proteome (\log_2 (iBAQ+ 1)). *Significantly higher in LSECs, #significantly higher in KCs. Significance level: FDR \leq 0.05 and $|\log_2$ fold change| \geq 1. **a.** Gene products involved in antigen processing (immune proteases: Psme1, Psme2), transport of processed peptide into the endosome for loading into MHC molecules (Tap1, Tap2, Tapbp), accessory proteins in loading and sorting of MHC molecules to endolysosome (Ifi30, Pdia3), and the invariant chain (Cd74). **b.** Lysosomal hydrolases annotated to be associated with MHC class II antigen processing. **c.** MHC class II gene products. **d.** Co-stimulatory factors involved in lymphocyte activation

the CD11hi phenotype includes bone marrow macrophages that have migrated to the liver [78]. The CD11b/c MACS-purified liver macrophages in our study expressed high levels of CRiG (VSig4), CD68 and CD163, which are validated markers of resident KCs [79–81], indicating that they are KCs, but our study cannot confirm whether some have been recruited from bone marrow. However, the cells were isolated from young, healthy rats with normal livers, and the livers were perfused free of blood with perfusion buffer before starting the recirculation system with collagenase buffer

in order to disperse the cells, which minimizes the risk of isolating blood monocytes. The source of macrophages in liver has been reported to affect expression levels of enzymes and receptors [82]. Interestingly, two recent studies in mice showed that bone marrow-derived resident liver macrophages, and KCs of yolk sac origin have highly similar gene expression profiles, that is different from that of monocytes [72, 83].

CD45 is used as a negative selection criterion for isolation of human and mouse LSECs [36], whereas the same marker has been reported to be expressed in rat LSECs



[38, 84]. In our study we observed a low expression of this marker in the LSEC transcriptomes and proteome compared to KCs, and flow cytometry showed that 4% of SE-1 positive small NPCs with limited complexity were CD31⁺CD45⁺ cells, which indicates CD45 expression in a small subpopulation of rat LSECs. Expression of CD45 in rat LSECs has been linked to recruitment of LSECs from bone marrow [66, 84].

Several SRs and C-type lectins were expressed at high density in the rat LSECs and KCs. This enables the two cells to recognize a wide variety of foreign and endogenous, modified substances, thus maintaining homeostasis [5]. In LSECs, the very high expression of stabilin-1, stabilin-2, FcγRIIb2, and the macrophage mannose receptor suggests that these are the crucial receptors contributing to the remarkably high endocytic capacity of LSECs [5, 16, 18]. In contrast to stabilin-1/-2 and the FcγRIIb2 which are LSEC specific in liver, the mannose receptor is also abundant in KCs. This receptor has traditionally been associated with M2 polarized macrophages but is present in LSECs of all mammalian species examined (rat, mouse, pig, human), while its expression in KCs varies between studies [5]. Interestingly, the macrophage mannose receptor has been reported to be absent in human KCs [85]. Functional studies in rat show that after intravenous injection of soluble ligands for this receptor, such as lysosomal enzymes [86–88], C-terminal procollagen propeptides [13], or ovalbumin [89], much of the ligand is rapidly cleared from blood by uptake in LSECs, which show a higher uptake per cell than in KCs. This points to LSECs as more efficient pinocytotic cells.

We also observed mRNA expression in LSEC of some SRs not previously reported in these cells at steady state - including members of SR-class A (Marco), SR-class D (Cd68, Ackr3), SR-class G (Lgals3bp, Cxcl16) and SR-class I (Cd5l, Cd163 and Dmbt1). However, these SRs were either not detected or showed low expression in the LSEC proteome. This may be due to post-transcriptional, translational, and/or protein degradation regulation, and/or the effect of the isolation procedure which may affect the expression. A previous microarray study [39] indicated changes in rat LSEC gene expression already after 2 h in culture. Importantly, proteomics is biased towards identification of highly abundant proteins. Despite high LSEC and KC purity in our experiments we cannot exclude that a low level in the other cell type might result from minute numbers of contaminating cells for some of the genes. Nonetheless, the expression pattern of these SRs was similar to that of LRP1, which has been functionally validated in LSECs [90], and CD45, which we showed by flow cytometry to be expressed in 4% of the LSECs. This suggests that a minor subset of LSECs may express these markers. However, this needs to be further explored in single cell experiments in rat liver cells.

Immune regulatory factors are important in maintaining liver homeostasis, and their dysregulation causes sustained inflammation. In the present study of cells at steady state we found that LSECs predominantly expressed Csf1, Ccl24 and Cxcl12, which affect recruiting, maintenance and homeostasis of other immune cells [63, 91, 92]. Our observation that LSECs express the chemokine scavenger receptor Ackr3 suggests a role for these cells in creating chemokine gradients and thus regulating the overall immune milieu of the sinusoids. KCs on the other hand, more abundantly expressed cytokines such as Il1b and TNF-α known to affect LSEC endocytic functions [93]. In accordance with a proteomics study in mice [42], rat KCs were also more tuned to positive regulation of complement activation by higher expression of triggers of complement activation. Interestingly, rat LSECs and KCs respond to inflammatory mediators in a generally similar manner, developing into pro- and anti-inflammatory subpopulations, indicating that both cells contribute to innate immune responses in liver [94].

Furthermore, we found that rat LSECs express gene products associated with processing and presentation of antigen required for activation of naïve (CD4⁺ and CD8⁺) T cells. Most of these genes were significantly lower expressed in LSECs than in KCs and their function in rat LSECs will need further validation. This finding nevertheless supports functional studies in mouse models concluding that LSECs are antigen presenting cells [1, 32, 95–98]. In physiological conditions, LSECs contribute to generation of T regulatory cells and induction of immune tolerance. However, after fibrotic liver injury due to hepatotoxins, mouse LSECs become proinflammatory, and induce an immunogenic T cell phenotype [99].

Conclusions

Good resolution was achieved between rat LSECs and KCs, enabling reliable and comprehensive molecular characterization of the cells at steady state. The study showed complementarity of scavenging and immune functions in LSECs and KCs. Both cells expressed high levels of SRs and immune lectins, of which some were present in both cells. Of note, inter-species expression differences for some receptors, as evident from the literature, highlight the need for thorough studies on gene expression in different animal models. We propose that the many common phenotypic and functional traits shared between LSECs and KCs is a consequence of the specialized sinusoidal environment along with the functional demand of the sinusoid, causing the cells to develop complementary and overlapping functions. Our study underlines the importance of taking both cells into consideration in studies of liver immunity. Furthermore, LSECs and KCs play a major role in the, often unwanted,

liver uptake of large molecule biopharmaceuticals and nano-formulations [23] preventing drugs from reaching their intended targets. Of note, major off-target drug accumulation in these cells may cause LSEC toxicity, which subsequently may result in liver toxicity. Our results contribute to understanding these uptake mechanisms to a greater detail, which is a prerequisite to develop remedies to reduce unwanted liver uptake.

Methods

Animals and ethics statement

Sprague Dawley, Crl:CD (SD), male rats, aged 6–11 weeks were used in the experiments. The animals were obtained directly from Charles River Laboratories (Sulzfeld, Germany). The rats were group housed (3 rats per cage) in 1354G Eurostandard type III conventional cages (Tecniplast, Italy) with aspen bedding (Scanbur, Norway), and with nesting material, houses, and aspen bricks (all from Datasand Ltd., Manchester, UK) as environmental enrichment. The rats were housed under controlled conditions ($21\text{ }^{\circ}\text{C} \pm 1\text{ }^{\circ}\text{C}$, relative humidity $55\% \pm 10\%$, and 12 h light/12 h dark cycle) at the specific pathogen free animal research facility at the University of Tromsø (UiT) – The Arctic University of Norway. The rats had free access to water and standard chow (RM1-E, Special Diet Service, UK), and were acclimatized for at least one week before experiments. Prior to the experiment and during acclimation period, animal health was assessed daily by experienced animal technicians. The experimental protocols and animal handling were approved by the competent institutional authority and the National Animal Research Authority at the Norwegian Food Safety Authority (Mattilsynet; Approval IDs: 4001, 8455, and 0817), and experiments were performed in compliance with the European Convention for the protection of Vertebrate Animals used for Experimental and Other Scientific Purposes. A total of 25 rats were used in this study. All animals were euthanized. While in deep surgical anesthesia (for anesthesia protocol see Method section “Rat liver perfusion, LSEC and KC isolation, and cell purity evaluation”), the vena cava was cut causing exsanguination. For liver tissue sampling for immune histochemistry, the animal was euthanized by CO_2 according to the requirement in Directive 2010/63/EU in a pre-set system ensuring gradual fill and appropriate exposure time (“Automatic CO_2 Delivery System”, Vet Tech Ltd., UK), and organs were sampled from the dead animal.

Rat liver perfusion, LSEC and KC isolation, and cell purity evaluation

Non-parenchymal liver cells (NPCs) were isolated essentially as described in [100], with some modifications. The surgical procedure was performed in the morning

(between 8 a.m. and 10 a.m.) in the animal research facility at UiT - The Arctic University of Norway. The rats (body weight 200–320 g) were anesthetized with either 1) a combination of ketamine hydrochloride (Ketalar 50 mg/mL; Pfizer, Norway) and medetomidine hydrochloride (Domitor vet 1 mg/mL, Orion Corporation, Finland); dose of mixture: 0.15 mL Ketalar/100 g BW and 0.05 mL Domitor /100 g BW, administered subcutaneously; or 2) with a mixture (ZRF-mix) of zolazepam /tiletamine hydrochloride 12.9/12.9 mg/mL (Zoletil forte vet, Virbac, Norway), xylazine 1.8 mg/mL (Rompun, Bayer Nordic, Norway) and fentanyl 10.3 $\mu\text{g}/\text{mL}$ (Actavis, Norway); dose of mixture: 2 mL/kg BW, administered intraperitoneally. Anesthetic depth was assessed prior to and during the operation procedure to ensure deep surgical anesthesia. The abdomen was opened in the midline, and the intestines gently pushed to the side in order to expose the liver and portal vein. A catheter connected to a peristaltic pump driven perfusion system was inserted into the portal vein and fixed to the vein by a suture, and the caudal vena cava was cut to allow outflow of buffer from the liver and exsanguination of the animal. The liver was then separated from the surrounding tissues by cutting all ligaments and placed on a mesh on the top of a cylinder, where run-through buffer was collected. The liver lobes were perfused free of blood with 250 ml of a calcium-free HEPES-based buffer [100], then perfused for 10 min (flow rate 30 ml/min) in a recirculation system, with 50 ml of a calcium-containing HEPES-based buffer [100] with 0.6 mg/ml collagenase (Worthington, Lot: X4B7108, Worthington Biochemical Corp., Lakewood, NJ). Hepatocytes were sedimented by low speed differential centrifugation (50 g, 2 min \times 3) leaving mainly NPCs in the supernatant which was decanted and centrifuged (300 g, 10 min). The resulting pellet was resuspended, loaded onto a two-step Percoll gradient (GE Healthcare, Uppsala, Sweden), and centrifuged at 1350 g for 30 min. Cells at the 25–45% Percoll interface, enriched in KCs and LSECs, were collected. To purify LSECs, NPCs were incubated with the M-rSE-1 antibody targeting Fc γ RIIb2 (CD32b) [45] (Table 1) for 30 min at $4\text{ }^{\circ}\text{C}$ in autoMACS rinsing solution with 1% BSA (Miltenyi Biotec Norden AB, Lund, Sweden), washed, and incubated with anti-mouse IgG2a + b MicroBeads for 30 min at $4\text{ }^{\circ}\text{C}$. To purify KCs, NPCs were incubated with a biotinylated-CD11b/c antibody (Table 1) followed by incubation with Streptavidin MicroBeads. Labeled NPCs were eluted through an LS-column in a MidiMACS Separator (Miltenyi) according to the manufacturer’s protocol. Typical cell yields were 30–40 million LSECs, and 10 million KCs per rat liver. LSECs and KCs were harvested from separate animals to maximize cell yields.

LSECs (0.25 million cells/cm²) were seeded in 100 mm tissue culture dishes (RNA-seq: Nunclon, ThermoFisher

Scientific, Waltham, MA; Proteomics: Sarstedt, Nümbrecht, Germany) coated with 2.9 µg/ml bovine collagen type I (Advanced BioMatrix, San Diego, CA, Cat.#5005), in RPMI-1640 cell culture medium supplemented with 20 mM sodium bicarbonate, 0.0006% penicillin, and 0.01% streptomycin (Sigma-Aldrich, St. Louis, MO, Cat.#R8758), and allowed to attach for 1 h. KCs (0.17 million cells/cm²) were seeded on uncoated 100 mm dishes, and incubated for 30 min. The cells were then gently washed with pre-warmed (37 °C) medium before extraction of RNA for high throughput RNA-sequencing, or protein for non-label quantitative proteomics.

The purity and morphology of MACS-isolated cells were assessed by phase contrast microscopy (all cultures), scanning electron microscopy (SEM; LSECs for transcriptomic and proteomic analyses, and KCs for proteomic analyses), and immune cytochemistry (LSECs and KCs for proteomic analyses) using antibodies against glial fibrillary acidic protein (GFAP; stellate cell marker), stabilin-2 (LSEC marker) [24, 25], CD11b/c, and SE-1/FcγRIIb2 (Table 1). The cells for purity assessment by SEM and immune cytochemistry were from the same preparations and cultured in parallel to the cells used for omics experiments, and were seeded in similar density, incubated and washed as for the omics experiments.

LSEC and KC mRNA transcriptome sequencing

Total RNA was extracted with the RNeasy Mini Kit (Qiagen, Hilden, Germany, Cat.#74,104). PolyA-enriched RNA from LSECs was then purified by MicroPoly(A)-Purist™ Kit (Life Technologies, ThermoFisher Scientific), whereas Dynabeads® mRNA DIRECT™ Micro Kit (Ambion, ThermoFisher, Cat.#61,021) was used to purify mRNA from KCs. Quality and quantity of mRNA were measured with Agilent RNA 6000 Pico Kit (Agilent Technologies, Santa Clara, CA, Cat.#5067–1513). The mRNAs were fragmented and reverse transcribed by Ion Total RNA-Seq Kit v2 (Life Technologies) according the manufacturer's instructions. Three LSEC transcriptome libraries representing 3 biological replicates, each from one individual rat, and three KC transcriptome libraries (3 biological replicates; each from the pooled KC mRNA from 2 rats) were constructed. Templates were prepared by Ion OneTouch™ 200 Template Kit v2 DL and Ion PGM™ Sequencing 300 Kit, loaded on Ion 316 chips, and sequenced with the Ion Torrent Personal Genome Machine (Life Technologies). We generated 1.09 billion nucleotide sequence data from the LSEC pool, corresponding to approximately 8.2 million mapped reads, and 0.93 billion nucleotide sequence data from the KS pool, corresponding to 6.5 million mapped reads. Additional file 10 lists the information on number of raw reads, reads after trimming, average length of the

trimmed sequences and the number of reads mapped to the reference genome for each biological replicate.

Transcriptomic data analyses

Bioinformatics analyses were performed with the CLC Genomics Workbench 8.0.2 (Qiagen® Bioinformatics), and the Bioconductor project. Raw sequencing reads were subjected to adaptor trimming, followed by quality trimming (Ambiguous limit = 2 and Quality limit = 0.05). Based on quality reports the reads were filtered based on length (minimum 15 and maximum 300 nucleotides); then 10 nucleotides from the 5' end, and 20 nucleotides from the 3' end were removed. All samples from the 6 experiments (LSECs, $n = 3$; KCs, $n = 3$) were included in the analysis as they were deemed homogenous with respect to 5-mer analysis and GC contents, and were free of ambiguous bases. RNA-seq analysis was performed with CLC Genomics Grid Worker 7.0.1. The reads were mapped to *Rattus norvegicus* reference genome (Rnor_6.0 [101]), which generated the gene expression counts and RPKM (reads per kilobase of exon model per million mapped reads [56]) values. Other parameter values used in mapping were: mismatch cost = 2, insertion cost = 3, deletion cost = 3, length and similarity fraction = 0.8 each, allowed maximum number of hits for a read = 10, and map to inter-genic regions. We used the edgeR (3.28.0)-limma (3.42.0) workflow as described in [102] to analyze the gene-level count data, using the following criteria: genes with low expression were filtered out using the filterByExpr function, and the remaining genes were considered to be expressed and were used in subsequent data analyses. Heteroscedasticity of the data was removed with voomWithQualityWeights function available in the limma package [103], after trimmed mean of M-values (TMM) normalization.

Preparation of samples for quantitative proteomics, and tandem mass spectrometry (LC-MS/MS)

MACS-isolated cells were allowed to adhere for 30 min (KC, $n = 4$ biological replicates, each from one individual rat) or 1 h (LSECs, $n = 3$ biological replicates, each from one individual rat) to 100 mm petri dishes as described under "Rat liver perfusion, LSEC and KC isolation, and cell purity evaluation". The cells were washed with RPMI-1640 (37 °C) to remove non-adherent cells, then immediately scraped out in triethylammonium bicarbonate (TEAB) solution (ThermoFisher) to collect protein lysate, which was centrifuged to remove cellular debris. Protein pellets were resuspended in 2 M urea and 50 mM TEAB. Samples of 20 µg protein were digested for 6 h in 1:100 (w/w) Lysyl Endopeptidase® (Fujifilm Wako Chemicals Europe GmbH, Neuss, Germany), then diluted to 1 M urea and digested overnight with 1/20 (w/w) trypsin (V511A, Promega Corporation, Madison,

WI). OMIX C18 tips (Varian Inc., Palo Alto, CA) were used for sample cleanup and concentration. Peptide mixtures containing 0.1% formic acid were loaded onto the Thermo Fisher Scientific EASY-nLC1000 system and EASY-Spray column (C18, 2 μm , 100 \AA , 50 μm , 50 cm). Peptides were fractionated using a 2–100% acetonitrile gradient in 0.1% formic acid over 50 min at a flow rate of 250 nl/min. Separated peptides were analyzed using Thermo Scientific Q-Exactive mass spectrometer. Data was collected in data dependent mode using a Top10 method.

Label-free proteomics analyses

Raw files from the Q-Exactive MS/MS were analysed using the quantitative proteomics software MaxQuant [104] (version 1.5.6.0). Proteins were identified using the built in Andromeda search engine using the UniProtKB *Rattus norvegicus* database (Jan 2017). Main search peptide tolerance was set to 4.5 ppm and MS/MS mass tolerance was set to 20 ppm. An FDR ratio of 0.01 was needed to give a protein identification. At least 2 peptides had to be quantified to give a quantitation value.

To estimate protein abundance, iBAQ values (i.e. the sum of peak intensities of all tryptic peptides matching to a specific protein divided by the number of theoretically observable peptides [105]) were generated with MaxQuant, and used for downstream quantitative proteomic analysis with Perseus (version 1.6.02). Perseus, R statistical computing (version 3.4.1), and Bioconductor (version 3.5) environments were used for bioinformatics and statistical analyses. The generated list of proteins was filtered to remove protein hits that were annotated as only identified by site, contaminants and reverse hits in Perseus. All samples for proteomics were run twice on LC-MS/MS and the median of the iBAQ values of the two runs was considered as the expressed iBAQ value. The annotation of the protein IDs and the corresponding genes were carefully curated. The iBAQ values of all protein IDs corresponding to a specific gene were added to remove redundancy in gene annotation. The resulting iBAQ values were then scaled to make an equal column sum. Protein with low expression were filtered using the filterByExpr function in edgeR-limma. The filtered data were rescaled to per million using the cpm function, followed by TMM normalization. The term “iBAQ” in figures and text refers to these normalized values and were used in the subsequent analyses. The same edgeR-limma workflow as used in the RNA-seq data analysis was used for the subsequent differential analysis of the proteomics data.

Data integration and visualization

In order to compare RNA-seq data with proteomics data the expression of gene products in the RNA-seq dataset

that corresponded to protein IDs in the proteomics data were reevaluated by summing up the counts of all relevant genes. Log_2 transformed expression values with prior addition of an offset of 1 were used in the visualization, unless mentioned otherwise.

Immune labeling of cells and liver tissue

MACS isolated LSECs and KCs (parallel cultures to proteomics experiments) were seeded on collagen coated glass coverslips (LSECs) or uncoated glass coverslips (KCs) at similar density as with the omics experiments, and incubated and washed in the same way, before fixation 15 min in 4% paraformaldehyde (PFA) in PBS, pH 7.2. NPCs from the 25–45% interface of the Percoll gradient were seeded on collagen-coated glass coverslips, incubated for 1 h, washed and fixed 15 min in 4% PFA. Liver samples were embedded in TissueTek OCT compound (Sakura Finetek, Zoeterwoude, Netherlands), snap frozen in liquid nitrogen, and stored at -70°C . Cryosections, 8–10 μm , were fixed in cold acetone for 10 min, then incubated in blocking buffer for 1 h, and immune labeled. All antibodies (Table 1) were diluted in blocking buffer, which was 1% BSA and 2% goat serum in PHEM buffer (w/v: 1.81% PIPES, 0.65% HEPES, 0.38% EGTA, 0.1% MgSO_4), pH 7, when labeling cryosections, and 1% BSA in tris buffered saline, 0.05% Tween 20, pH 8.4, when labeling cells. Sections and cells were incubated with primary antibody at 4°C overnight, then washed and labeled with secondary antibody for 1 h at room temperature. Isotype controls or non-immune IgG controls were used in all immune staining experiments. Nuclei were stained with DAPI (1:1000 in PBS; Sigma-Aldrich). Confocal microscopy was performed using a Zeiss LSM780 system (Carl Zeiss, Oberkochen, Germany). For purity assessment by differential counting of immune labeled MACS isolated cells, images were taken from 5 different areas of the cultures, including at least 350 cells from each CD11b/c-MACS isolation, and 700 cells from each SE-1-MACS isolation in the differential cell count.

Scanning Electron Microscopy (SEM)

SE-1-MACS-isolated LSECs (parallel cultures to proteomics experiments) were seeded on collagen coated 24-well tissue culture plates for 1 h, whereas CD11b/c MACS-isolated KCs were seeded for 30 min on uncoated 24-well plates. Cells were gently washed with medium before fixation in McDowell's fixative (4% PFA, 1% glutaraldehyde, in phosphate buffer, pH 7.2). Fixed cultures were stamped out from the plate and cells processed for SEM using the following protocol: 1) 3x wash in PHEM buffer, pH 7; 2) 1 h incubation with 1% tannic acid in PHEM; 3) 3x wash in PHEM; 4) 30 min in 1% osmium tetroxide in H_2O ; 5) 3x wash in PHEM; 6) dehydration

in graded ethanol (30–100%); 7) drying in hexamethyldisilazane (Sigma-Aldrich). Specimens coated with 10 nm gold/palladium were scanned and imaged in a Zeiss Sigma Field Emission Scanning electron microscope (Carl Zeiss) at 2 kV. For cell purity assessment, high resolution overview images were taken at random from at least 5 different areas per cell culture (LSEC and KC samples for proteomics experiments), or at least 3 areas per culture (LSEC samples for RNA-seq experiments). Cells from all areas were included in the differential cell count, including at least 600 cells per KC sample, and 800 cells per LSEC sample in the cell purity assessment for proteomics, and 280–470 cells per LSEC sample in the cell purity assessment for RNA-seq.

Flow cytometry

Samples of $0.5\text{--}1 \times 10^6$ NPCs collected from the 25–45% interface of the Percoll gradient were stained with antibodies to CD45, CD31, and SE-1/FcγRIIb2 (Table 1) at 4 °C in dark for 20 min. Data acquisition and analysis were performed in a BD LSRFortessa™ Cell Analyzer (BD Biosciences, San Jose, CA) with BD FACSDiva Software version 8.0.1. The laser configuration and the PTM voltage were calibrated prior running the samples. The PTM voltage was adjusted during the experiments using the single stained controls. The data were further quality checked and analyzed with FlowJo V10.7.1 software (BD Biosciences). The AutoSpill/AutoSpread spillover algorithm available in FlowJo 10.7.1 was used to address the compensation issue using single stained controls post acquisitions. Isotype controls, single antibody controls, and FMO controls were used to properly interpret the acquired data. DAPI staining was performed to discriminate between live and dead NPCs. An excess of 100,000 events were recorded and analyzed in every test within each biological replicate ($n = 4$), each representing one individual rat.

Statistical tests

The descriptive and inferential statistical analyses and graphical plots of the transcriptomics and proteomics data were performed either in the R/Bioconductor or the Perseus environment. RNA-seq analysis was performed with CLC Genomics Grid Worker 7.0.1. The genes/proteins retained after filtering of low expressed gene/protein using filterByExpr function were deemed to be expressed and were used in subsequent data analyses. Heteroscedasticity of the data was removed with voom-WithQualityWeights function available in the limma package [103], after trimmed mean of M-values (TMM) normalization. Differential expression analysis of the transcriptomics and the proteomics data was tested with edgeR (3.28.0)-limma (3.42.0) workflow as described in [102], with FDR multiple correction [103], as described

under “Transcriptomic data analyses” and “Label-free proteomics analyses”. The genes/proteins were identified as differentially expressed when the $|\log_2$ fold change $|\geq 1$ and $\text{FDR} \leq 0.05$. All samples were included in the omics analyses. LSECs and KCs were compared at functional level using gene set enrichment analysis (GSEA) [49, 50] on gene lists ranked based on expression level with priori defined collection of annotated gene sets from Molecular Signatures Database. The gene sets were considered significantly enriched if $\text{FDR } q\text{-value} \leq 0.05$.

Supplementary Information

The online version contains supplementary material available at <https://doi.org/10.1186/s12860-020-00331-9>.

Additional file 1. Gene set enrichment analysis. The Excel file (.xls) shows the output of gene set enrichment analysis (GSEA) [49, 50] of pre-ranked gene lists from the rat LSEC and KC RNA-seq datasets, associated with Gene Ontology (GO) biological processes (BP). The genes were pre-ranked based on expression. We have used the C5 collection of annotated gene sets in the Molecular Signatures Database (release 6.2; BP) [53] which consists of gene sets derived from GO [51, 52]. Name of worksheets: “GSEA_plot”, “GSEA_RNAseq_LSEC_BP”, and “GSEA_RNAseq_KC_BP”. The worksheet named “GSEA_Plot” contains the selected enriched BPs shown in Fig. 4.

Additional file 2. List of all expressed genes in the RNA-seq and proteomics datasets. Excel file (.xls) with all genes and proteins that were deemed expressed, as defined in Methods, and used in the downstream analysis and visualization of data. The worksheet named “RNA_seq_whole expressed” contains the data from the RNA-seq experiments (expression values in RPKM), and differential expression analysis results. The worksheet named “Proteomics_whole expressed” contains the data from the label-free proteomic experiments (expression values in iBAQ), and differential expression analysis results.

Additional file 3. Genes and proteins associated with immune system processes. Excel file (.xls) with the list of genes and proteins associated with the term immune system processes (GO:0002376) presented in the two heatmaps in Fig. 5a, along with their associated expression values (RPKM, or iBAQ). The two worksheets are named “Immune genes_RPKM_RNAseq”, and “Immune genes_iBAQ_proteomics”. Of note, for visualization, $\log_2(\text{RPKM} + 1)$ and $\log_2(\text{iBAQ} + 1)$ were used in the heatmaps in Fig. 5a.

Additional file 4. Scavenger receptors and C-type lectins. Excel file (.xls) with the list of genes and proteins presented in the two heatmaps in Fig. 6a, along with their associated expression values (RPKM, or iBAQ). The two worksheets are named “SRs&lectins_RPKM_RNAseq” and “SRs&lectins_iBAQ_proteomics”. For visualization, $\log_2(\text{RPKM} + 1)$ and $\log_2(\text{iBAQ} + 1)$ were used in Fig. 6.

Additional file 5. Immune histochemistry for CD68. Immune histochemistry of acetone-fixed frozen sections of rat liver showing the distribution pattern of CD68 in the liver lobule. Sections were labeled with an antibody to CD68 (red fluorescence) and stabilin-2 (Stab2, green fluorescence) and subjected to confocal laser scanning microscopy. Antibodies are listed in Table 1. Nuclei were stained with DAPI (blue).

Additional file 6. Immune regulatory factors. Excel file (.xls) with the list of expressed genes annotated to cytokine receptor binding (GO:0005126), cytokine receptor activity (GO:0004896), complement activation (GO:0006956), or complement receptor activity (GO:0004875) in rat LSECs and KCs. The file shows their corresponding abundance in the RNA-seq datasets (RPKM values; worksheet named “Immunereg.factors_RPKM_RNAseq”) and label-free proteomics datasets (iBAQ values; worksheet named “Immunereg.factors_iBAQ_LFP”) along with differential expression analysis outputs. For visualization of the selected genes shown in Fig. 7, $\log_2(\text{RPKM} + 1)$ was used.

Additional file 7. Genes annotated to antigen processing and presentation and lymphocyte co-stimulation. Excel file (.xls) with the list of expressed genes associated with antigen processing and presentation (GO:0019882), and lymphocyte co-stimulation (GO:0031294) in LSECs and KCs. The file shows their corresponding abundance in the RNA-seq datasets (RPKM values; worksheet named "Immuneactivation_RPKM_RNAseq") and label-free proteomics datasets (iBAQ values; worksheet named "Immuneactivation_iBAQ_LFP") along with differential expression analysis outputs. For visualization of the selected genes and proteins shown in Fig. 8, \log_2 (RPKM+ 1), and \log_2 (iBAQ+ 1) were used.

Additional file 8. Immune histochemistry for CD31 and CD45, and controls for SE-1, CD31, CD45 flow cytometry experiments. a-b: Immune histochemistry of acetone-fixed frozen sections of rat liver showing the distribution pattern of stabilin-2, CD31 and CD45 in the liver lobule. a: Sections were labeled with antibodies to CD31 (red fluorescence) and stabilin-2 (Stab2, green fluorescence) and subjected to confocal laser scanning microscopy. CD31 stained all hepatic endothelia; in the sinusoids the CD31 staining overlapped with the stabilin-2 staining (arrows). b: Sections labeled with antibodies to CD45 (red fluorescence) and stabilin-2 (Stab2, green fluorescence). a-b: Pv, portal vein/venule. Antibodies are listed in Table 1. Nuclei were stained with DAPI (blue). c: The figure panel contains the contour profiles (of the singlet, small, low complexity, live-gated non-parenchymal liver cells) of the three single antibody staining controls on the different fluorophore channels used during the acquisition of the data in the flow cytometry experiment presented in Fig. 9. d: The figure contains the contour profiles of the three FMO controls and tests used to verify the gating used to interpret the experiment in Fig. 9.

Additional file 9. Analysis of microarray expression data obtained from Nolan et al. 2013 [35]. Excel file (.xls) with the comparative analysis of expression data obtained from a microarray profiling study of mouse (*Mus musculus*) primary microvascular endothelial cells, published by Nolan DJ, Ginsberg M, Israely E, Palikuqi B, Poulos MG, James D, et al. Molecular signatures of tissue-specific microvascular endothelial cell heterogeneity in organ maintenance and regeneration [35]. The microarray data was downloaded from the GEO public database-Series GSE47067. Title of dataset: In vivo endothelial cell heterogeneity. The first worksheet, named "Pairwise_DGE (Nolan_2013)", shows pairwise analysis of the expression data of endothelial cells from different organs. The second worksheet, named "DAVID_liver specific genes", presents the DAVID enrichment analysis [54, 55] output of genes that were consistently significantly abundant in mouse liver sinusoidal endothelial cells (LSECs) in every pairwise comparison of LSECs with other microvascular endothelial cells in the dataset (Significance level: FDR \leq 0.05, and \log_2 fold change \geq 1).

Additional file 10. Ion Torrent sequencing results. Excel file (.xls) summarizing the Ion Torrent PGM sequencing results, including number of mapped sequences and average lengths.

Abbreviations

FDR: False discovery rate; GO: Gene ontology; GSEA: Gene set enrichment analysis; MACS: Magnetic-activated cell separation; KC: Kupffer cell; LSEC: Liver sinusoidal endothelial cell; NPC: Non-parenchymal liver cell; SR: Scavenger receptor

Acknowledgements

We thank Dr. Jack-Ansgar Bruun for help with the LC/MS-MS work.

Authors' contributions

Study concept and design: SB, RL, JS, SJ, PM, BS, IM, KS; acquisition of data: SB, RL, JS, KS; bioinformatics and statistical analysis: SB; analysis, interpretation, and visualization of data: SB, RL, JS, BS, IM, KS; drafting of manuscript: SB, RL, JS, BS, KS; critical revision of the manuscript for important intellectual content: SB, RL, JS, PM, SJ, IM, BS, KS; obtained funding: BS, PM, KS. All authors had access to the study data and have reviewed and approved the final manuscript.

Funding

This work was supported by the University of Tromsø (UiT) - The Arctic University of Norway, and by a grant from Tromsø Research Foundation to Bård Smedsrød. The study sponsor had no role in study design, collection, analysis or interpretation of data. The publication charges for this article have been funded by a grant from the publication fund of UiT The Arctic University of Norway.

Availability of data and materials

The datasets supporting the conclusions of this article are included within the article and its additional files. Additional data generated and analyzed during this study are available from the corresponding author on reasonable request.

The RNA-sequencing datasets generated and analysed during the current study are available in the NCBI Sequence Read Archive (SRA). SRA accession number to dataset: PRJNA574898. [<https://www.ncbi.nlm.nih.gov/bioproject/PRJNA574898/>].

The mass spectrometry proteomics datasets generated and analysed during the current study are available in the ProteomeXchange Consortium PRIDE database. ProteomeXchange accession: PXD012080. [<https://www.ebi.ac.uk/pride/archive/projects/PXD012080>].

Ethics approval and consent to participate

Experimental protocols using rats were approved by the competent institutional authority and the National Animal Research Authority at the Norwegian Food Safety Authority (Mattilsynet; Approval IDs: 4001, 8455, and 0817). Housing, handling and procedures were performed in compliance with Directive 2010/63/EU and the European Convention for the protection of Vertebrate Animals used for Experimental and Other Scientific Purposes (ETS 123, European Council). The experiments included are in vitro (euthanasia before tissue sampling) or terminal experiments where the anesthetized animal was euthanized during the surgical procedure, as described in Methods.

Competing interests

The authors declare no competing interests.

Author details

¹Department of Medical Biology, Vascular Biology Research Group, University of Tromsø (UiT) -The Arctic University of Norway, Hansine Hansens veg 18, N-9037 Tromsø, Norway. ²Faculty of Biosciences and Aquaculture, Nord University, Bodø, Norway. ³Department of Clinical Medicine, UiT -The Arctic University of Norway, Tromsø, Norway.

Received: 16 February 2020 Accepted: 18 November 2020

Published online: 27 November 2020

References

- Knolle PA, Wohlleber D. Immunological functions of liver sinusoidal endothelial cells. *Cell Mol Immunol*. 2016;13(3):347–53.
- Shetty S, Lalor PF, Adams DH. Liver sinusoidal endothelial cells - gatekeepers of hepatic immunity. *Nat Rev Gastroenterol Hepatol*. 2018;15(9):555–67.
- Bilzer M, Roggel F, Gerbes AL. Role of Kupffer cells in host defense and liver disease. *Liver Int*. 2006;26(10):1175–86.
- van Furth R, Cohn ZA, Hirsch JG, Humphrey JH, Spector WG, Langevoort HL. The mononuclear phagocyte system: a new classification of macrophages, monocytes, and their precursor cells. *Bull World Health Organ*. 1972;46(6):845–52.
- Sørensen KK, McCourt P, Berg T, Crossley C, Le Couteur D, Wake K, et al. The scavenger endothelial cell: a new player in homeostasis and immunity. *Am J Physiol Regul Integr Comp Phys*. 2012;303(12):R1217–30.
- Seternes T, Sørensen K, Smedsrød B. Scavenger endothelial cells of vertebrates: a nonperipheral leukocyte system for high-capacity elimination of waste macromolecules. *Proc Natl Acad Sci U S A*. 2002;99(11):7594–7.
- Eriksson S, Fraser JR, Laurent TC, Pertoff H, Smedsrød B. Endothelial cells are a site of uptake and degradation of hyaluronic acid in the liver. *Exp Cell Res*. 1983;144(1):223–8.
- Skogh T, Blomhoff R, Eskild W, Berg T. Hepatic uptake of circulating IgG immune complexes. *Immunology*. 1985;55(4):585–94.

9. Smedsrød B, Johansson S, Pertoft H. Studies in vivo and in vitro on the uptake and degradation of soluble collagen alpha 1(I) chains in rat liver endothelial and Kupffer cells. *Biochem J*. 1985;228(2):415–24.
10. Melkko J, Hellevik T, Risteli L, Risteli J, Smedsrød B. Clearance of NH₂-terminal propeptides of types I and III procollagen is a physiological function of the scavenger receptor in liver endothelial cells. *J Exp Med*. 1994;179(2):405–12.
11. Smedsrød B, Melkko J, Araki N, Sano H, Horiuchi S. Advanced glycation end products are eliminated by scavenger-receptor-mediated endocytosis in hepatic sinusoidal Kupffer and endothelial cells. *Biochem J*. 1997;322(Pt 2): 567–73.
12. Smedsrød B, Einarsson M. Clearance of tissue plasminogen activator by mannose and galactose receptors in the liver. *Thromb Haemost*. 1990;63(1): 60–6.
13. Smedsrød B, Melkko J, Risteli L, Risteli J. Circulating C-terminal propeptide of type I procollagen is cleared mainly via the mannose receptor in liver endothelial cells. *Biochem J*. 1990;271(2):345–50.
14. Dahl LB, Laurent TC, Smedsrød B. Preparation of biologically intact radioiodinated hyaluronan of high specific radioactivity: coupling of 125I-tyramine-cellobiose to amino groups after partial N-deacetylation. *Anal Biochem*. 1988;175(2):397–407.
15. Smedsrød B, Pertoft H, Gustafson S, Laurent TC. Scavenger functions of the liver endothelial cell. *Biochem J*. 1990;266(2):313–27.
16. Sørensen KK, Simon-Santamaria J, McCuskey RS, Smedsrød B. Liver sinusoidal endothelial cells. *Compr Physiol*. 2015;5(4):1751–74.
17. Malovic I, Sørensen KK, Elvevold KH, Nedredal GI, Paulsen S, Erofeev AV, et al. The mannose receptor on murine liver sinusoidal endothelial cells is the main denatured collagen clearance receptor. *Hepatology*. 2007;45(6):1454–61.
18. Elvevold K, Simon-Santamaria J, Hasvold H, McCourt P, Smedsrød B, Sørensen KK. Liver sinusoidal endothelial cells depend on mannose receptor-mediated recruitment of lysosomal enzymes for normal degradation capacity. *Hepatology*. 2008;48(6):2007–15.
19. Ganesan LP, Mohanty S, Kim J, Clark KR, Robinson JM, Anderson CL. Rapid and efficient clearance of blood-borne virus by liver sinusoidal endothelium. *PLoS Pathog*. 2011;7(9):e1002281.
20. Simon-Santamaria J, Rinaldo CH, Kardas P, Li R, Malovic I, Elvevold K, et al. Efficient uptake of blood-borne Bk and JC polyomavirus-like particles in endothelial cells of liver sinusoids and renal vasa recta. *PLoS One*. 2014;9(11):e111762.
21. Mates JM, Yao Z, Cheplowitz AM, Suer O, Phillips GS, Kwiek JJ, et al. Mouse liver sinusoidal endothelium eliminates HIV-like particles from blood at a rate of 100 million per minute by a second-order kinetic process. *Front Immunol*. 2017;8(35):35.
22. Simon-Santamaria J, Malovic I, Warren A, Oteiza A, Le Couteur D, Smedsrød B, et al. Age-related changes in scavenger receptor-mediated endocytosis in rat liver sinusoidal endothelial cells. *J Gerontol A Biol Sci Med Sci*. 2010; 65(9):951–60.
23. Godfrey C, Desviat LR, Smedsrød B, Pietri-Rouxel F, Denti MA, Disterer P, et al. Delivery is key: lessons learnt from developing splice-switching antisense therapies. *EMBO Mol Med*. 2017;9(5):545–57.
24. McCourt PA, Smedsrød BH, Melkko J, Johansson S. Characterization of a hyaluronan receptor on rat sinusoidal liver endothelial cells and its functional relationship to scavenger receptors. *Hepatology*. 1999;30(5):1276–86.
25. Politz O, Gratchev A, McCourt PA, Schledzewski K, Guillot P, Johansson S, et al. Stabilin-1 and -2 constitute a novel family of fasciclin-like hyaluronan receptor homologues. *Biochem J*. 2002;362(Pt 1):155–64.
26. Mousavi SA, Sporstol M, Fladeby C, Kjeker R, Barois N, Berg T. Receptor-mediated endocytosis of immune complexes in rat liver sinusoidal endothelial cells is mediated by FcγmabR1b2. *Hepatology*. 2007;46(3):871–84.
27. Uhrig A, Banafsche R, Kremer M, Hegenbarth S, Hamann A, Neurath M, et al. Development and functional consequences of LPS tolerance in sinusoidal endothelial cells of the liver. *J Leukoc Biol*. 2005;77(5):626–33.
28. Martin-Armas M, Simon-Santamaria J, Pettersen I, Moens U, Smedsrød B, Sveinbjornsson B. Toll-like receptor 9 (TLR9) is present in murine liver sinusoidal endothelial cells (LSECs) and mediates the effect of CpG-oligonucleotides. *J Hepatol*. 2006;44(5):939–46.
29. Wu J, Meng Z, Jiang M, Zhang E, Trippler M, Broering R, et al. Toll-like receptor-induced innate immune responses in non-parenchymal liver cells are cell type-specific. *Immunology*. 2010;129(3):363–74.
30. Knolle PA, Germann T, Treichel U, Uhrig A, Schmitt E, Hegenbarth S, et al. Endotoxin down-regulates T cell activation by antigen-presenting liver sinusoidal endothelial cells. *J Immunol*. 1999;162(3):1401–7.
31. Limmer A, Ohl J, Kurts C, Ljunggren HG, Reiss Y, Groettrup M, et al. Efficient presentation of exogenous antigen by liver endothelial cells to CD8+ T cells results in antigen-specific T-cell tolerance. *Nat Med*. 2000;6(12):1348–54.
32. Limmer A, Ohl J, Wingender G, Berg M, Jungerkes F, Schumak B, et al. Cross-presentation of oral antigens by liver sinusoidal endothelial cells leads to CD8 T cell tolerance. *Eur J Immunol*. 2005;35(10):2970–81.
33. Steffan AM, Gendrault JL, McCuskey RS, McCuskey PA, Kim A. Phagocytosis, an unrecognized property of murine endothelial liver cells. *Hepatology*. 1986;6(5):830–6.
34. Chi JT, Chang HY, Haraldsen G, Jahnsen FL, Troyanskaya OG, Chang DS, et al. Endothelial cell diversity revealed by global expression profiling. *Proc Natl Acad Sci U S A*. 2003;100(19):10623–8.
35. Nolan DJ, Ginsberg M, Israely E, Palikuqi B, Poulos MG, James D, et al. Molecular signatures of tissue-specific microvascular endothelial cell heterogeneity in organ maintenance and regeneration. *Dev Cell*. 2013;26(2): 204–19.
36. DeLeve LD, Maretta-Mira AC. Liver sinusoidal endothelial cell: an update. *Semin Liver Dis*. 2017;37(4):377–87.
37. Elvevold K, Smedsrød B, Martinez I. The liver sinusoidal endothelial cell: a cell type of controversial and confusing identity. *Am J Physiol Gastrointest Liver Physiol*. 2008;294(2):G391–400.
38. Xie G, Wang L, Wang X, Wang L, DeLeve LD. Isolation of periportal, midlobular, and centrilobular rat liver sinusoidal endothelial cells enables study of zoned drug toxicity. *Am J Physiol Gastrointest Liver Physiol*. 2010; 299(5):G1204–10.
39. Geraud C, Schledzewski K, Demory A, Klein D, Kaus M, Peyre F, et al. Liver sinusoidal endothelium: a microenvironment-dependent differentiation program in rat including the novel junctional protein liver endothelial differentiation-associated protein-1. *Hepatology*. 2010;52(1):313–26.
40. Martinez I, Nedredal GI, Øie CI, Warren A, Johansen O, Le Couteur DG, et al. The influence of oxygen tension on the structure and function of isolated liver sinusoidal endothelial cells. *Comp Hepatol*. 2008;7:4.
41. Azimifar SB, Nagaraj N, Cox J, Mann M. Cell-type-resolved quantitative proteomics of murine liver. *Cell Metab*. 2014;20(6):1076–87.
42. Ding C, Li Y, Guo F, Jiang Y, Ying W, Li D, et al. A cell-type-resolved liver proteome. *Mol Cell Proteomics*. 2016;15(10):3190–202.
43. Tokairin T, Nishikawa Y, Doi Y, Watanabe H, Yoshioka T, Su M, et al. A highly specific isolation of rat sinusoidal endothelial cells by the immunomagnetic bead method using SE-1 monoclonal antibody. *J Hepatol*. 2002;36(6):725–33.
44. Ohmura T, Enomoto K, Satoh H, Sawada N, Mori M. Establishment of a novel monoclonal antibody, SE-1, which specifically reacts with rat hepatic sinusoidal endothelial cells. *J Histochem Cytochem*. 1993;41(8):1253–7.
45. March S, Hui EE, Underhill GH, Khetani S, Bhatia SN. Microenvironmental regulation of the sinusoidal endothelial cell phenotype in vitro. *Hepatology*. 2009;50(3):920–8.
46. Yoshida M, Nishikawa Y, Omori Y, Yoshioka T, Tokairin T, McCourt P, et al. Involvement of signaling of VEGF and TGF-beta in differentiation of sinusoidal endothelial cells during culture of fetal rat liver cells. *Cell Tissue Res*. 2007;329(2):273–82.
47. Geraud C, Koch PS, Zierow J, Klapproth K, Busch K, Olsavszky V, et al. GATA4-dependent organ-specific endothelial differentiation controls liver development and embryonic hematopoiesis. *J Clin Invest*. 2017;127(3):1099–114.
48. Low TY, van Heesch S, van den Toorn H, Giansanti P, Cristobal A, Toonen P, et al. Quantitative and qualitative proteome characteristics extracted from in-depth integrated genomics and proteomics analysis. *Cell Rep*. 2013;5(5): 1469–78.
49. Subramanian A, Tamayo P, Mootha VK, Mukherjee S, Ebert BL, Gillette MA, et al. Gene set enrichment analysis: a knowledge-based approach for interpreting genome-wide expression profiles. *Proc Natl Acad Sci U S A*. 2005;102(43):15545–50.
50. Mootha VK, Lindgren CM, Eriksson KF, Subramanian A, Sihag S, Lehar J, et al. PGC-1alpha-responsive genes involved in oxidative phosphorylation are coordinately downregulated in human diabetes. *Nat Genet*. 2003;34(3):267–73.
51. Ashburner M, Ball CA, Blake JA, Botstein D, Butler H, Cherry JM, et al. Gene ontology: tool for the unification of biology. *The Gene Ontology Consortium*. *Nat Genet*. 2000;25(1):25–9.
52. The Gene Ontology C. The gene ontology resource: 20 years and still GOing strong. *Nucleic Acids Res*. 2019;47(D1):D330–D8.
53. Liberzon A, Birger C, Thorvaldsdóttir H, Ghandi M, Mesirov Jill P, Tamayo P. The molecular signatures database Hallmark gene set collection. *Cell Syst*. 2015;1(6):417–25.

54. Huang da W, Sherman BT, Lempicki RA. Systematic and integrative analysis of large gene lists using DAVID bioinformatics resources. *Nat Protoc* 2009; 4(1):44–57.
55. Huang DW, Sherman BT, Lempicki RA. Bioinformatics enrichment tools: paths toward the comprehensive functional analysis of large gene lists. *Nucleic Acids Res.* 2009;37(1):1–13.
56. Mortazavi A, Williams BA, McCue K, Schaeffer L, Wold B. Mapping and quantifying mammalian transcriptomes by RNA-Seq. *Nat Methods.* 2008;5(7): 621–8.
57. Malerod L, Juvet K, Gjoen T, Berg T. The expression of scavenger receptor class B, type I (SR-BI) and caveolin-1 in parenchymal and nonparenchymal liver cells. *Cell Tissue Res.* 2002;307(2):173–80.
58. Strauss O, Phillips A, Ruggiero K, Bartlett A, Dunbar PR. Immunofluorescence identifies distinct subsets of endothelial cells in the human liver. *Sci Rep.* 2017;7:44356.
59. Li R, Oteiza A, Sørensen KK, McCourt P, Olsen R, Smedsrød B, et al. Role of liver sinusoidal endothelial cells and stabilins in elimination of oxidized low-density lipoproteins. *Am J Physiol Gastrointest Liver Physiol.* 2011;300(1): G71–81.
60. Geraud C, Evdokimov K, Straub BK, Peitsch WK, Demory A, Dorflinger Y, et al. Unique cell type-specific junctional complexes in vascular endothelium of human and rat liver sinusoids. *PLoS One.* 2012;7(4): e34206.
61. Liu W, Tang L, Zhang G, Wei H, Cui Y, Guo L, et al. Characterization of a novel C-type lectin-like gene, LSEctin: demonstration of carbohydrate binding and expression in sinusoidal endothelial cells of liver and lymph node. *J Biol Chem.* 2004;279(18):18748–58.
62. Aizarani N, Saviano A, Sagar, Mailly L, Durand S, Herman JS, et al. A human liver cell atlas reveals heterogeneity and epithelial progenitors. *Nature.* 2019; 572(7768):199–204.
63. Stutchfield BM, Antoine DJ, Mackinnon AC, Gow DJ, Bain CC, Hawley CA, et al. CSF1 restores innate immunity after liver injury in mice and serum levels indicate outcomes of patients with acute liver failure. *Gastroenterology.* 2015;149(7):1896–909 e14.
64. Xu H, Cao D, Guo G, Ruan Z, Wu Y, Chen Y, et al. *Diagn Pathol.* 2012;7:142.
65. Scoazec JY, Feldmann G. In situ immunophenotyping study of endothelial cells of the human hepatic sinusoid: results and functional implications. *Hepatology.* 1991;14(5):789–97.
66. Harb R, Xie G, Lutzko C, Guo Y, Wang X, Hill CK, et al. Bone marrow progenitor cells repair rat hepatic sinusoidal endothelial cells after liver injury. *Gastroenterology.* 2009;137(2):704–12.
67. DeLeve LD, Wang X, Hu L, McCuskey MK, McCuskey RS. Rat liver sinusoidal endothelial cell phenotype is maintained by paracrine and autocrine regulation. *Am J Physiol Gastrointest Liver Physiol.* 2004; 287(4):G757–63.
68. MacParland SA, Liu JC, Ma XZ, Innes BT, Bartzak AM, Gage BK, et al. Single cell RNA sequencing of human liver reveals distinct intrahepatic macrophage populations. *Nat Commun.* 2018;9(1):4383.
69. Lalor PF, Lai WK, Curbishley SM, Shetty S, Adams DH. Human hepatic sinusoidal endothelial cells can be distinguished by expression of phenotypic markers related to their specialised functions in vivo. *World J Gastroenterol.* 2006;12(34):5429–39.
70. Poisson J, Lemoine S, Boulanger C, Durand F, Moreau R, Valla D, et al. Liver sinusoidal endothelial cells: physiology and role in liver diseases. *J Hepatol.* 2017;66(1):212–27.
71. Lynch RW, Hawley CA, Pellicoro A, Bain CC, Iredale JP, Jenkins SJ. An efficient method to isolate Kupffer cells eliminating endothelial cell contamination and selective bias. *J Leukoc Biol.* 2018;104(3):579–86.
72. Bonnardel J, T'Jonck W, Gaubomme D, Browaeys R, Scott CL, Martens L, et al. Stellate Cells, Hepatocytes, and Endothelial Cells Imprint the Kupffer Cell Identity on Monocytes Colonizing the Liver Macrophage Niche. *Immunity.* 2019;51(4):638–54 e9.
73. Mouta Carreira C, Nasser SM, di Tomaso E, Padera TP, Boucher Y, Tomarev SJ, et al. LYVE-1 is not restricted to the lymph vessels: expression in normal liver blood sinusoids and down-regulation in human liver cancer and cirrhosis. *Cancer Res.* 2001;61(22):8079–84.
74. Ishikawa T, Yokoyama H, Matsuura T, Fujiwara Y. Fc gamma RIIb expression levels in human liver sinusoidal endothelial cells during progression of non-alcoholic fatty liver disease. *PLoS One.* 2019;14(1): e0211543.
75. Smedsrød B, Pertoft H, Eggertsen G, Sundstrom C. Functional and morphological characterization of cultures of Kupffer cells and liver endothelial cells prepared by means of density separation in Percoll, and selective substrate adherence. *Cell Tissue Res.* 1985;241(3):639–49.
76. Bouwens L, Baekeland M, de Zanger R, Wisse E. Quantitation, tissue distribution and proliferation kinetics of kupffer cells in normal rat liver. *Hepatology.* 1986;6(4):718–22.
77. Guillot A, Tacke F. Liver macrophages: old dogmas and new insights. *Hepatol Commun.* 2019;3(6):730–43.
78. Nishiyama K, Nakashima H, Ikarashi M, Kinoshita M, Nakashima M, Aosasa S, et al. Mouse CD11b+Kupffer Cells Recruited from Bone Marrow Accelerate Liver Regeneration after Partial Hepatectomy. *PLoS One.* 2015;10(9): e0136774 e.
79. Krenkel O, Tacke F. Liver macrophages in tissue homeostasis and disease. *Nat Rev Immunol.* 2017; 17(5):306–21.
80. Helmy KY, Katschke KJ Jr, Gorgani NN, Kljavin NM, Elliott JM, Diehl L, et al. CRIg: A macrophage complement receptor required for phagocytosis of circulating pathogens. *Cell.* 2006;124(5):915–27.
81. Zeng Z, Surewaard BGJ, Wong CHY, Geoghegan JA, Jenne CN, Kubes P. CRIg functions as a macrophage pattern recognition receptor to directly bind and capture blood-borne gram-positive bacteria. *Cell Host Microbe.* 2016;20(1):99–106.
82. Naito M, Hasegawa G, Ebe Y, Yamamoto T. Differentiation and function of Kupffer cells. *Med Electron Microscopy.* 2004;37(1):16–28.
83. Scott CL, Zheng F, De Baetselier P, Martens L, Saey Y, De Prijck S, et al. Bone marrow-derived monocytes give rise to self-renewing and fully differentiated Kupffer cells. *Nat Commun.* 2016;7.
84. Wang L, Wang X, Xie G, Wang L, Hill CK, DeLeve LD. Liver sinusoidal endothelial cell progenitor cells promote liver regeneration in rats. *J Clin Invest.* 2012;122(4):1567–73.
85. Martens JH, Kzhyshkowska J, Falkowski-Hansen M, Schledzewski K, Gratchev A, Mansmann U, et al. Differential expression of a gene signature for scavenger/lectin receptors by endothelial cells and macrophages in human lymph node sinuses, the primary sites of regional metastasis. *J Pathol.* 2006; 208(4):574–89.
86. Hubbard AL, Wilson G, Ashwell G, Stukenbrok H. An electron microscope autoradiographic study of the carbohydrate recognition systems in rat liver. I. Distribution of 125I-ligands among the liver cell types. *J Cell Biol.* 1979; 83(1):47–64.
87. Dalen DPP-V, De Leeuw AM, Brouwer A, Knook DL. Rat liver endothelial cells have a greater capacity than kupffer cells to endocytose N-acetylglucosamine- and mannose-terminated glycoproteins. *Hepatology.* 1987;7(4):672–9.
88. Bijsterbosch MK, Donker W, van de Bilt H, van Weely S, van Berkel TJ, Aerts JM. Quantitative analysis of the targeting of mannose-terminal glucocerebrosidase. Predominant uptake by liver endothelial cells. *Eur J Biochem.* 1996;237(2):344–9.
89. Kindberg GM, Stang E, Andersen KJ, Roos N, Berg T. Intracellular transport of endocytosed proteins in rat liver endothelial cells. *Biochem J.* 1990;270(1): 205–11.
90. Øie CI, Appa RS, Hilden I, Petersen HH, Gruhler A, Smedsrød B, et al. Rat liver sinusoidal endothelial cells (LSECs) express functional low density lipoprotein receptor-related protein-1 (LRP-1). *J Hepatol.* 2011;55(6):1346–52.
91. Zimmermann N, Hogan SP, Mishra A, Brandt EB, Bodette TR, Pope SM, et al. Murine eotaxin-2: a constitutive eosinophil chemokine induced by allergen challenge and IL-4 overexpression. *J Immunol.* 2000;165(10):5839–46.
92. Miles A, Liaskou E, Eksteen B, Lalor PF, Adams DH. CCL25 and CCL28 promote alpha4 beta7-integrin-dependent adhesion of lymphocytes to MAdCAM-1 under shear flow. *Am J Physiol Gastrointest Liver Physiol.* 2008; 294(5):G1257–67.
93. Martinez I, Sveinbjornsson B, Vidal-Vanaclocha F, Asumendi A, Smedsrød B. Differential cytokine-mediated modulation of endocytosis in rat liver endothelial cells. *Biochem Biophys Res Commun.* 1995;212(1):235–41.
94. Liu Y, Gardner CR, Laskin JD, Laskin DL. Classical and alternative activation of rat hepatic sinusoidal endothelial cells by inflammatory stimuli. *Exp Mol Pathol.* 2013;94(1):160–7.
95. Schildberg FA, Hegenbarth SI, Schumak B, Scholz K, Limmer A, Knolle PA. Liver sinusoidal endothelial cells veto CD8 T cell activation by antigen-presenting dendritic cells. *Eur J Immunol.* 2008;38(4):957–67.
96. Knolle PA, Gerken G. Local control of the immune response in the liver. *Immunol Rev.* 2000;174:21–34.

97. Onoe T, Ohdan H, Tokita D, Shishida M, Tanaka Y, Hara H, et al. Liver sinusoidal endothelial cells tolerize T cells across MHC barriers in mice. *J Immunol.* 2005;175(1):139–46.
98. Carambia A, Freund B, Schwinge D, Heine M, Laschtowitz A, Huber S, et al. TGF-beta-dependent induction of CD4(+)CD25(+)Foxp3(+) Tregs by liver sinusoidal endothelial cells. *J Hepatol.* 2014;61(3):594–9.
99. Connolly MK, Bedrosian AS, Malhotra A, Henning JR, Ibrahim J, Vera V, et al. In hepatic fibrosis, liver sinusoidal endothelial cells acquire enhanced immunogenicity. *J Immunol.* 2010;185(4):2200–8.
100. Smedsrød B, Pertoft H. Preparation of pure hepatocytes and reticuloendothelial cells in high yield from a single rat liver by means of Percoll centrifugation and selective adherence. *J Leukoc Biol.* 1985;38(2): 213–30.
101. Zerbino DR, Achuthan P, Akanni W, Amode MR, Barrell D, Bhai J, et al. Ensembl 2018. *Nucleic Acids Res.* 2018;46(D1):D754–D61.
102. Law CW, Alhamdoosh M, Su S, Dong X, Tian L, Smyth GK, et al. RNA-seq analysis is easy as 1–2–3 with limma, Glimma and edgeR. *F1000Res.* 2016;5: 1408.
103. Ritchie ME, Phipson B, Wu D, Hu Y, Law CW, Shi W, et al. limma powers differential expression analyses for RNA-sequencing and microarray studies. *Nucleic Acids Res.* 2015;43(7):e47.
104. Cox J, Mann M. MaxQuant enables high peptide identification rates, individualized p.p.b.-range mass accuracies and proteome-wide protein quantification. *Nat Biotechnol.* 2008;26(12):1367–72.
105. Schwanhauser B, Busse D, Li N, Dittmar G, Schuchhardt J, Wolf J, et al. Global quantification of mammalian gene expression control. *Nature.* 2011; 473(7347):337–42.

Publisher's Note

Springer Nature remains neutral with regard to jurisdictional claims in published maps and institutional affiliations.

Ready to submit your research? Choose BMC and benefit from:

- fast, convenient online submission
- thorough peer review by experienced researchers in your field
- rapid publication on acceptance
- support for research data, including large and complex data types
- gold Open Access which fosters wider collaboration and increased citations
- maximum visibility for your research: over 100M website views per year

At BMC, research is always in progress.

Learn more biomedcentral.com/submissions



Paper II

Li, R., Bhandari, S., Martinez, I., Bruun, J.A., Urbarova, I., Smedsrød, B., Simon-Santamaria, J. & Sørensen, K.K.

Changes in the proteome and secretome of rat liver sinusoidal endothelial cells during early primary culture and effects of dexamethasone.

(Manuscript).

Changes in the proteome and secretome of rat liver sinusoidal endothelial cells during early primary culture and effects of dexamethasone

Ruomei Li^{1*}, Sabin Bhandari^{1*}, Inigo Martinez², Jack-Ansgar Bruun¹, Ilona Urbarova³, Bård Smedsrød¹, Jaione Simon-Santamaria¹, Karen Kristine Sørensen^{1,#}

¹Department of Medical Biology, UiT – The Arctic University of Norway, Tromsø, Norway.

²Department of Clinical Medicine, UiT – The Arctic University of Norway, Tromsø, Norway.

³Department of Community Medicine, UiT – The Arctic University of Norway, Tromsø, Norway.

*Shared first author. #Corresponding author: E-mail: karen.sorensen@uit.no

Authors' contribution:

Conceptualization: RL, SB, IM, BS, JS, KS

Investigation, methodology, analysis, and visualization: RL, SB, JB, JS, KS

Data curation: SB, JB, IU

Funding acquisition: BS, KS

Writing – original draft: RL, SB, KS

Writing – review & editing: RL, SB, IM, JB, IU, BS, JS, KS

Abstract

Liver sinusoidal endothelial cells (LSECs) are fenestrated endothelial cells and specialized scavenger cells involved in the elimination of modified plasma proteins and tissue turnover waste macromolecules from blood. LSECs also participate in liver immune responses. A challenge when studying LSEC biology is the rapid loss of the *in vivo* cell phenotype in culture. In this study, we have examined biological processes and pathways affected during early-stage primary culture of rat LSECs and checked for cell responses to the pro-inflammatory cytokine interleukin (IL)-1 β and the anti-inflammatory drug dexamethasone.

Methods: LSECs from male Sprague Dawley rats were cultured on type I collagen in a 5% oxygen atmosphere in DMEM with serum-free supplements for 2 and 24 h. Quantitative proteomics using tandem mass tag technology, differential expression, and functional enrichment analyses were used to examine proteins in cells and supernatants. Validation was done with ELISA and multiplex immunobead assays, cell ultrastructure was examined by scanning electron microscopy, and scavenger function by quantitative endocytosis assays.

Results: LSECs cultured for 24 h showed a pro-inflammatory phenotype both in the presence and absence of IL-1 β , with upregulation of cellular responses to cytokines and interferon- γ , cell-cell adhesion, and glycolysis, and downregulation of membrane/endocytosis receptors (MCAM, STAB1, STAB2, LYVE-1, CLEC4G) and proteins involved in pyruvate metabolism, citric acid cycle, fatty acid elongation, amino acid metabolism, and oxidation-reduction processes. Dexamethasone improved LSEC viability in culture and repressed the culture-induced stimulation of glycolysis, inflammatory and immune regulatory pathways, and secretion of pro-inflammatory cytokines while increasing interleukin-10 secretion compared to the time-matched control. The number of sieve plates in LSECs was markedly reduced at 24 h both in the presence and absence of dexamethasone but the cells showed a more quiescent phenotype with dexamethasone.

Conclusion: Rat LSECs are activated towards a pro-inflammatory phenotype during early culture. Dexamethasone represses LSEC activation and improves cell viability.

Keywords

Rats, liver, endothelial cells, liver sinusoidal endothelial cell(s), scavenger receptors, secretome, TMT isobaric tag labeling, proteomics, endothelial activation, dexamethasone, glucocorticoid(s), IL-1 β , phenotype, capillaries, cell survival, proteome

Introduction

Endothelial cells from different vascular beds vary in their gene expression profile and structure, reflecting organ-specific functions (1, 2). The liver sinusoidal endothelial cells (LSECs) have a unique morphology and function essential for hepatic and systemic homeostasis. The cells lack an organized basal lamina and are highly perforated with transcellular, membrane-bound pores or fenestration (appr. 50-300 nm in diameter (3)) that allow a bidirectional flow of plasma proteins, lipoproteins, and solutes between the sinusoidal blood and hepatocytes (4-7). LSECs are also highly active scavenger cells (8, 9), equipped with a wide repertoire of scavenger receptors and C-type lectins (10, 11) and a well-developed endocytic apparatus (9, 12). Studies over the last four decades have shown a pivotal role of the cells in blood clearance of many modified plasma proteins and lipoproteins, extracellular matrix molecules, viruses, and other nanoparticles (9, 13). In addition, LSECs participate in immune responses in the liver and are suggested to have a key role in the maintenance of liver immune tolerance (14, 15). Paracrine signals from LSECs are essential for the normal function of other sinusoidal cells and hepatocytes, not least for proper organ regeneration after partial hepatectomy (16-21). Despite increasing awareness of the role of LSECs in liver health and disease (22-27), there are still few reports describing the LSEC proteome (10, 28-30) and information about the LSEC secretome, which is dependent on studies in cultured cells remains incomplete.

One challenge with LSEC studies *in vitro* is that the cells rapidly lose their specific *in vivo* phenotype in culture, including altered gene expression of cell markers, loss of cell fenestration, and scavenger functions (31, 32). LSEC culture can, to some extent, be improved by co-culture with other liver cells, confirming the cells' dependence on the sinusoidal microenvironment (33). However, few studies have investigated the detailed molecular mechanisms behind the reported *in vitro* changes in LSEC monocellular cultures. Geraud *et al.* (2010) compared the gene expression profiles of freshly isolated (0 and 2h) rat LSECs with LSECs at 42 h post-seeding and rat lung microvascular endothelial cells (32). They found that rat LSECs showed significant time-dependent downregulation in growth and transcription factors essential for LSEC differentiation, as well as down-regulation of the LSEC markers stabilin-1, stabilin-2, FcγRIIb2, and LYVE-1. LSECs in 42 h culture also became more similar to lung microvascular endothelial cells. One of the downregulated transcription factors was GATA4. GATA4 (34), and GATA4 in combination with c-MAF and MEIS2 (35), have later been suggested as major transcriptional regulators of LSEC differentiation and specialization.

We recently reported and compared the bulk transcriptomes and non-labelled proteomes of freshly isolated rat LSECs and Kupffer cells, revealing cell-specific and complementary scavenger and

immune features of the sinusoidal liver cells (10). In the present study we have explored the rat LSEC proteome at 2 and 24 h post-seeding under pro- and anti-inflammatory conditions by quantitative proteomics, using an isobaric tandem mass tag (TMT) sixplex labeling approach combined with liquid chromatography and tandem mass spectrometry (LC-MS/MS).

The aim of the study was two-fold: 1) To reveal biological pathways and processes that are affected during early primary culture of rat LSECs at the proteome level, as this is incompletely described in the literature, and 2) examine the effect of the pro-inflammatory cytokine interleukin (IL)-1 β , and the anti-inflammatory drug dexamethasone (Dex) on the cell-associated and secreted proteomes of the cells. In addition, we have looked at the effects of Dex on rat LSEC ultrastructure, scavenger function, and viability in culture. Dex is a synthetic glucocorticoid routinely used in the clinic and shows anti-inflammatory activity and modulatory effects on metabolism in many cell types (36). Glucocorticoids, including Dex, are also frequently used as a medium supplement for *in vitro* primary cultures of different cell types. Most cells in the body express the glucocorticoid receptor (NR3C1), a nuclear receptor of the steroid /thyroid hormone receptor superfamily and regulator of glucocorticoid responses. However, the response to glucocorticoids varies between tissues and is highly cell type-dependent in terms of the individual genes and pathways affected (37-39). It is therefore of interest to know the detailed effects of these drugs in LSECs.

Material and methods

Animals and Ethics statement

Male Sprague Dawley (CrI:CD (SD)) rats were purchased from Charles River Laboratories, (Sulzfeld, Germany) at the age of 6 weeks. The rats were housed under controlled conditions ($21^{\circ}\text{C} \pm 1^{\circ}$, relative humidity $55\% \pm 10\%$ and 12 h light/12 h dark cycle) at the specific pathogen-free animal research facility, UiT – The Arctic University of Norway, Tromsø, Norway, and were acclimatized for at least one week before the experiments. The rats were group housed (2-3 rats per cage) in 1354G Eurostandard type III conventional cages (Tecniplast, Italy) with aspen bedding (Scanbur Norway), and with nesting material, houses, and aspen bricks (Datasand Ltd, Manchester, UK) as environmental enrichment. The rats had free access to water and standard chow (RM1-E, Special Diet Service, UK). The experimental protocols were approved by the National Animal Research Authority at the Norwegian Food Safety Authority (Mattilsynet; Approval IDs: 6233 and 8455) and experiments were performed in compliance with the European Convention for the protection of Vertebrate Animals used for Experimental and Other Scientific Purposes. All experiments were terminal experiments, and all animals were euthanized by the following procedure: While in deep surgical anesthesia, the vena cava was cut, causing exsanguination of the animal. The anesthesia protocol is described in section “LSEC isolation, purification and culture”.

LSEC isolation, purification, and culture

Rat LSECs were isolated and purified essentially as described (40). In short, the rats were anaesthetized with a mixture of zolazepam /tiletamine hydrochloride 12.9/12.9 mg/ml (Zoletil forte vet, Virbac, Norway), xylazine 1.8 mg/ml (Rompun, Bayer Nordic, Norway), and fentanyl 10.3 $\mu\text{g}/\text{ml}$ (Actavis, Norway); a dose of mixture: 2 ml/kg BW, administered intraperitoneally. Anesthetic depth was assessed prior to and during the operation procedure to ensure deep surgical anesthesia. After the opening of the abdomen, a catheter connected to a peristaltic pump-driven perfusion system was inserted into the portal vein, and the caudal vena cava was cut to allow outflow of a buffer from the liver and exsanguination of the animal. The liver was dissected out and placed on a mesh on the top of a cylinder where run-through buffer was collected. The liver lobes were perfused free of blood with 250 ml of a calcium-free HEPES-based buffer, and the buffer was discarded. Then the liver was perfused with 50 ml of a calcium-containing HEPES-based buffer with 0.6 mg/ml collagenase (Worthington Biochemical Corp., Lakewood, NJ) in a recirculation system (flow rate 30 ml/min) until the cells could be released by gentle shaking. After removal of hepatocytes by low-speed differential centrifugation (50 g, 2 min x 3), the non-parenchymal liver cells (NPCs) in the supernatant

were pelleted (300 g, 10 min), and loaded onto a two-step 25%-45% Percoll gradient (GE Healthcare, Uppsala, Sweden), and centrifuged at 1350 g for 30 min. Cells at the Percoll 25%-45% interface were collected and LSECs were purified by selective adherence: first, the cell suspension was seeded onto non-coated tissue culture plates and incubated at 37°C for 30 min, leaving Kupffer cells but not LSECs to attach to the substrate; then the non-adherent cells, highly enriched in LSECs were collected and used in the experiments. The average yield of LSECs for proteomics experiments was approximately 60 million cells per liver (body weight: 250-300 gram), and LSECs from two rat livers were pooled in each experiment.

Purified LSECs were seeded on bovine type I collagen (2.9 µg/ml; Advanced BioMatrix, San Diego, CA) coated tissue culture plates (100 mm; Sarstedt, Nümbrecht, Germany), or 24-well tissue culture plates (Sarstedt) at a density of 0.3×10^6 cells/cm² in Dulbecco's modified Eagle's cell culture medium (DMEM, Sigma, St. Louis, MO). The cells were first incubated for 30 min (37°C), then washed with prewarmed medium to remove debris and non-attached cells, before further incubation in DMEM supplemented with Insulin-transferrin-sodium selenite supplement (ITS, Sigma, Cat. No I3146), ascorbic acid (62 µg/ml, Sigma, Cat. No A4403), sodium pyruvate (1mM, Gibco, Cat. No 11360039), glutamax (2 mM of L-alanyl-L-glutamine dipeptide, Gibco, Cat. No 35050-038), penicillin (100 units/ml) and streptomycin (0.1 mg/ml) (Sigma), with or without the addition of 1 µg/ml of Dex (FortecortinTM Inject 4 mg/ml, Merck Serono GmbH, Darmstadt, Germany) (dose as in (41)) and/or 100 IU/ml of human recombinant interleukin-1β (IL-1β) (PeproTech, NJ, Cat. No 200-01B) (42). All cultures were incubated in low oxygen (5% O₂) and 5% CO₂ at 37°C, as recommended in (31).

The purity of LSECs was assessed by scanning electron microscopy (SEM). Cells isolated for quantitative proteomic analysis (n=3; each biological replicate representing the pooled LSECs from two rat livers) showed $93.2\% \pm 1.5\%$ fenestrated endothelial cells, which is the hallmark of LSECs. Cells for SEM were from the same cell isolation as used for proteomics and were seeded in similar density as for the proteomics experiments and incubated and washed in the same way (the SEM preparation protocol is included in section "Scanning electron microscopy"). Parallel LSEC cultures were also immune labelled with an antibody to whole rat stabilin-2 (43) resulting in $91.8\% \pm 0.7\%$ positive cells (n=3). Contaminating cells were identified as Kupffer cells (CD163 positive) and hepatic stellate cells (glial fibrillary acidic protein, GFAP, positive) by immune labeling with mouse monoclonal anti-rat CD163 (Bio-Rad, Kidlington, UK, Cat. No MCA342GA), and rabbit polyclonal anti-rat glial fibrillary acidic protein (GFAP) (Dako, Glostrup, Denmark, Cat. No Z0334). The purity of LSEC cultures for Luminex analyses were also assessed by SEM. The percentage of LSECs (*i.e.*,

fenestrated endothelial cells) in cultures incubated for 24 h were 94.0 % \pm 3.5% without Dex (n=3), and 97.3% \pm 1.2% with Dex (n=3).

Proteomic sample preparation and analysis

The supernatant of LSECs cultured for 24 h was collected and passed through a filter (pore size 0.2 μ m) to remove debris, then concentrated on Vivaspin columns (3kD cut-off, Sartorius AG, City, State). The protein solution was washed 3 times with PBS in the column and the volume was reduced to 0.2 ml.

Cellular protein extracts of LSEC cultures incubated for either 2 or 24 h were prepared according to the protocol provided in the TMTsixplexTM Isobaric Mass Tagging Kit (Thermo Fisher Scientific, Waltham, MA) with the following modification: Denaturing reagent was 5% sodium deoxycholate in 100 mM TEAB (triethylammonium bicarbonate). Protein concentrations of concentrated supernatant and cellular extracts were measured with Direct DetectTM Infrared Spectrometer (Millipore).

The proteins in cell extracts and supernatants were reduced according to the protocol provided in the TMTsixplexTM Isobaric Mass Tagging Kit, except that the reducing reagent was 5 mM dithiothreitol (Sigma) instead of tri (2-carboxyethyl)-phosphine. Proteins were precipitated with acetone and the pellet was collected by centrifugation at 8000 g for 10 min. The protein pellet (25 μ g) was resuspended in 2 M urea, 50 mM TEAB. Proteins were digested for 6 h by 1:100 (w/w) lysyl endopeptidase (Fujifilm Wako Chemicals Europe GmbH, Neuss, Germany). The samples were diluted to 1 M urea and digested overnight with 1:20 (w/w) trypsin (V511A, Promega Corporation, Wisconsin, USA). Peptides from each sample were labelled with the TMTsixplexTM Isobaric Mass Tagging Kit according to the manufacturer's protocol. OMIX C18 tips (Varian, Inc., Palo Alto, CA, USA) were used for sample cleanup and concentration. Peptide mixtures containing 0.1% formic acid were loaded onto Thermo Fisher Scientific EASY-nLC1000 system and EASY-Spray column (C18, 2 μ m, 100 \AA , 50 μ m, 50 cm). Peptides were fractionated using a 2-100% acetonitrile gradient in 0.1% formic acid over 180 min at a flow rate of 250 nl/min. The separated peptides were analyzed using a Thermo Scientific Q-Exactive mass spectrometer. Data was collected in data-dependent mode using a Top10 method. Raw data were processed using MaxQuant (version 1.5.0.30), and proteins were identified using the integrated Andromeda search engine. Tandem mass spectrometry (MS/MS) data were searched against the UniProt Rattus norvegicus (Rat) reference proteome (44). A false discovery rate (FDR) ratio of 0.01 was needed to give a protein identification.

An overview of the experimental setup for the quantitative TMT proteomics experiments is shown in **Fig. 1**.

Data analysis

The resulting output from MaxQuant, was pre-processed with Perseus (version 1.6.10.43). The generated list of proteins was filtered to remove protein hits that were annotated as only identified by site, contaminants, and reverse hits in Perseus. The annotation of the protein IDs to their corresponding gene symbols was manually curated with the UniProt Knowledgebase (UniProtKB; (44)). Redundant gene symbols were summed to get the expression values before doing the differential expression analysis. The tag-reporter intensity corrected output from the MaxQuant was used for protein quantification. Each single TMT run contained all the experimental groups from one rat (=one biological replicate; see the experimental setup in **Fig. 1**), and the reporter intensity was therefore dependent both on the run and the rat. The runs are separately scaled, followed by internal reference scaling normalization (45, 46). Finally, the data was normalized for compositional bias using edgeR TMM normalization (Bioconductor (47)). These normalized intensities were then used in differential protein expression analysis using the edgeR-limma workflow described in (10, 48).

In addition, the differential protein expression in the supernatant datasets was checked by adjusting the normalized data for the total amount of histone and ribosomal proteins. The result displayed no significant difference prior to and after scaling for histone and ribosomal proteins in terms of the differential expression analyses (not shown). Therefore, supernatant datasets without additional histone and ribosomal proteins scaling were used for the subsequent analysis and illustration. We wanted to keep the normalization steps to a minimum to prevent inadvertent bias due to inherent variability in the expression of histone and ribosomes in our data.

Gene set enrichment analysis (GSEA)

Protein IDs were converted to gene symbol before loading into GSEA-4.1.0 (49, 50). The normalized reporter intensity data were fed for the functional enrichment analysis. Signal-to-noise weighted scoring schemes were used for the enrichment statistics. Gene set permutation of 10,000 times was done to obtain the null distribution of p-values. Gene sets with an FDR q-value ≤ 0.05 were considered significantly enriched.

Endocytosis experiments

LSECs (0.3×10^6 cells/cm² in collagen-coated 24-well plates) were cultured as described under “LSEC isolation, purification and culture”, with or without supplementation of 1 µg/ml Dex. Formaldehyde-denatured bovine serum albumin (FSA), prepared as described in (51) was labeled with either fluorescein isothiocyanate (FITC) by incubating FSA and FITC in sodium carbonate buffer (0.5 ml/L, pH 9.5) at a protein-dye ratio of 4:1 at 4°C overnight, and dialyzed against PBS, or with carrier-free Na¹²⁵I using Iodogen as an oxidizing agent, as described by the manufacturer (Pierce Chemicals, Rockford, IL). FSA labeled with ¹²⁵I was separated from unbound ¹²⁵I on a PD-10 column (GE Health, Uppsala, Sweden). The resulting specific radioactivity was approximately 1×10^6 cpm per µg protein.

Endocytosis experiments were carried out as described (52). In short, LSEC cultures were incubated with ¹²⁵I-FSA, 0.1 µg/ml, in Roswell Park Memorial Institute (RPMI-1640) medium (Sigma) with 1% human serum albumin (Octapharma, Heidelberg, Germany) for 2 h at 37°C in 5% O₂, 5% CO₂. The supernatant was then removed and intact proteins in the supernatant pelleted with 20% trichloroacetic acid (Merck), while cell cultures were washed with cold PBS and lysed in 1% sodium dodecyl sulphate before measuring cell-associated radioactivity, and acid-soluble radioactivity in supernatants (representing degraded ligand (52)) in a gamma counter. Each experiment was done in triplicate and repeated with 3 biological replicates.

For measurements of cell numbers in cultures, 5 areas per culture per treatment were imaged before starting the endocytosis experiments, using a Nikon inverted microscope (Nikon, Tokyo, Japan) equipped with a Zeiss AxioCam MRc digital camera (Carl Zeiss, Göttingen, Germany). Cell numbers were counted manually with Fiji software (53).

In a separate series of experiments, LSECs were incubated with 20 µg/ml of FITC-labeled FSA in RPMI-1640 with 1% human serum albumin (Octapharma) for 30 min, then the medium with ligand was removed and the cells incubated further in medium alone for another 1.5h before fixation of cells in 4% formaldehyde in PBS, pH 7.2. Cell nuclei were stained with DAPI (Sigma-Aldrich). Cultures were imaged as described above.

Scanning electron microscopy (SEM)

LSECs (0.3×10^6 cells/cm²) were seeded in collagen-coated 24-well plates and treated as described under “LSEC isolation, purification, and culture” before fixation in McDowell’s fixative for electron microscopy (54) at 2 or 24 h after seeding. Fixed cultures were stamped out from the plate and processed for SEM using the protocol in (10). In short, the cells were washed in PHEM buffer, post-fixed in 1% tannic acid, then in 1% osmium tetroxide in double-distilled water, dehydrated in a graded

ethanol series (30-100%), chemically dried in hexamethyldisilazane (Sigma Aldrich; cells for morphology analysis and sieve plate counts), or critical point dried (cells for purity tests for proteomics), mounted on aluminum stubs, and sputter coated with gold/palladium alloy. Specimen were imaged in a Zeiss Sigma field emission scanning electron microscope (Carl Zeiss, Oberkochen, Germany), run at 2 kV. High-resolution overview images were taken from 3-5 different regions per culture, and high magnification images were obtained within these areas.

When comparing the number of sieve plates per cell area in rat LSEC cultures incubated for 2 or 24 h, fenestrae were defined as open trans-cytoplasmic holes < 500 nm in diameter, whereas holes above this size were defined as gaps. Sieve plates were defined as clusters of ≥ 5 fenestration. The image analysis was done in a semi-quantitative way, where the area covered by cells in each image was divided with a grid into areas of $20\ \mu\text{m} \times 20\ \mu\text{m}$ ($400\ \mu\text{m}^2$) using Image J, and the number of sieve plates was counted per area. More than 100 areas of $400\ \mu\text{m}^2$ were analyzed from each culture. When establishing the method for this analysis, 35 randomly selected grid areas were evaluated independently by three experienced LSEC researchers (RL, KKS, BS). Without counting the actual number of sieve plates, each researcher was asked to score the number of sieve plates within each grid area as high, medium, and low according to their experience. More than 90% consensus was reached between the researchers. The number of sieve plates in the areas scored as high, medium, or low fenestrated were then counted, and the criteria of each category was set as follows: 1) Low: 0-4 sieve plates/ $400\ \mu\text{m}^2$, 2) medium: 5-14 sieve plates/ $400\ \mu\text{m}^2$, and 3) high: ≥ 15 sieve plates/ $400\ \mu\text{m}^2$.

Cell viability assay

LSECs ($0.3\ \text{million cells/cm}^2$) were seeded in collagen-coated 24-well plates and treated as described under “LSEC isolation, purification and culture”. At 2 or 24 h, the fluorescent dye mixture from the LIVE/DEAD Cell Imaging Kit (Thermo Scientific) was added to each culture and the cells incubated according to the manufacturer’s instructions. The cultures were imaged as described under “Endocytosis experiments”, and the number of positively stained cells were counted with Image J and corrected manually when two cells were closely attached to each other.

Enzyme-linked immunosorbent assay (ELISA)

IL-6 production was measured after treatment with IL-1 β , or Dex. Supernatants were harvested from LSECs (0.3×10^6 cells/ cm^2 seeded per well in 24-well plates) at specified time points, and the concentration of IL-6 was determined with the Rat IL-6 DuoSet ELISA kit (R&D Systems). When titrating the IL-1 β dose for the proteomic experiments the IL-6 production was measured at 6, 18,

and 24 h. Doses tested were 0, 10, 50, 100, 1000, 5000 IU/ml. Of these 100 IU/ml gave the highest IL-6 production at 18 and 24 h relative to 6h and were used in the proteomics experiments.

Luminex – Multiplex immunobead assay

Supernatants of the LSEC cultures used for SEM morphology analysis were collected at 24 h, filtered, and concentrated as described for cell supernatants under “Proteomic sample preparation and analysis”. The concentration of IL-1 β , IL-10, IL-6, monocyte chemoattractant protein-1 (MCP-1; CCL2), MCP-3 (CCL7), and macrophage inflammatory protein-1 alfa (MIP-1 α) in supernatants were measured with the Rat Custom ProcartaPlex 6-plex Kit (Thermo Fisher) following the ProcartaPlex Multiplex Immunoassay user guide MAN0017083. Specific luminescence in samples and standards were differentiated and analyzed by Luminex 100/200 (Thermo Fisher).

Statistical analysis, and visualization

The initial data annotation and filtrations were done in the Perseus environment (version 1.6.10.43). TMT data processing and normalization (as described under “Data analysis”), and the subsequent differential expression analysis were performed in the R/Bioconductor environment (55). The normalized intensities were subjected to the exact test implemented in the edgeR package and proteins that showed $|\log_2 FC| \geq 0.5$ and $FDR \leq 0.05$ were determined significantly different. The gene enrichment analysis was performed in the GSEA-4.1.0 software (49, 50), and the gene sets with FDR q-value ≤ 0.05 were identified as significantly enriched. Figures were generated using the R packages factoextra, ggplot2, ggpubr, pheatmap, and the plugin EnrichmentMap from Cytoscape, InstantClue, and Microsoft Office Excel. Panels were made in Adobe Illustrator.

Results

Global information about the rat LSEC proteome in early primary culture

An overview of the experimental setup is presented in **Fig. 1**. We quantitatively catalogued 2537 protein IDs in the cell lysates (*i.e.*, cell-associated proteins) and 1432 proteins in the filtered supernatants of the LSEC cultures in the 3 experiments (**Supplemental file 1**). The LSEC supernatants were harvested at 24 h. Approximately 18% (260) of the proteins identified in the supernatants were not identified in the cell lysates (**Fig. 2A**), and the supernatants contained more of proteins/protein isoforms predicted to be secreted (**Fig. 2B**; detailed in **Supplemental file 1**) using the protein class annotation in the Human Protein Atlas (56).

Principal component analysis (PCA) clustered the cell-associated proteomes into three groups (**Fig. 2C**): 1) Samples from freshly isolated LSECs cultured for 2 h with no treatment, 2) samples from LSECs cultured for 24 h with no treatment or with IL-1 β alone, and 3) samples from LSECs cultured for 24 h with Dex alone or with Dex plus IL-1 β . The proteomes from the culture supernatants (harvested after 24 h) clustered into two groups in the PCA plot (**Fig. 2D**): 1) Samples from LSECs cultured with no treatment or with IL-1 β alone, and 2) samples from LSECs incubated in the presence of Dex alone or with Dex plus IL-1 β .

Dex induced significant changes both in the LSEC cell-associated proteome and the proteome from the LSEC supernatants, while the effect of IL-1 β was low as illustrated in the scatter plots in **Figs. 2E-H**. We here compared the ranks obtained from a pairwise comparison of protein expression in cultures with different combinations of treatments. The high correlation across the protein ranks obtained from the pairwise comparison between the proteomes of cells (**Fig. 2E**, $R=0.78$), or supernatants (**Fig. 2F**, $R=0.93$) of [Dex-treated LSECs vs 24 h non-treated LSECs] and [Dex-treated LSECs vs IL-1 β -treated LSECs] suggests that the expression level of proteins in IL-1 β stimulated cultures were almost similar to that of non-treated cultures. Furthermore, the low correlation across the protein ranks obtained from the pairwise comparison between the proteomes of cells (**Fig. 2G**, $R=0.29$), or supernatants (**Fig. 2H**, $R= -0.19$) of [Dex-treated LSECs vs 24 h non-treated LSECs] and [IL-1 β treated LSECs vs 24 h non-treated LSECs] indicates that Dex induced a significantly different proteomic response in LSECs than IL-1 β .

Since non-treated LSECs and LSECs exposed to IL-1 β showed highly similar protein expression levels, we have focused the further analysis and presentation of results on the effect of Dex on the LSEC proteome.

Rat LSECs developed a pro-inflammatory phenotype and showed major changes in metabolic pathways during the first 24 h in culture

In order to unravel proteome changes that occur in the early primary culture of rat LSECs, we first compared the protein expression profiles of the cell lysates from LSECs cultured for 24 h with the profile of LSECs cultured for 2 h.

Row-wise k-means cluster analysis on the cell-associated proteomes of non-treated (2 h, 24 h) and Dex-treated LSECs resulted in four modules, where proteins within each module showed a similar direction in their pattern of expression (**Fig. 3A**). Fig. 3A also shows enriched processes and pathways that are associated with each module (resulting from functional enrichment analysis in DAVID). The significantly up-, or downregulated proteins within each of the four modules are shown in the scaled heatmaps in **Figs. 3B-E**.

Maintaining rat LSECs in culture for 24 h evoked substantial changes in the cell proteome. The majority of these changes were not significantly altered by Dex treatment (**Fig. 3A - modules 1 and 2, Figs. 3B, 3C**). Module 1 contained the proteins that were downregulated at 24 h both in the presence and absence of Dex. Functional enrichment analysis of significantly altered proteins ($FDR \leq 0.05$, and $|\log_2 FC| \geq 0.25$) in this module showed downregulation of pyruvate metabolism, citrate cycle, oxidation-reduction processes, fatty acid elongation, amino acid metabolism, and peroxisome functions (**Fig. 3A - module 1**). Several LSEC signature membrane receptors, including the scavenger receptors stabilin-1 (STAB1) and stabilin-2 (STAB2), lymphatic vessel endothelial hyaluronan receptor 1 (LYVE-1), C-type lectin domain family member 4 (CLEC4G, or LSECtin), and melanoma cell adhesion molecule (MCAM, or CD146), were also significantly downregulated at 24 h ($FDR \leq 0.05$, and $|\log_2 FC| \geq 0.5$) (**Fig. 3B**). Fc γ RIIb and mannose receptor (MRC1, CD206) were also reduced at 24 h but with $|\log_2 FC| = 0.44$ ($FDR \leq 0.05$).

Module 2 (**Figs. 3A, 3C**) contained proteins that were upregulated at 24 h in all cultures. Enriched processes and pathways were glycolysis/gluconeogenesis, mRNA transport and initiation of translation, biosynthesis of amino acids, and cell-cell adhesion.

Module 3 (**Figs. 3A, 3D**) contained proteins that were upregulated at 24 h in LSEC cultures without Dex but repressed in the presence of Dex. Significantly altered proteins in this cluster were closely associated with immune functions and inflammatory processes.

Module 4 (**Figs. 3A, 3E**) include proteins that were upregulated at 24 h only in presence of Dex. Enriched processes and pathways were linked to responses to glucose and glucocorticoids, and mineral absorption.

Dex suppressed the induction of an inflammatory-like phenotype in cultured LSECs

In order to evaluate the effect of Dex on LSECs in more detail, we compared the proteomes from Dex-treated and non-treated cultures at 24 h focusing both on the cell-associated proteome and proteins in culture supernatants. Approximately 1.2% (33) of the cell-associated proteins were differentially expressed in the presence of Dex (**Fig. 4A**), whereas 19% (178) of all supernatant proteins were significantly altered by Dex (**Fig. 4B**). Significantly up-, or downregulated proteins in the supernatants are listed in the two scaled heatmaps in **Figs. 4C-D**.

Proteins in culture supernatants may stem from several sources, including Golgi-mediated secretory pathways, shedding of extracellular vesicles, histone release (57), fusion of endosomes/lysosomes with the plasma membrane, or leakage from dead or dying cells. The LSEC secretome has not been fully characterized in any animal model, and we do not know the exact source of all proteins in the supernatant. We, therefore, focused the GSEA on proteins annotated as secreted proteins according to the Human Protein Atlas (58). This included 115 protein orthologs of the 1432 protein IDs in the LSEC supernatants. GSEA and leading-edge analysis of these secreted proteins showed that Dex led to downregulation of cell-cell signaling, and cellular responses to oxygen-containing compounds, chemotaxis, and leukocyte migration (**Figs. 5A, B; Supplementary Fig. 1**).

In the cell-associated proteome of LSEC, Dex significantly downregulated many proteins in the inflammatory response (**Fig. 6A**), including intercellular adhesion molecule 1 (ICAM-1), CD14, CD44, nitric oxide synthase 2 (NOS2, or inducible nitric oxide synthase, iNOS), hexokinase 2 (HK2), and guanylate binding protein 2 and 5 (GBP2, GBP5). CD14 regulates LPS-induced endocytosis of toll-like receptor 4 and modulates responses in monocytes and LSECs (59), whereas CD44 is a receptor for matrix molecules such as hyaluronan, osteopontin, and matrix metalloproteinases and is involved in lymphocyte activation and homing (15). Glycolytic proteins were also suppressed in Dex-treated LSECs compared to non-treated LSECs at 24 h but enhanced compared to 2 h (**Fig. 6B**).

The proteins that showed the highest upregulation in the presence of Dex at 24 h were fatty acid-binding proteins (FAB4, FAB5), metallothioneins (MT1, MT1M), and the microtubule-associated protein 1B (MAP1B) (**Fig. 6C**). Fatty acid binding proteins are ubiquitously expressed, with different

isoforms depending on the tissue, and are active in fatty acid metabolism (60). Metallothionein is the part of thiol antioxidants that are involved in heavy metal detoxification and are elevated in response to prolonged oxidative stress, controlled by the Nrf2-antioxidant response element signaling pathway (61).

LSEC cytokine secretion and effect of Dex

To validate some of the cytokines and chemokines affected by Dex in the quantitative proteomic study (**Figs. 4, 5, Supplementary Fig. 1**), we used a multiplex immunobead assay to measure the production of IL-1 β , IL-6, CCL2 (MCP-1), CCL7 (MCP-3), IL-10, and MIP-1 α in supernatants harvested from non-treated and Dex-treated LSEC cultures at 24 h (**Figs. 7A-E**). The LSEC secretion of IL-1 β , IL-6, and CCL2 was downregulated, whereas the secretion of IL-10 was enhanced in cells exposed to Dex, validating the quantitative proteomics results, while CCL7 was either enhanced or not changed. MIP-1 α was out of range (too high, not shown).

LSECs are important producers of IL-6 in the liver, and Dex is a well-known inhibitor of IL-6 (62). To investigate more in detail LSEC production of IL-6 in early cultures and the effect of Dex, we incubated freshly isolated cells with 1 μ g/ml Dex and measured IL-6 in supernatants at 12, 18, and 24 h (**Fig. 7F**). The IL-6 production in the absence of Dex was 3 times higher at 24 h compared to 12 h post-seeding. Dex efficiently suppressed IL-6 production in LSECs at all time points.

Dex-mediated preservation of LSEC endocytosis in culture may be a function of improved cell viability

A core *in vivo* function of LSECs is the effective removal, via clathrin-mediated endocytosis of many modified plasma proteins, and blood-borne macromolecules from tissue turnover processes (13). Dex improved rat LSEC viability in culture (**Fig. 8A; Supplementary Fig. 2**). To test if the increased viability also preserved the LSEC scavenger function, we examined the cellular uptake and subsequent degradation of modified albumin (FSA). FSA is a scavenger receptor ligand and is efficiently endocytosed by LSECs both *in vivo* and *in vitro* (63, 64). Active endocytosis of FSA is also used as a functional marker for these cells (13, 65, 66).

First, we measured the rate of uptake of radiolabeled FSA in LSECs. This was done by incubating LSEC cultures with ¹²⁵I-FSA (0.1 μ g/ml) for 2 h, starting at 2 or 24 h post-seeding, and measure how much of the added ligand that had been internalized and processed by the cells during the 2 h incubation period (**Fig. 8B**). The total uptake of ¹²⁵I-FSA was 67% (\pm 2.6%, n=3) of added ligand in the freshly plated LSEC cultures. In 24 h old LSEC cultures, the uptake of ¹²⁵I-FSA was reduced to

74% of this value in Dex-treated cells, and to 53 % in non-treated cells (**Fig. 8B**). The decrease in endocytosis of ^{125}I -FSA with time in culture corresponded with the decrease in cell numbers in culture, suggesting that the higher uptake in the Dex-treated LSEC cultures may be explained by higher cell survival. The proportion of degraded ligand vs cell-associated ligand was almost similar at 2 and 24 h, with or without Dex, suggesting efficient degradation of internalized ligand in all groups.

Experiments with radiolabeled ligands only measure uptake per cell culture. In order to examine if all cells in the cultures, or only a fraction of the cells were able to endocytose the ligand, we incubated LSECs with FITC-labelled FSA and examined the accumulation of ligand in the cells by fluorescence microscopy (**Fig. 8C**). In these experiments the cells were first incubated with 20 $\mu\text{g}/\text{ml}$ FITC-FSA for 30 min, followed by incubation for 1.5 h in medium without ligand. This revealed that in all experimental groups nearly all cells were able to internalize the ligand both at 2 and 24 h post-seeding.

Dex effects on LSEC morphology in culture

The effect of Dex on rat LSEC morphology and fenestration was analyzed by SEM (**Fig. 9**). At 2 h post-seeding, LSECs were highly fenestrated with most fenestrae organized in sieve plates (**Fig. 9A**). At 24 h, the number of sieve plates was markedly reduced, and in the cultures without Dex, the cells also showed an increased number of larger holes, *i.e.*, gaps, which were located especially at the edges of the cells and between cells (**Fig. 9B**). Dex-treated LSECs also showed marked defenestration at 24 h with loss of sieve plates. However, the cells had fewer gaps than cells without Dex, and the cell borders had a smooth appearance, with close contact between cells (**Fig. 9C**), reflecting a more quiescent phenotype.

In order to estimate the reduction in sieve plates in cells at 24 h (\pm Dex) compared to 2 h, we counted the number of sieve plates per cell area ($400\ \mu\text{m}^2$) as described in Methods. At 2 h, approximately 79% of the cell surface had a high density of sieve plates (defined as ≥ 15 sieve plates/area). At 24 h, the percentage of cell surface area with a high density of sieve plates dropped to 10% in LSECs cultured without Dex, and 3% in Dex-treated LSECs (**Fig. 9D**).

Discussion

In this study, we report how the rat LSEC proteome changes in 2D culture, including analyses of both the cell-associated proteome and secreted proteins and the modulating effect of Dex. We used the TMT multiplexing strategy to accommodate all treatments belonging to a biological replicate in the same run to improve quantitation and consequently enhance the proteomic comparison applied henceforth. Having all samples from one experiment in one block simplifies the subsequent normalization between the runs and makes the quantitative comparisons between samples more valid (67), securing proteomic data that are suitable and sensitive to uncover culture-induced phenotypic and functional changes with accuracy and precision.

Deregulation of LSEC morphology and functions in culture is well acknowledged in the literature (13, 66, 68). However, the information about culture-induced changes at the level of processes and pathways is limited. Also, we have limited knowledge about the changes in LSEC proteome in response to pro- and anti-inflammatory stimuli *in vitro*. We found that primary rat LSECs developed an activated phenotype in early culture with elevated expression of pro-inflammatory cytokines, chemokines, and cell adhesion molecules, both in the presence and absence of IL-1 β . This interpretation was supported by enrichment in processes associated with cellular responses to cytokines and interferon- γ and cell-cell adhesion. Dex in the dose tested (1 μ g/ml, (41)) substantially repressed the culture-induced stimulation of inflammatory and immune regulatory pathways, as well as the expression of intercellular adhesion molecule 1 (ICAM-1) and inflammatory mediators such as NF- κ B1, NF- κ B2, NOS2, and other components of interferon responses. Dex also suppressed LSEC production and release of pro-inflammatory cytokines while increasing the secretion of the anti-inflammatory cytokine IL-10.

Importantly, Dex had a clear positive effect on LSEC survival *in vitro*, and significantly downregulated the expression of proapoptotic CASP3 (\log_2 FC = 0.45, FDR < 0.05, **Supplemental file 1**). Cells in medium with Dex also showed a more quiescent morphology compared with non-treated cells. However, Dex was not able to prevent the defenestration of LSECs, which probably occurs due to a lack of paracrine factors in culture. Vascular endothelial growth factor (VEGF), derived from hepatocytes and stellate cells, are important for the regulation of LSEC fenestration and acts through nitric oxide (NO)-dependent and NO-independent pathways (69).

In accordance with previous reports (32, 35, 69-72), membrane receptors that are constitutively highly expressed in LSECs and regarded as LSEC signature genes/proteins were downregulated in the rat

LSEC cultures at 24 h compared to 2 h. These included stabilin-1 (STAB1), stabilin-2 (STAB2), LYVE-1, and LSECtin (CLEC4G). The two stabilins are homologous proteins (73). Both are broad-spectrum scavenger receptors with partly overlapping ligand binding properties (11, 13, 73) and have been suggested as the major work-horses in LSEC clearance of modified plasma proteins, oxidized lipoproteins, and soluble waste material from connective tissue turnover (9). LYVE-1 is a hyaluronan binding protein constitutively expressed by lymphatic vascular endothelial cells, LSECs, and spleen sinusoids (13) and is often downregulated during liver inflammation and in fibrosis in both humans and animal model (74). The C-type lectin LSECtin has a postulated role in viral infection of cells and interacts with envelope glycoproteins on Japanese encephalitis virus (75), lymphocytic choriomeningitis virus (76), and ebolavirus (77), and SARS-CoV-1 spike glycoproteins (77). Although Dex improved cell viability and suppressed cell activation, Dex did not significantly affect the expression of these receptors. Our study lacks sufficient proteome coverage to look at culture- and Dex-induced effects on LSEC transcription factors. However, GATA4 (34), together with c-MAF and MEIS2 (35), are critical regulators of LSEC phenotype, and downregulation of these factors promoted the dedifferentiation of LSECs in culture (34, 35).

Pathway analysis revealed a shift in LSEC metabolism at 24 h compared to 2 h, including enhanced glycolysis (extent of the increase was relatively lesser with Dex treatment) and a reduction in pyruvate metabolism, citrate cycle, fatty acid elongation, amino acid metabolism, oxidation-reduction processes, peroxisome, and PPAR signaling. There are few studies on LSEC metabolism. LSECs are reported to generate most ATPs and biosynthetic precursors from glutamine and palmitate oxidation and less (appr. 20%) from glucose metabolism (78). In accordance with this, we found decreased expression of glutamate dehydrogenase in the rat LSEC proteome at 24 h compared to 2 h, suggesting the diminished ability of the cells to utilize glutamine in culture. Recently, Kalucka *et al.* (2018) demonstrated that another type of endothelial cell, human umbilical vein endothelial cells also rely on fatty acid oxidation to sustain NADPH regeneration critical for redox homeostasis and endothelial quiescence (79).

In conclusion, our study extends the knowledge about culture-induced changes in LSEC metabolism, receptor expression, and functions in culture. The supplementation of Dex to the culture system significantly improved LSEC survival and repressed the culture-induced upregulation of pro-inflammatory proteins and mediators.

Acknowledgements

We thank Randi Olsen and Augusta Hlin Aspar Sundbø at the UiT Core Facility for Advanced Microscopy for excellent help with preparation of samples for scanning electron microscopy.

References

1. Aird WC. Phenotypic Heterogeneity of the Endothelium. *Circ Res.* 2007;100(2):174-90.
2. Butler LM, Hallstrom BM, Fagerberg L, Ponten F, Uhlen M, Renne T, et al. Analysis of Body-wide Unfractionated Tissue Data to Identify a Core Human Endothelial Transcriptome. *Cell Syst.* 2016;3(3):287-301 e3.
3. Zapotoczny B, Szafranska K, Kus E, Chlopicki S, Szymonski M. Quantification of fenestration in liver sinusoidal endothelial cells by atomic force microscopy. *Micron.* 2017;101:48-53.
4. Wisse E, De Zanger RB, Charels K, Van Der Smissen P, McCuskey RS. The liver sieve: considerations concerning the structure and function of endothelial fenestrae, the sinusoidal wall and the space of Disse. *Hepatology.* 1985;5(4):683-92.
5. Wisse E. An ultrastructural characterization of the endothelial cell in the rat liver sinusoid under normal and various experimental conditions, as a contribution to the distinction between endothelial and Kupffer cells. *J Ultrastruct Res.* 1972;38(5-6):528-62.
6. Fraser R, Cogger VC, Dobbs B, Jamieson H, Warren A, Hilmer SN, et al. The liver sieve and atherosclerosis. *Pathology.* 2012;44(3):181-6.
7. Fraser R, Bosanquet AG, Day WA. Filtration of chylomicrons by the liver may influence cholesterol metabolism and atherosclerosis. *Atherosclerosis.* 1978;29(2):113-23.
8. Seternes T, Sørensen K, Smedsrød B. Scavenger endothelial cells of vertebrates: a nonperipheral leukocyte system for high-capacity elimination of waste macromolecules. *Proc Natl Acad Sci U S A.* 2002;99(11):7594-7.
9. Sørensen KK, McCourt P, Berg T, Crossley C, Le Couteur D, Wake K, et al. The scavenger endothelial cell: a new player in homeostasis and immunity. *Am J Physiol Regul Integr Comp Physiol.* 2012;303(12):R1217-30.
10. Bhandari S, Li R, Simon-Santamaria J, McCourt P, Johansen SD, Smedsrød B, et al. Transcriptome and proteome profiling reveal complementary scavenger and immune features of rat liver sinusoidal endothelial cells and liver macrophages. *BMC Mol Cell Biol.* 2020;21(1):85.
11. Pandey E, Nour AS, Harris EN. Prominent Receptors of Liver Sinusoidal Endothelial Cells in Liver Homeostasis and Disease. *Front Physiol.* 2020;11:873.
12. Kjekken R, Mousavi SA, Brech A, Gjoen T, Berg T. Fluid phase endocytosis of [125I]iodixanol in rat liver parenchymal, endothelial and Kupffer cells. *Cell Tissue Res.* 2001;304(2):221-30.
13. Sørensen KK, Simon-Santamaria J, McCuskey RS, Smedsrød B. Liver Sinusoidal Endothelial Cells. *Compr Physiol.* 2015;5(4):1751-74.

14. Knolle PA, Wohlleber D. Immunological functions of liver sinusoidal endothelial cells. *Cell Mol Immunol*. 2016;13(3):347-53.
15. Shetty S, Lalor PF, Adams DH. Liver sinusoidal endothelial cells - gatekeepers of hepatic immunity. *Nat Rev Gastroenterol Hepatol*. 2018;15(9):555-67.
16. Koch PS, Olsavszky V, Ulbrich F, Sticht C, Demory A, Leibing T, et al. Angiocrine Bmp2 signaling in murine liver controls normal iron homeostasis. *Blood*. 2017;129(4):415-9.
17. Ding BS, Cao Z, Lis R, Nolan DJ, Guo P, Simons M, et al. Divergent angiocrine signals from vascular niche balance liver regeneration and fibrosis. *Nature*. 2014;505(7481):97-102.
18. Ding BS, Nolan DJ, Butler JM, James D, Babazadeh AO, Rosenwaks Z, et al. Inductive angiocrine signals from sinusoidal endothelium are required for liver regeneration. *Nature*. 2010;468(7321):310-5.
19. DeLeve LD, Wang X, Guo Y. Sinusoidal endothelial cells prevent rat stellate cell activation and promote reversion to quiescence. *Hepatology*. 2008;48(3):920-30.
20. Herrera B, Addante A, Sánchez A. BMP Signalling at the Crossroad of Liver Fibrosis and Regeneration. *Int J Mol Sci*. 2017;19(1).
21. Maretti-Mira AC, Wang X, Wang L, DeLeve LD. Incomplete differentiation of engrafted bone marrow endothelial progenitor cells initiates hepatic fibrosis in the rat. *Hepatology*. 2018.
22. DeLeve LD. Liver sinusoidal endothelial cells in hepatic fibrosis. *Hepatology*. 2015;61(5):1740-6.
23. Poisson J, Lemoine S, Boulanger C, Durand F, Moreau R, Valla D, et al. Liver sinusoidal endothelial cells: Physiology and role in liver diseases. *J Hepatol*. 2017;66(1):212-27.
24. Sun X, Harris EN. New aspects of hepatic endothelial cells in physiology and nonalcoholic fatty liver disease. *Am J Physiol Cell Physiol*. 2020;318(6):C1200-C13.
25. Lafoz E, Ruart M, Anton A, Oncins A, Hernandez-Gea V. The Endothelium as a Driver of Liver Fibrosis and Regeneration. *Cells*. 2020;9(4).
26. Gracia-Sancho J, Caparros E, Fernandez-Iglesias A, Frances R. Role of liver sinusoidal endothelial cells in liver diseases. *Nat Rev Gastroenterol Hepatol*. 2021.
27. Ramachandran P, Dobie R, Wilson-Kanamori JR, Dora EF, Henderson BEP, Luu NT, et al. Resolving the fibrotic niche of human liver cirrhosis at single-cell level. *Nature*. 2019;575(7783):512-8.
28. Ölander M, Wiśniewski JR, Artursson P. Cell-type-resolved proteomic analysis of the human liver. *Liver Int*. 2020;40(7):1770-80.

29. Ding C, Li Y, Guo F, Jiang Y, Ying W, Li D, et al. A Cell-type-resolved Liver Proteome. *Mol Cell Proteomics*. 2016;15(10):3190-202.
30. Azimifar SB, Nagaraj N, Cox J, Mann M. Cell-type-resolved quantitative proteomics of murine liver. *Cell Metab*. 2014;20(6):1076-87.
31. Martinez I, Nedredal GI, Oie CI, Warren A, Johansen O, Le Couteur DG, et al. The influence of oxygen tension on the structure and function of isolated liver sinusoidal endothelial cells. *Comp Hepatol*. 2008;7:4.
32. Geraud C, Schledzewski K, Demory A, Klein D, Kaus M, Peyre F, et al. Liver sinusoidal endothelium: a microenvironment-dependent differentiation program in rat including the novel junctional protein liver endothelial differentiation-associated protein-1. *Hepatology*. 2010;52(1):313-26.
33. March S, Hui EE, Underhill GH, Khetani S, Bhatia SN. Microenvironmental regulation of the sinusoidal endothelial cell phenotype in vitro. *Hepatology*. 2009;50(3):920-8.
34. Geraud C, Koch PS, Zierow J, Klapproth K, Busch K, Olsavszky V, et al. GATA4-dependent organ-specific endothelial differentiation controls liver development and embryonic hematopoiesis. *J Clin Invest*. 2017;127(3):1099-114.
35. de Haan W, Øie C, Benkheil M, Dheedene W, Vinckier S, Coppiello G, et al. Unraveling the transcriptional determinants of liver sinusoidal endothelial cell specialization. *Am J Physiol Gastrointest Liver Physiol*. 2020;318(4):G803-G15.
36. Kuo T, McQueen A, Chen T-C, Wang J-C. Regulation of Glucose Homeostasis by Glucocorticoids. *Adv Exp Med Biol*. 2015;872:99-126.
37. Franco LM, Gadkari M, Howe KN, Sun J, Kardava L, Kumar P, et al. Immune regulation by glucocorticoids can be linked to cell type-dependent transcriptional responses. *J Exp Med*. 2019;216(2):384-406.
38. Grøntved L, John S, Baek S, Liu Y, Buckley JR, Vinson C, et al. C/EBP maintains chromatin accessibility in liver and facilitates glucocorticoid receptor recruitment to steroid response elements. *Embo j*. 2013;32(11):1568-83.
39. Quatrini L, Ugolini S. New insights into the cell- and tissue-specificity of glucocorticoid actions. *Cell Mol Immunol* 2020.
40. Smedsrød B, Pertoft H, Eggertsen G, Sundstrom C. Functional and morphological characterization of cultures of Kupffer cells and liver endothelial cells prepared by means of density separation in Percoll, and selective substrate adherence. *Cell Tissue Res*. 1985;241(3):639-49.
41. Martinez I, Sveinbjørnsson B, Smedsrød B. Nitric oxide down-regulates endocytosis in rat liver endothelial cells. *Biochem Biophys Res Commun*. 1996;222(3):688-93.

42. Martinez I, Sveinbjornsson B, Vidal-Vanaclocha F, Asumendi A, Smedsrød B. Differential cytokine-mediated modulation of endocytosis in rat liver endothelial cells. *Biochem Biophys Res Commun.* 1995;212(1):235-41.
43. McCourt PA, Smedsrød BH, Melkko J, Johansson S. Characterization of a hyaluronan receptor on rat sinusoidal liver endothelial cells and its functional relationship to scavenger receptors. *Hepatology.* 1999;30(5):1276-86.
44. UniProt C. UniProt: a worldwide hub of protein knowledge. *Nucleic Acids Res.* 2019;47(D1):D506-D15.
45. Plubell DL, Wilmarth PA, Zhao Y, Fenton AM, Minnier J, Reddy AP, et al. Extended Multiplexing of Tandem Mass Tags (TMT) Labeling Reveals Age and High Fat Diet Specific Proteome Changes in Mouse Epididymal Adipose Tissue. *Mol Cell Proteom.* 2017;16(5):873-90.
46. Khan SY, Ali M, Kabir F, Renuse S, Na CH, Talbot CC, Jr., et al. Proteome Profiling of Developing Murine Lens Through Mass Spectrometry. *Invest Ophthalmol Vis Sci.* 2018;59(1):100-7.
47. Robinson MD, Oshlack A. A scaling normalization method for differential expression analysis of RNA-seq data. *Genome Biol.* 2010;11(3):R25.
48. Law CW, Alhamdoosh M, Su S, Dong X, Tian L, Smyth GK, et al. RNA-seq analysis is easy as 1-2-3 with limma, Glimma and edgeR. *F1000Res.* 2016;5:1408.
49. Subramanian A, Tamayo P, Mootha VK, Mukherjee S, Ebert BL, Gillette MA, et al. Gene set enrichment analysis: a knowledge-based approach for interpreting genome-wide expression profiles. *Proc Natl Acad Sci U S A.* 2005;102(43):15545-50.
50. Mootha VK, Lindgren CM, Eriksson KF, Subramanian A, Sihag S, Lehar J, et al. PGC-1alpha-responsive genes involved in oxidative phosphorylation are coordinately downregulated in human diabetes. *Nat Genet.* 2003;34(3):267-73.
51. Mego JL, Bertini F, McQueen JD. The use of formaldehyde-treated 131-I-albumin in the study of digestive vacuoles and some properties of these particles from mouse liver. *J Cell Biol.* 1967;32(3):699-707.
52. Hansen B, Svistounov D, Olsen R, Nagai R, Horiuchi S, Smedsrød B. Advanced glycation end products impair the scavenger function of rat hepatic sinusoidal endothelial cells. *Diabetologia.* 2002;45(10):1379-88.
53. Schindelin J, Arganda-Carreras I, Frise E, Kaynig V, Longair M, Pietzsch T, et al. Fiji: an open-source platform for biological-image analysis. *Nat Methods.* 2012;9(7):676-82.
54. McDowell EM, Trump BF. Histologic fixatives suitable for diagnostic light and electron microscopy. *Arch Pathol Lab Med.* 1976;100(8):405-14.

55. Gentleman RC, Carey VJ, Bates DM, Bolstad B, Dettling M, Dudoit S, et al. Bioconductor: open software development for computational biology and bioinformatics. *Genome Biol.* 2004;5.
56. Thul PJ, Åkesson L, Wiking M, Mahdessian D, Geladaki A, Ait Blal H, et al. A subcellular map of the human proteome. *Science.* 2017;356(6340).
57. Chen R, Kang R, Fan XG, Tang D. Release and activity of histone in diseases. *Cell Death Dis.* 2014;5(8):e1370.
58. Uhlén M, Karlsson MJ, Hober A, Svensson AS, Scheffel J, Kotol D, et al. The human secretome. *Sci Signal.* 2019;12(609):eaaz0274.
59. Uhrig A, Banafsche R, Kremer M, Hegenbarth S, Hamann A, Neurath M, et al. Development and functional consequences of LPS tolerance in sinusoidal endothelial cells of the liver. *J Leukoc Biol.* 2005;77(5):626-33.
60. Smathers RL, Petersen DR. The human fatty acid-binding protein family: evolutionary divergences and functions. *Hum Genomics.* 2011;5(3):170-91.
61. Han ES, Muller FL, Pérez VI, Qi W, Liang H, Xi L, et al. The in vivo gene expression signature of oxidative stress. *Physiol Genomics.* 2008;34(1):112-26.
62. Waage A, Slupphaug G, Shalaby R. Glucocorticoids inhibit the production of IL6 from monocytes, endothelial cells and fibroblasts. *Eur J Immunol.* 1990;20(11):2439-43.
63. Blomhoff R, Eskild W, Berg T. Endocytosis of formaldehyde-treated serum albumin via scavenger pathway in liver endothelial cells. *Biochem J.* 1984;218(1):81-6.
64. Li R, Oteiza A, Sørensen KK, McCourt P, Olsen R, Smedsrød B, et al. Role of liver sinusoidal endothelial cells and stabilins in elimination of oxidized low-density lipoproteins. *Am J Physiol Gastrointest Liver Physiol.* 2011;300(1):G71-81.
65. Elvevold K, Smedsrød B, Martinez I. The liver sinusoidal endothelial cell: a cell type of controversial and confusing identity. *Am J Physiol Gastrointest Liver Physiol.* 2008;294(2):G391-400.
66. DeLeve LD, Maretta-Mira AC. Liver Sinusoidal Endothelial Cell: An Update. *Semin Liver Dis.* 2017;37(4):377-87.
67. Arul AB, Robinson RAS. Sample Multiplexing Strategies in Quantitative Proteomics. *Anal Chem.* 2019;91(1):178-89.
68. Cogger VC, Hunt NJ, Le Couteur DG. Fenestration in the Liver Sinusoidal Endothelial Cell. *The Liver2020.* p. 435-43.
69. Xie G, Wang X, Wang L, Wang L, Atkinson RD, Kanel GC, et al. Role of differentiation of liver sinusoidal endothelial cells in progression and regression of hepatic fibrosis in rats. *Gastroenterology.* 2012;142(4):918-27 e6.

70. Xie G, Choi SS, Syn WK, Michelotti GA, Swiderska M, Karaca G, et al. Hedgehog signalling regulates liver sinusoidal endothelial cell capillarisation. *Gut*. 2013;62(2):299-309.
71. Duan JL, Ruan B, Yan XC, Liang L, Song P, Yang ZY, et al. Endothelial Notch activation reshapes the angiocrine of sinusoidal endothelia to aggravate liver fibrosis and blunt regeneration in mice. *Hepatology*. 2018;68(2):677-90.
72. Desroches-Castan A, Tillet E, Ricard N, Ouarne M, Mallet C, Belmudes L, et al. Bone Morphogenetic Protein 9 Is a Paracrine Factor Controlling Liver Sinusoidal Endothelial Cell Fenestration and Protecting Against Hepatic Fibrosis. *Hepatology*. 2019;70(4):1392-408.
73. Politz O, Gratchev A, McCourt PA, Schledzewski K, Guillot P, Johansson S, et al. Stabilin-1 and -2 constitute a novel family of fasciclin-like hyaluronan receptor homologues. *Biochem J*. 2002;362(Pt 1):155-64.
74. Arimoto J, Ikura Y, Suekane T, Nakagawa M, Kitabayashi C, Iwasa Y, et al. Expression of LYVE-1 in sinusoidal endothelium is reduced in chronically inflamed human livers. *J Gastroenterol*. 2010;45(3):317-25.
75. Shimojima M, Takenouchi A, Shimoda H, Kimura N, Maeda K. Distinct usage of three C-type lectins by Japanese encephalitis virus: DC-SIGN, DC-SIGNR, and LSECtin. *Arch Virol*. 2014;159(8):2023-31.
76. Shimojima M, Ströher U, Ebihara H, Feldmann H, Kawaoka Y. Identification of cell surface molecules involved in dystroglycan-independent Lassa virus cell entry. *J Virol*. 2012;86(4):2067-78.
77. Gramberg T, Hofmann H, Möller P, Lalor PF, Marzi A, Geier M, et al. LSECtin interacts with filovirus glycoproteins and the spike protein of SARS coronavirus. *Virology*. 2005;340(2):224-36.
78. Spolarics Z, Lang CH, Bagby GJ, Spitzer JJ. Glutamine and fatty acid oxidation are the main sources of energy for Kupffer and endothelial cells. *Am J Physiol*. 1991;261(2 Pt 1):G185-90.
79. Kalucka J, Bierhansl L, Conchinha NV, Missiaen R, Elia I, Bruning U, et al. Quiescent Endothelial Cells Upregulate Fatty Acid beta-Oxidation for Vasculoprotection via Redox Homeostasis. *Cell Metab*. 2018;28(6):881-94 e13.
80. Huang da W, Sherman BT, Lempicki RA. Bioinformatics enrichment tools: paths toward the comprehensive functional analysis of large gene lists. *Nucleic Acids Res*. 2009;37(1):1-13.
81. Huang da W, Sherman BT, Lempicki RA. Systematic and integrative analysis of large gene lists using DAVID bioinformatics resources. *Nat Protoc*. 2009;4(1):44-57.

Figure legends

Fig. 1: Overview of the experimental setup for the quantitative TMT proteomics study

The figure shows the experimental setup for the quantitative proteomics experiment. The whole experiment was repeated three times with cells from different rats. Each biological replicate included pooled LSECs from two rat livers. The dose of Dex was 1 $\mu\text{g/ml}$ (41). The dose of IL-1 β was 100 IU/ml, which was chosen after testing the effect of different doses on IL-6 production in LSECs as described in Material and Methods. NT: not treated with either Dex or IL-1 β .

Fig. 2: Global characterization of proteins in cell lysates and supernatants from rat LSEC primary cultures

A) Venn diagram showing the number of proteins identified in cell lysates and supernatants of LSEC cultures and overlapping protein expression in the two sample types.

B) Protein composition of cell lysates and supernatants of LSECs cultured for 24 h. Results are presented in percent of total protein in the respective datasets and annotated to the major protein categories in Human Protein Atlas (56).

C) Non-scaled principal component analysis (PCA) plot of proteomes of cell lysates of LSECs cultured for 2 or 24 h with Dex, IL-1 β , a combination of Dex and IL-1 β , or with no treatment (NT).

D) Non-scaled PCA plot of proteomes obtained from supernatants of LSECs cultured for 24 h with Dex, IL-1 β , or a combination of Dex and IL-1 β , or with no treatment (NT).

E-H) Scatter plots showing ranked proteomes in response to Dex and IL-1 β compared to non-treated (NT) control cultures at 24 h. The plots in E (proteomes from cell lysates) and F (proteomes from supernatants) show the correlation between the Dex vs IL-1 β comparison and the Dex vs 24 h NT comparison. The plots in G (proteomes from cell lysates) and H (proteomes from supernatants) show the correlation between the Dex vs 24 h NT comparison and the IL-1 β vs 24 h NT comparison.

Fig. 3: Cluster analysis of the cell-associated proteomes of 2 h vs 24 h LSEC cultures

The figure shows proteins that are significantly differentially expressed between 2 and 24 h rat LSEC cultures. A) Row-wise k-means clustering on the whole cell lysate proteome of non-treated LSECs (NT 2 h, 24 h) and Dex-treated LSECs (Dex 24 h) resulted in four different modules. Proteins within each module 1-4 showed a similar expression pattern. These are illustrated in the parallel line (profile)

plots with corresponding Z score (standardized TMT reporter intensities). In each profile plot significantly up- and downregulated proteins belonging to each module are highlighted in red, and the other proteins are shown in grey. Significantly regulated proteins are named in the scaled heatmaps in B-E. The list of proteins from each module with at least $|\log_2 \text{FC}| \geq 0.25$, and $\text{FDR} \leq 0.05$ in at least one pairwise comparison between the NT 2 h, NT 24 h, or Dex 24 h group were feed into DAVID (v 6.8) (<https://david.ncifcrf.gov/home.jsp>) (80, 81) for functional annotation and enrichment analysis. The enriched processes/pathways associated with each module are listed below the corresponding parallel line plot.

B) Scaled heatmap of proteins downregulated at 24 h in the presence and absence of Dex.

C) Scaled heatmap of proteins upregulated at 24 h in the presence and absence of Dex.

D) Scaled heatmap of proteins upregulated at 24 h in non-treated cultures only.

E) Scaled heatmaps of proteins upregulated at 24 h in Dex-treated cultures only.

Significance level in B-E: $\text{FDR} \leq 0.05$, and $|\log_2 \text{FC}| \geq 0.5$.

Fig. 4: Comparison of the proteomes of cell lysates and supernatants of 24 h LSEC cultures incubated with or without Dex

A-B) Volcano plots illustrating differently expressed genes in A) the LSEC cell-associated proteome at 24 h \pm Dex, and B) the LSEC supernatants \pm Dex. The Top 10 differentiated proteins are illustrated with symbols. Significance level: $\text{FDR} \leq 0.05$, and $|\log_2 \text{FC}| \geq 0.5$. NS, not significant.

C-D) Scaled heat maps of significantly differentially expressed proteins in the supernatants of Dex-treated LSEC cultures compared to non-treated (NT) cultures at 24 h ($\text{FDR} \leq 0.05$ and $|\log_2 \text{FC}| \geq 0.5$). Proteins or isoforms identified to be secreted or predicted to be secreted in the Human Protein Atlas (58) are underlined.

Fig. 5: Gene set enrichment analysis (GSEA) of LSEC secreted proteins

GSEA leading-edge analysis including only proteins in the LSEC culture supernatants that were annotated as secreted proteins (n=115) in the Human Protein Atlas (58).

A) GSEA map showing processes that were significantly changed (all were downregulated) in the presence of Dex. The line thickness reflects the relative number of proteins that were affected.

B) Heatmap with the leading-edge proteins contributing to the enrichment of the processes in A. The color of the heatmap corresponds to the amplitude of \log_2 fold change between the Dex group and the non-treated control group.

Fig. 6: Differential protein expression in selected cellular processes affected by Dex

- A) Proteins in the LSEC cell-associated proteome contributing to the inflammatory-like phenotype of the cells at 24 h post-seeding. All proteins were significantly upregulated (#) during the 24 h culture period in non-treated (NT) cells compared to 2 h NT cultures and were significantly repressed (*) in the presence of Dex at 24 h compared to 24 h NT.
- B) Proteins in the LSEC cell-associated proteome that are involved in the glycolysis shift in culture. The proteins were significantly upregulated (#) during the culture period compared to 2 h NT control and were to some extent suppressed in the presence of Dex (significant* for hexokinase 2 (HK2)).
- C) Lipid binding proteins and metallothioneins in the LSEC cell-associated proteome. These proteins were upregulated during the culture period compared to 2 h NT cultures. The upregulation was more pronounced in the presence of Dex compared to 24 h NT cultures. # Significant between 24 h NT and 2 h NT; *Significant between 24 h Dex and 24 h NT.

In each figure (A-C) the bars represent the standardized \log_2 TMT reporter intensities for each protein per time point and treatment. Results are average values of 3 biological replicates. Error bars show 95% confidence intervals.

Fig. 7: Cytokine production in rat LSECs treated with Dex

- A-E) Expression of selected cytokines and chemokines in supernatants of rat LSEC cultures \pm 1 μ g/ml Dex, measured by Luminex multiplex immunobead assay (n=3).
- F) IL-6 production (single ELISA) at 12, 18, and 24 h in rat LSEC cultures \pm 1 μ g/ml Dex (n=3).

Fig. 8: Effect of Dex on rat LSEC viability and endocytosis function in culture

- A) Number of adherent cells in LSEC cultures at the indicated time points. Results show the average value (% of 2 h value) of 3 biological replicates. NT, no treatment; Dex, dexamethasone.
- B) Endocytosis of radiolabeled formaldehyde-treated serum albumin (FSA) in LSECs. LSECs were cultured for 2 or 24 h; then incubated with 0.1 μ g/ml 125 I-FSA for another 2 h. Total uptake per culture during the 2 h incubation period with radiolabeled ligand represents the sum of cell-associated and degraded ligand as described in Methods. Results are given in % of uptake in the fresh (2 h) cultures

(\pm standard deviation), and the figure shows the average values of 3 biological replicates. The average uptake of ^{125}I -FSA in the fresh cultures was 67% ($\pm 2.6\%$) of added ligand.

C) LSECs were cultured for 2 or 24 h; then incubated with 20 $\mu\text{g/ml}$ FITC-FSA (green fluorescence) for 30 min, washed, and incubated in ligand-free medium for 90 min, and fixed in 4% formaldehyde. Nuclei were stained with DAPI (blue), and cells were imaged in a Nikon inverted fluorescence microscope.

The dose of Dex was 1 $\mu\text{g/ml}$ in all experiments.

Fig. 9: Effect of Dex on rat LSEC morphology in early cultures

A-C) Scanning electron micrographs of LSECs cultured for the indicated time points in the presence or absence of 1 $\mu\text{g/ml}$ Dex (D). Inserts show sieve plates (A-C), and details of cell borders (B, C) at higher magnification.

D) Extent of LSEC surface area with high density (H, ≥ 15 sieve plates (SP)/area), medium density (M, 5-14 SP/area), and low density (L, 0-4 SP/area) of fenestrae organized in SP in percent of total LSEC surface area at the indicated time point and treatment. The number of SP was counted per 400 μm^2 squares on images from randomly picked larger areas in the LSEC cultures. At least 100 squares were scored for each treatment in each experiment. The average values of 3 biological replicates are presented in the figure.

Figure 1

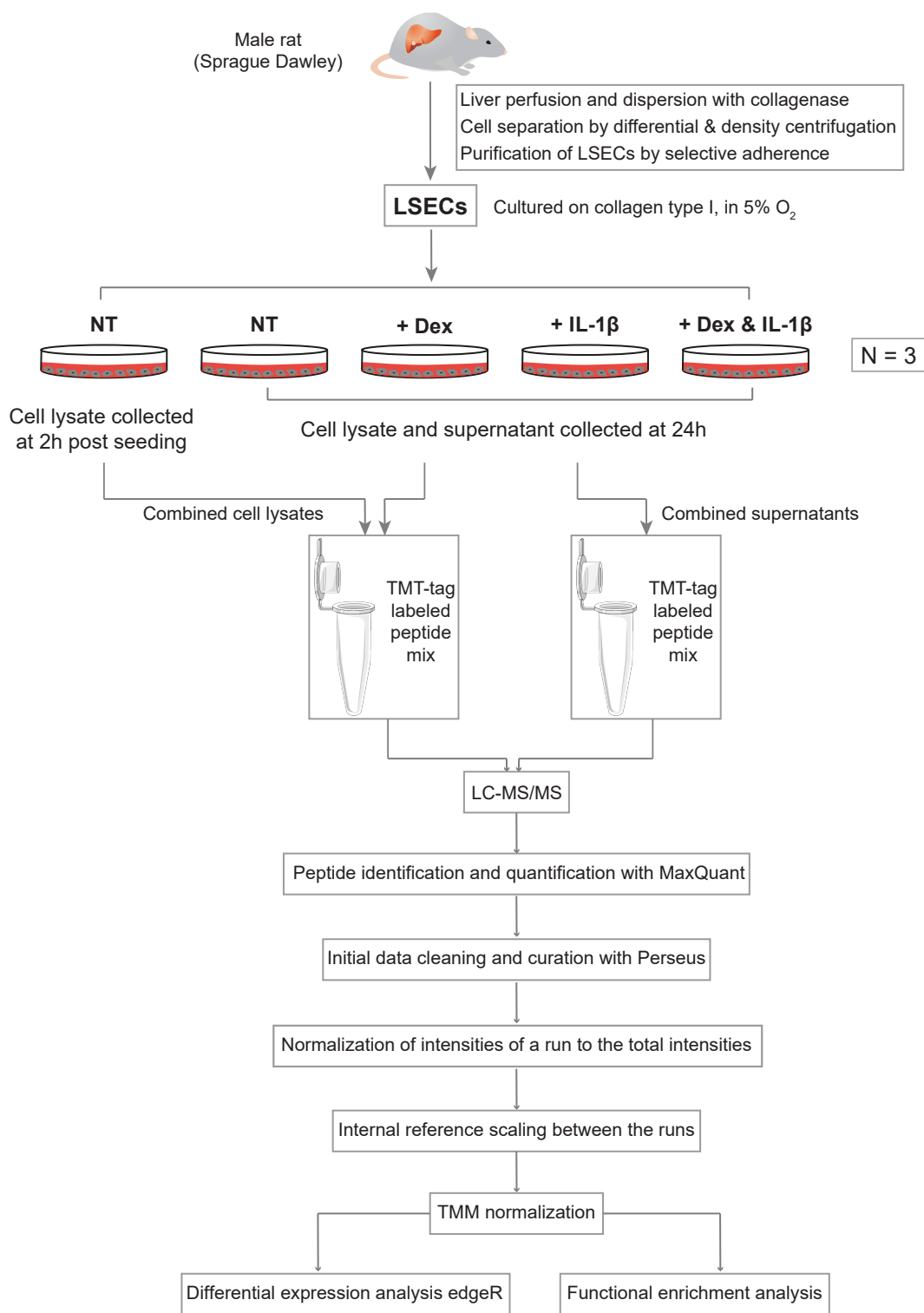


Figure 2

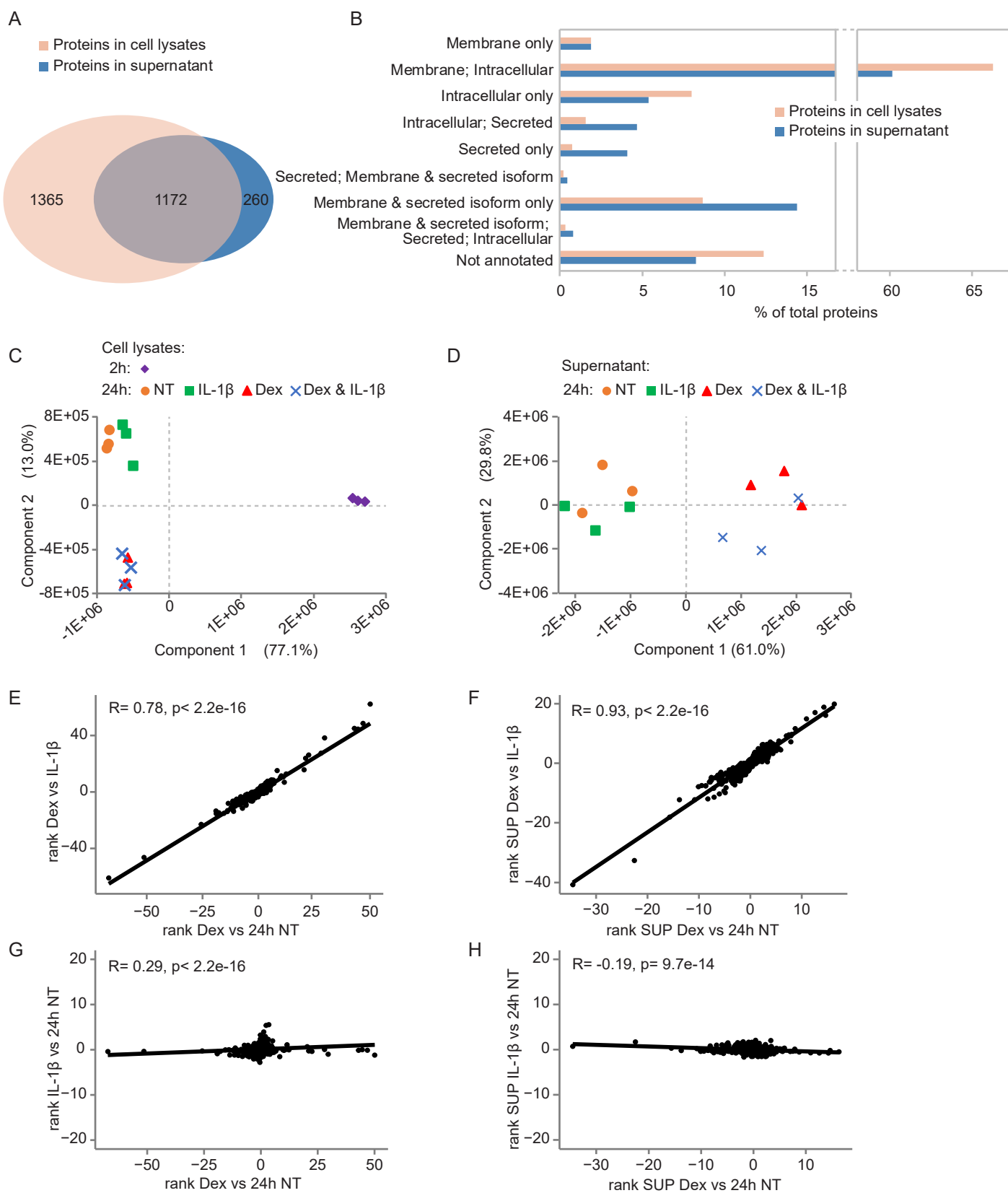


Figure 3

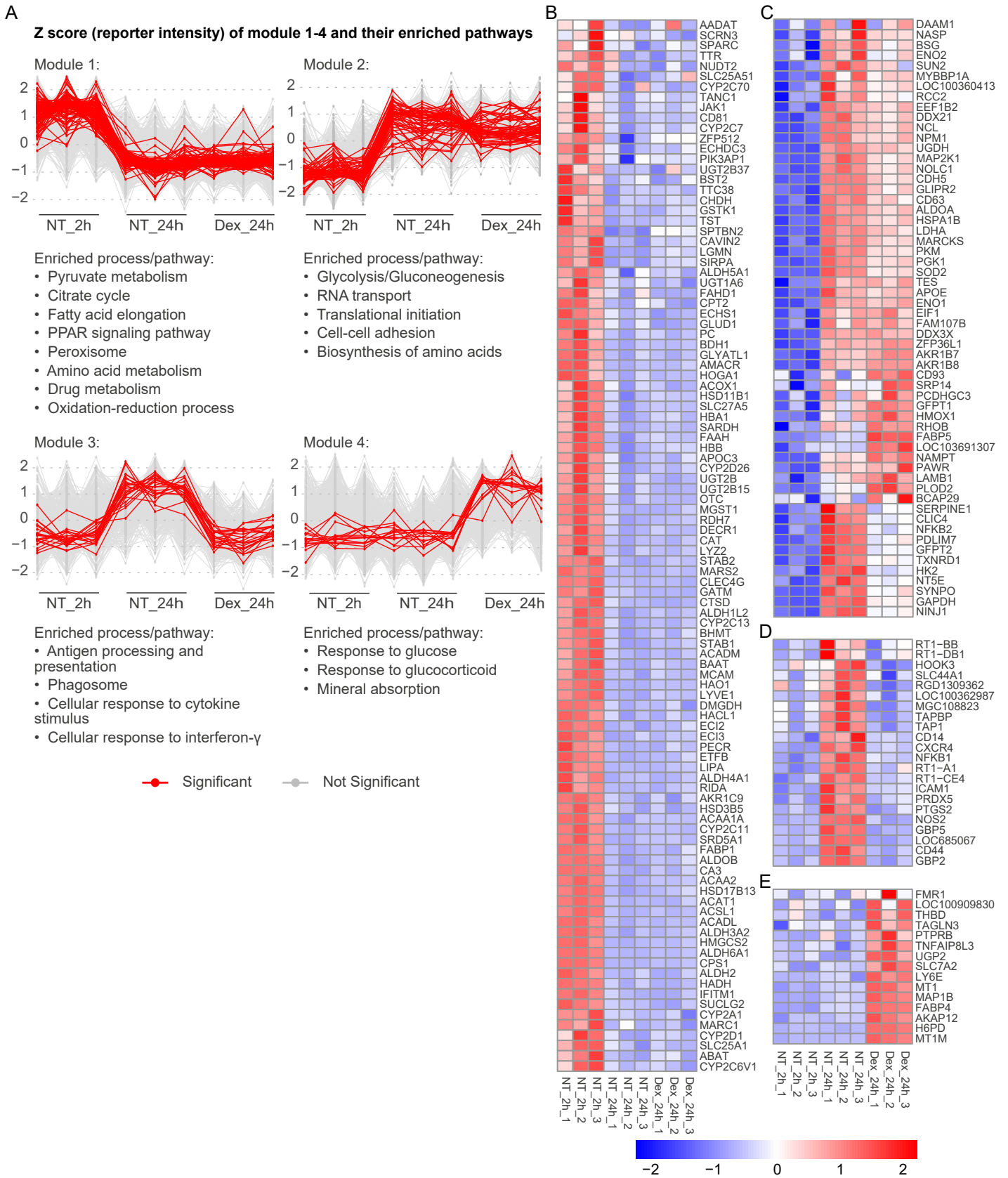
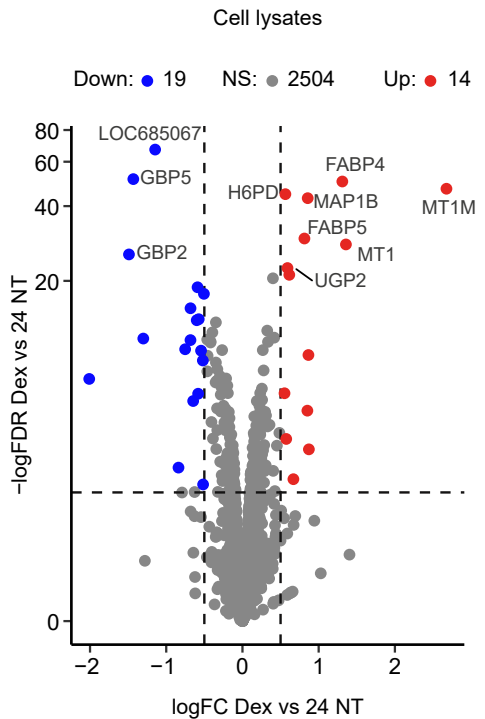
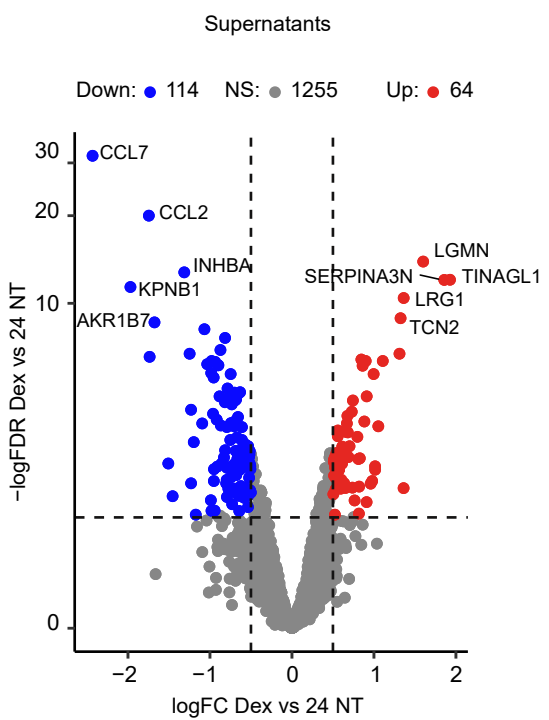


Figure 4

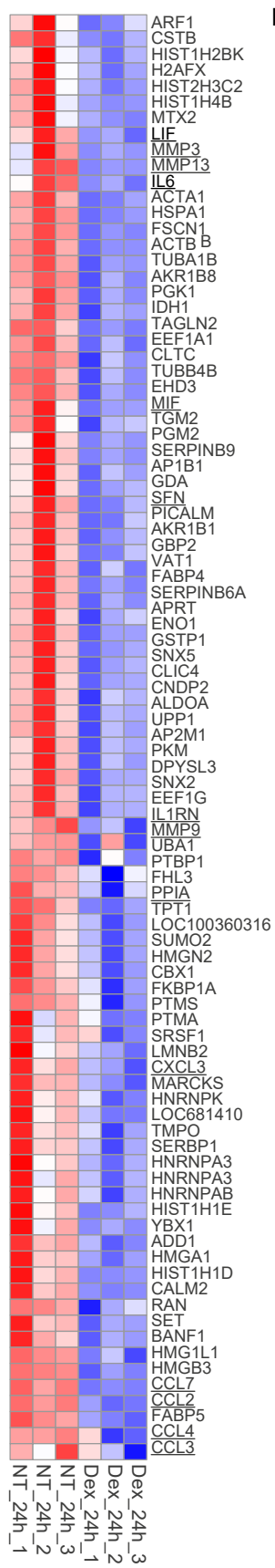
A



B



C



D

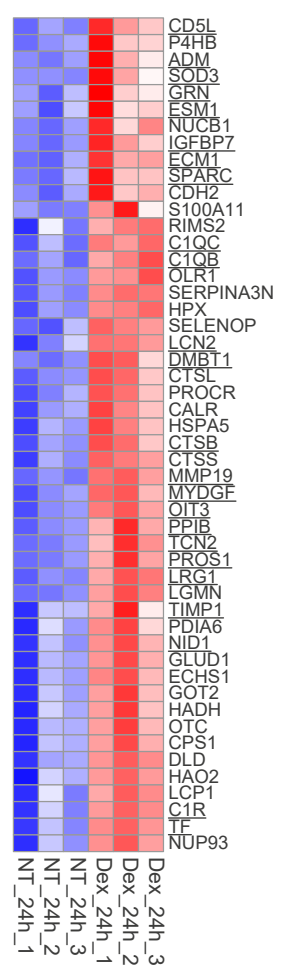
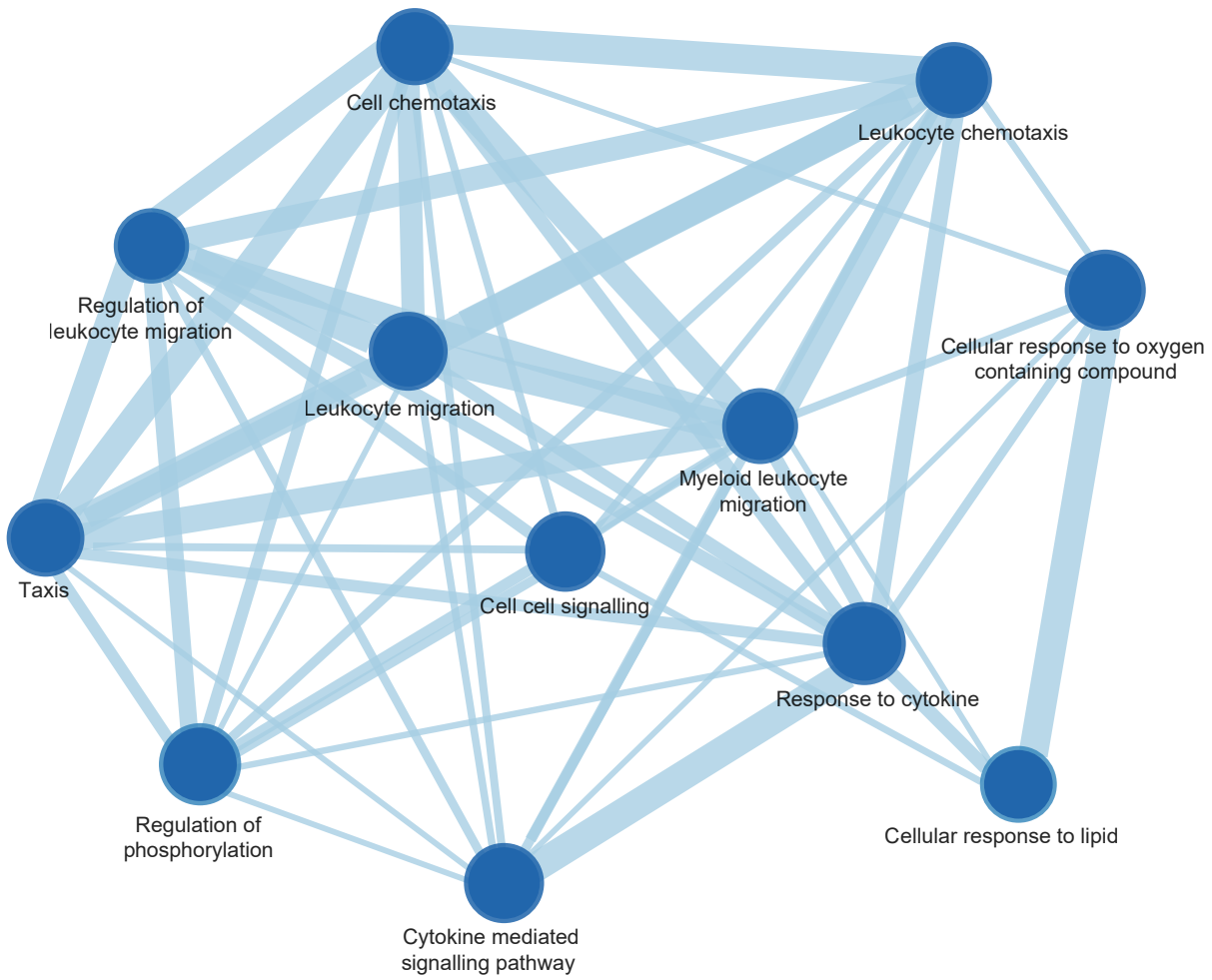


Figure 5
A



B

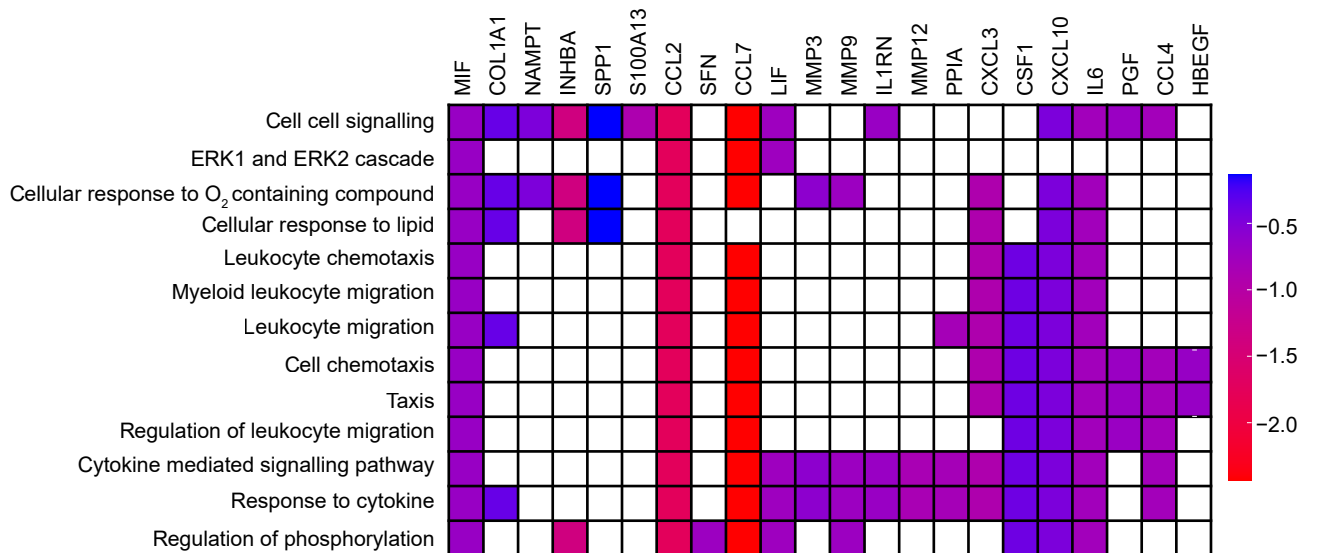


Figure 6

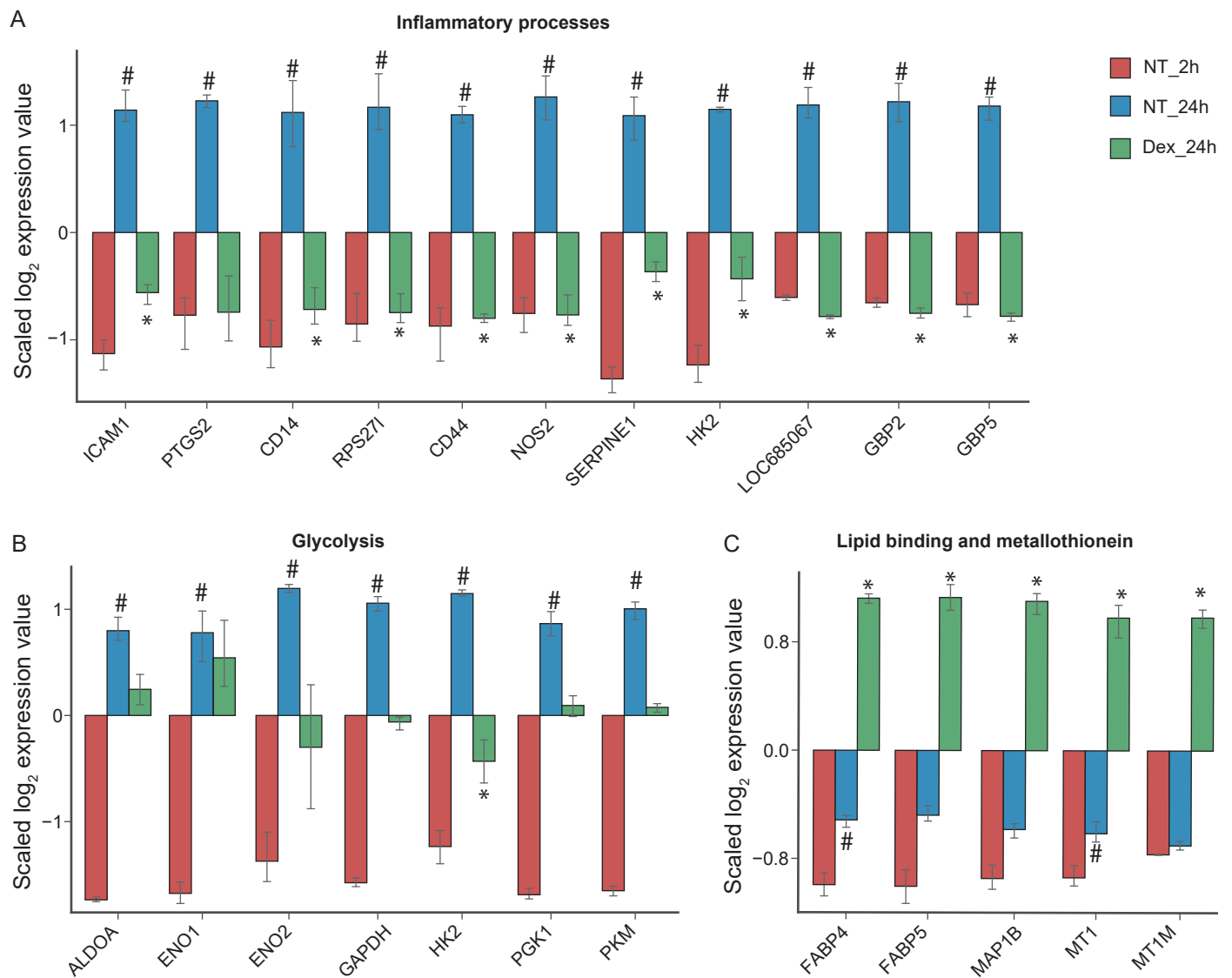


Figure 7

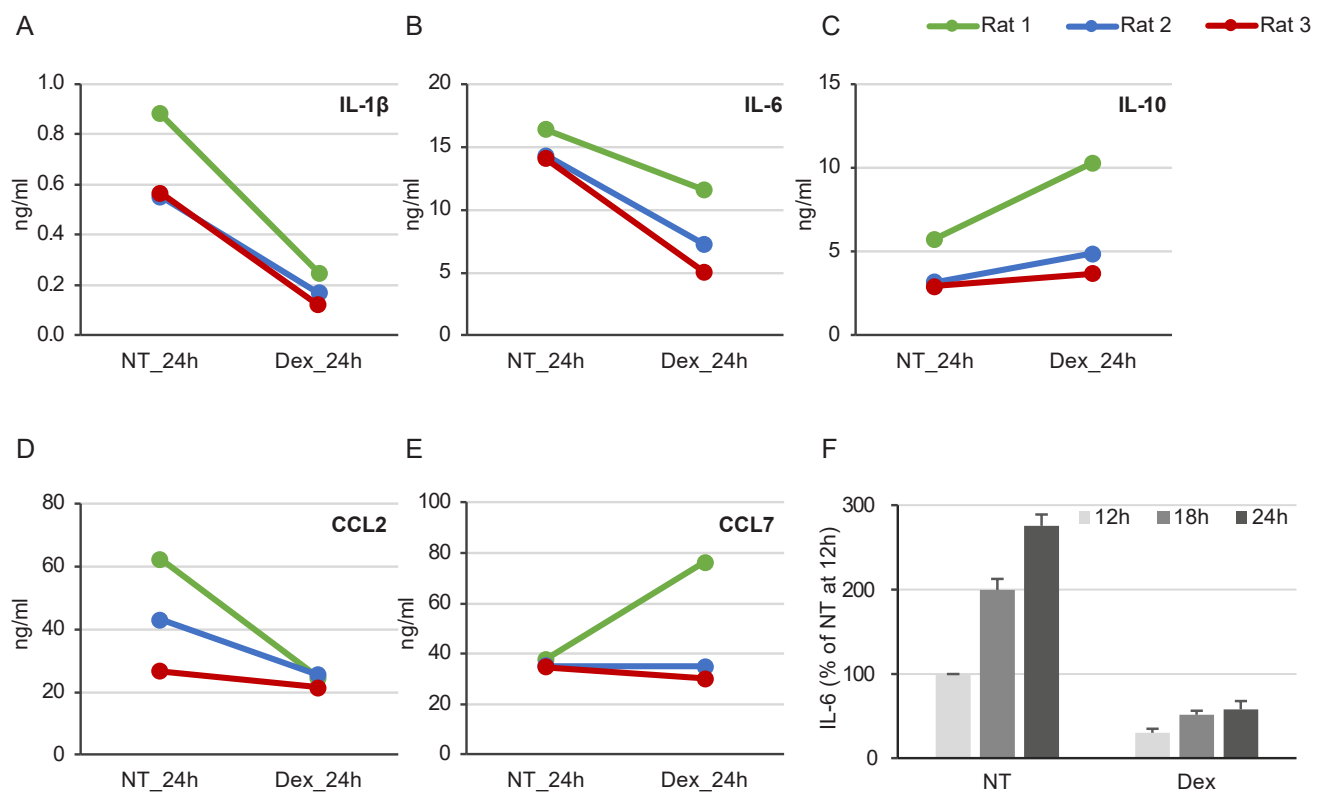


Figure 8

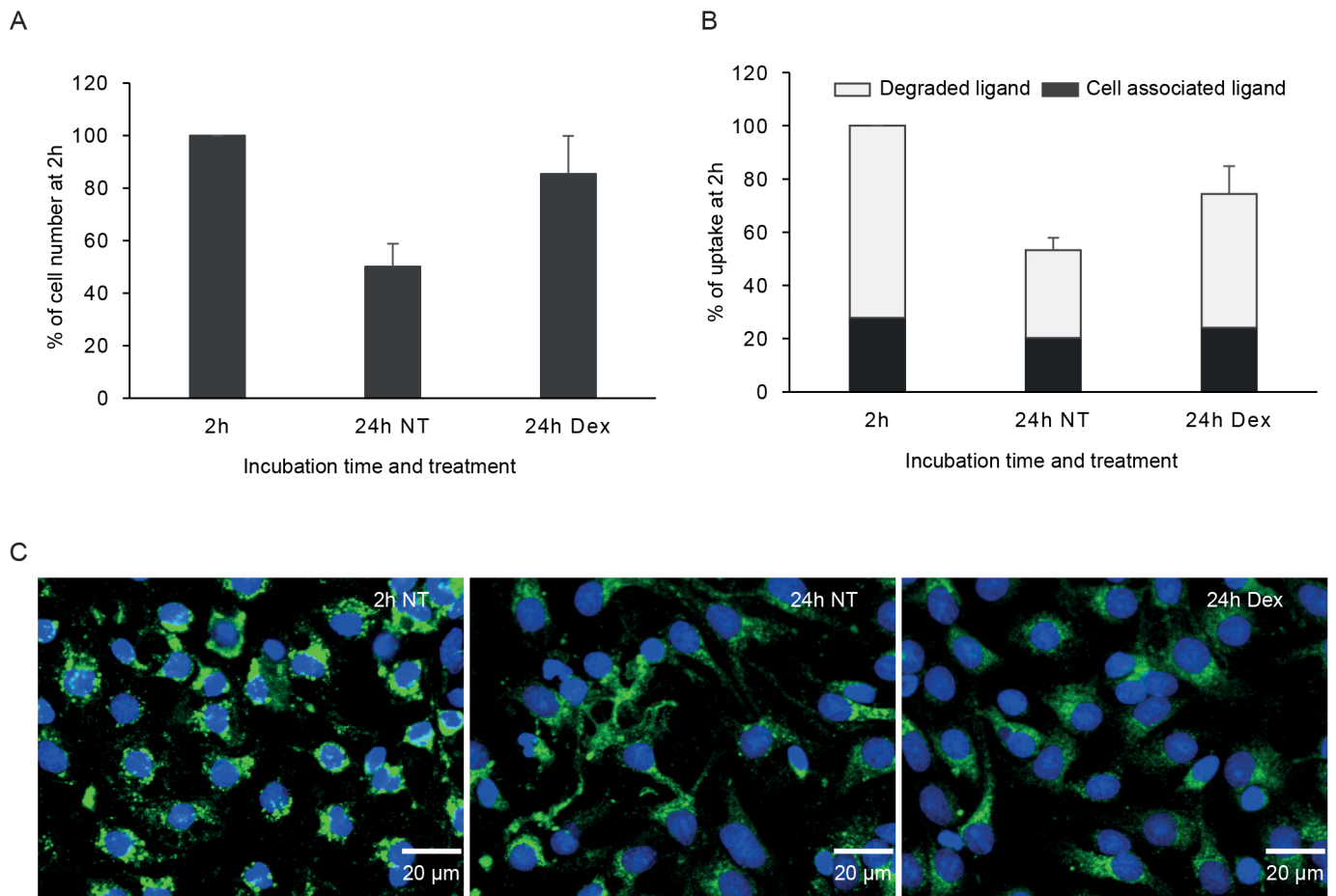
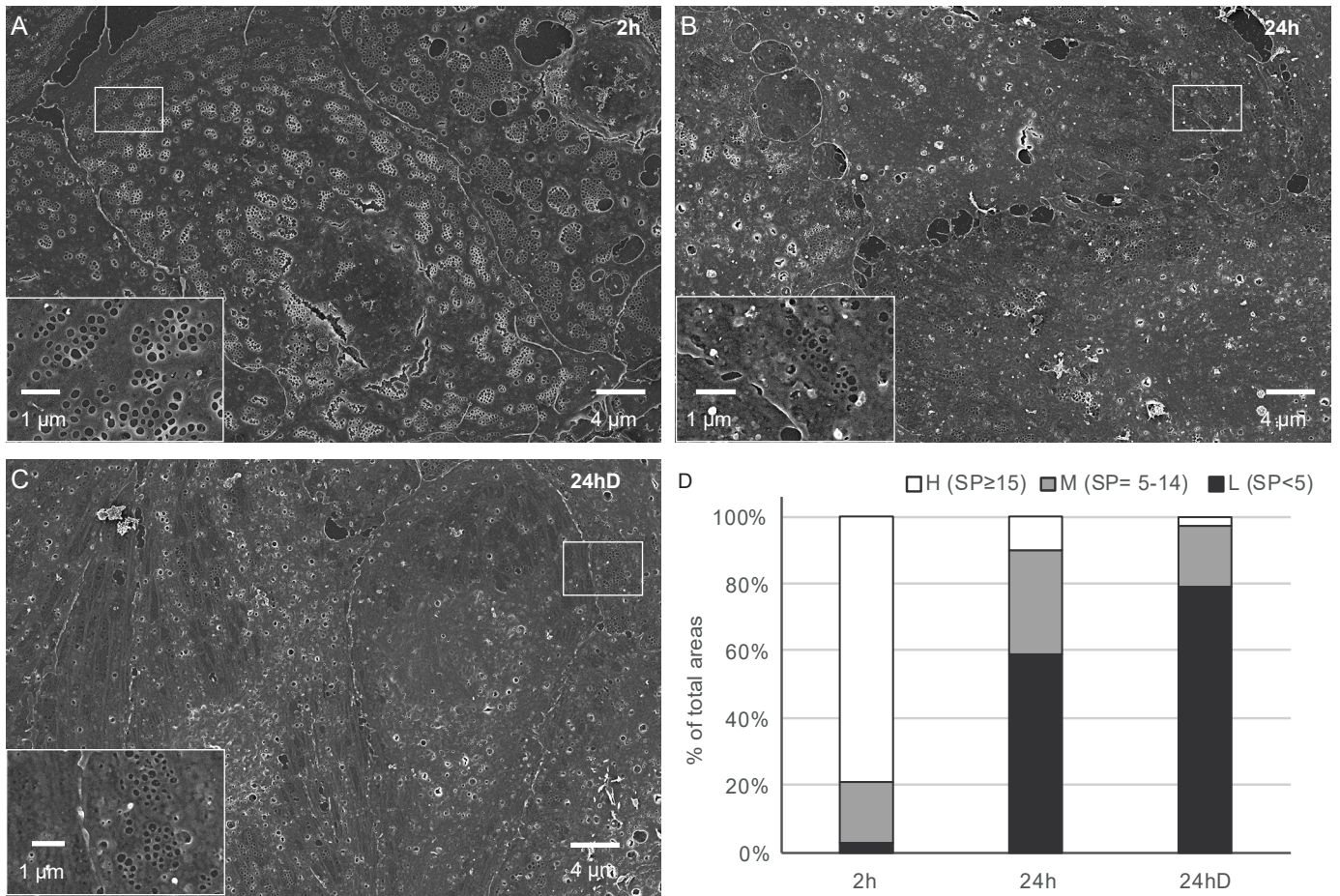


Figure 9



Supplementary information

Supplemental file 1: The processed proteome – whole dataset

Supplemental file 1 is available at

<https://dataverse.no/privateurl.xhtml?token=a8c147c3-0e2d-4142-8081-1369103c506b>

The link will take you to the UiT Open Research Data repository. There are three txt files - the one on top “00_README_Rat_LSEC_proteome.txt” contains all the meta-information about the two main data files:-

- a. “Rat_LSEC_cell_associated_processed_6plexTMT.txt”
- b. “Rat_LSEC_supernatant_TMT6plex_proteomic.txt”

Supplementary Fig. 1: Pro- and anti-inflammatory mediators in LSEC supernatants and effects of Dex

The figure shows the differential expression (scaled \log_2 expression values) of selected proteins in supernatants (n=3). NT, not treated; Dex, dexamethasone. Results are average of 3 biological replicates. Error bars show 95% confidence interval. *Significantly altered between the two groups ($FDR \leq 0.05$ and $|\log_2 FC| \geq 0.5$).

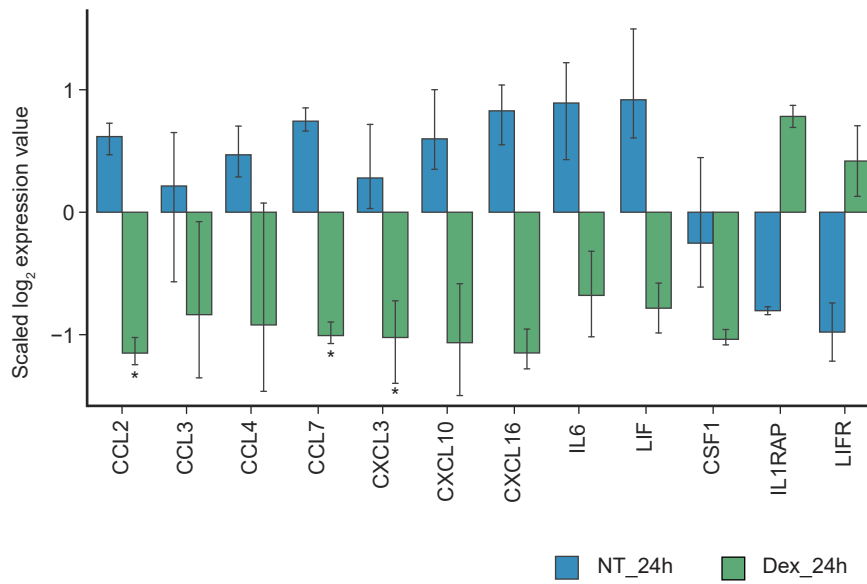
Supplementary Fig. 2: Live-dead cell viability assay

Freshly isolated LSECs were cultured for the indicated time points in 5% O₂, and 5% CO₂ in a DMEM-based serum-free medium \pm 1 μ g/ml Dex (D) and/or 100 IU/ml IL-1 β . The cultures were incubated with fluorescent dyes that indicate live and dead cells, and number of positively stained cells was counted manually with ImageJ. Results are presented in % of attached cells at 2 h (set as 100%) and are the average of 3 biological replicates.

Supplementary figure 1

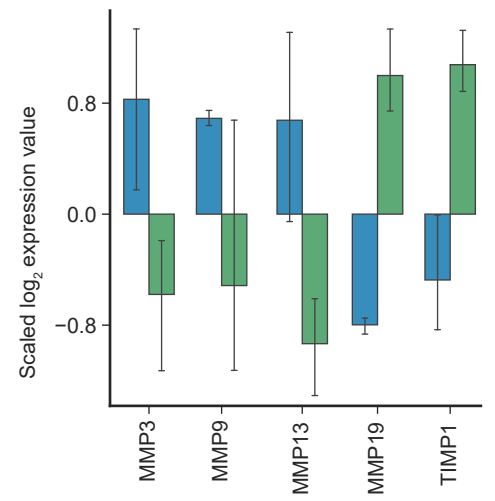
A

Cytokines and cytokine receptors

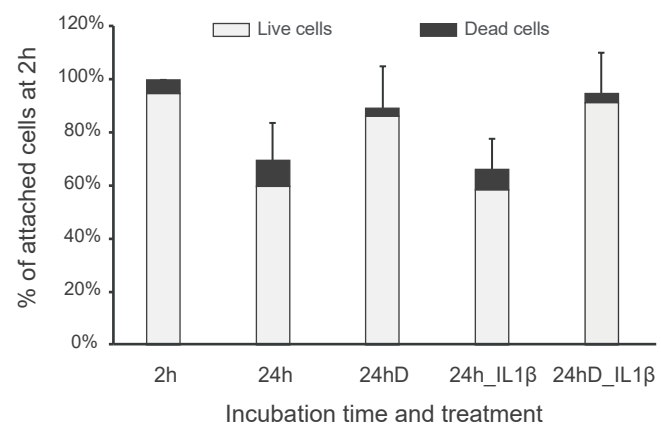


B

Matrix metalloprotease and inhibitors



Supplementary figure 2



Paper III

Bhandari, S., Kyrrestad, I., Simon-Santamaria, J., Li, R., Smedsrød, B. & Sørensen, K.K.

Mouse liver sinusoidal endothelial cell responses to the glucocorticoid receptor agonist dexamethasone in vitro.

(Manuscript).

Mouse liver sinusoidal endothelial cell responses to the glucocorticoid receptor agonist dexamethasone *in vitro*

Sabin Bhandari¹, Ingelin Kyrrestad¹, Jaione Simon-Santamaria¹, Ruomei Li¹, Bård Smedsrød¹, Karen Kristine Sørensen^{1#}.

¹Department of Medical Biology, UiT - The Arctic University of Norway, Tromsø, Norway.

#Corresponding author: E-mail: karen.sorensen@uit.no

Authors' contribution:

Conceptualization: SB, IK, JS, RL, BS, KS

Investigation, methodology, analysis, and visualization: SB, IK, JS, RL, KS

Data curation and analysis: SB

Writing – original draft preparation: SB, IK, BS, KS

Writing – review & editing: SB, IK, JS, RL, BS, KS

Funding acquisition: BS, KS

Abstract

Liver sinusoidal endothelial cells (LSECs) which make up the fenestrated wall of the hepatic sinusoids, are highly active scavenger cells and are also involved in liver immune functions. The glucocorticoid dexamethasone is commonly used as an anti-inflammatory drug and as a cell culture supplement. Dexamethasone effects are dependent on cell type. In this study, we have characterized and catalogued the proteome of primary (C57Bl/6) mouse LSECs cultured for 1, 10, or 48 h in serum-free AIM-V medium in 5% oxygen (LSEC “normoxia”) in the presence, and absence of dexamethasone (1 μ M) to elucidate time-dependent and dexamethasone-specific cell responses. We also investigated dose- and time-dependent effects (up to 5 days) of dexamethasone on LSEC morphology, viability, interleukin-6 expression, and scavenger functions. Doses up to at least 100 μ M were non-toxic to the cells. A tandem mass tag (TMT) sixplex strategy was used to study all groups of each proteomics experiment simultaneously. More than 6000 protein IDs were quantified (FDR value 1%) using the SPS MS3 method on an Orbitrap Fusion Lumos mass spectrometer. The enrichment of hallmark gene sets from the Molecular Signatures Database showed early activation of mouse LSECs towards a pro-inflammatory phenotype, and a rapid shift in LSEC metabolism *in vitro*, with upregulation of glycolysis and concomitant downregulation of the tricarboxylic acid cycle and oxidative phosphorylation. Dexamethasone suppressed the activation of LSECs and improved cell survival through anti-apoptotic mechanisms. Dexamethasone delayed but did not inhibit culture-induced cell defenestration. Mouse LSECs in AIM-V medium were competent to rapidly endocytose a radiolabeled SR-ligand even after 5 days in culture, but the cell’s max capacity for endocytosis was reduced at 48 h compared to freshly plated cells both in the presence or absence of dexamethasone, correlating with diminished expression of major scavenger receptors, and altered expression of proteins in the endocytic machinery.

Conclusion: This study presents a detailed overview of biological processes and pathways affected by dexamethasone in mouse LSEC *in vitro*. Dexamethasone significantly inhibits cell activation and improves cell survival in culture.

Keywords

Mice, proteome, liver sinusoidal endothelial cell(s), proteomics, tandem mass tag (TMT), endothelial dysfunction, endothelial activation, dexamethasone, endocytosis, scavenger receptors, transcription factors, cell survival, capillaries, phenotype, endocytosis

Introduction

Liver sinusoidal endothelial cells (LSECs) are unique among endothelial cells considering their morphology, gene expression, and physiological functions. This includes a high endocytic (“scavenger”) activity towards many modified plasma proteins and lipoproteins, waste macromolecules from tissue turnover processes, and exogenous substances that have gained access to the blood circulation (1, 2). Morphologically, LSECs are highly porous cells, with numerous open holes, or fenestrae of approximately 50-300 nm in diameter (3, 4) that ease the traffic of lipoproteins, plasma proteins, and solutes between the blood and hepatocytes (5-7). Loss of LSEC fenestrae and functional features such as the large clearance capacity for potentially harmful waste materials may contribute to various hepatic and extra-hepatic pathologies (8-10).

Primary LSECs rapidly lose their specialized phenotype in culture including fenestrae, receptor expression, and endocytic function (5, 11-14), which poses a challenge for the interpretation of results from *in vitro* studies and sets a limit for the type of studies that are feasible in these cells. Analyses of the transcriptome of rat LSECs harvested at 0-42 h post-seeding showed that LSECs could not sustain their cell-specific gene expression program and became more like lung microvascular endothelial cells at 42 h in culture (15). Another study in mice has also underscored a time-dependent downregulation of transcription factors that may regulate the LSEC phenotype *in vitro* (16). Culture-induced dysregulation in the VEGF-cGC-cGMP pathway (17) and Hedgehog pathway (18) is suggested to lead to LSEC defenestration and dedifferentiation *in vitro*. However, our knowledge regarding processes and pathways affected *in vitro* is still incomplete at the proteomic level.

Glucocorticoids (GCs) are steroid hormones released from the adrenal glands in a diurnal pattern and as a response to stress or inflammatory stimuli via activation of the hypothalamic-pituitary-adrenal axis (19). GCs are involved in many physiological processes, control glucose metabolism, and are potent regulators of inflammatory responses. Dexamethasone (Dex) is a potent, long-acting synthetic GC (derivative of the natural hormone cortisol), which is widely used as an anti-inflammatory drug, and a cell culture supplement, *e.g.*, in hepatocyte culture. Dex readily permeates the cell membrane and mediates its action mainly via binding to the intracellular glucocorticoid receptor (GR; NR3C1). The Dex-bound GR complex is translocated into the nucleus and acts as a transcriptional regulator (20). In addition, Dex can induce immediate effects in cells by causing rapid non-genomic changes such as inducing phosphorylation of target kinases, increasing intracellular calcium concentrations, or altering the production of reactive oxygen and nitrogen species (21).

The effect of GCs is dependent on cell type (22) and cell state (23, 24). Cumulative evidence from *in vitro* studies supports a hepatoprotective effect of Dex, and even a low concentration (100 nM) inhibits primary hepatocytes from undergoing apoptosis (25, 26). Dex can also induce apoptosis in a cell type and context-dependent manner, *e.g.*, in combined chemotherapy in malignant myeloma, suggesting a pleiotropic action of the drug (27). Further, Dex-induced responses cause differential effects on cell growth, cell differentiation, and functional activity, especially in immune cells in a dose- and time-dependent manner (20). Additionally, Dex influences cellular metabolism to a large extent, and prolonged use of Dex leads to hyperglycemia due to increased glycogenolysis and gluconeogenesis, and subsequently insulin resistance, ultimately leading to hepatic enlargement and steatosis (28).

Few studies have assessed GC-induced responses in LSECs (29-31). We recently examined the proteome of rat LSECs in early primary culture by analyzing samples from cells incubated for 2 and 24 h and found that the cells had acquired an activated pro-inflammatory phenotype at 24 h, which was significantly suppressed by Dex (paper II in this thesis). In the present study in C57BL/6 mice, we have implemented a time series design (1, 10, and 48 h), more advanced mass spectrometry (MS), and improved workflow to gain the depth, accuracy, and precision to discern the mechanistic details of time- and Dex-dependent changes in LSECs kept in 2D monocellular cultures. We have also investigated dose- and time-dependent effects (up to 5 days) of Dex on LSEC ultrastructure, viability, and scavenger functions. We hypothesized that exposure of LSECs to stress-related stimuli during the process of liver cell isolation, purification, and establishment of primary cultures triggers the sequence of alterations leading to the loss of specialized *in vivo* features and that early suppression of these responses using Dex prolongs LSEC survival *in vitro* by preserving *in vivo* functions. It is essential to know the effects of this drug on mouse LSEC biological processes and pathways to predict how Dex may affect the outcome of different tests and experiments carried out with these cells in immunology and toxicology studies.

Materials and Methods

Animals and Ethics

The proteomics experiments and most functional experiments were done with liver cells from C57Bl/6J male mice obtained from Charles River Laboratory (Sulzfeld, Germany). Some experiments were done with liver cells from male C57BL/6JRj mice obtained from Janvier Lab (France). All mice were obtained directly from the vendors at the age of 5-6 weeks. The animals were acclimatized for at least 5 days, before being included in the experiments at the age of 6-12 weeks. The mice were group-housed (3 mice per cage) in single-use filter-top mouse cages with aspen bedding (Scanbur, Norway), nesting material, houses, and aspen bricks (all from Datasand Ltd, Manchester, UK) as environmental enrichment. All mice had free access to fresh water and a standardized mouse diet and were kept under controlled conditions (21 °C ± 1 °C, relative humidity 55% ± 10%, and 12 h light/12 h dark cycle) at the animal research facility at the University of Tromsø (UiT) - The Arctic University of Norway. In the period before the experiment, the health of the animals was supervised daily by experienced animal technicians.

All experiments were performed with liver cells isolated from mice that had been euthanized by cervical dislocation immediately prior to the start of experiments. The animals were anaesthetized with Zoletil-mixture for mice before the cervical dislocation. The Zoletil-mixture for mice consists of a combination of zolazepam/tiletamine hydrochloride 3.3/3.3 mg/ml (Zoletil forte vet, Virbac, Norway), xylazine 0.45 mg/ml (Rompun, Bayer Nordic, Norway), and fentanyl 2.6 µg/ml (Actavis, Norway); dose of mixture: 0.1 ml/10 g body weight, administered by intraperitoneal injection. The experimental protocol and animal handling were approved by the competent institutional authority at the UiT-The Arctic University of Norway, which is licensed by the National Animal Research Authority at the Norwegian Food Safety Authority (Mattilsynet, Approval IDs: UiT 03/19, 02/20, 24/20), and experiments were performed in compliance with the European Convention for the protection of Vertebrate Animals used for Experimental and Other Scientific Purposes.

Mouse liver perfusion and cell isolation

Liver perfusions started shortly after the euthanasia of the animal. The procedure was performed between 8 a.m. and 10 a.m., in the animal research facility at UiT - The Arctic University of Norway, Tromsø, Norway.

The abdomen of the carcass was opened, and the intestines moved to the side to expose the liver and portal vein. A venous catheter connected to a peristaltic pump-driven perfusion system was inserted

into the portal vein, and the inferior vena cava was cut to allow the escape of blood and buffer from the liver. The liver was first perfused with 10-20 ml calcium-free perfusion buffer (32) to remove all blood from the liver (flow rate 8 ml/min). At this point, the perfusion buffer was changed to 50 ml perfusion buffer supplied with 1- 1.2 mg Liberase™ (Roche, Cat. No 05401127001) and 4.76 mM CaCl₂ (flow rate 8 ml/min). The digested liver was separated from the surrounding tissues, the gall bladder was removed, and the liver was placed in a Petri dish with cold perfusion buffer with 1% bovine serum albumin (BSA; Applichem, Albumin Fraction V, Cat No A1391,0250)). After removing the Glisson's capsule, the liver was gently shaken to release the cells.

The hepatocytes were removed from the cell suspension by 2x differential centrifugation at 35 g for 2 min at 4 °C, leaving the non-parenchymal liver cells (NPCs) in the supernatant. The final supernatant was centrifuged at 300 g for 10 min at 4 °C to spin down the NPCs, which were then resuspended in autoMACs rinsing solution with 1% BSA (Miltenyi Biotec Norden AB, Lund, Sweden). The cells were counted, spun down at 300 g for 10 min at 4 °C, and incubated with CD146 MicroBeads (1 µl per 10⁶ cells: Miltenyi, Cat. No 130-092-007), in dilution 1:10 in MACS rinsing solution for 15 min at 4 °C in a rotator. Unbound microbeads were washed away by centrifugation at 300 g for 5 min, and the enriched cells were resuspended in MACs rinsing solution with 1% BSA and passed through a MACs positive selection column on a MACs separator following the provider's instructions. The eluted cell suspension was centrifuged at 300 g for 10 min, and the pelleted cells were resuspended in AIM-V medium (Gibco; Thermo Fisher Scientific, Waltham, MA), counted and seeded on human fibronectin-coated Petri dishes (21 cm²; Sarstedt, Nümbrecht, Germany), or tissue culture plates (Sarstedt: 24-well, 48-well plates; Corning Costar® 3903, Merck: 96-well plates). The LSEC cultures were incubated at 37 °C in 5% O₂ and 5% CO₂. The cultures were washed with prewarmed medium 30 min post-seeding and then incubated further in AIM-V with or without Dex (Fortecortin™, Merck), at the indicated concentrations for the duration of the respective experiments. The total number of LSECs purified from one mouse liver was 4-12x10⁶ cells. The protocol for CD146 MACS purification of LSECs from liver NPCs resulted in highly pure LSEC cultures with > 95% endothelial cells displaying fenestrae, which is the hallmark of LSECs (2, 33) as assessed by scanning electron microscopy (SEM; described in the next section).

Assessment of LSEC morphology by scanning electron microscopy (SEM)

CD146 MACS purified LSECs were seeded on fibronectin-coated 24-well tissue culture plates at the same density as used in the proteomics study (0.3x10⁶ cells/cm²), and incubated in AIM-V medium for 30 min, washed, and incubated further in AIM-V with 0, 0.1, 1.0, or 2.5 µM of Dex for up to 2 h

(only without Dex), 24, 48, 72, or 120 h (with or without Dex), and then fixed in McDowell's fixative for electron microscopy (34). Medium was changed after 24 and 72 h. The fixed LSEC cultures were stamped out from the culture plate and processed for SEM as described in (35). In short, the cultures were washed 3x in PHEM buffer, pH 7, incubated for 1 h in 1% tannic acid in PHEM buffer, washed 3x in PHEM, incubated 30 min in OsO₄ in H₂O, and dehydrated in 30-100% ethanol before chemical drying in hexamethyldisilazane (Sigma-Aldrich, Merck Life Science, Norway). The specimens were mounted on aluminum stubs, sputter-coated with 10 nm gold/palladium alloy and scanned in a Zeiss Sigma Field Emission Scanning electron microscope (Carl Zeiss, Oberkochen, Germany) run at 2kV. At each time point and treatment, high-resolution overview images were taken at random from at least 3 areas per cell culture, and higher magnification images were taken within these areas for detailed analysis.

In a separate set of experiments LSEC cultures established as described above were incubated with 0, 1, 10, 100, or 1000 μ M of Dex for 48 and 72 h for repeated measurements of lactate dehydrogenase release into the medium, then fixed and prepared for SEM at the end of the experiment. The specimens were scanned in a Zeiss Gemini scanning electron microscopy (Carl Zeiss) run at 2 kV.

To validate the CD146 MACS method of LSEC purification, a differential cell count was carried out on the 2 h cultures. At least 400 cells were included in the differential cell count per biological replicate (n=4) to assess the purity of CD146 MACS-isolated LSECs. This showed that the method of purification of LSECs from liver NPCs produced cultures with > 95% (up to 99%) fenestrated endothelial cells. Nearly 100% LSEC purity was also observed at later time points by SEM.

Sample preparation, TMT labelling, and fractionation

The set-up for the proteomics experiment is described in **Fig. 1**. LSECs (0.3×10^6 cells/cm²) were seeded on 21 cm² fibronectin-coated tissue culture plates in AIM-V medium, one plate per treatment and time point, and gently washed with a prewarmed medium at 30 min post-seeding. Dex treatment (1 μ M = 0.4 μ g/ml) started immediately thereafter. Supernatants were removed and the cell-associated proteins extracted at 1 h (LSECs in AIM-V alone), 10 h (LSECs \pm Dex), or 48 h (LSECs \pm Dex) post-seeding. The experiment was repeated with 3 biological replicates, each consisting of the pooled LSECs from 4-5 mouse livers.

The protein extracts were prepared according to the protocol provided in the TMTsixplex Isobaric Mass Tagging Kit (Thermo Fisher Scientific) with the following modification: Denaturing reagent was 5% sodium deoxycholate in 100 mM triethylammonium bicarbonate (TEAB). Protein

concentrations were measured with Direct DetectTM Infrared Spectrometer (Millipore). The proteins were then reduced according to the protocol (Thermo Fisher Scientific), except that the reducing reagent was 5 mM dithiothreitol (Sigma) instead of tri (2-carboxyethyl)-phosphine. Proteins were precipitated with acetone and the pellet was collected by centrifugation at 8000 g for 10 min. The protein pellet (25 µg) was resuspended in 2 M urea, 50 mM TEAB. Proteins were digested for 6 h with 1:100 (w/w) lysyl endopeptidase (Fujifilm Wako Chemicals Europe GmbH, Neuss, Germany). The samples were diluted to 1 M urea and digested overnight with 1:20 (w/w) trypsin (V511A, Promega Corporation, WI). Peptides from each sample were then labelled with the TMTsixplexTM Isobaric Mass Tagging Kit according to the manufacturer's protocol. OMIX C18 tips (Varian Inc., Palo Alto, CA) were used for sample cleanup and concentration.

The labelled peptides were fractionated by high pH reversed-phase chromatography (36) using an Ultimate 3000 offline HPLC: 100 µg of peptides were reconstituted in 200 mM ammonium formate, pH 10, and loaded onto an RP column (Acuity UPLC BEH, C18, 1.7 µm, 2.1 x 100 mm column; Waters Chemistry, Milford, MA). The samples were then fractionated using a linear gradient of B increasing from 0% B to 60% B (B: 90% acetonitrile, 20 mM ammonium formate, pH 10) at a fixed flow rate of 150 µl/min for 60 min. Forty-two fractions were collected from each TMT mix and pooled into 21 fractions using the mixing strategy Fr1+Fr22, Fr 2+Fr23, etc. The fractions were dried in a SpeedVac concentrator (SC250, Thermo Fisher Scientific) and frozen at -80°C until MS. The samples were then reconstituted in 0.1% formic acid and injected into a trap column (Acclaim PepMap 75 µm x 2 cm, C18, 3 µm, 100 Å; Thermo Fisher Scientific) for desalting before elution to the separation column (EASY-Spray column, C18, 2 µm, 100 Å, 50 µm, 50 cm; Thermo Fisher Scientific). Peptides were fractionated using a 4–40% gradient of increasing amounts of 80% acetonitrile in water over 120 min at a flow rate of 300 nl/min. The mobile phase contained 0.1% formic acid. Samples were analyzed by an Orbitrap Fusion Lumos mass spectrometer (Thermo Fisher Scientific), using the TMT synchronous precursor selection (SPS) multi-notch MS3 quantitative (37).

TMT data preparation and analysis

The raw files from Orbitrap Fusion Lumos were fed into MaxQuant (version 1.6.10) for processing and generation of peak lists. Peak lists were searched for identification with the MaxQuant integrated Andromeda search engine against the UniProt *Mus musculus* (mouse) reference proteome (38) with the following parameters: 2 missed cleavages were allowed at max; carbamidomethyl and TMT labelling (at N-terminus and lysine residue) were set as fixed modification, while oxidation at methionine and acetylation at the protein N-terminus were set as variable modifications. The mass tolerance was set to 4.5 ppm and 20 ppm, respectively, for the precursor ions and the fragment ions.

None of the peaks were excluded for any known contaminants. A false discovery rate (FDR) of 1% was applied to eliminate false positives at both peptide and protein levels.

The protein groups output text file from the MaxQuant was uploaded into Perseus (version 1.6.14.0 (39)) for initial data processing to filter out irrelevant protein groups with identification tag “Only identified by site”, “Reverse” and “Potential contaminants”. The annotation of the protein IDs to their corresponding gene symbols was manually curated with the UniProt Knowledgebase (38) using Retrieve/ID mapping. The tag-reporter intensity corrected from MaxQuant was used for protein quantification. The intensity corresponding to redundant gene symbols associated with a protein group was summed beforehand of differential expression analysis. Each TMT run had all five samples from a biological replicate; see experimental set up in **Fig. 1**. A factor for global scaling normalization was determined separately for each run. Subsequently, after scaling the dataset, internal reference scaling normalization (40) was used to correct the effect of the different TMT runs. Finally, the compositional bias was corrected using TMM normalization (41) and was tested for differential expression with edgeR (3.30.0) (42).

Caspase assay

LSECs were plated at a density of 1×10^5 cells per well in fibronectin-coated white, clear bottom 96-well plates (Corning Costar® 3903), washed 30 min post-seeding and replenished with 100 μ l of AIM-V medium alone, or AIM-V with 1 μ M Dex \pm CD95 antibody (BD Pharmingen™, BD Biosciences, CA, Cat. No 554255) (10 ng/ml), then incubated for 2 h, or 24 h. All biological replicates (n=3), each in duplicate, were run in the same plate, with one plate for each time point. The caspase activity was assessed with Caspase-Glo® 3/7 (Promega Corporation, Cat. No G8090). The tetrapeptide DEVD sequence provided as substrate emits a luminescent signal when cleaved by caspase-3, or -7. The luminescence was measured in a CLARIOstar Plus microplate reader (BMG Labtech GmbH, Ortenberg, Germany).

Enzyme-linked immunosorbent assay (ELISA) – Interleukin (IL)-6, ICAM-1, VCAM-1

LSECs were plated in fibronectin-coated 24-well plates (Sarstedt) at a density of 6×10^5 cells per well, washed after 30 min, and replenished with fresh AIM-V medium \pm Dex (doses indicated in figures). Supernatants were collected in low protein binding Eppendorf tubes, centrifuged at 300g for 10 min at 4°C, aliquoted, and stored at -70 °C until analysis. Biological replicates were 2 (IL-6) or 3 (ICAM-1, VCAM-1), and all treatments were done in duplicate. DuoSet ELISA kits for IL-6 (Cat. No DY406), ICAM-1 (Cat. No DY796), and VCAM-1 (Cat. No DY643) were purchased from R&D

systems (Bio-Techne Corporation, Minneapolis, MN), and the assays were performed in accordance with the provided instructions. The raw optical density reads (from CLARIOstar Plus) were used for four parameters logistic regression to determine the concentration based on the standards.

GSH assays

GSH in LSECs was measured with the GSH-Glo™ Glutathione assay (Promega Corporation, Cat. No V6911). LSECs were plated in fibronectin-coated white, clear bottom 96-well plates (Corning Costar® 3903) at a density of 1×10^5 cells per well, washed after 30 min, and replenished with 100 μ l of AIM-V alone, AIM-V with 1 μ M Dex, or AIM-V with 1% H₂O₂. The plates were incubated at 37°C, in 5% CO₂ and 5% O₂ for 2 h prior to the assays (n=3). The experiments were performed according to the manufacturer's protocols. Luminescence was measured in a CLARIOstar Plus microplate reader.

Lactate dehydrogenase (LDH) cytotoxicity assay

Dex cytotoxicity was analyzed with the Promega LDH-Glo Cytotoxic assay (Cat. No J2380). LSEC cultures established in fibronectin-coated 24-well plates (6×10^5 cells seeded per well) were incubated in 0.5 ml AIM-V medium plus 0, 1, 10, 100, and 1000 μ M Dex, and incubated at 37 °C in 5% O₂, 5% CO₂ for 48 or 72 h. At 2, 24, 48, and 72 h, 25 μ l of the medium was collected and frozen at -20 °C in LDH storage buffer, until analysis. Parallel cultures were dissolved in Triton X-100 (final concentration 0.1%) and used as a positive control for each time point. Luminescence was detected at emission 540-550 nm in a CLARIOstar Plus microplate reader. At the end of the experiments, all cultures were imaged in a Nikon inverted photomicroscope before removing the medium, then the cells were fixed and prepared for SEM as described in the section "Assessment of LSEC morphology by scanning electron microscopy (SEM)".

Endocytosis assays

Ligand labeling: Formaldehyde-treated bovine serum albumin (FSA) was prepared as described (43), and labeled with carrier-free Na¹²⁵I, using Iodogen as an oxidizing agent as described by the manufacturer (Pierce Chemicals, Rockford, IL), and separated from unbound ¹²⁵I on a PD-10 column (GE Health, Uppsala, Sweden). The resulting specific radioactivity was $1-2 \times 10^6$ counts per minute (cpm) per μ g protein.

Endocytosis assays: LSECs (0.3×10^6 cells/well) were established in fibronectin-coated 48-well tissue culture plates (Sarstedt) in AIM-V medium, washed after 30 min, and incubated for various periods

in AIM-V in the presence or absence of Dex, before starting the endocytosis experiments. Two series of endocytosis experiments were performed.

In experimental series 1 (biological replicates: $n=3$, each done in duplicate), the uptake of trace amounts of ^{125}I -FSA per 2 h (in % of added radiolabeled ligand) was measured in LSECs that had been cultured for 2, 24, 48, 72, or 120 h in AIM-V with 0, 0.1, 1.0, or 2.5 μM Dex, at 37°C in 5% O_2 , 5% CO_2 , before the start of the experiment. The medium was then removed, and 100 μl of AIM-V with 1% human serum albumin and ^{125}I -FSA (approximately 0.1 $\mu\text{g}/\text{ml}$) were added to each culture. The cultures were incubated for 2 h at 37 °C in 5% O_2 , 5% CO_2 before cell-associated and degraded ligand was measured as described (44). Prior to the start of each endocytosis experiment, cultures were imaged in a Nikon inverted microscope for estimation of cell numbers per culture.

In experimental series 2 (biological replicates: $n=3$, each done in duplicate or triplicate), the LSEC capacity of endocytosis of FSA was measured in cells that had been cultured for 48 h in AIM-V with or without 1 μM Dex, and results compared to the endocytic capacity of freshly plated LSECs for the same ligand. All cultures were incubated for 2 h with 100 μl of AIM-V with 1% human serum albumin and ^{125}I -FSA (approximately 0.1 $\mu\text{g}/\text{ml}$) plus 0, 10, 20, 40, or 80 $\mu\text{g}/\text{ml}$ of non-labeled FSA. In each biological replicate, parallel cultures (seeded in the same concentration, and washed and treated in the same way as those used for endocytosis) were fixed after 2 and 48 h for cell counting, using Axio Observer (Carl Zeiss). Cell nuclei were stained with DAPI (Sigma-Aldrich).

In both experimental series, the supernatant was removed at the end of the 2 h incubation period with FSA, and cell-associated, and degraded ligand calculated as described (44). In short, intact proteins in the supernatant, along with one wash of PBS were pelleted with 20% trichloroacetic acid, whereas the acid-soluble radioactivity in the supernatant represented the degraded ligand (44). The cells were then lysed in 1% sodium dodecyl sulphate, and radioactivity in cell lysates and supernatants were measured in an automated gamma counter (Cobra II, Packard). Total endocytosis was calculated as the sum of cell-associated and degraded ligand.

Statistical analysis and visualization

Preprocessing, annotation, curation, and filtrations of the proteomics data were done in the Perseus environment (ver. 1.6.14.0; (39)). The R/Bioconductor environment (<https://bioconductor.org>) was used to normalize the TMT data, and the edgeR integrated exact test (45) was implemented to identify differential protein expression. Proteins that had $|\log_2 \text{fold change}| \geq 1$, and $\text{FDR} \leq 0.05$ between the comparisons were deemed significantly different. The gene sets with $\text{FDR } q\text{-value} \leq 0.05$ obtained

from gene set enrichment analysis (GSEA) were identified as significantly enriched gene sets. Most figures were generated using R packages including factoextra, ggplot2, ggpubr, pheatmap, and the plugins EnrichmentMap and String from Cytoscape. Some figures were generated in Microsoft Office Excel, and the panels were made in Adobe Illustrator or Microsoft Office PowerPoint. Protein expression values are presented with 95% confidence intervals.

Results

Dose and time-dependent effects of dexamethasone on mouse LSEC morphology, viability, and IL-6 production in culture

As a fundament for choosing the dose and treatment time of Dex in the quantitative proteomics experiments, we did a series of experiments to examine how Dex affected mouse LSEC morphology, viability, and cytokine production in culture.

In vivo, LSECs are highly fenestrated cells with most fenestrae organized in sieve plates (5, 33). To evaluate the effect of Dex on LSEC survival and ultrastructure, freshly isolated cells were incubated in AIM-V with 0, 0.1, 1, or 2.5 μM Dex for 24, 48, 72, and 120 h and examined by SEM, and compared to fresh (2 h) cultures ($n=3$). At 2 h, more than 95% (up to 99%) of the cells in culture were highly fenestrated endothelial cells, proving their identity as LSECs (**Fig. 2A**). LSECs seeded at a density of 0.3×10^6 per cm^2 formed a continuous cell layer for at least 5 days in the presence or absence of Dex (**Supplementary Fig. 1**). In all experiments, Dex-treated cultures appeared denser, compared to time-matched control cultures without Dex. LSECs cultured in the presence of Dex further showed smoother cell borders. This difference was most prominent at 48-120 h (**Fig. 2A**). LSECs gradually lost their fenestrae with time in culture. At 72 h, some fenestrae could still be observed in almost all cells in the cultures. However, the degree of fenestration varied much between individual cells within each culture from nearly absent in some cells to more abundant in others. At 120 h, cells with sieve plates were still observed in the Dex-treated cultures, whereas cultures without Dex were almost totally defenestrated (**Fig. 2A**).

Increased LDH activity in cell culture supernatants is used as a marker of alterations in plasma membrane integrity and cytotoxicity. LDH activity in supernatants did not differ significantly between LSEC cultures treated with up to 1000 μM Dex for up to 72 h (**Fig. 2B**), suggesting that Dex was well tolerated by the cells, confirmed by phase-contrast microscopy (**Supplementary Figs. 2A, B**). However, at 72 h, increased cell death was observed in cultures with 1000 μM Dex by SEM (**Supplemental Fig. 2C**).

LSECs are among the major producers of IL-6 in the liver, and the production is upregulated in inflammation (46) and early LSEC culture (paper II in this thesis). When testing the effect of 0.1 and 1 μM Dex on IL-6 production in mouse LSECs after 3, 6, 10, and 20 h we found that Dex immediately reduced IL-6 production, compared to non-treated control cultures, with 1 μM Dex having the most pronounced effect over time (**Fig. 2C**).

Based on these results, we went for a time-course design in the quantitative proteomics experiment to determine 1) early effects of Dex, from 1-10 h, and 2) later effects, from 10-48 h. We also chose to use the 1 μ M Dex dose, as this was well tolerated by the cells, anticipated to be more physiological than the higher doses (22), had a positive effect on cell morphology, and suppressed the IL-6 production in culture.

LSECs cultured with or without Dex shared global proteome changes with time in culture

The general workflow of the TMT quantitative proteomic study is illustrated in **Fig. 1**. Proteins were collected from LSEC cultures at 1, 10, and 48 h. The two later time points included two samples at each point; one from cells exposed to Dex and one from cells cultured without Dex. A total of 6030 non-redundant protein IDs were identified, quantified, and used in the subsequent downstream analyses (**Supplemental file 1**).

Principal component analysis (PCA, **Fig. 3A**) showed a large dispersion between the samples corresponding to three time points, suggesting a substantial effect of time in culture on the LSEC proteome, irrespective of Dex exposure. However, at 48 h the samples from the Dex-treated and non-treated cells were segregated into two separate clusters.

Despite the dominant time-dependent effect on the LSEC proteome, the higher global correlation between the proteome of LSECs cultured for 48 h in the presence of Dex and the proteome of freshly plated cells ($R=0.929$), compared to the correlation between LSECs cultured for 48 h without Dex and freshly plated cells ($R=0.917$), indicates that Dex to some extent preserved the LSEC molecular phenotype *in vitro* (**Fig. 3B**).

We further found a moderately high correlation ($R = 0.71$, $p < 2.2e-16$) between the ranks obtained from pairwise comparison of the samples without Dex [(48 h vs 1 h) vs (10 h vs 1 h)], and the samples with Dex [(48 h+Dex vs 1 h) vs (10 h+Dex vs 1 h)] using a generalized linear model from edgeR (**Fig. 3C**). As illustrated by the scatter plot in **Fig. 3C**, the expression of several proteins was either unaffected (74.4%) or affected in a similar direction in the presence or absence of Dex with time in culture (9.6%). The scatter plot also highlights proteins affected only in a time-dependent (8.4%) or Dex-specific manner (7.4%). It also shows a small number of proteins, expression of which were completely reciprocated by Dex in contrast to the time-dependent changes induced *in vitro* (0.2%).

Taken together, the results showed a substantial effect of time in culture on the LSEC proteome, which was modified by the presence of Dex.

LSEC shift in metabolism in culture, and effects of Dex

To get a global overview of affected biological pathways or processes in LSECs in response to culture time and Dex treatment across the five different sample phenotypes, we performed GSEA with the hallmark gene sets and the canonical KEGG pathway gene sets defined in the Molecular Signatures Database (MsigDB ver 7.2 (47)). The whole proteomic data set with normalized TMT reporter intensities were used for the GSEA. Gene sets significantly enriched in at least one of the pairwise comparisons are shown in **Fig. 4A**. The hierarchical clustering based on the enrichment scores of the enriched gene sets representing metabolism, across the sample comparisons reflected a significant shift in canonical metabolic pathways in cultured LSECs. This shift was chiefly a time-dependent phenomenon and less a result of Dex treatment.

Changes in the glucose metabolism (*i.e.*, glycolysis and gluconeogenesis, and the pentose phosphate pathway) showed a strong dependence on time in culture. Compared to 1 h incubation, these pathways increased at 10 h and stayed high even at 48 h, in the presence or absence of Dex (**Fig. 4A**). However, at 10 h, glucose metabolism was suppressed in the Dex-treated LSECs compared to the time-matched untreated control cells (**Fig. 4A**).

The shift in glucose metabolism as a function of time in culture was even more evident if one considers the proteins contributing to the enrichment (**Fig. 4B**). Of note, Dex was found to augment the expression of some of the enzymes, including the rate-limiting enzyme phosphofructokinase (PFKP), allosteric regulator of PFKP (PFKFB3), phosphoglucomutase-2 (PGM2), and hexose-6-phosphate dehydrogenase (H6PD) (**Fig. 4B**), suggesting that Dex might enhance the glucose flux along the glycolytic and pentose phosphate pathways. Lactate dehydrogenase A (LDHA), which converts pyruvate to lactate, was also upregulated in response to Dex (**Fig. 4B**). High production of lactate in LSEC cultures was reported already in 1984 (rat model, (48)). In the present proteomics experiment, we also observed a time-dependent increase in LSEC expression of the monocarboxylate transporter 4 (SLC16a3) in culture (**Fig. 4B**). That may endow the cells with enhanced capacity to maintain lactate production by increasing lactate efflux out of the cell.

The GSEA further showed that the tricarboxylic acid (TCA) cycle, oxidative phosphorylation (Oxphos), and organic acid metabolism were significantly declined in LSECs at 10 h compared to 1 h in a direction opposite to the glycolysis (**Fig. 4A**). At the pathway level, LSECs in culture showed diminished expression of most proteins involved in the TCA cycle (**Fig. 4C**). Dex increased the amplitude of the change for most of the proteins involved in the TCA cycle except for isocitrate dehydrogenase (IDH1) (not statistically significant) (**Fig. 4C**). LSECs also

showed diminished expression of proteins involved in Oxphos (**Fig. 4D**), and upregulation of proteins in the pentose phosphate pathway with increased time in culture (**Fig. 4E**).

LSEC activation occurs early in culture and is partly suppressed by Dex

The *in vitro* shift in metabolism with increased dependency on glucose for energy production (**Fig. 4**) showed an altered LSEC state in culture. To assess the LSEC state in the different treatment groups, we performed GSEA with the hallmark gene sets defined in MsigDB. The outcome showed enrichment of the hallmark gene sets of the inflammatory response, INF- α response, IFN- γ -response, TGF- β signalling, TNF- α signalling via NF- κ B, and IL-6/JAK/STAT3 signalling at 10 and 48 h, compared to 1 h (**Fig. 5A**), reflecting an early activated LSEC phenotype in culture. Dex treatment downregulated the proteins associated with these hallmark gene sets.

The suppressive effect of Dex over LSEC activation was most apparent at the pathway level at 48 h (**Fig. 5A**). However, Dex treatment suppressed TNF- α signalling via NF- κ B and the inflammatory response already at 10 h. The significant Dex-mediated suppression of the IL-6/JAK/STAT3 signalling pathway (**Fig. 5A**) corroborated with the observed repression of IL-6 release from Dex-treated LSECs in ELISA experiments (**Fig. 2C**).

The average relative abundance of all proteins linked to the inflammatory response is presented in **Fig. 5B**. The scaled averages of proteins associated with the inflammatory response (MsigDB, hallmark proteins) increased over the *in vitro* period, while Dex treatment blunted the increase, albeit partially.

To ascertain the inflammatory-like LSECs phenotype, we investigated proteins specifically linked with toll-like receptor (TLR) signalling, cytokine-cytokine receptor signalling, chemokine signalling, and focal adhesion as defined in the KEGG pathway database. All these processes were significantly changed either in a time-dependent, or Dex-specific manner as presented in the protein-protein interaction map in **Fig. 5C**. Network analysis with cytoHubba (Cytoscape plugin) using the maximal clique centrality (MCC) method, identified AP-1 transcription factor subunit (JUN, AP-1), signal transducer and activator of signalling 1 and 3 (STAT1, STAT3), and Janus kinase 3 (JAK3) as the topmost hub proteins of the network. JUN (AP-1) is well-characterized as an immediate-early gene in the inflammatory response (49).

We also found a strong upregulation of cell adhesion molecules in the LSEC proteome (**Fig. 5D**). Unlike other endothelial cells, quiescent LSECs at steady-state do not express selectins (50), and the proteomics data showed low expression at 1 h of selectin-E and -P (SELE, SELP), as well as of the

IgG superfamily members ICAM-1 and VCAM-1. However, all of these were significantly increased already after 10 h in culture. ELISA experiments with LSEC culture supernatants also showed the time-dependent increase in ICAM-1 (**Fig. 5E**) and VCAM-1 (**Fig. 5F**). It also confirmed that Dex treatment significantly repressed the *in vitro* induction. Increased expression of ICAM-1 and VCAM-1 (both cell-bound and soluble) has often used as biomarkers for endothelial activation (51, 52).

The LSEC proteome changes *in vitro* reflect a scenario of limited bioavailability of NO, and redox imbalance that may promote endothelial dysfunction

Nitric oxide synthase 3 (NOS3, eNOS) was significantly downregulated in all LSEC cultures at 48 h regardless of Dex treatment, whereas inducible nitric oxide synthase (NOS2, iNOS) showed a time-dependent upregulation in LSEC cultures without Dex and was downregulated in the presence of Dex (**Fig. 6A**). Moreover, the transcriptional regulators E74-like factor 1 (ELF1), E26 avian leukemia oncogene 1, 5' domain (ETS1), and the enhancer ETS related gene (ERG), which enhance *Nos3* promoter activity (53), were downregulated congruent with the diminished level of NOS3 in LSECs (**Supplementary Fig. 2A**). Proteins affecting posttranslational modification and enzymatic activity of NOS3 are illustrated in **Fig. 6B**. Time-dependent and Dex-specific changes in these regulators indicated an altered NOS3 activity in LSECs in culture that may promote endothelial dysfunction.

Tetrahydrobiopterin (BH₄) is an indispensable cofactor for NOS3-dependent NO production. Limited BH₄ availability induces uncoupling of the process, rendering NOS3 incapable of sustaining NO production (54). We have not measured BH₄ levels but the time-dependent augmentation of the rate-limiting enzyme glutamate cysteine ligase 1 (GCH1) (**Fig. 6C**) suggests enhanced *de novo* synthesis of BH₄ (54) in LSECs *in vitro*. Similarly, the elevated levels of dihydrofolate reductase (DHFR) (**Fig. 6C**), which is involved in the regeneration of BH₄ from BH₂ (54), suggest reinforced availability of BH₄ at 48 h. Dex significantly reduced the level of DHFR but not GCH1 in LSECs at 48 h compared with the time-matched control.

The differential protein expression analysis also showed derangement of the redox system in LSECs *in vitro*, another essential factor driving endothelial dysfunction (**Figs. 6A, D**). Glutathione peroxidase 3 (GPX3) and catalase (CAT) were significantly downregulated, whereas superoxide dismutase 2 (SOD2), peroxiredoxin-1, and -5 (PRDX1, PRDX5), NAD(P)H: quinone oxidoreductase-1 (NQO1), sulfiredoxin-1 (SRXN1), and glutathione-disulfide reductase (GSR) were upregulated. Xanthine dehydrogenase (XDH), which is involved in the normal breakdown of purines but can also be involved in the production of superoxide radicals (55), was specifically upregulated in the Dex-treated cultures. To further investigate the LSEC oxidative status and effects of Dex, we

measured the level of glutathione (GSH) (**Fig. 6E**) in LSEC cultures incubated for 2 h with or without Dex. This showed increased GSH level with Dex supplement.

Inability to regulate the vascular tone is caused by endothelial cell dysfunction. In line with this, we observed that the Endothelin B receptor (EDNRB) that binds with endothelin 1 (ET1) to bring about vasoconstriction *in vivo* (56), was significantly upregulated in cultured LSECs, but was repressed by Dex (**Supplementary Fig. 2A**). Moreover, the data also exhibited culture-induced alterations in junction-associated proteins including differential regulation of tight junction proteins in the presence (upregulated VAPA (Vesicle-associated membrane protein-associated protein A), EPB41 (Protein 4.1)) and absence of Dex (upregulated F11R (Junctional adhesion molecule A), CLDN5 (Claudin-5)), time-dependent upregulation of adherens junctions (particularly Cadherin-5 (CDH5), Nectin-2 (NECTIN2)), and gap junction-associated proteins and upregulation of BCAM (Basal cell adhesion molecule) (**Supplementary Fig. 2B**).

Effects of culture time and Dex on LSEC endocytosis

A hallmark function of LSECs is the high rate of clathrin-mediated endocytosis of modified plasma proteins, lysosomal enzymes, and many extracellular matrix waste macromolecules that gain access to the general circulation (2). A commonly used test ligand for LSEC clathrin-mediated endocytosis is formaldehyde-treated serum albumin (FSA) which is internalized via scavenger receptors in LSECs (57). The plasma half-life of this ligand is only a few minutes when injected intravenously into a mouse or rat, with LSECs as the major site of uptake and intracellular degradation (58, 59). To study how long mouse LSEC cultures retain the ability to rapidly internalize trace amount of FSA, we measured the uptake of ¹²⁵I-FSA per culture (appr. 10 ng added per culture) during a 2 h incubation period in 0-5 days old cultures that had been treated with 0, 0.1, 1, or 2.5 μ M Dex (**Fig. 7A**). This showed that the uptake of ¹²⁵I-FSA was high (approx. 45% of added ligand/culture/2 h) up to 72 h post-seeding in all treatment groups and then dropped at 120 h post-seeding. At 120 h, ¹²⁵I-FSA uptake was highest with 2.5 μ M Dex, which may be explained by higher cell viability. Of note, this assay does not measure the maximum cell capacity for ligand uptake, which may have been reduced despite a preserved high rate of endocytosis of trace amounts of ligands (60).

We, therefore, did a different set of experiments to test the capacity of uptake of FSA per LSEC at 48 h post-seeding in cultures with or without 1 μ M Dex. In these experiments, non-labeled FSA (10-80 μ g/ml) was added to the culture in addition to trace amounts of ¹²⁵I-FSA and results compared with the endocytic capacity of freshly isolated cells (2 h post-seeding). Cell counts were done in parallel cultures with a similar number of cells that were treated and incubated in the same way as the cultures

with the ligand. This showed that the uptake capacity per cell was significantly reduced in LSECs that had been cultured for 48 h (**Fig. 7B**), with no significant difference between Dex-treated and non-treated cells.

In order to examine the mechanisms responsible for these observations, we studied the expression of essential components and regulators of endocytosis (**Figs. 7C-E**).

The expression of LSEC signature scavenger receptors and C-type lectins was decreased at 48 h in the presence or absence of Dex (**Fig. 7C**). However, Dex stimulated the expression of CD14, which is involved in LPS binding and forms the LPS receptor complex together with TLR4 (61). This effect of Dex was also observed in rat LSEC cultures (paper II in this thesis).

The effect of time in culture and Dex exposure on the expression of essential components and regulators of endocytosis in LSECs are shown in **Fig. 7D**. The figure illustrates differential expression of proteins involved in regulation of endocytosis, as a function of time in culture and Dex treatment. The regulatory proteins that were upregulated in a time-dependent manner regardless of Dex were associated with membrane deformation and tubulation (62). On the contrary, those that were downregulated during culture were the ones associated with endocytosis receptor recycling. Interestingly, we found that Dex treatment of mouse LSECs upregulated different sets of proteins involved in endocytosis receptor recycling and the hydrolase USP8 that deubiquitinates endocytosis-associated proteins preventing their lysosomal degradation (63, 64). We also found that the major coat proteins clathrin light chain A and B (CLTA, CLTB) as well as early-arriving, pioneer proteins (65) that function in the early step of clathrin-mediated endocytosis (*i.e.*, F-bar domain only protein 2 (FCHO2), formin-binding protein (FNBP1), and SH3 domain-containing kinase-binding protein 1 (SH3KBP1)) were downregulated in a time-dependent manner (**Fig. 7E**). Exceptions were sorting nexin-18 (SNX18) which was upregulated by Dex at 48 h, and SNX9 which was upregulated at 48 h in the presence or absence of Dex. Sorting nexins are multifunctional proteins that are also involved in clathrin-coated pit maturation and fission (66).

Dex enhanced LSEC survival *in vitro* by inhibition of apoptosis

Dex treatment improved LSECs survival *in vitro* (**Fig. 2**). The average expression of proteins involved in three different cell death modalities is displayed in **Fig. 8A**, indicating elevated cell death *in vitro*. Dex significantly downregulated the cell death pathways at 48 h and was confirmed in a caspase 3/7 activity assay (**Fig. 8B**). The assay also showed improved Dex mediated LSEC survival even in the presence of apoptotic inducer CD95 (FAS).

The proteomic data illustrated significant time-dependent upregulation of proapoptotic proteins (**Fig. 8C**). Significant increase in expression of tumor necrosis factor receptor superfamily member 10B (TNFRSF10B, also known as death receptor 5), CD40 (Tumor necrosis factor receptor superfamily member 5), CASP3 (caspase 3), and cathepsins (not shown) indicates accentuated caspase-dependent apoptosis in cultured LSECs (67-69). Notably, Dex significantly downregulated TNFRSF10B, CD40, and CASP3.

In addition, prolonged culture (48 h) significantly induced the expression of the apoptosis regulator BAX, BH3-interacting domain death agonist (BID), sequestosome-1 (SQSTM1, p62), and protein mono-ADP-ribosyltransferase (PARP10) (**Fig. 8D**). Dex treatment upregulated the expression of Bcl-2-like protein 1 (BCL2L1, BCL-XL) in LSECs (**Fig. 8D**). BCL2L1 protects against BAX-induced apoptosis by sequestering BAX in a complex (70), which may partly explain the enhanced survival of LSECs in cultures with Dex.

Dex-treatment also stimulated the expression of the transcriptional repressor Bcl-2-associated transcription factor 1 (BCLAF1), known as a proapoptotic protein (71). However, co-expression of BCLAF1 with BCL2-XL may reverse the apoptotic effect of BCLAF1(71). Similarly, the expression of MCL1 (another anti-apoptotic protein) was stimulated in the presence of Dex to some extent, compared to time-matched controls. Dex further stimulated LSECs to significantly induce the expression of proteins that are known to enhance survival, including forkhead box protein O1 (FOXO1) (72, 73), insulin-like growth factor 1 receptor (IGF1R), and insulin receptor (INSR) (74) (**Fig. 8D**).

Transcription regulators which may be critical for maintenance of LSECs in culture

This study enlisted several transcriptional regulators that may impact the LSEC phenotype in early *in vitro* culture, during prolonged culture, and in the presence of Dex. In total, we identified and catalogued 349 transcription regulators (TRs) out of 1346 TRs defined in the following databases: MGI (Mouse Genome Informatics (75)), mouse tissue transcription factor atlas (76)), and Cistrome DB (77). Of these, 103 TRs were regulated in a time-dependent or Dex-specific manner *in vitro*.

Additionally, we implemented Lisa models based on CistromeDB TR ChIP-seq (77) to predict TRs from the list of differentially regulated proteomes while in culture, including early changes (10 h vs 1 h) (**Fig. 9A**), later changes (48 h vs 10 h) (**Fig. 9C**), and by Dex, comparing [(48 h+Dex vs 10 h+Dex) vs (10 h+Dex vs 1 h)] vs [(48 h vs 10 h) vs (10 h vs 1 h)] (**Fig. 9E**). Interestingly, the top predicted TRs from the Lisa models were also the ones that were significantly altered in the proteomic

datasets, further affirming their role in mediating the observed changes in LSECs *in vitro* and in eliciting the response to Dex. Among the top predicted TRs, JUNB (Transcription factor jun-B), MAFK (Transcription factor MafK), and CEBPB (CCAAT/enhancer-binding protein beta) were upregulated, whereas FLI1 (Friend leukemia integration 1 transcription factor), ERG (Transcriptional regulator ERG), and STAT3 (Signal transducer and activator of transcription 3) were downregulated in LSECs at 10 h compared to 1 h (**Fig. 9B**). However, during the prolonged culture (48 h) LSECs displayed elevated expression of the top predicted TRs NOTCH1 (Neurogenic locus notch homolog protein 1), STAT1 (Signal transducer and activator of transcription 1), CEBPB (CCAAT/enhancer-binding protein beta), CAPG (Macrophage-capping protein) and SMAD2&3 (Mothers against decapentaplegic homolog 2 and 3) important for angiocrine factors, whereas the expression of the top predicted TRs GATA4 (transcription factor GATA-4), CREBBP (CREB-binding protein), ELF1 (ETS-related transcription factor Elf-1), STAT5B (Signal transducer and activator of transcription 5B) and IRF7 (Interferon regulatory factor 7) were repressed (**Fig. 9D**). GATA4 is reported as a crucial transcription factor for the development and maintenance of LSEC phenotype (78) and is previously reported to be downregulated in LSEC culture (15, 16).

One of the top 10 TRs inferred was the glucocorticoid receptor NR3C1 (nuclear receptor subfamily 3, group C), which was downregulated in LSECs in a time-dependent manner (**Figs. 9E, F**). NR3C1 expression was notably subverted in the Dex-treated samples (**Fig. 9F**), coinciding with the reports of Dex-stimulated NR3C1 downregulation and degradation (79-82). Similarly, STAT1, ETS1 (Protein C-ets-1), NOTCH1 (Neurogenic locus notch homolog protein 1), FOXO1 (Forkhead box protein O1), and TCF4 (Transcription factor 4) (**Fig. 9F**) were among the top TRs which were identified as regulated both in a time and Dex-specific manner in our study (**Figs. 9D, F**). Unlike NR3C1, the expression of NOTCH1 and STAT1 were significantly upregulated with time, and the presence of Dex significantly reciprocated their expression (**Fig. 9F**). The level of ETS1, which activates the expression of cytokine and chemokines genes in various cellular contexts (83), was upregulated at 48 h in control cultures while suppressed in the presence of Dex (**Fig. 9F**). Dex significantly upregulated the expression of FOXO1 and TCF4 at 48 h (**Fig. 9F**).

Discussion

In this study, we have generated a fine-grained snapshot of the mouse LSEC proteome at several time points (1, 10, and 48 h) post-seeding to uncover hitherto undescribed changes in the LSEC proteome *in vitro* and cell-specific responses towards Dex in culture.

A main effect of Dex was the improved cell survival in culture. The pro-survival effect of Dex on the mouse LSECs *in vitro* may be partly explained by the repression of pro-apoptotic proteins, and the enhanced expression of anti-apoptotic proteins. This was supported by the diminished caspase 3/7 activity in the presence of Dex, regardless of Fas ligand stimulation. Congruently, Dex treatment significantly suppressed the LSEC expression of death receptor 5 (TNFRSF10B), caspases, and cathepsins in culture, which are proteins associated with increased apoptosis (67-69, 84).

The influence of Dex on cell survival and apoptosis varies depending on cell type, dose, and context of use (20). In the clinic, Dex is used both as an anti-inflammatory drug and in cancer treatment where pro-apoptotic effects are sought (85). Of note, Dex was well tolerated by mouse LSECs in doses up to at least 100 μ M (tested up to 3 days in culture).

The proteomic results further reflected a substantial and immediate shift in LSEC metabolism in culture, indicating increased glycolysis and diminished TCA or oxidative phosphorylation both in the presence or absence of Dex. Upregulation of glycolytic proteins and downregulation of proteins associated with the TCA cycle and oxidative phosphorylation were evident as early as 10 h in culture. Interestingly, such metabolic shift was reported to be characteristic of pro-inflammatory immune cells (86, 87) and activated non-LSEC endothelial cells (88). Of note, Dex brought about anti-inflammatory activity in LSECs *in vitro* despite the elevation of glycolytic proteins.

In some cell types, including acute lymphoblastic leukemia cells (89) and alveolar macrophages (90, 91), Dex has been shown to inhibit the expression of glycolytic proteins. In contrast to this, we found that treatment of LSECs with 1 μ M Dex significantly elevated the expression of the rate-limiting enzyme phosphofructokinase (PFKP) and its allosteric regulator PFKFB3 (an enzyme that produces the PFKB allosteric activator β -D-Fructose-2,6 bisphosphate) compared with the time-matched controls signifying that Dex further increased glycolytic flux (92). In fact, the expression pattern of the glycolytic proteins indicates that LSECs could cope with the increased glycolytic flux by preventing energy stress caused by accumulating glycolytic intermediates (92). To maintain the glycolytic flux, cell need to sustain the supply of NAD⁺ and balance protons by converting pyruvate to lactate. The conversion is catalyzed by LDHA which was upregulated in

LSECs by Dex. The upregulation of the monocarboxylate transporter 4 (SLC16A3) in culture also ensures maintenance of high glycolytic flux by the efflux of lactate out of the cell. We have not measured lactate production in this study, however, elevated lactate in rat LSEC culture supernatants was reported previously (13) and then correlated with an improved LSEC phenotype *in vitro*. The low oxygen tension (5%) of the sinusoidal blood (13) combined with the low number of mitochondria in LSECs (93, 94) also signify a comparatively low degree of oxidative phosphorylation and largely anaerobic metabolism in LSECs, yielding high amounts of lactate and acetate (95, 96). Our recently published mRNA and protein expression data of freshly plated rat LSECs and KCs at steady-state also signify anaerobic metabolism in LSECs showing higher expression of proteins associated with glycolysis in LSECs, compared to the higher expression of proteins associated with oxidative phosphorylation in KCs (35).

It has been suggested that rat LSECs generate 80% of their ATP from glutamine and palmitate oxidation *in vitro* (97). However, our present studies of LSECs in mice and rats (paper II in this thesis) suggest downregulation of fatty acid oxidation and amino acid degradation in culture, supporting that LSECs *in vitro* largely depend on glycolysis for ATP regeneration. Surprisingly, the data did not show any notable increase in any of the facilitative glucose transporter expression, and rather showed significant time-dependent downregulation of SLC2A2 (GLUT2, major facilitative glucose transporter between blood and liver cells). An additional source for substrates is lysosomal degradation products, and several lysosomal hydrolases were upregulated with time in culture.

The Dex-induced upregulation of GDH/6PGL endoplasmic bifunctional protein (H6PD) may increase the traffic of phosphorylated monosaccharides into the pentose phosphate pathway, preventing the accumulation of phosphorylated monosaccharides and enhancing glycolytic flux. The reaction facilitated by H6PD is important in NADPH regeneration which is critical for endoplasmic reticulum redox balance (98). Recently, it was reported that quiescent non-LSEC endothelial cells exhibit a 3-4-fold higher rate of fatty acid oxidation compared to activated angiogenic endothelial cells (88, 99), suggesting that fatty acid oxidation feeds the TCA cycle to sustain NADPH regeneration which is critical to maintaining redox homeostasis and endothelial quiescence (88). As already mentioned, our data showed diminished fatty acid oxidation in LSEC in culture in the presence or absence of Dex. One may therefore speculate that Dex-mediated increase in H6PD is also contributing to the more quiescent LSEC phenotype.

Mouse LSECs in cultures without Dex immediately acquired an activated phenotype, like rat LSECs *in vitro* (paper II in this thesis), featured by elevated expression of pro-inflammatory proteins and cell

adhesion molecules which was validated in functional experiments. This is likely caused by the stress response to the cell isolation procedure and non-physiological substrate as discussed in (14, 100-103).

It was previously reported that maintaining LSECs in 5% O₂ significantly dampened cell activation compared to incubation in 20% O₂ reducing the expression of IL-6 and ICAM-1 in culture (13). The present study showed that maintaining LSECs in the presence of Dex further suppresses the expression of pro-inflammatory cytokines and CAMs and significantly improves LSEC functions and morphology in culture. Derangement in angiocrine factors such as NOTCH1, HGF, BMP6, and WNT is another feature of endothelial activation (104). The present data showed upregulation of NOTCH1 in the LSEC cultures at 48 h, supporting LSEC activation. NOTCH-1 activation has been shown to cause LSEC dedifferentiation and inflammatory activation in mouse studies (105, 106).

We also found that mouse LSECs *in vitro* showed decreased expression of NOS3, and increased expression of NOS2 suggesting a deranged redox system. Dex downregulated the NOS2 expression but did not affect NOS3 compared to time-matched controls. NO signalling affects endothelial cell physiology and pathophysiology including metabolism, vascular tone, and immune responses (107). The two major sources of NO in the liver are NOS3 (eNOS) and NOS2 (nitric oxide synthase 2, inducible) (108). NOS3 dependent NO release is hepatoprotective and maintains LSEC fenestration as well as promotes hepatic stellate cell and Kupffer cell quiescence (17, 108). NOS3 is upregulated in response to VEGF, shear stress (via the transcription factor Krüppel- like factor 2 (KLF2)), and transcriptional enhancers such as ELF1, ES1, and ERG, and downregulation of NOS3 expression in our *in vitro* system may be explained by lack of VEGF and the static monocellular culture system.

In contrast, NOS2 is induced through activation of NF-κB and STAT-pathways (109) and increases NO production in response to pro-inflammatory stimuli. NOS2-derived NO contributes to reactive nitrogen species and promotes inflammation (108). Dex-mediated downregulation of NOS2 may therefore be a consequence of repressed NF-κB and diminished STAT1 expression in LSECs *in vitro*. Moreover, an elevated level of NO in response to prolonged pro-inflammatory cytokine exposure or exogenous NO donor (sodium nitroprusside) was reported to downregulate endocytosis in rat LSECs via scavenger- and mannose receptors in culture (29).

We also saw upregulation of NOTCH1 at 48 h into the culture, which was significantly decreased with Dex. Activated NOTCH1 was reported to interfere with the NOS/sGC signaling pathway inducing downregulation of KDR (VEGFR2) and NOS3 in mouse LSECs exacerbating defenestration *in vitro* (106). The diminished expression of NOS3, the elevated expression of NOS2, and other proteome changes (particularly downregulation of AKT1) *in vitro* favor uncoupling of

NOS3 effects (which leads to the production of reactive oxygen species instead of NO) and represents a likely scenario of limited NO bioavailability in LSEC culture (108). In addition, activation of NOTCH1 and limited NO bioavailability may be among the factors contributing to inflammatory changes of LSECs in culture.

The anti-inflammatory action of Dex depends prominently on the nuclear receptor NR3C1. Dex-bound NR3C1 translocates into the nucleus to activate anti-inflammatory gene expression and represses NF- κ B and AP-1 mediated pro-inflammatory gene expression (110). Interestingly, NR3C1 was downregulated in a time-dependent manner in LSECs *in vitro*. The NR3C1 repression was more pronounced in LSECs cultured with Dex. Dex-mediated degradation of NR3C1 has been shown in other cell models (81, 82, 111). Dex treatment for 48 h also resulted in the elevated level of the co-chaperone FKBP5, which inhibits NR3C1 translocation into the nucleus (112), suggesting that LSECs might lose sensitivity towards Dex in prolonged culture, as reported for other cells (112, 113).

Efficient clathrin-mediated endocytosis of soluble macromolecules via SRs is a hallmark of LSEC integrity (13). FSA is used as a model ligand for SR-mediated endocytosis in LSECs (2, 114), and uptake in LSECs is mediated via stabilin-1 and stabilin-2 (57, 115). FSA is also likely to bind to other SRs. We found that mouse LSECs in AIM-V medium in the presence or absence of Dex were able to rapidly endocytose trace doses of radio-iodinated FSA even after 5 days in culture. At day 5 this ability was best preserved in Dex-treated cultures. However, the maximum capacity for FSA uptake per cell was markedly reduced (measured at 48 h vs 2 h), with no significant improvement by Dex. In accordance with the findings in the functional assays, the proteomics data showed that many SRs, regulators of endocytosis, and pioneer proteins involved in clathrin-mediated coat formation showed diminished expression at 48 h in the presence or absence of 1 μ M Dex. Of note, Dex suppressed the culture-induced downregulation of stabilin-1 and upregulated some critical components of clathrin-mediated endocytosis, along with regulators involved in receptor recycling. The higher uptake at 5 days of trace doses of radiolabeled FSA in cultures with Dex may therefore be partly explained by a positive effect of Dex but also by the fact that Dex increased LSEC survival in long-term primary culture. Dex (2.5 μ M) was previously reported to enhance endocytosis of radiolabeled ligands (trace doses) via SR and mannose receptors in rat LSEC cultures (29), however, that study did not include a capacity of uptake experiment.

In conclusion, we report in detail the effect of time in culture on the mouse LSEC proteome, cell morphology, scavenger function, and metabolism, and how Dex affects these parameters. Dex is widely used in the clinic, and therefore, it is vital to know how the drug affects different cell types.

Additionally, a deep understanding of the proteomic changes that occur in LSECs *in vitro* may support the work to improve LSECs in culture systems and interpretation of *in vitro* studies in these cells. Early management of the inflammatory changes and sustaining the expression of the transcriptional regulators significantly altered *in vitro* may be a way to improve LSEC *in vitro* system making LSECs more accessible for research.

Acknowledgement

The proteomics used in this study was performed at the Tromsø University Proteomics Platform (TUPP). We would like to express our gratitude to Dr. Jack-Ansgar Brun for help with the proteomic experiments, and Randi Olsen and Augusta Hlin Aspar Sundbø for help with preparation of samples for SEM.

Financial support

The study was supported by the Norwegian Research Council (Grant No. 262438), the Tromsø Research Foundation, and UiT The Arctic University of Norway.

References

1. Smedsrød B, Pertoft H, Gustafson S, Laurent TC. Scavenger functions of the liver endothelial cell. *Biochem J.* 1990;266(2):313-27.
2. Sørensen KK, Simon-Santamaria J, McCuskey RS, Smedsrød B. Liver Sinusoidal Endothelial Cells. *Compr Physiol.* 2015;5(4):1751-74.
3. Zapotoczny B, Szafranska K, Kus E, Braet F, Wisse E, Chlopicki S, et al. Tracking Fenestrae Dynamics in Live Murine Liver Sinusoidal Endothelial Cells. *Hepatology.* 2019;69(2):876-88.
4. Braet F, Wisse E. Structural and functional aspects of liver sinusoidal endothelial cell fenestrae: a review. *Comp Hepatol.* 2002;1(1):1.
5. Wisse E, De Zanger RB, Charels K, Van Der Smissen P, McCuskey RS. The liver sieve: considerations concerning the structure and function of endothelial fenestrae, the sinusoidal wall and the space of Disse. *Hepatology.* 1985;5(4):683-92.
6. Fraser R, Cogger VC, Dobbs B, Jamieson H, Warren A, Hilmer SN, et al. The liver sieve and atherosclerosis. *Pathology.* 2012;44(3):181-6.
7. Fraser R, Bosanquet AG, Day WA. Filtration of chylomicrons by the liver may influence cholesterol metabolism and atherosclerosis. *Atherosclerosis.* 1978;29(2):113-23.
8. Gracia-Sancho J, Caparros E, Fernandez-Iglesias A, Frances R. Role of liver sinusoidal endothelial cells in liver diseases. *Nat Rev Gastroenterol Hepatol.* 2021.
9. Sørensen KK, Smedsrød B. The Liver Sinusoidal Endothelial Cell. *The Liver2020.* p. 422-34.
10. Le Couteur DG, Fraser R, Cogger VC, McLean AJ. Hepatic pseudocapillarisation and atherosclerosis in ageing. *Lancet.* 2002;359(9317):1612-5.
11. Hang TC, Lauffenburger DA, Griffith LG, Stolz DB. Lipids promote survival, proliferation, and maintenance of differentiation of rat liver sinusoidal endothelial cells in vitro. *Am J Physiol Gastrointest Liver Physiol.* 2012;302(3):G375-88.
12. Elvevold KH, Nedredal GI, Revhaug A, Smedsrød B. Scavenger properties of cultivated pig liver endothelial cells. *Comp Hepatol.* 2004;3(1):4.
13. Martinez I, Nedredal GI, Oie CI, Warren A, Johansen O, Le Couteur DG, et al. The influence of oxygen tension on the structure and function of isolated liver sinusoidal endothelial cells. *Comp Hepatol.* 2008;7:4.
14. March S, Hui EE, Underhill GH, Khetani S, Bhatia SN. Microenvironmental regulation of the sinusoidal endothelial cell phenotype in vitro. *Hepatology.* 2009;50(3):920-8.
15. Geraud C, Schledzewski K, Demory A, Klein D, Kaus M, Peyre F, et al. Liver sinusoidal endothelium: a microenvironment-dependent differentiation program in rat including the novel

- junctional protein liver endothelial differentiation-associated protein-1. *Hepatology*. 2010;52(1):313-26.
16. de Haan W, Øie C, Benkheil M, Dheedene W, Vinckier S, Coppiello G, et al. Unraveling the transcriptional determinants of liver sinusoidal endothelial cell specialization. *Am J Physiol Gastrointest Liver Physiol*. 2020;318(4):G803-G15.
 17. Xie G, Wang X, Wang L, Wang L, Atkinson RD, Kanel GC, et al. Role of differentiation of liver sinusoidal endothelial cells in progression and regression of hepatic fibrosis in rats. *Gastroenterology*. 2012;142(4):918-27 e6.
 18. Xie G, Choi SS, Syn WK, Michelotti GA, Swiderska M, Karaca G, et al. Hedgehog signalling regulates liver sinusoidal endothelial cell capillarisation. *Gut*. 2013;62(2):299-309.
 19. Whirlledge S, DeFranco DB. Glucocorticoid Signaling in Health and Disease: Insights From Tissue-Specific GR Knockout Mice. *Endocrinology*. 2018;159(1):46-64.
 20. Quatrini L, Ugolini S. New insights into the cell- and tissue-specificity of glucocorticoid actions. *Cell Mol Immunol* 2020.
 21. Panettieri RA, Schaafsma D, Amrani Y, Koziol-White C, Ostrom R, Tliba O. Non-genomic Effects of Glucocorticoids: An Updated View. *Trends Pharmacol Sci*. 2019;40(1):38-49.
 22. Franco LM, Gadkari M, Howe KN, Sun J, Kardava L, Kumar P, et al. Immune regulation by glucocorticoids can be linked to cell type-dependent transcriptional responses. *J Exp Med*. 2019;216(2):384-406.
 23. John S, Sabo PJ, Thurman RE, Sung MH, Biddie SC, Johnson TA, et al. Chromatin accessibility pre-determines glucocorticoid receptor binding patterns. *Nat Genet*. 2011;43(3):264-8.
 24. Grøntved L, John S, Baek S, Liu Y, Buckley JR, Vinson C, et al. C/EBP maintains chromatin accessibility in liver and facilitates glucocorticoid receptor recruitment to steroid response elements. *Embo j*. 2013;32(11):1568-83.
 25. Bailly-Maitre B, de Sousa G, Boulukos K, Gugenheim J, Rahmani R. Dexamethasone inhibits spontaneous apoptosis in primary cultures of human and rat hepatocytes via Bcl-2 and Bcl-xL induction. *Cell Death Differ*. 2001;8(3):279-88.
 26. Zhao B, Xie GJ, Li RF, Chen Q, Zhang XQ. Dexamethasone protects normal human liver cells from apoptosis induced by tumor necrosis factor-related apoptosis-inducing ligand by upregulating the expression of P-glycoproteins. *Mol Med Rep*. 2015;12(6):8093-100.
 27. Burwick N, Sharma S. Glucocorticoids in multiple myeloma: past, present, and future. *Ann Hematol*. 2019;98(1):19-28.

28. Tamez-Perez HE, Quintanilla-Flores DL, Rodriguez-Gutierrez R, Gonzalez-Gonzalez JG, Tamez-Pena AL. Steroid hyperglycemia: Prevalence, early detection and therapeutic recommendations: A narrative review. *World J Diabetes*. 2015;6(8):1073-81.
29. Martinez I, Sveinbjörnsson B, Smedsrød B. Nitric oxide down-regulates endocytosis in rat liver endothelial cells. *Biochem Biophys Res Commun*. 1996;222(3):688-93.
30. Melgert BN, Weert B, Schellekens H, Meijer DK, Poelstra K. The pharmacokinetic and biological activity profile of dexamethasone targeted to sinusoidal endothelial and Kupffer cells. *J Drug Target*. 2003;11(1):1-10.
31. Melgert BN, Olinga P, Jack VK, Molema G, Meijer DKE, Poelstra K. Dexamethasone coupled to albumin is selectively taken up by rat nonparenchymal liver cells and attenuates LPS-induced activation of hepatic cells. *J Hepatol*. 2000;32(4):603-11.
32. Smedsrød B, Pertoft H. Preparation of pure hepatocytes and reticuloendothelial cells in high yield from a single rat liver by means of Percoll centrifugation and selective adherence. *J Leukoc Biol*. 1985;38(2):213-30.
33. Wisse E. An electron microscopic study of the fenestrated endothelial lining of rat liver sinusoids. *J Ultrastruct Res*. 1970;31(1):125-50.
34. McDowell EM, Trump BF. Histologic fixatives suitable for diagnostic light and electron microscopy. *Arch Pathol Lab Med*. 1976;100(8):405-14.
35. Bhandari S, Li R, Simon-Santamaria J, McCourt P, Johansen SD, Smedsrød B, et al. Transcriptome and proteome profiling reveal complementary scavenger and immune features of rat liver sinusoidal endothelial cells and liver macrophages. *BMC Mol Cell Biol*. 2020;21(1):85.
36. Stein DR, Hu X, McCorrister SJ, Westmacott GR, Plummer FA, Ball TB, et al. High pH reversed-phase chromatography as a superior fractionation scheme compared to off-gel isoelectric focusing for complex proteome analysis. *Proteomics*. 2013;13(20):2956-66.
37. Navarrete-Perea J, Yu Q, Gygi SP, Paulo JA. Streamlined Tandem Mass Tag (SL-TMT) Protocol: An Efficient Strategy for Quantitative (Phospho)proteome Profiling Using Tandem Mass Tag-Synchronous Precursor Selection-MS3. *J Proteome Res*. 2018;17(6):2226-36.
38. UniProt C. UniProt: the universal protein knowledgebase in 2021. *Nucleic Acids Res*. 2021;49(D1):D480-D9.
39. Tyanova S, Temu T, Sinitcyn P, Carlson A, Hein MY, Geiger T, et al. The Perseus computational platform for comprehensive analysis of (prote)omics data. *Nat Methods*. 2016;13(9):731-40.

40. Plubell DL, Wilmarth PA, Zhao Y, Fenton AM, Minnier J, Reddy AP, et al. Extended Multiplexing of Tandem Mass Tags (TMT) Labeling Reveals Age and High Fat Diet Specific Proteome Changes in Mouse Epididymal Adipose Tissue. *Mol Cell Proteom.* 2017;16(5):873-90.
41. Robinson MD, Oshlack A. A scaling normalization method for differential expression analysis of RNA-seq data. *Genome Biol.* 2010;11(3):R25.
42. Robinson MD, McCarthy DJ, Smyth GK. edgeR: a Bioconductor package for differential expression analysis of digital gene expression data. *Bioinformatics.* 2010;26(1):139-40.
43. Mego JL, Bertini F, McQueen JD. The use of formaldehyde-treated ¹³¹I-albumin in the study of digestive vacuoles and some properties of these particles from mouse liver. *J Cell Biol.* 1967;32(3):699-707.
44. Hansen B, Arteta B, Smedsrød B. The physiological scavenger receptor function of hepatic sinusoidal endothelial and Kupffer cells is independent of scavenger receptor class A type I and II. *Mol Cell Biochem.* 2002;240(1-2):1-8.
45. Robinson MD, Smyth GK. Small-sample estimation of negative binomial dispersion, with applications to SAGE data. *Biostatistics.* 2008;9.
46. Schmidt-Arras D, Rose-John S. IL-6 pathway in the liver: From physiopathology to therapy. *J Hepatol.* 2016;64(6):1403-15.
47. Subramanian A, Tamayo P, Mootha VK, Mukherjee S, Ebert BL, Gillette MA, et al. Gene set enrichment analysis: a knowledge-based approach for interpreting genome-wide expression profiles. *Proc Natl Acad Sci U S A.* 2005;102(43):15545-50.
48. Smedsrød B, Pertoft H, Eriksson S, Fraser JR, Laurent TC. Studies in vitro on the uptake and degradation of sodium hyaluronate in rat liver endothelial cells. *Biochem J.* 1984;223(3):617-26.
49. Bahrami S, Drabløs F. Gene regulation in the immediate-early response process. *Adv Biol Regul.* 2016;62:37-49.
50. Wong J, Johnston B, Lee SS, Bullard DC, Smith CW, Beaudet AL, et al. A minimal role for selectins in the recruitment of leukocytes into the inflamed liver microvasculature. *J Clin Invest.* 1997;99(11):2782-90.
51. Ridker PM, Hennekens CH, Roitman-Johnson B, Stampfer MJ, Allen J. Plasma concentration of soluble intercellular adhesion molecule 1 and risks of future myocardial infarction in apparently healthy men. *Lancet* 1998;351(9096):88-92.
52. Li H, Cybulsky MI, Gimbrone MA, Jr., Libby P. An atherogenic diet rapidly induces VCAM-1, a cytokine-regulatable mononuclear leukocyte adhesion molecule, in rabbit aortic endothelium. *Arterioscler Thromb.* 1993;13(2):197-204.

53. Oliveira-Paula GH, Lacchini R, Tanus-Santos JE. Endothelial nitric oxide synthase: From biochemistry and gene structure to clinical implications of NOS3 polymorphisms. *Gene*. 2016;575(2 Pt 3):584-99.
54. Yuyun MF, Ng LL, Ng GA. Endothelial dysfunction, endothelial nitric oxide bioavailability, tetrahydrobiopterin, and 5-methyltetrahydrofolate in cardiovascular disease. Where are we with therapy? *Microvasc Res*. 2018;119:7-12.
55. Nishino T, Okamoto K, Eger BT, Pai EF, Nishino T. Mammalian xanthine oxidoreductase - mechanism of transition from xanthine dehydrogenase to xanthine oxidase. *FEBS J*. 2008;275(13):3278-89.
56. Finney SJ. Critical Care. In: Gatzoulis MA, Webb GD, Daubeney PEF, editors. *Diagnosis and Management of Adult Congenital Heart Disease*: Elsevier; 2018. p. 209-15.
57. Li R, Oteiza A, Sørensen KK, McCourt P, Olsen R, Smedsrød B, et al. Role of liver sinusoidal endothelial cells and stabilins in elimination of oxidized low-density lipoproteins. *Am J Physiol Gastrointest Liver Physiol*. 2011;300(1):G71-81.
58. Blomhoff R, Eskild W, Berg T. Endocytosis of formaldehyde-treated serum albumin via scavenger pathway in liver endothelial cells. *Biochem J*. 1984;218(1):81-6.
59. Elvevold K, Simon-Santamaria J, Hasvold H, McCourt P, Smedsrød B, Sørensen KK. Liver sinusoidal endothelial cells depend on mannose receptor-mediated recruitment of lysosomal enzymes for normal degradation capacity. *Hepatology*. 2008;48(6):2007-15.
60. Simon-Santamaria J, Malovic I, Warren A, Oteiza A, Le Couteur D, Smedsrød B, et al. Age-related changes in scavenger receptor-mediated endocytosis in rat liver sinusoidal endothelial cells. *J Gerontol A Biol Sci Med Sci*. 2010;65(9):951-60.
61. Zanoni I, Ostuni R, Marek LR, Barresi S, Barbalat R, Barton GM, et al. CD14 controls the LPS-induced endocytosis of Toll-like receptor 4. *Cell*. 2011;147(4):868-80.
62. van Weering JR, Verkade P, Cullen PJ. SNX-BAR proteins in phosphoinositide-mediated, tubular-based endosomal sorting. *Semin Cell Dev Biol*. 2010;21(4):371-80.
63. Grant BD, Donaldson JG. Pathways and mechanisms of endocytic recycling. *Nat Rev Mol Cell Biol*. 2009;10(9):597-608.
64. MacDonald E, Urbé S, Clague MJ. USP8 controls the trafficking and sorting of lysosomal enzymes. *Traffic*. 2014;15(8):879-88.
65. Mettlen M, Chen PH, Srinivasan S, Danuser G, Schmid SL. Regulation of Clathrin-Mediated Endocytosis. *Annu Rev Biochem*. 2018;87(1):871-96.
66. Kaksonen M, Roux A. Mechanisms of clathrin-mediated endocytosis. *Nat Rev Mol Cell Biol*. 2018;19(5):313-26.

67. Walczak H, Degli-Esposti MA, Johnson RS, Smolak PJ, Waugh JY, Boiani N, et al. TRAIL-R2: a novel apoptosis-mediating receptor for TRAIL. *Embo j.* 1997;16(17):5386-97.
68. Oberst A, Pop C, Tremblay AG, Blais V, Denault JB, Salvesen GS, et al. Inducible dimerization and inducible cleavage reveal a requirement for both processes in caspase-8 activation. *J Biol Chem.* 2010;285(22):16632-42.
69. Pitti RM, Marsters SA, Ruppert S, Donahue CJ, Moore A, Ashkenazi A. Induction of apoptosis by Apo-2 ligand, a new member of the tumor necrosis factor cytokine family. *J Biol Chem.* 1996;271(22):12687-90.
70. Dejean L, Hermida OT, Ganesan YT, Renault T, Antonsson B, Manon S. Interactions Between Bcl-2, Bcl-xl, and Bax at the Mitochondria: Keep Your Friends Close but Your Enemies Closer. *Biophys J.* 2011;100(3):40-.
71. Kasof GM, Goyal L, White E. Btf, a novel death-promoting transcriptional repressor that interacts with Bcl-2-related proteins. *Mol Cell Biol.* 1999;19(6):4390-404.
72. Greer EL, Brunet A. FOXO transcription factors at the interface between longevity and tumor suppression. *Oncogene.* 2005;24(50):7410-25.
73. Burgering BM, Medema RH. Decisions on life and death: FOXO Forkhead transcription factors are in command when PKB/Akt is off duty. *J Leukoc Biol.* 2003;73(6):689-701.
74. Heidegger I, Kern J, Ofer P, Klocker H, Massoner P. Oncogenic functions of IGF1R and INSR in prostate cancer include enhanced tumor growth, cell migration and angiogenesis. *Oncotarget.* 2014;5(9):2723-35.
75. Bult CJ, Blake JA, Smith CL, Kadin JA, Richardson JE. Mouse Genome Database (MGD) 2019. *Nucleic Acids Res.* 2019;47(D1):D801-d6.
76. Zhou Q, Liu M, Xia X, Gong T, Feng J, Liu W, et al. A mouse tissue transcription factor atlas. *Nat Commun.* 2017;8(1):15089.
77. Qin Q, Fan J, Zheng R, Wan C, Mei S, Wu Q, et al. Lisa: inferring transcriptional regulators through integrative modeling of public chromatin accessibility and ChIP-seq data. *Genome Biol.* 2020;21(1):32.
78. Geraud C, Koch PS, Zierow J, Klapproth K, Busch K, Olsavszky V, et al. GATA4-dependent organ-specific endothelial differentiation controls liver development and embryonic hematopoiesis. *J Clin Invest.* 2017;127(3):1099-114.
79. Ramamoorthy S, Cidlowski JA. Ligand-induced repression of the glucocorticoid receptor gene is mediated by an NCoR1 repression complex formed by long-range chromatin interactions with intragenic glucocorticoid response elements. *Mol Cell Biol.* 2013;33(9):1711-22.

80. Wandler AM, Huang BJ, Craig JW, Hayes K, Yan H, Meyer LK, et al. Loss of glucocorticoid receptor expression mediates in vivo dexamethasone resistance in T-cell acute lymphoblastic leukemia. *Leukemia*. 2020;34(8):2025-37.
81. Wallace AD, Cidlowski JA. Proteasome-mediated glucocorticoid receptor degradation restricts transcriptional signaling by glucocorticoids. *J Biol Chem*. 2001;276(46):42714-21.
82. Silva CM, Powell-Oliver FE, Jewell CM, Sar M, Allgood VE, Cidlowski JA. Regulation of the human glucocorticoid receptor by long-term and chronic treatment with glucocorticoid. *Steroids*. 1994;59(7):436-42.
83. Russell L, Garrett-Sinha LA. Transcription factor Ets-1 in cytokine and chemokine gene regulation. *Cytokine*. 2010;51(3):217-26.
84. Machuca C, Mendoza-Milla C, Cordova E, Mejia S, Covarrubias L, Ventura J, et al. Dexamethasone protection from TNF-alpha-induced cell death in MCF-7 cells requires NF-kappaB and is independent from AKT. *BMC Cell Biol*. 2006;7(1):9.
85. Lin K-T, Wang L-H. New dimension of glucocorticoids in cancer treatment. *Steroids*. 2016;111:84-8.
86. Jha AK, Huang SC, Sergushichev A, Lampropoulou V, Ivanova Y, Loginicheva E, et al. Network integration of parallel metabolic and transcriptional data reveals metabolic modules that regulate macrophage polarization. *Immunity*. 2015;42(3):419-30.
87. Wculek SK, Khouili SC, Priego E, Heras-Murillo I, Sancho D. Metabolic Control of Dendritic Cell Functions: Digesting Information. *Front Immunol*. 2019;10(775):775.
88. Kalucka J, Bierhansl L, Conchinha NV, Missiaen R, Elia I, Bruning U, et al. Quiescent Endothelial Cells Upregulate Fatty Acid beta-Oxidation for Vasculoprotection via Redox Homeostasis. *Cell Metab*. 2018;28(6):881-94 e13.
89. Aoki S, Morita M, Hirao T, Yamaguchi M, Shiratori R, Kikuya M, et al. Shift in energy metabolism caused by glucocorticoids enhances the effect of cytotoxic anti-cancer drugs against acute lymphoblastic leukemia cells. *Oncotarget*. 2017;8(55):94271-85.
90. Talreja J, Bauerfeld C, Sendler E, Pique-Regi R, Luca F, Samavati L. Derangement of Metabolic and Lysosomal Gene Profiles in Response to Dexamethasone Treatment in Sarcoidosis. *Front Immunol*. 2020;11(779):779.
91. Buentke E, Nordström A, Lin H, Björklund AC, Laane E, Harada M, et al. Glucocorticoid-induced cell death is mediated through reduced glucose metabolism in lymphoid leukemia cells. *Blood Cancer J*. 2011;1(7):e31.
92. Tanner LB, Goglia AG, Wei MH, Sehgal T, Parsons LR, Park JO, et al. Four Key Steps Control Glycolytic Flux in Mammalian Cells. *Cell Syst*. 2018;7(1):49-62.e8.

93. Wisse E. An ultrastructural characterization of the endothelial cell in the rat liver sinusoid under normal and various experimental conditions, as a contribution to the distinction between endothelial and Kupffer cells. *J Ultrastruct Res.* 1972;38(5-6):528-62.
94. Fujii Y, Ohno N, Li Z, Terada N, Baba T, Ohno S. Morphological and histochemical analyses of living mouse livers by new 'cryobiopsy' technique. *J Electron Microsc* 2006;55(2):113-22.
95. Eriksson S, Fraser JR, Laurent TC, Pertoft H, Smedsrød B. Endothelial cells are a site of uptake and degradation of hyaluronic acid in the liver. *Exp Cell Res.* 1983;144(1):223-8.
96. Smedsrød B. Cellular events in the uptake and degradation of hyaluronan. *Adv Drug Deliv Rev.* 1991;7(2):265-78.
97. Spolarics Z, Lang CH, Bagby GJ, Spitzer JJ. Glutamine and fatty acid oxidation are the main sources of energy for Kupffer and endothelial cells. *Am J Physiol.* 1991;261(2 Pt 1):G185-90.
98. Lavery GG, Walker EA, Turan N, Rogoff D, Ryder JW, Shelton JM, et al. Deletion of hexose-6-phosphate dehydrogenase activates the unfolded protein response pathway and induces skeletal myopathy. *J Biol Chem.* 2008;283(13):8453-61.
99. Falkenberg KD, Rohlenova K, Luo Y, Carmeliet P. The metabolic engine of endothelial cells. *Nat Metab.* 2019;1(10):937-46.
100. Juin A, Planus E, Guillemot F, Horakova P, Albiges-Rizo C, Genot E, et al. Extracellular matrix rigidity controls podosome induction in microvascular endothelial cells. *Biol Cell.* 2013;105(1):46-57.
101. Kidambi S, Natarajan V, Casey C, Harris E. Matrix Stiffness Regulate Liver Sinusoidal Endothelial Cells (LSECs) Function: Importance for Liver Fibrosis Progression. *Faseb J.* 2019;33(S1):496.39-.39.
102. Denisenko E, Guo BB, Jones M, Hou R, de Kock L, Lassmann T, et al. Systematic assessment of tissue dissociation and storage biases in single-cell and single-nucleus RNA-seq workflows. *Genome Biol.* 2020;21(1):130.
103. O'Flanagan CH, Campbell KR, Zhang AW, Kabeer F, Lim JLP, Biele J, et al. Dissociation of solid tumor tissues with cold active protease for single-cell RNA-seq minimizes conserved collagenase-associated stress responses. *Genome Biol.* 2019;20(1):210.
104. Csiszar A, Wang M, Lakatta EG, Ungvari Z. Inflammation and endothelial dysfunction during aging: role of NF-kappaB. *J Appl Physiol.* 2008;105(4):1333-41.
105. Zhang P, Yue K, Liu X, Yan X, Yang Z, Duan J, et al. Endothelial Notch activation promotes neutrophil transmigration via downregulating endomucin to aggravate hepatic ischemia/reperfusion injury. *Sci China Life Sci.* 2020;63(3):375-87.

106. Duan JL, Ruan B, Yan XC, Liang L, Song P, Yang ZY, et al. Endothelial Notch activation reshapes the angiocrine of sinusoidal endothelia to aggravate liver fibrosis and blunt regeneration in mice. *Hepatology*. 2018;68(2):677-90.
107. Oliveira-Paula GH, Lacchini R, Tanus-Santos JE. Clinical and pharmacogenetic impact of endothelial nitric oxide synthase polymorphisms on cardiovascular diseases. *Nitric Oxide*. 2017;63:39-51.
108. Iwakiri Y, Kim MY. Nitric oxide in liver diseases. *Trends Pharmacol Sci*. 2015;36(8):524-36.
109. Farlik M, Reutterer B, Schindler C, Greten F, Vogl C, Muller M, et al. Nonconventional initiation complex assembly by STAT and NF-kappaB transcription factors regulates nitric oxide synthase expression. *Immunity*. 2010;33(1):25-34.
110. Smoak KA, Cidrowski JA. Mechanisms of glucocorticoid receptor signaling during inflammation. *Mech Ageing Dev*. 2004;125(10-11):697-706.
111. Sengupta S, Wasylyk B. Ligand-dependent interaction of the glucocorticoid receptor with p53 enhances their degradation by Hdm2. *Genes Dev*. 2001;15(18):2367-80.
112. Guidotti G, Calabrese F, Anacker C, Racagni G, Pariante CM, Riva MA. Glucocorticoid receptor and FKBP5 expression is altered following exposure to chronic stress: modulation by antidepressant treatment. *Neuropsychopharmacology*. 2013;38(4):616-27.
113. Mata-Greenwood E, Stewart JM, Steinhorn RH, Pearce WJ. Role of BCL2-associated athanogene 1 in differential sensitivity of human endothelial cells to glucocorticoids. *Arterioscler Thromb Vasc Biol*. 2013;33(5):1046-55.
114. DeLeve LD, Maretta-Mira AC. Liver Sinusoidal Endothelial Cell: An Update. *Semin Liver Dis*. 2017;37(4):377-87.
115. McCourt PA, Smedsrød BH, Melkko J, Johansson S. Characterization of a hyaluronan receptor on rat sinusoidal liver endothelial cells and its functional relationship to scavenger receptors. *Hepatology*. 1999;30(5):1276-86.
116. Zhang J, Defelice AF, Hanig JP, Colatsky T. Biomarkers of endothelial cell activation serve as potential surrogate markers for drug-induced vascular injury. *Toxicol Pathol*. 2010;38(6):856-71.

Figure Legends

Fig. 1: Experimental design and workflow of the proteomics experiment and analyses

Illustration of the workflow for the generation of samples for proteomic analyses from purified mouse LSECs. Liver cells were isolated by warm *in situ* liver perfusion with Liberase™, as described in Materials and Methods. The obtained single-cell suspension was then kept at 4°C during LSEC purification. LSECs were enriched from non-parenchymal liver cells on a MACS column using beads with antibodies to CD146. The cells were established on fibronectin-coated tissue culture plates and incubated at 37°C in 5% CO₂ and 5% O₂ atmosphere and allowed to attach for 30 min before washing with prewarmed medium. The plates were examined for cell density and purity and incubated with fresh medium with or without Dex for 10 and 48 h, and cells lysed to collect protein at the specified time points. The lysates were enzymatically digested to generate peptides that were labelled with TMT reporters. The samples were pre-run to determine the mixing ratio to generate the final 1:1:1:1 TMT mix. The labelled peptides were fractionated before LC-MS/MS/MS. The subsequent data processing is described in Materials and Methods.

Fig. 2: Dose and time-dependent effects of Dex on mouse LSEC morphology, viability, and IL-6 production in culture

- A. Scanning electron micrographs of freshly isolated mouse LSECs cultured for 2 h-5 days in AIM-V medium \pm 1 μ M Dex. Dex-treated cells showed better preservation of fenestrae, but still lost their fenestrae over time in culture.
- B. LDH activity in LSEC culture medium from cells incubated for 48-72 h in the presence of 0, 1, 10, 100, or 1000 μ M Dex. LDH was measured at 2, 24, 48, and 72 h. Parallel control cultures were treated with Triton-X100 (TX-100) at 2, 24, 48, and 72 h. Results are average values of 4 (2-48 h) or 2 biological replicates (72 h) \pm SD.
- C. IL-6 production in LSECs from 3-20 h, and effects of Dex. Results are average of 2 biological replicates \pm SD.

Fig. 3: Global aspects of the proteomics data sets

- A. Principal component analysis (PCA) plot based on scaled TMT reporter intensities of all samples included in the proteomics experiment.

- B. Correlation plot between samples at different time points and treatment. The size of the circle corresponds to the magnitude of the respective Pearson's correlation coefficient between the time in culture and Dex treatment (\pm Dex).
- C. Scatter plot elucidates Dex-mediated changes on top of the time-dependent *in vitro* changes. This was done by plotting the ranks calculated from the generalized linear model with edgeR of [(48 h-10 h) - (10 h-1 h)] against [(48 h+Dex vs 10 h+Dex) vs (10 h+Dex vs 1 h)]. The majority of the proteins were similarly affected with respect to time in culture, independent of treatment (open circles). The red circles show proteins that were changed as a function of time only. The blue circles show proteins that were changed in a Dex-specific manner. The green circles show proteins whose time-dependent changes were completely reciprocated by Dex.

Fig. 4: Metabolic changes in LSECs during *in vitro* maintenance

- A. Scaled heatmap illustrating enriched KEGG pathways in at least one of the comparisons between samples, based on MSigDB (ver.7.2) with GSEA analysis (47). Only gene sets with FDR $q \leq 0.05$ were identified as enriched. We used the Signal2Noise parameter for ranking genes and weighted options for enrichment statistics during GSEA. The color code is based on the normalized enrichment score obtained from the GSEA analysis. The columns represent the individual comparison in an order obtained from hierarchical clustering based on Euclidean distance.
- B. Schematic drawing of the glycolytic pathway based on the KEGG pathway illustration. Unfilled circles represent the glycolytic metabolites. Arrowheads show the direction of the reactions driven by the glycolytic enzymes. The arrowhead (o-) represents the allosteric enhancer of PFKP. Proteins written in red were upregulated in a time-dependent manner with/without Dex, while unaltered proteins are written in black. Proteins written in blue were upregulated in the presence of Dex. Proteins in green were downregulated in the presence of Dex. Proteins in orange were upregulated in culture only with the comparison between 10 h vs 1 h. G6PDx (purple box) was upregulated with time in cultures without Dex and downregulated in the presence of Dex.
- C.-E. Bar charts showing the standardized \log_2 TMT reporter intensities of C) proteins involved in the TCA cycle; D) the average of the leading-edge genes of the oxidative phosphorylation pathway; and E) the average of the genes associated with the MSigDB integrated KEGG pentose phosphate pathway (PPP). In C, * indicates that the protein level was significantly changed ($|\log_{2FC}| \geq 0.5$, FDR ≤ 0.05 , exact test in edgeR) compared to 1 h samples. The time of sample collection is written directly above the spheres, Dex treatment is indicated by '+' and untreated controls by '-'. Error bars show 95% confidence intervals.

Fig. 5: LSECs display an activated inflammatory-like phenotype *in vitro*

- A. Scaled heatmap illustrating the enriched hallmarks gene sets indicating inflammatory response, cytokine signaling, response to hypoxia, and release of complement factors in at least one of the comparisons, based on MSigDB (ver. 7.2) with GSEA analysis. Only the gene sets with ($FDR \leq 0.05$) were identified as enriched. We used the Signal2Noise parameter for ranking genes and weighted options for enrichment statistics during GSEA. The color code is based on the normalized enrichment score obtained from the GSEA analysis. The columns represent the individual comparison in an order obtained from hierarchical clustering based on Euclidean distance.
- B. Dot plot illustrating the time-dependent increase in expression of inflammatory proteins. The averages of inflammatory protein and basal protein intensities (rest minus inflammatory proteins) are presented by blue and red spheres, respectively.
- C. Protein-protein interaction map of proteins involved in endothelial activation, that are significantly altered ($|\logFC| \geq 0.5$, $FDR \leq 0.05$, pairwise exact test in edgeR) in the presence of Dex, or with time in culture. The nodes represent the proteins, the edges represent an interaction between proteins, and edge colour indicates the nature of the interaction.
- D. Bar chart illustrating the averages of the standardized \log_2 TMT reporter intensities of cell adhesion molecules that are considered as biomarkers of endothelial activation (116). The * over the bar indicates significantly altered expression compared to 1 h culture. The α over the bar indicates significantly altered expression at 48 h compared to both 1 h and 10 h control culture while the # indicated significant changes in the presence of Dex compared to its time-matched control. Dex treatment is indicated by +.
- E. Box plot illustrating the changes in the concentration of ICAM-1 in supernatants of mouse LSECs with time in culture, and in the presence of Dex (n=3). Red boxes represent the supernatants from untreated cultures; blue boxes represent the supernatants from Dex-treated cultures. The significance of the effect of Dex on ICAM-1 level in supernatants was evaluated with a paired t-test ($p \leq 0.05$ was considered significant represented by *) against the time-matched control.
- F. Box plot illustrating the changes in the concentration of VCAM-1 in the supernatant of mouse LSECs with time in culture, and in the presence of Dex (n=3). Red boxes represent the supernatants from untreated cultures; blue boxes represent the supernatants from Dex-treated cultures. The significance of the effect of Dex on VCAM-1 level in supernatants was evaluated with paired t-test ($p \leq 0.05$ was considered significant represented by *) against the time-matched control.
- Error bars show 95% confidence intervals.

Fig. 6: Proteins involved in endothelial-dependent NO production, and LSEC redox systems

A-D. The bar charts in (A - D) illustrate the averages of the standardized \log_2 TMT reporter intensities of A) the two isoforms of nitric oxide synthase; B) proteins involved in posttranslational modification of eNOS (NOS3), which directly affects endothelial-dependent NO production; C) proteins involved in regeneration and recycling of tetrahydrobiopterin (BH₄), a vital cofactor of eNOS (NOS3), which also directly affects the physiological activity of eNOS (54); and D) proteins involved in LSEC redox balance. The * over the bar indicates significantly altered expression compared to 1 h culture. The α over the bar indicates significantly altered expression at 48 h compared to both 1 h and 10 h culture while the # indicates the significant changes in the presence of Dex compared to its time-matched control. The “+” sign indicates Dex (1 μ M). Error bars show 95% confidence intervals.

E. The box plot shows the level of intracellular glutathione (in μ M) in LSEC cultures after 2 h incubation with or without Dex, or H₂O₂. The exposure of LSEC cultures to H₂O₂ significantly decreased the level of glutathione. A paired t-test ($p < 0.05$). Error bars show 95% confidence intervals.

Fig. 7: Mouse LSEC scavenger function in culture

A. Endocytosis of low dose of formaldehyde-treated serum albumin (FSA) in LSECs. LSECs were kept in medium \pm dexamethasone (Dex) for 2, 24, 48, 72, or 120 h after primary culture establishment, and then incubated with ¹²⁵I-FSA (approximately 0.1 μ g/ml) for 2 h at 37 °C. Endocytosis was measured as described in Material and Method, and results are given in percent of added radioactivity (\pm SE). The results for the different treatment groups are slightly separated in the figure for visualization only and experiments started similarly at the indicated time points.

B. Endocytic capacity of freshly plated (2 h) LSECs and LSECs cultured for 48 h in medium \pm 1 μ M Dex. The cultures were incubated with ¹²⁵I-FSA (approximately 0.1 μ g/ml) alone or together with nonlabelled FSA (10-80 μ g/ml) for 2 h at 37 °C. Error bars represent SE.

C-E. The bar charts in (C - E) illustrate the averages of the standardized \log_2 TMT reporter intensities (\pm 95% confidence intervals) of C) major scavenger receptors and lectins, D) proteins associated with endocytosis regulation, and E) proteins associated with clathrin coat formation and vesicle maturation, in LSECs cultured for 1, 10, or 48 h in the presence (+), or absence (-) of Dex. The * over the bar indicates significantly altered expression compared to 1 h culture. The α over the bar indicates significantly altered expression at 48 h compared to both 1 and 10 h control culture, the # indicates the significant changes in the presence of Dex compared to its time-matched control,

while ~ indicates the significant changes between 10 h vs 48 h compared with treatment-matched samples.

Fig. 8: Dexamethasone protects LSECs in culture from apoptosis

- A. Box plot illustrating changes in the average of TMT reporter intensities of proteins associated with apoptotic cell death, autophagy, and pyroptosis in LSECs. Student's t-test was used to evaluate significant differences between comparisons, indicated by the roofs over the bar with the corresponding p-value on top. "+" indicates Dex treatment and "-" indicates the time-matched control.
- B. Box plot illustrating changes in the relative luminescence unit, corresponding to apoptotic cell death in mouse LSECs cultured for 24 h in the presence of 1 μ M Dex, CD95, 1 μ M Dex + CD95, or with no treatment (n=3). Differences between treatments were identified as significant if the $p \leq 0.05$ in a paired t-test; the p-values are inserted on the roofs over the bars.
- C-D. Bar charts illustrating the average of the standardized \log_2 TMT reporter intensities of C) pro-apoptotic proteins involved in the induction of cell death; D) anti-apoptotic proteins providing a protective effect against cell death. The * over the bar indicates significantly altered expression compared to 1 h culture. The α over the bar indicates significantly altered expression at 48 h compared to both 1 and 10 h control culture while the # indicates the significant changes in the presence of Dex compared to its time-matched control. "+" indicates Dex treatment and "-" indicates the time-matched control.

Error bars in A-D show 95% confidence intervals.

Fig. 9: Effect of time in culture and dexamethasone on LSEC transcription regulators in the proteomic data set

- A. Scatter plot showing the transcriptional regulators predicted by Lisa using the Cistrome DB (77), corresponding to up- and downregulated gene sets identified as significantly different between 10 h non-Dex samples against 1 h. Proteins with $|\log_{2}FC| \geq 0.5$ and $FDR \leq 0.05$ in a pairwise comparison using an exact test in edgeR were identified as differentially expressed. Each solid sphere indicates a transcriptional regulator in Cistrome DB. The grey spheres represent predicted proteins that were not detected in our TMT datasets. The light-yellow spheres were below the significant threshold of $|\log_{2}FC| \geq 0.5$ and $FDR \leq 0.05$. The black spheres represent transcriptional regulators that were downregulated in LSECs at 10 h compared to 1 h, whereas the red-colored spheres show the ones that were upregulated at 10 h.

- B. Bar chart illustrating the average of the standardized \log_2 TMT reporter intensities of transcriptional regulators that were significantly changed early *in vitro*, predicted by the Lisa model (in A) based on the list of differentially expressed proteins between 10 h non-Dex samples vs 1 h. The * over the bar indicates significantly altered expression compared to 1 h while the # indicates significant changes in the presence of Dex compared to the time-matched control. Dex treatment is indicated by +.
- C. Scatter plot showing transcriptional regulators predicted by Lisa using the Cistrome DB, corresponding to up- and downregulated gene sets identified as significantly different between 48 h non-Dex samples against 10 h non-Dex samples. Proteins with $|\log_{FC}| \geq 0.5$ and $FDR \leq 0.05$ in a pairwise comparison using an exact test in edgeR were identified as differentially expressed. Each solid sphere indicates a transcriptional regulator in Cistrome DB.
- D. Bar chart illustrating the averages of the standardized \log_2 TMT reporter intensities of transcription regulators significantly changed late *in vitro* which were predicted by the Lisa model (in c) based on the list of differentially expressed proteins between 48 h vs 10 h non-Dex treated samples. The * over the bar indicates significantly altered expression compared to 10 h culture. The # over the bar indicates significantly altered expression at 48 h in Dex treated samples compared to 48 h non-treated controls. Dex treatment is indicated by +.
- E. Scatter plot showing the transcriptional regulators predicted by Lisa using the Cistrome DB, corresponding to up- and downregulated gene sets identified as significantly different between Dex-treated 48 h samples against 48 h non-treated control samples. Proteins with $|\log_{FC}| \geq 0.5$ and $FDR \leq 0.05$ in a pairwise comparison using an exact test in edgeR were identified as differentially expressed. Each solid sphere indicates a transcriptional regulator in the Cistrome DB.
- F. Bar chart illustrating the average of the standardized \log_2 TMT reporter intensities of transcriptional factors significantly changed late *in vitro* in a Dex specific manner, predicted by the Lisa model based on the list of differentially expressed proteins between Dex-treated samples at 48 h vs 48 h controls. The * over the bar indicates significantly altered expression in the presence of Dex at 48 h compared to 1 h control. The # over the bar indicates significantly altered expression at 48 h Dex-treated compared to 48 h control. Dex treatment is shown by +.
- Error bars in B, D, F show 95% confidence intervals.

Figure 1

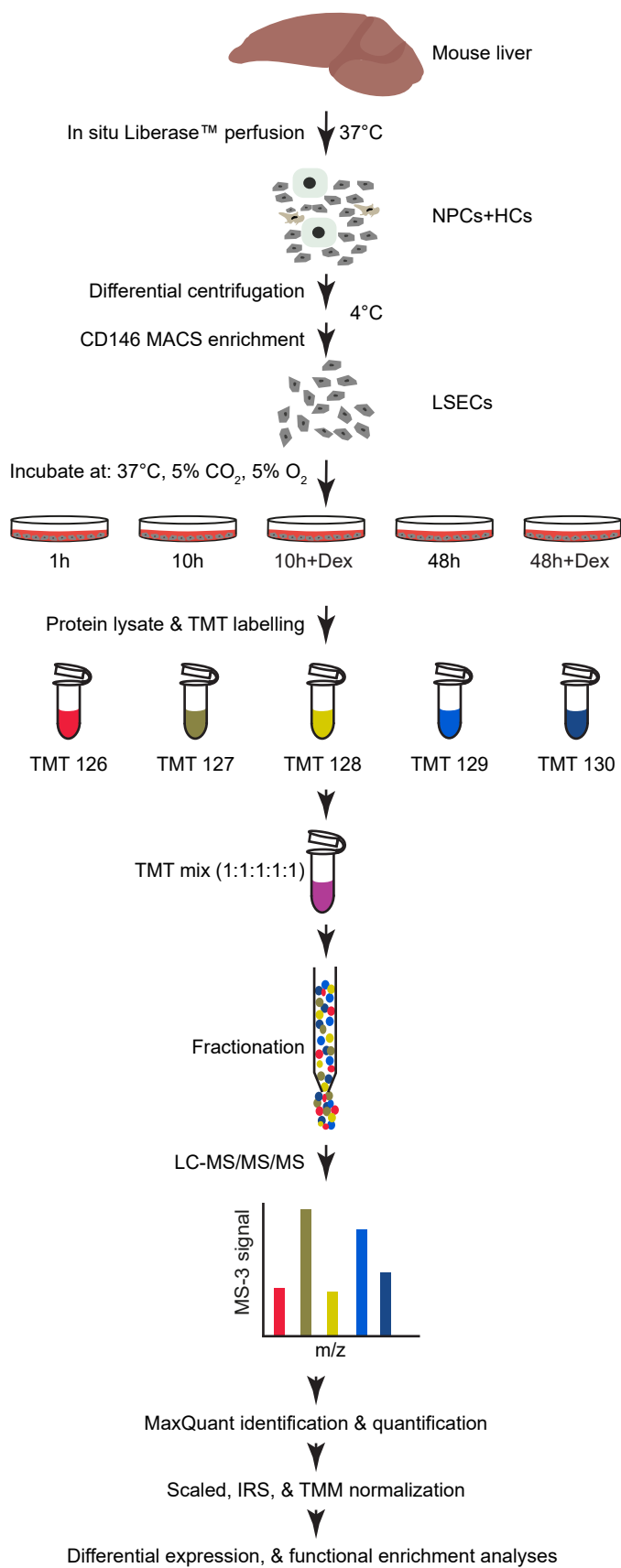


Figure 2

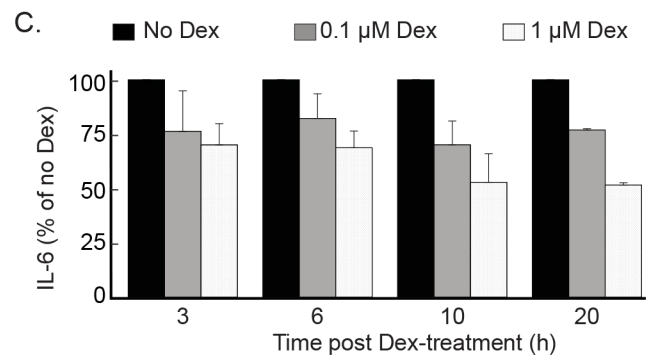
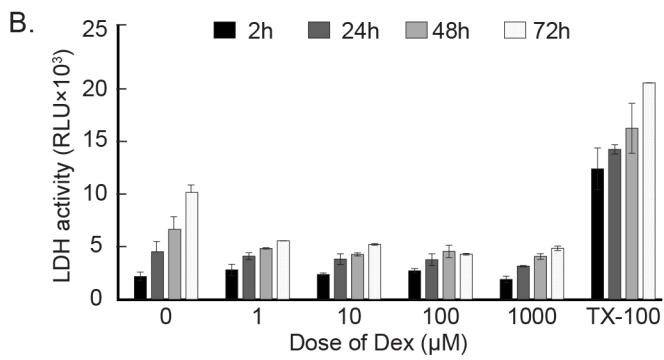
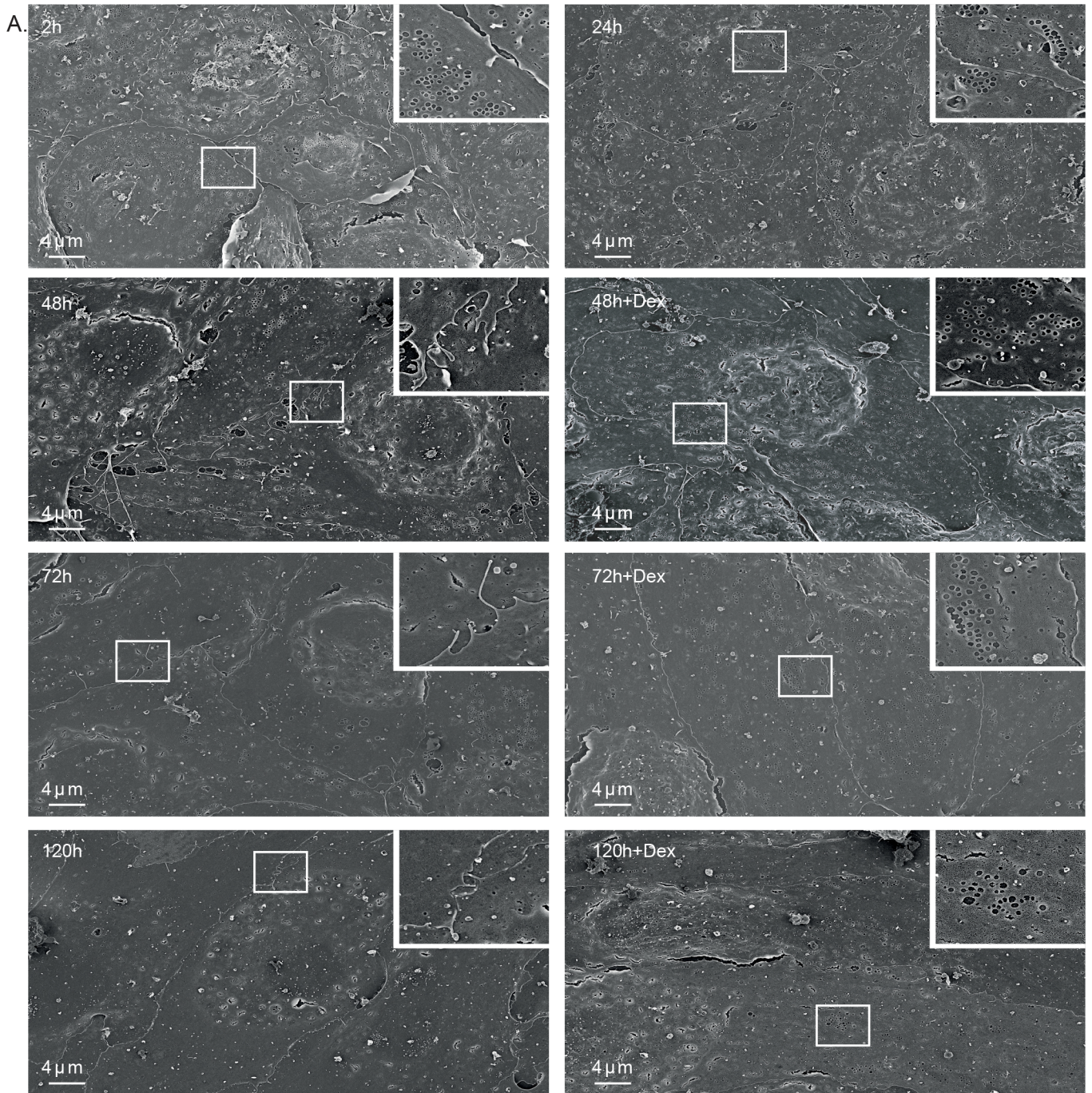


Figure 3

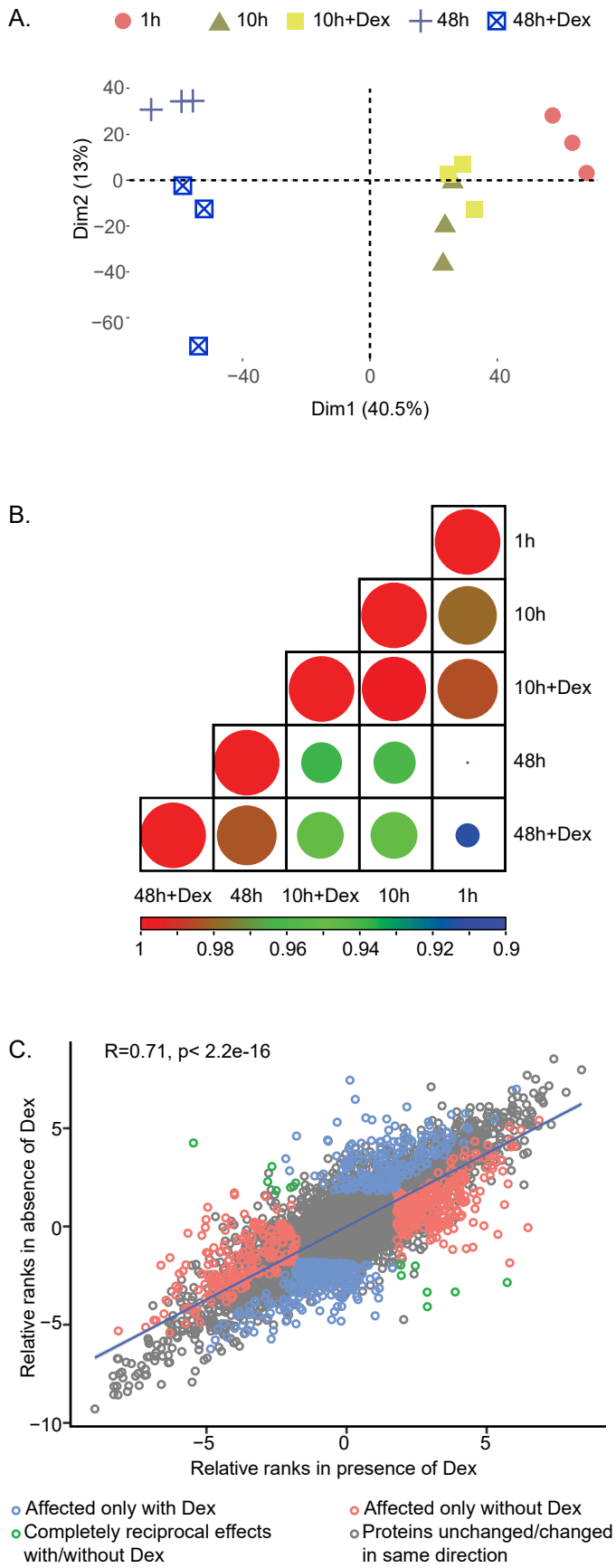


Figure 4

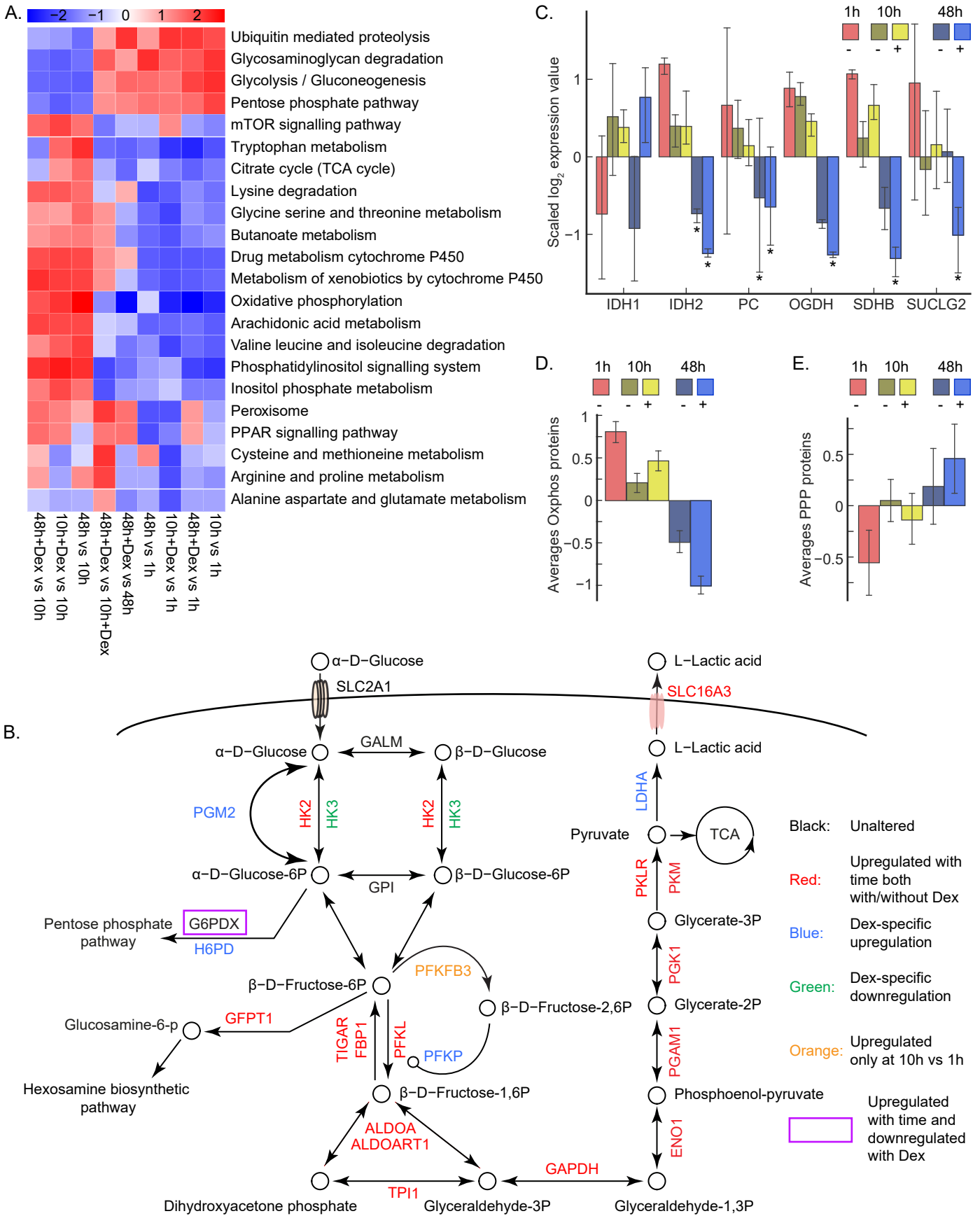


Figure 5

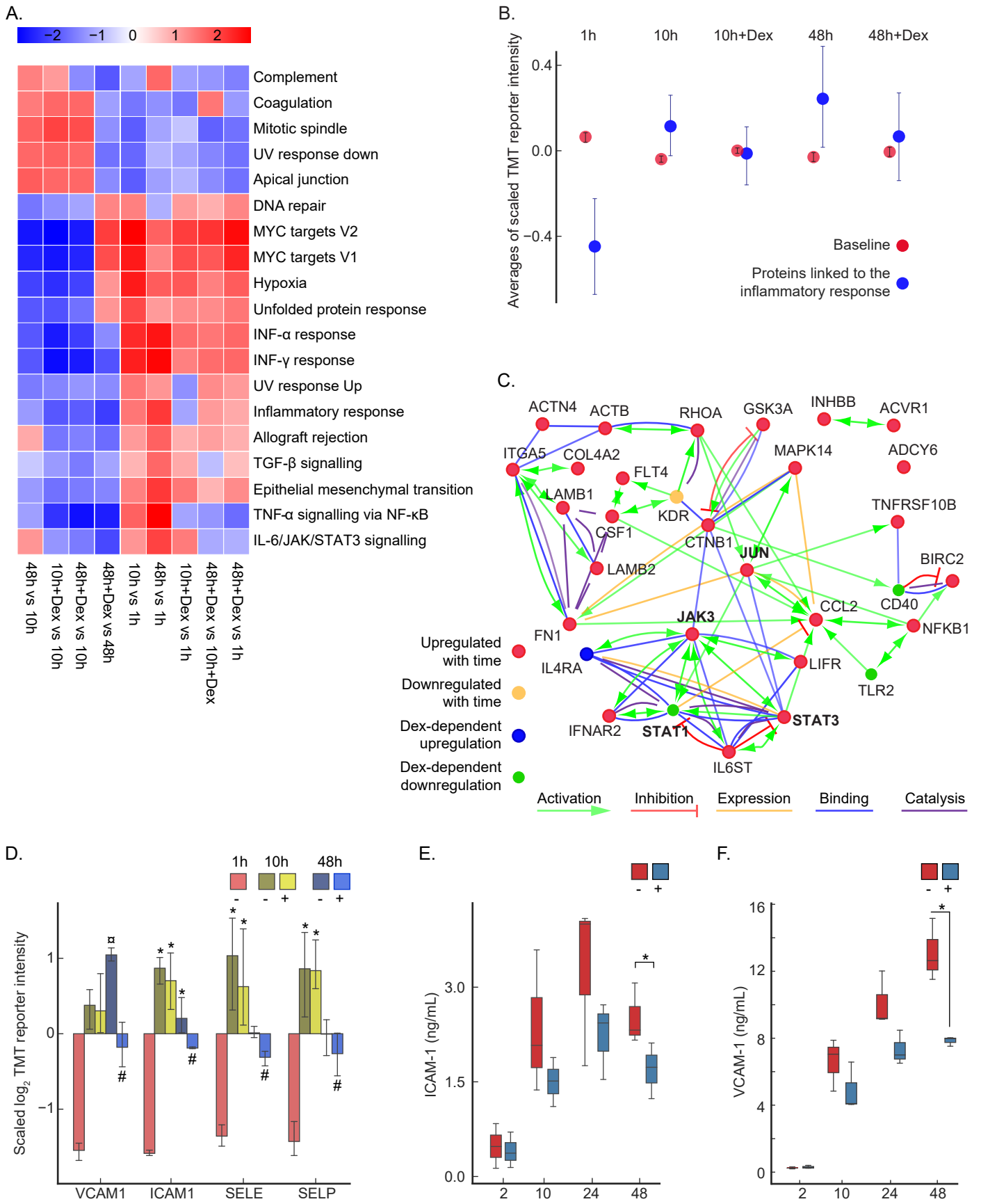


Figure 6

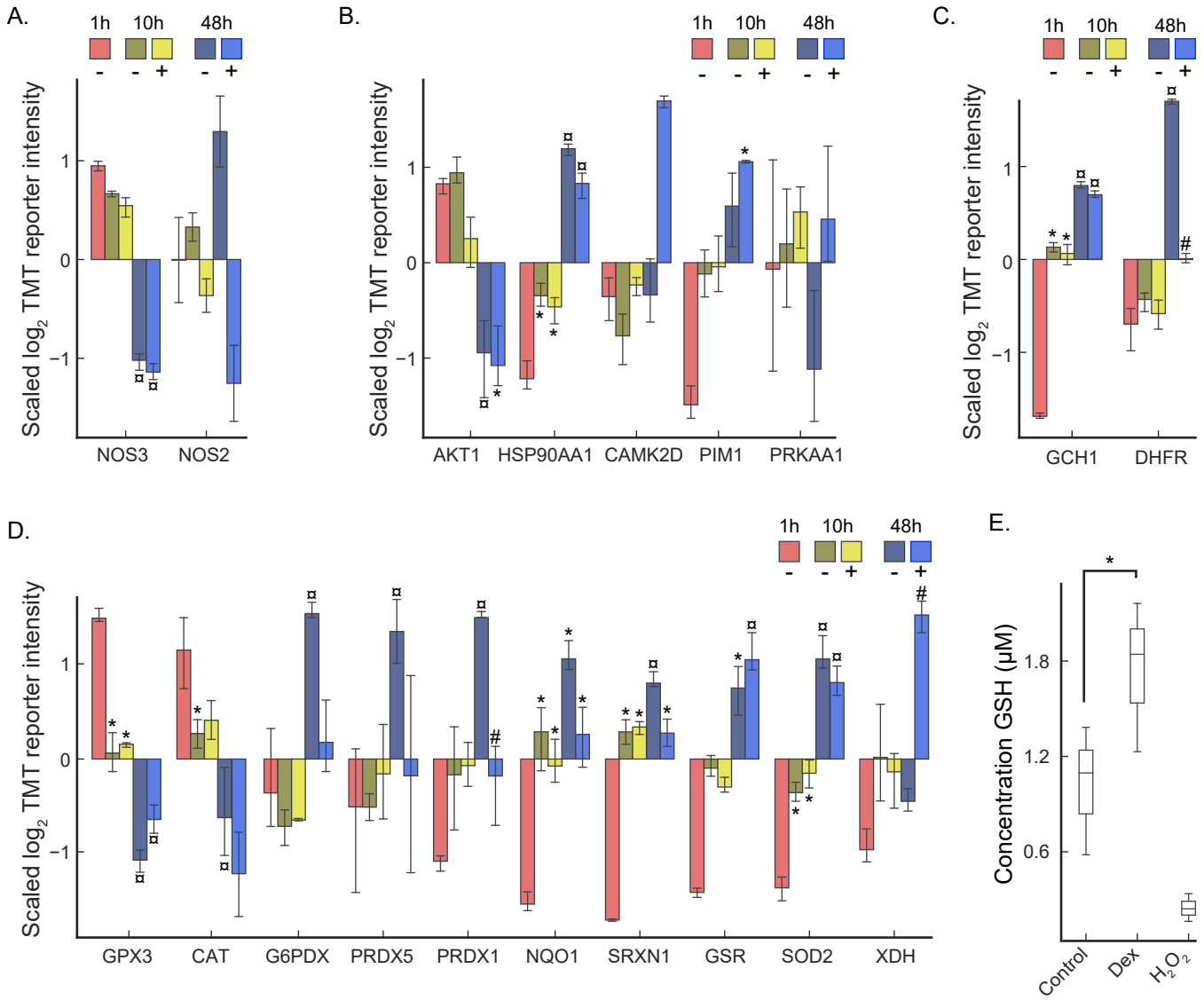


Figure 7

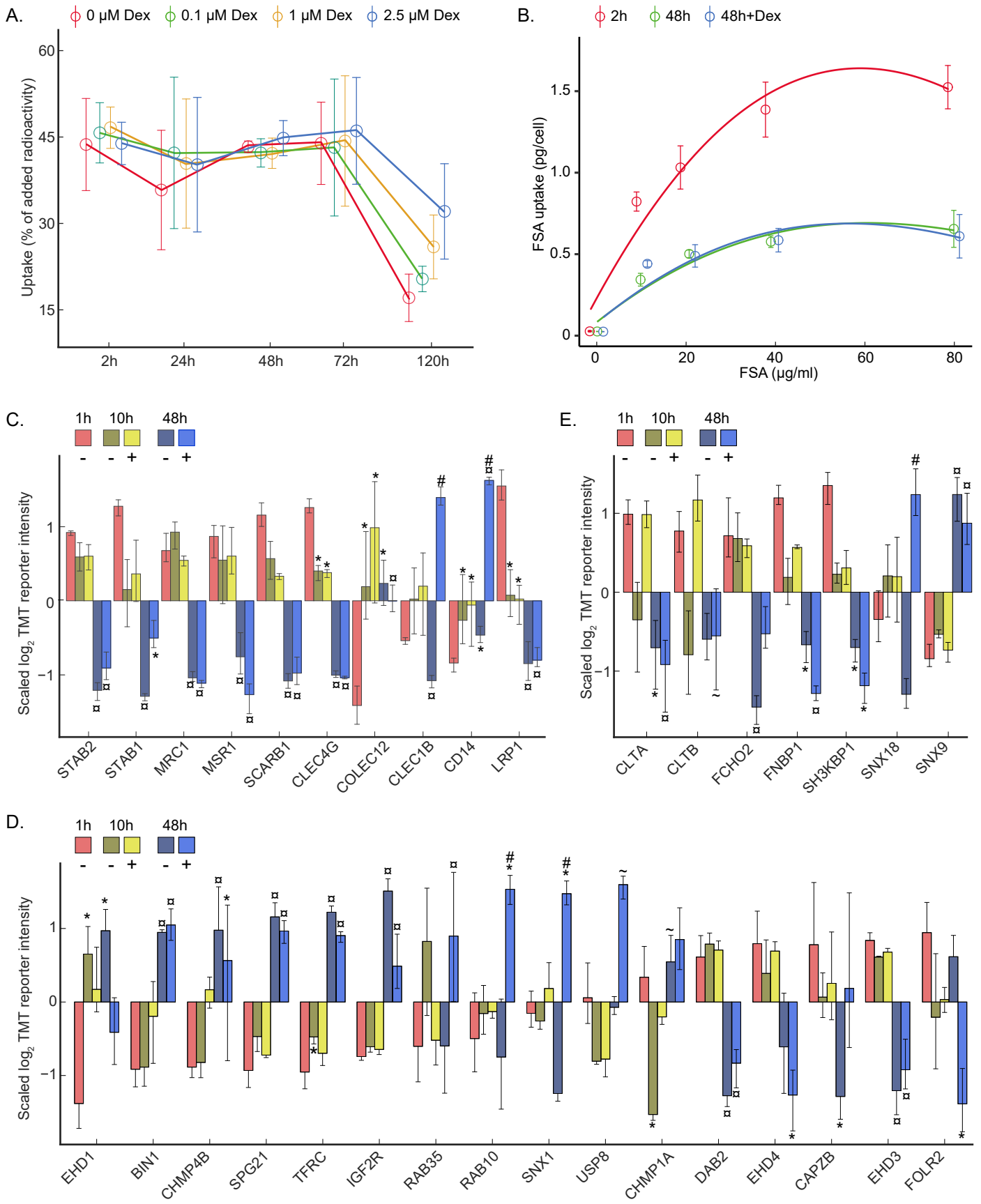


Figure 8

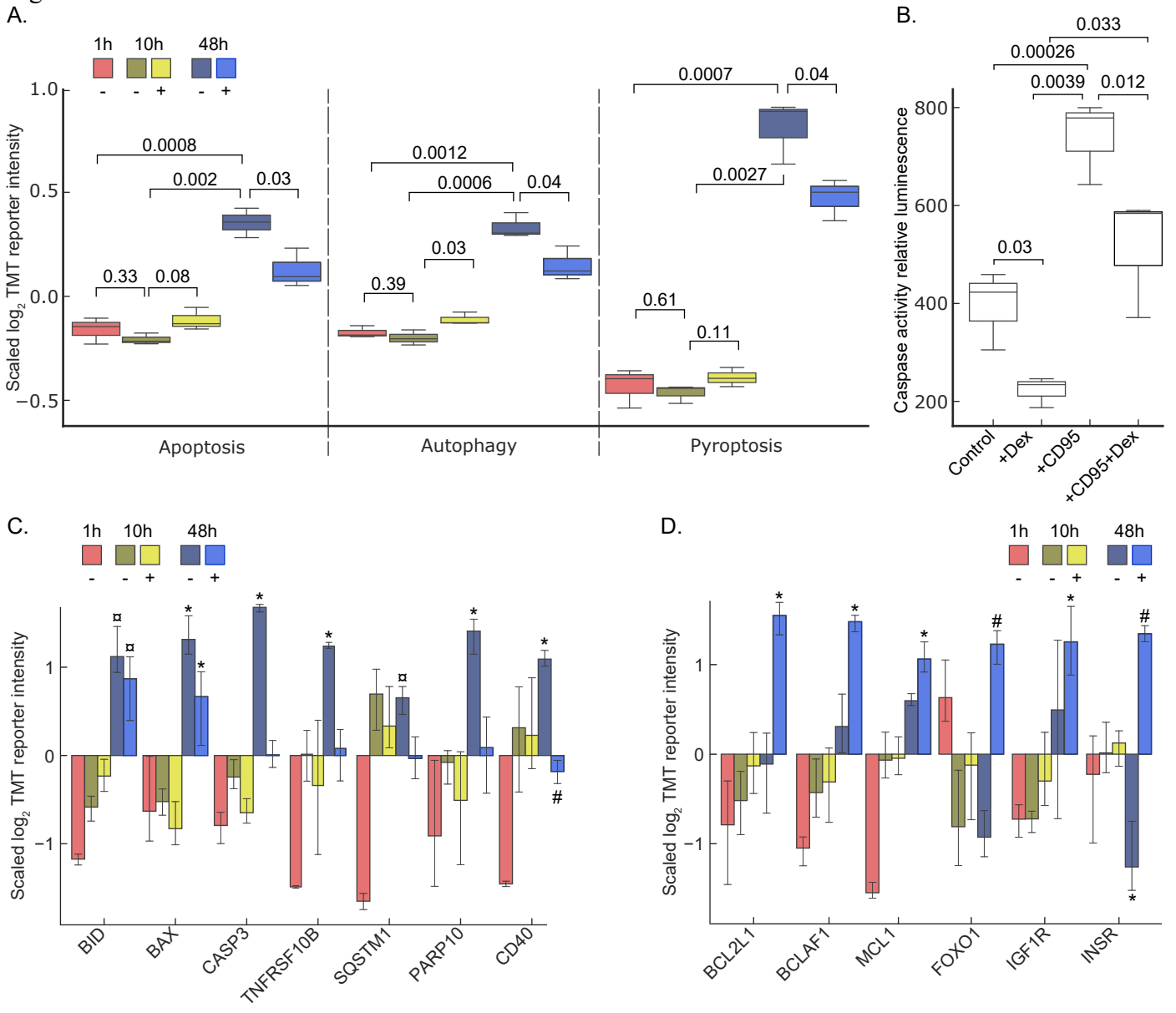
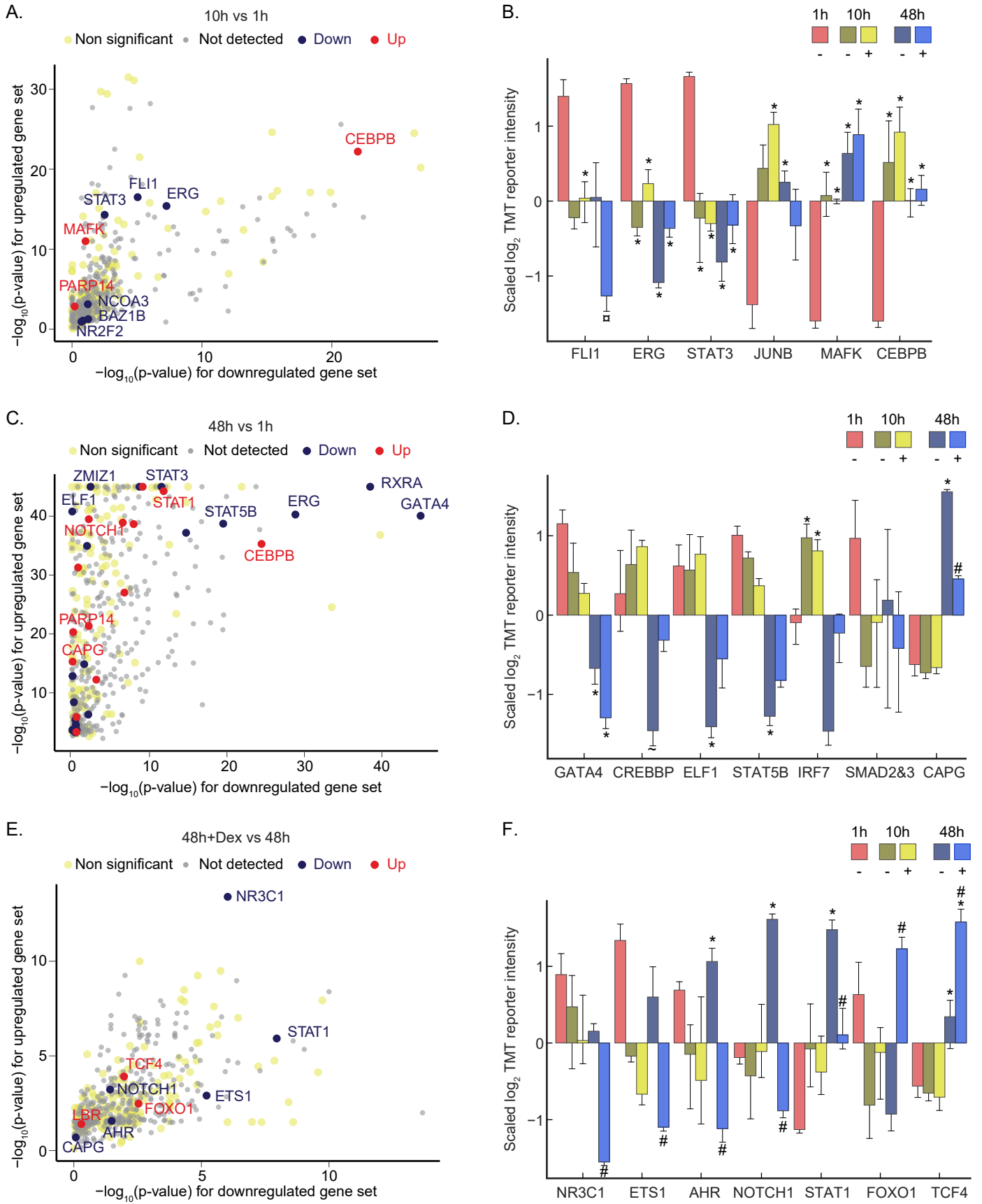


Figure 9



Supplementary information

Supplementary Fig. 1: Primary mouse LSEC cultures 5 days post-seeding

Freshly isolated cells were cultured in AIM-V medium in 5% oxygen atmosphere, in the absence and presence of dexamethasone at indicated doses.

Supplementary Fig. 2: Micrographs of primary mouse LSEC cultures used for measurements of LDH release to the culture medium (Fig. 2B)

A, B) Phase-contrast images of LSEC cultures incubated with 0-1000 μ M Dex for 48-72 h. C) Scanning electron micrographs of LSECs incubated with 1000 μ M Dex for 48 or 72 h. Arrow points to a dead cell.

Supplementary Fig. 3: Regulators of NO signaling, endocytic regulators, and clathrin coat proteins and initiators

The bar charts in A-B illustrate the average of the standardized \log_2 TMT reporter intensities of A) regulators and interacting partners of NOS3; B) proteins associated with cell-cell and cell-substrate adhesion. The * over the bar indicates significantly altered expression compared to 1 h culture, \square over the bar indicates significantly altered expression at 48 h compared to 1 h and 10 h culture, # over the bar indicates significantly altered expression at 48 h of Dex-treated samples compared to 48 h control samples, while ~ indicates the significant changes between 10 h vs 48 h compared with treatment-matched samples. Treatments are represented by different fills in legends as well as with + for Dex treatment, and – for the time-matched control. Error bars show 95% confidence intervals.

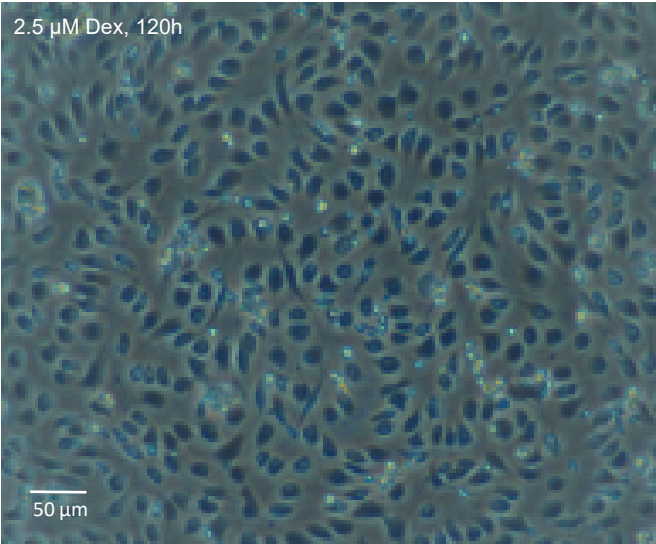
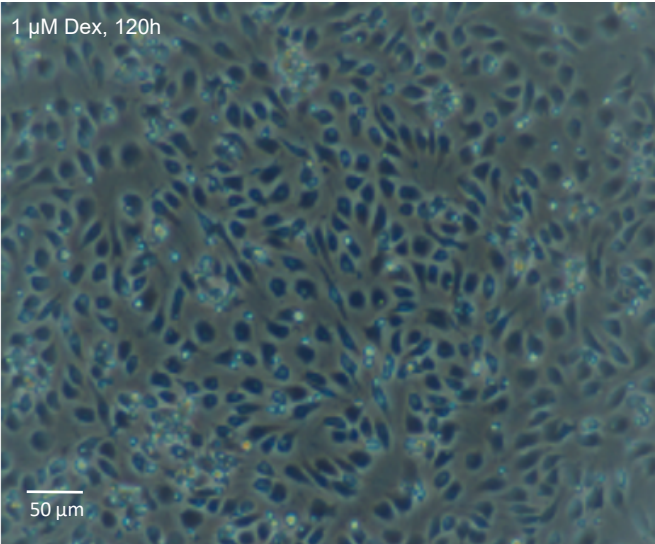
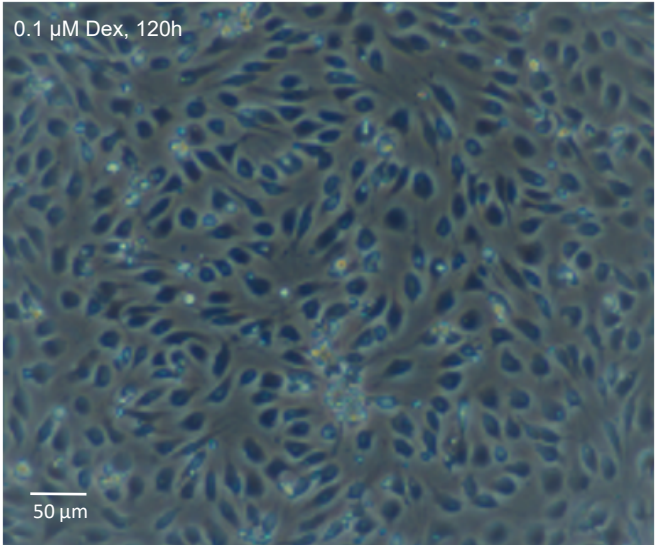
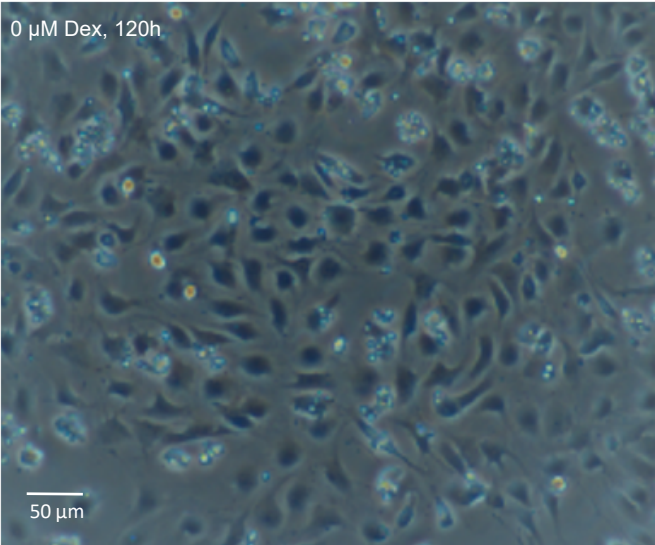
Supplemental file 1: The processed proteomics dataset

Supplemental file 1 is available at

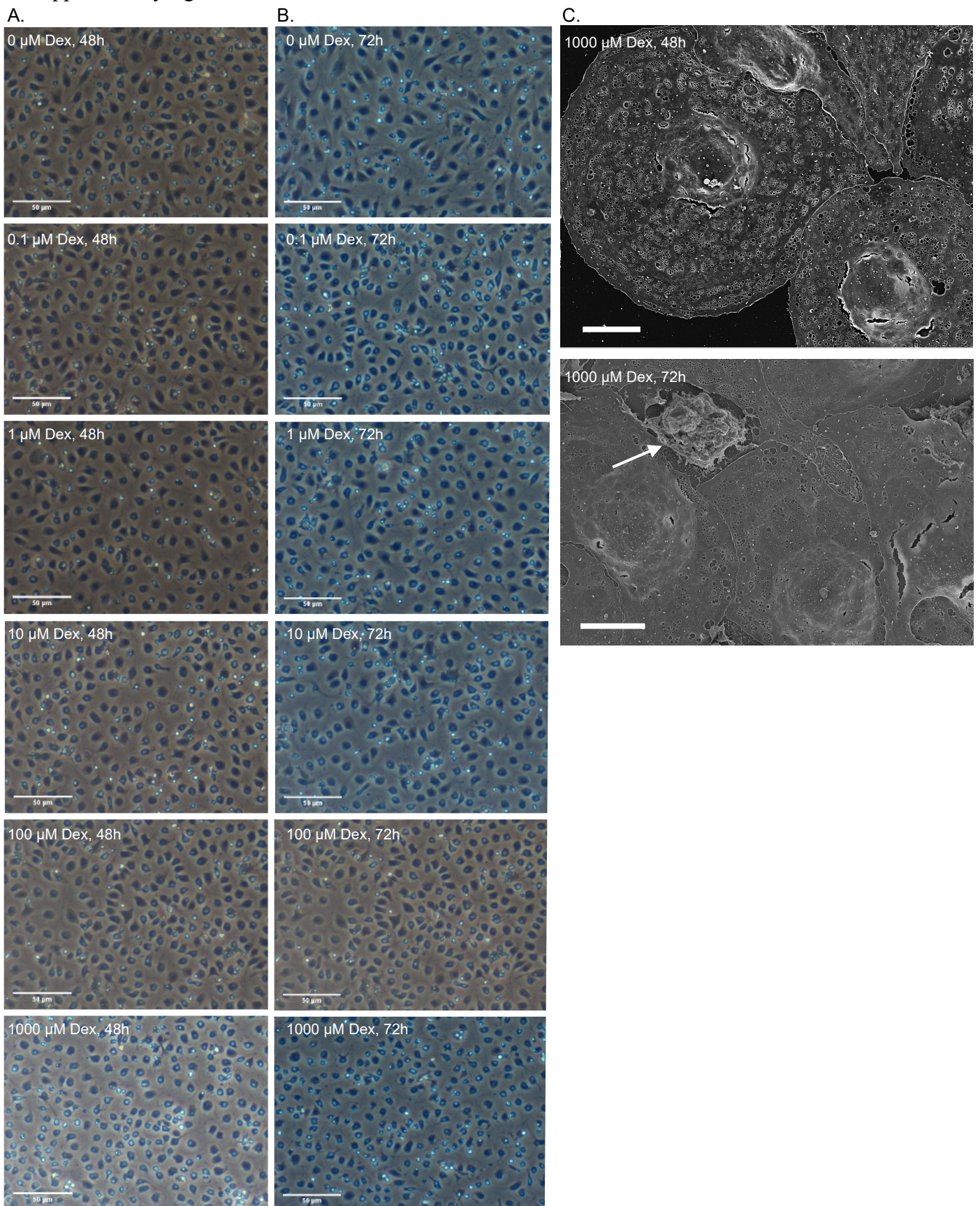
<https://dataverse.no/privateurl.xhtml?token=a64cce05-be19-42b2-b5a1-7a1252433028>

The link will take you to the UiT Open Research Data repository. There are two txt files - the one on top “00_README_Murine_LSEC_proteome.txt” contains all the meta-information about the main data file “Murine_LSEC_timeseries_processed_TMTproteomics.txt”.

Supplementary figure 1



Supplementary figure 2



Supplementary figure 3

